Bergische Universität Wuppertal

Fachbereich C- Mathematik und Naturwissenschaften

Design of drugs for the inhibition of the cancer related proteins MIA, Rheb and K-Ras

Dissertation

zur Erlangung des Grades eines
Dr. rer. nat.

von
Jasmin Müller
geboren in Remscheid
am 25. Mai 1988

Die Dissertation kann wie folgt zitiert werden:

urn:nbn:de:hbz:468-20180806-114148-2
[http://nbn-resolving.de/urn/resolver.pl?urn=urn%3Anbn%3Ade%3Ahbz%3A468-20180806-114148-2]

Der Mensch hat dreierlei Wege, klug zu handeln:
Erstens durch Nachdenken – das ist der edelste;
zweitens durch Nachahmen – das ist der leichteste;
und drittens durch Erfahrung – das ist der bitterste.
Konfuzius

Lernen und nicht denken ist unnütz,
Denken und nicht lernen ist zwecklos,
Denken, ohne etwas gelernt zu haben, ist gefährlich.
Konfuzius

Das schönste Glück des denkenden Menschen ist,
das Erforschliche erforscht zu haben
und das Unerforschliche zu verehren.
Johann Wolfgang von Goethe

Danksagung

Ich möchte mich herzlich bei all den Menschen bedanken, die mich bei der Anfertigung dieser Thesis weitreichend unterstützt haben:

- Prof. Dr. Jürgen Scherkenbeck für die intensive Betreuung und viele konstruktive Kritik während der gesamten Zeit
- Prof. Dr. Raphael Stoll, Dr. Miriam Schöpel, Dr. King Yip Tuo sowie Oleksandr Shkura und Xueyin Zhong für die Kooperation, die ausführlichen Diskussionen und die Messung der 2D-NMR Spektren

Vielen lieben Dank auch an alle meine Laborkollegen, die mich täglich durch die guten wie auch die schlechten Zeiten begleitet haben, für die zahlreichen Diskussionen und Anregungen und das allgemein sehr angenehme Arbeitsklima:

- Sivatharushan Sivanathan, Govinda Babu Kotipalli, Marcel Mackwitz, Florian Körber
- Albert Lehnard, Isabell Geisler, Dario Wetterling und Julia Vollrodt für die Unterstützung bei den Synthesen während ihrer Bachelor- und Masterarbeiten

Weiterer Dank gilt dem technischen Personal der Bergischen Universität Wuppertal, ohne die sowohl NMR als auch LC-Messungen nicht möglich gewesen wären. Vielen Dank für eure unermüdliche Hilfe, egal mit welchem Problem ich zu euch kam:

- Simone Bettinger und Ilka Polanz für die Unterstützung bei den LC-Messungen
- Andreas Siebert für die NMR-Messungen

Mein größter Dank aber gilt meiner Familie. Danke, dass ihr immer für mich da wart.

Abstract

Cancer is one of the leading causes of morbidity and mortality worldwide. The three cancer-related proteins Rheb, *K*-Ras and MIA were chosen as targets. In the course of this thesis, the structure-activity-relationship of molecules, which bind to these proteins, were examined. During preliminary studies, four molecules were identified as good binders. The structure-activity-relationship of the compounds was thoroughly investigated. Molecular modelling was used as a tool to identify promising compounds. Complexes of the compounds and the corresponding proteins were computed using Autodock/Vina and/or Glide. Selected molecules were then synthesized and tested for their interaction with the protein by heteronuclear NMR measurements. The observed shifts were used for HADDOCK calculations to predict the binding conformation of the compound and the corresponding protein.

For Rheb, a molecule incorporating an additional hydroxy group in comparison to 4,4'-biphenol was found to exhibit a binding constant that is approximately six times stronger. Surprisingly, reducing the number of hydroxy groups has the same effect on the binding affinity. All in all, the Rheb protein tolerates only small additional substituents on the biphenol core structure.

In case of *K*-Ras, alterations of the bisphenol A core mostly led to inactive compounds. These will be interesting for other purposes than cancer treatment depending on the functional groups of the molecules. Similar to Rheb, the *K*-Ras protein does not tolerate introduction of large substituents into the bisphenol A core structure.

For the MIA protein, two molecules were identified from a screening of the ZINC database. The structure-activity-relationship of one of these compounds regarding its substituents was examined. In the following step, hybrid compounds derived from the two fragments were synthesized. Precursor molecules showed no activity towards the protein. Consequently, a comprehensive screening of the ZINC database was performed. A compound, which inflicts significant shifts of all protein peaks in the 2D-NMR spectrum, was found.

Contents

List of Abbreviations

Å	angstrom
aa	amino acid
Ac	acetyl
ACN	acetonitrile
ADP	adenosine diphosphate
AIR	ambiguous interaction restraints
Ala	alanine
aq.	aqueous
Arf	ADP ribosylation factor
Arg	arginine
Asn	asparagine
Asp	aspartate
BCC	basal-cell skin cancer
Bcl	B-cell lymphoma
bFGF	basic fibroblast growth factor
Boc	*tert*-butyloxycarbonyl
BPA	bisphenol A
C	cytosine
cal	calorie
calcd	calculated
CDI	carbonyldiimidazole
CH	cyclohexane
COSMIC	Catalogue of Somatic Mutations in Cancer
Cys	cysteine
d	days
Da	Dalton
dba	dibenzylideneacetone
DCAI	2-(4,6-dichloro-2-methyl-1*H*-indol-3-yl)ethanamine
DCC	*N*,*N*’-dicyclohexylcarbodiimide
DCM	dichloromethane
DIPA	diisopropylamine
DIPEA	diisopropylethylamine
DMAP	4-dimethylaminopyridine
DME	dimethoxyethane
DMF	dimethylformamide
DMSO	dimethylsulfoxide
DNA	deoxyribonucleic acid
DPPF	1,1’-ferrocenediyl-bis(diphenylphosphine)
E. coli	*Escherichia coli*
EDC	1-ethyl-3-(3-dimethylaminopropyl)carbodiimide
EtOAc	ethyl acetate
EGF	epidermal growth factor
EGFR	epidermal growth factor receptor
EM	energy minimization
equiv.	equivalents
ER	endoplasmatic reticulum
ERK	extracellular signal-regulated kinase
ESI	electrospray ionization
Et	ethyl
FBDD	fragment-based drug design
FN	fibronectin
FTI	farnesyl transferase inhibitor
G	guanine
GAP	GTPase activating protein
GDP	guanosine diphosphate
GEF	guanidine exchange factor
Glide	grid-based ligand docking with energetics
Gln	glutamine
Glu	glutamate

Gly	glycine
GppNHp	guanosine-5’-(β,γ-imido) triphosphate
Grb	growth factor receptor binding
GTP	guanosine triphosphate
HADDOCK	High Ambiguity Driven Docking
HATU	1-[Bis(dimethylamino) methylene]-1*H*-1,2,3-triazolo[4,5-b]pyridinium 3-oxid hexafluorophosphate
HEPES	2-[4-(2-hydroxyethyl) piperazin-1-yl] ethanesulfonic acid
His	histidine
HOBt	1-hydroxybenzotriazole
HPLC	high pressure liquid chromatography
H-Ras	Harvey rat sarcoma
HSQC	heteronuclear single quantum coherence spectroscopy
HTFP	heterogeneous transition-metal-based fluorescence polarization
HVR	hypervariable region
IC_{50}	half maximal inhibitory concentration
IGF	insulin-like growth factor
Ile	isoleucine
IPTG	isopropyl β-D-1-thiogalactopyranoside
IR	infrared
k_D	dissociation constant
K-Ras	Kirsten rat sarcoma
LB	lysogeny broth
Leu	leucine
Lys	lysine
MAPK	mitogen-activated protein kinase
Me	methyl
MEK	mitogen-activated protein kinase kinase
MEM	(2-methoxyethoxy)methyl
Met	methionine
MIA	melanoma inhibitory activity
MS	mass spectrometry
mTOR	mammalian target of rapamycin
mTORC1	mammalian target of rapamycin complex 1
NIS	*N*-iodosuccinimide
NMR	nuclear magnetic resonance
NTA	nitrilotriacetic acid
OD_{600}	optical density at 600 nm
PDB	protein data bank
PDGF	platelet-derived growth factor
PDK	3-phophoinositide-dependent protein kinase-1
Phe	phenylalanine
PI3K	phosphatidylinositol-3’-kinase
PIP2	phoaphatidylinositol-3,4-biphosphate
PKB	protein kinase B
PKC	protein kinase C
PLCε	phospholipase Cε
PLD1	phospholipase D1
P-loop	phosphate-binding loop
PPI	protein-protein-interaction
ppm	parts per million

Pro	proline
PTEN	phosphatase and tensin homologue
pTsOH	*para*-toluenesulfonic acid
Raf	rapid fibrosarcoma
RAL	Ras-related protein
RALGDS	RAL guanine nucleotide dissociation stimulator
Ran	Ras-related nuclear protein
Ras	rat sarcoma
RGL2	Ral guanine nucleotide dissociation stimulator-like 2
Rheb	Ras homologue enriched
RP	reversed phase
SA	simulated annealing
SAR	structure-activity-relationship
SCC	squamous-cell skin cancer
Ser	serine
SH	sarcoma homology
SOS	son of sevenless
SP	standard precision
STD	saturation transfer difference
T	thymine
TAD	torsion angle space
TEA	triethylamine
TFA	trifluoroacetic acid
THF	tetrahydrofurane
Thr	threonine
TIPS	triisopropylsilane
TOF	time of flight
TROSY	transverse relaxation-optimized spectroscopy
Trp	tryptophane
Tsc2	tuberous sclerosis complex 2
Tyr	tyrosine
UV	ultra-violet
Val	valine
XP	extra precision

1. Introduction

1.1. Cancer

“Cancer” is the common term for a family of diseases that are known to affect almost all tissues in the body. A similarity of all types of cancer is the abnormally increased growth of cells, which can be spread to other areas of the body in a process known as metastasis. In 2012, cancer was one of the leading causes of morbidity and mortality worldwide (14 million new cases and 8 million cancer related deaths). Over the next two decades, it is expected that the number of new cases will increase by approximately 70% to ~22 million.[1,2]

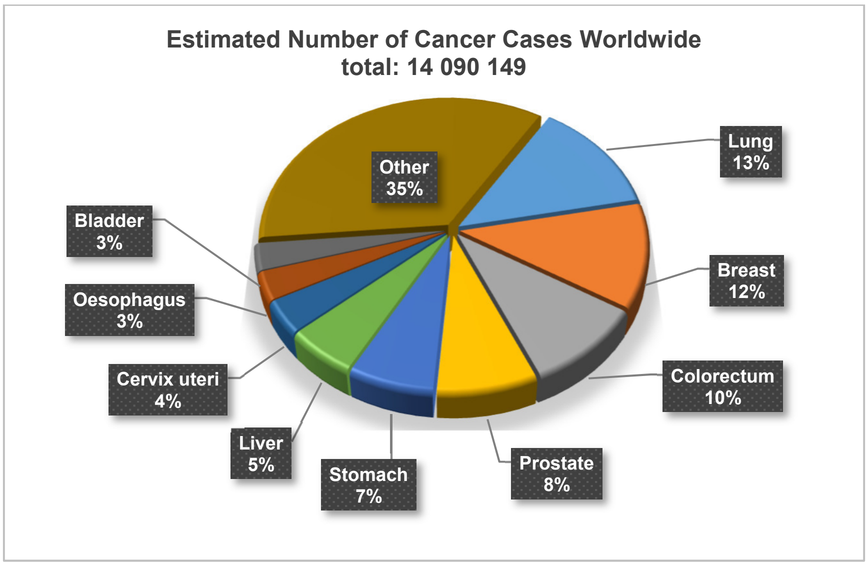

Figure 1: Estimated world cancer cases by major sites in both sexes in 2012.[1]

The estimated global annual numbers of new cases and cancer deaths for the most important types of cancer are summarized in Figure 1 for both sexes. Men and women show a different distribution of the organs most frequently infested by cancer. While men are most commonly affected by lung (16.7%), prostate (15.0%), colorectum (10.0%), stomach (8.5%) and liver cancers (7.5%), women are mainly diagnosed for breast (25.2%), colorectum (9.2%), lung (8.7%), cervix (7.9%) and stomach (4.8%) cancer. The highest incidence rates are reported for lung cancer (34.2 per 100 000) among men and breast cancer (43.3 per 100 000) for women (Figure 2).[1]

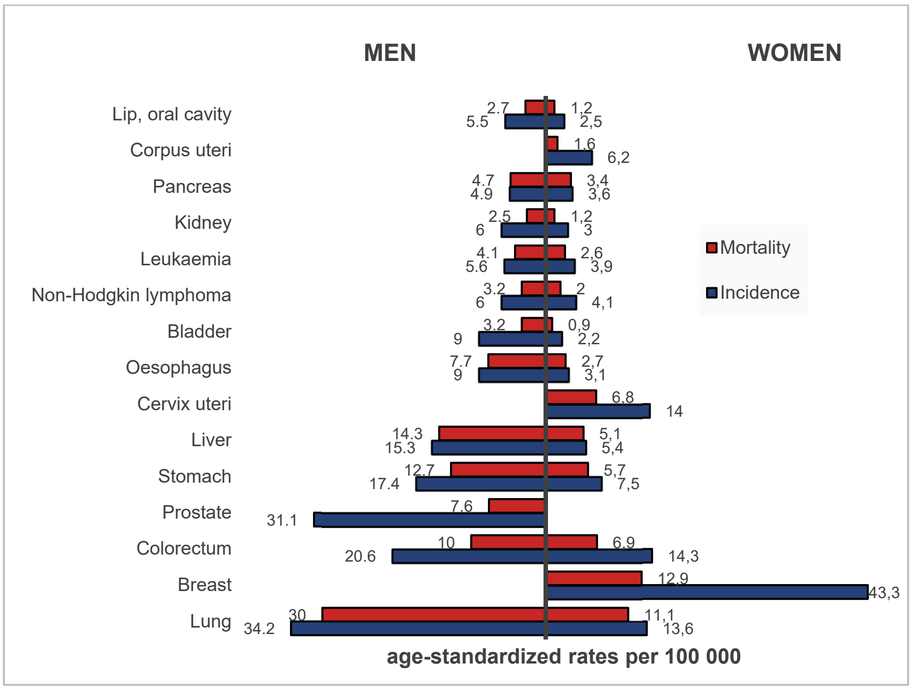

Figure 2: Estimated worldwide, age-standardized cancer incidence and mortality rates per 100 000 by major sites in 2012.[1]

North America and Western Europe account for the highest cancer incidence rates worldwide. Despite this, more than 60% of all cancer cases are associated with Africa, Asia as well as Central and South America. In these countries, 70% of the world's cancer deaths occur.

An outbreak of cancer begins with the mutation of a single cell through interaction of the genetic material with an external factor. These factors, also referred to as carcinogenic factors, can be of various natures such as physical (UV-light, ionizing and electromagnetic radiation), chemical (asbestos, aflatoxins, arsenic or tobacco smoke) or biological (viral, bacterial or parasitical infections).[2] Aberrations of the DNA or proteins such as the small GTPases *K*-Ras and Rheb or the growth-related protein MIA is the result. These proteins and especially their function and effect on cancer development will be explained in the following sections. Approximately one third of all cancer deaths are caused by the five most common behavioural and dietary risks (high body mass index, low fruit and vegetable intake, lack of physical activity, tobacco and alcohol consumption). The highest risk is posed by tobacco use causing around 20% of global cancer deaths and approximately 70% of global lung cancer deaths.[1]

The best method to heal cancer is to prevent it. The factors stated above cannot be avoided totally, but exposure to those risks can be minimized to reduce the chance of cancer affliction. In addition, a significant proportion of cancers can be cured by surgery, radiotherapy or chemotherapy, especially if they are detected early.[1]

1.2. Ras proteins and their functions

The Ras proteins, named after the Harvey and Kirsten **Ra**t **s**arcoma, belong to the eponymous superfamily of small GTPases with an average molecular weight of 20-25 kDa. For humans, it can be divided into five subfamilies: Ras, Rho, Rab, Arf and Ran.[3,4] The Ras subfamily expresses three isoforms of the Ras gene: *K*-Ras (spliced into the two modification *K*-Ras4A and *K*-Ras4B), *H*-Ras and *N*-Ras. While the four Ras isoforms differ slightly in size (189 amino acids for *H*-Ras, *K*-Ras4A and *N*-Ras and 188 amino acid for *K*-Ras4B), a sequence alignment shows nearly 79% sequence identity and therefore a high conservation.[5,6] *K*-Ras and its isoforms are involved in cellular signaling cascades responsible for growth regulation, proliferation, apoptosis and differentiation.[4,5,7,8] For biological activity, posttranslational prenylation (addition of farnesyl or geranylgeranyl groups) at the C-terminus of the Ras proteins is required. The hydrophobic modifications are necessary to anchor Ras proteins in the cell membrane.[3,7,8] An additional member of the Ras family is Rheb (**R**as **h**omologue **e**nriched in **b**rain), a protein consisting of 184 amino acids, which is expressed from two genes in mammals (Rheb1 and Rheb2). While Rheb1 is universally expressed and will therefore be referred to as Rheb in the following, Rheb2 is much more limited.[9] This protein plays a significant role in controlling cellular growth, protein biosynthesis, cell cycle progression, neuronal axon regeneration, autophagy, nutritional deprivation, oxygen stress and cellular energy status.[10,11]

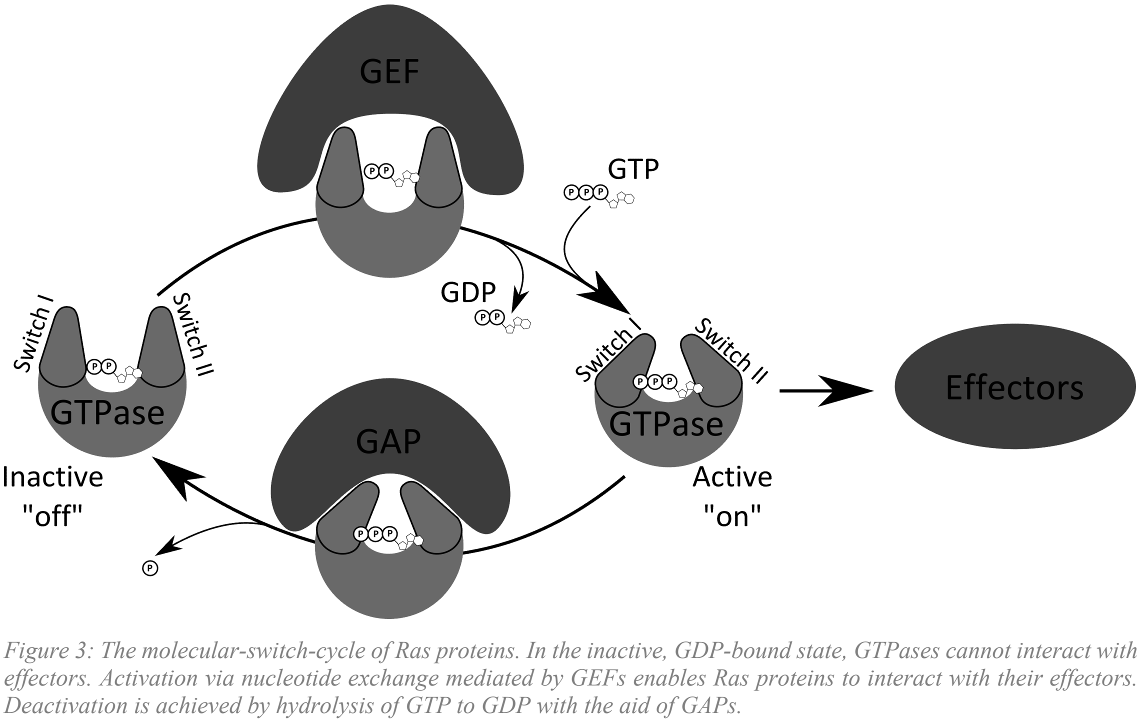

Figure 3: The molecular-switch-cycle of Ras proteins. In the inactive, GDP-bound state, GTPases cannot interact with effectors. Activation via nucleotide exchange mediated by GEFs enables Ras proteins to interact with their effectors. Deactivation is achieved by hydrolysis of GTP to GDP with the aid of GAPs.

All Ras proteins exhibit a strong affinity to guanosine triphosphate (GTP), which can be hydrolyzed to guanosine diphosphate (GDP). Although Ras proteins have an intrinsic ability to hydrolyze GTP independently, the hydrolysis rate (0.028 min^{-1})[12] is too low and therefore has to be enhanced by other proteins, the so-called GTPase activating proteins (GAPs). Those proteins accelerate the GTP hydrolysis by approximately 10^5 fold.[13] While the GTP-bound Ras proteins are in the "active" state and can interact with their various downstream effectors, GDP-bound Ras is "inactive". Their ability to alternate between two different states characterizes the Ras proteins as molecular switches (Figure 3). To activate GDP-bound (inactive) Ras, exchange of the nucleotide is required. The dissociation constants of both, GTP and GDP, are in the picomolar range (~10-100 pM)[14]. To activate Ras proteins, weakening of its interaction with GDP by so-called guanine nucleotide exchange factors (GEFs) is necessary.[3,4,7,15] Further information about effector interaction of *K*-Ras and Rheb is given in Chapter 1.2.2.

1.2.1. Structure of Ras proteins

The three-dimensional structure of Ras proteins has originally been determined from two different, C-terminally truncated *H*-Ras proteins by X-ray crystallography in 1988. In 1991, the crystal structures of *H*-Ras and *K*-Ras4B in complex with GDP, GTP and GppNHp (guanosine-5'-(β,γ-imido)triphosphate), a nonhydrolyzable analogue of GTP, were solved.[5]

The three-dimensional structure of Ras proteins, which is typical for all standard GTP-binding proteins consists of six β-strands (β1-β6) flanked by five α-helices (α1-α5) and 10 connecting loops.[5,7] Ras proteins show two structural compartments, the so-called G domain, which is the catalytically active part and the C-terminal hypervariable region (HVR). The G domain itself can be further divided into two lobes. One is responsible for effector binding (aa 1-86) and shows 100% sequence identity throughout all Ras isoforms. The other allosteric one is required for embedment in the cell membrane (aa 87-166).[6] This second lobe contains a more variable sequence among the Ras isoforms. The phosphate-binding loop (P-loop, aa 10-17) and the so-called switch I (aa 30-38) and switch II (aa 59-76) regions constitute the binding site for the nucleotide and a surface for the interaction with effector proteins.[4,5,8]

Depending on the bound nucleotide, switch I and II regions undergo a crucial conformational change known as the loaded spring model[16] (Figure 4). In the GppNHp bound state, mimicking the GTP-bound active state of the Ras protein, the γ-phosphate of GppNHp is involved in two hydrogen bonds with amino acids Gly60 (switch II) and Thr35 (switch I). The Mg^{2+}-ion is inevitable for GTP hydrolysis as it is involved in a charge transfer reaction. Theoretical calculations show that the Mg^{2+}-ion intermittently stores electrons, which are then set free during the cleavage of the γ-phosphate of GTP.[17] Therefore, Mg^{2+} is bidentately coordinated by the non-bridging oxygen atoms of the β- and γ-phosphates of GppNHp, Ser17 (P-loop) and three water molecules. Those interactions constrain the protein to a closed conformation. The loss of coordination between Mg^{2+} and Thr35 as well as no direct interaction of the β-phosphate with amino acids Thr35 and Gly60 results in a considerable conformational transition. This opens up the whole structure to allow nucleotide exchange.[5]

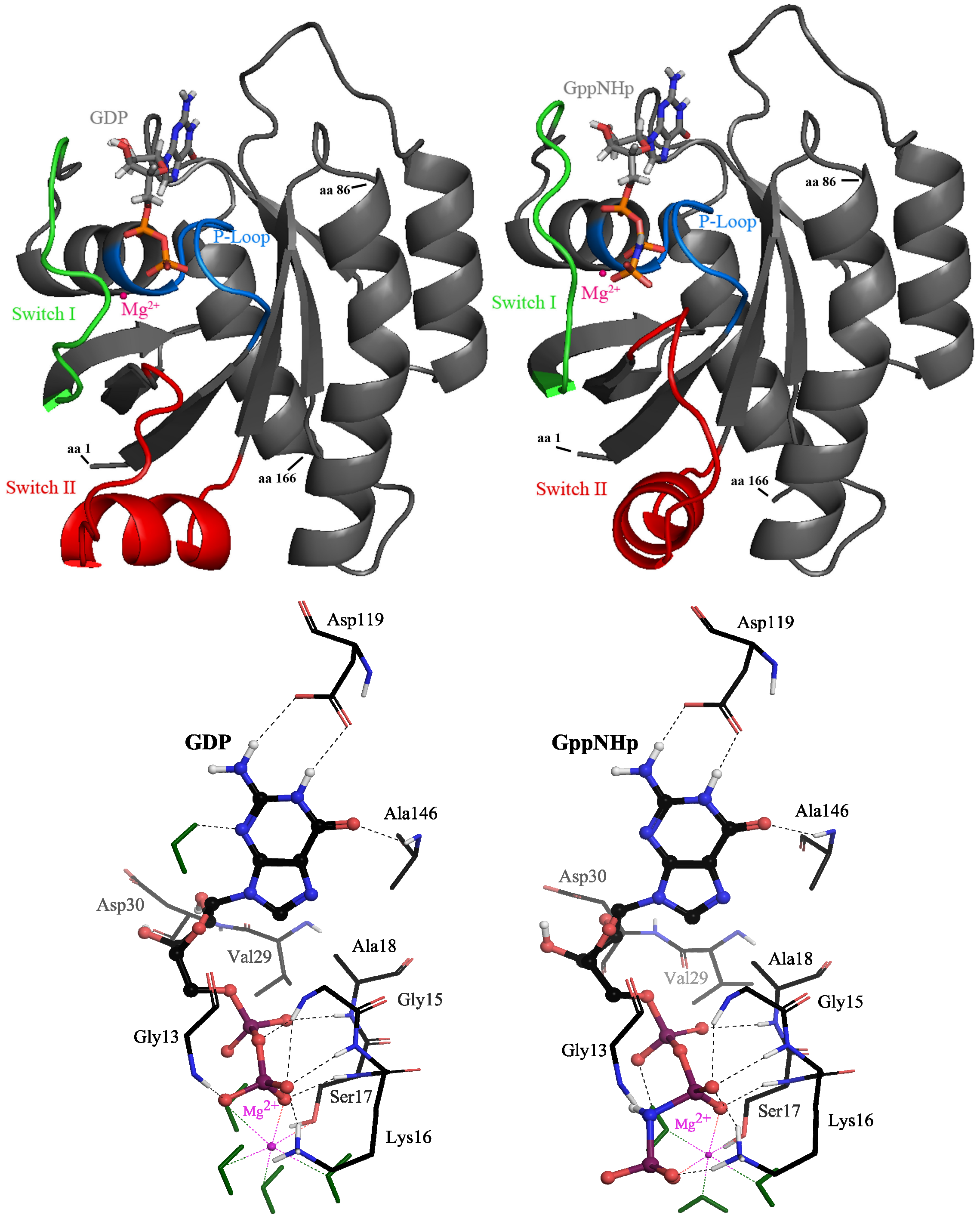

Figure 4: Top: Truncated K-Ras4B in complex with GDP (left) and GppNHp (right). The nucleotides are shown in stick representation while the protein is depicted in cartoon representation. The magnesium ion essential for nucleotide binding is shown as a pink sphere. Highlighted are the regions most important for nucleotide binding: switch I (green), switch II (red) and P-loop (blue). PDB IDs: 4LPK and 3GFT.[18] Bottom: Binding mode of the nucleotides GDP (left) and GppNHp (right). The relevant amino acids and water molecules (green), which are involved in nucleotide binding, are shown. PDB IDs: 4LPK and 5UFE.[18]

X-ray crystallography can only provide information on a "frozen" configuration of the protein often disregarding structural dynamics. Therefore, analysis of GDP and GppNHp bound *H*-Ras was repeated with heteronuclear 3D and 4D NMR spectroscopy. In solution, both switch regions of the GDP-bound state are flexible suggesting different conformations especially of the switch II region. With the exception of the switch regions, which show mobility in solution, the NMR structure is in accordance with the X-ray structure of GDP-bound *H*-Ras. GppNHp-bound *H*-Ras exhibits high flexibility of switch I, while switch II and the P-loop are more restricted. Apart from that, the MNR structure is in good agreement with the X-ray-structure.[5]

For Rheb, X-ray crystal structures bound to GDP, GTP and GppNHp have been solved in 2005.[19] The G domain consists of the 169 N-terminal amino acids, leaving the remaining 15 residues to form the HVR region.[9] The three-dimensional structure (Figure 5) adopts the typical canonical fold of small GTPases containing 6 β-strands, 5 α-helices and 10 connecting loops. As for all small GTPases, the nucleotide binding site is formed by the P-loop (aa 10-20), switch I (aa 33-41) and switch II (aa 63-79). These regions are essential for GAP, GEF and effector interactions.[9,11]
As it has been shown for other Ras proteins, the nucleotide present in the catalytically active site is bound by numerous hydrophobic and hydrophilic interactions with amino acid residues of the protein.[19] The structure of Rheb bound to GppNHp or GTP shows that the Mg^{2+}-ion is coordinated with nearly octahedral geometry by six oxygen atoms of the β- and γ-phosphate of the nucleotide, Ser20, Thr38 and two water molecules. The γ-phosphate of GppNHp forms multiple hydrogen bonds to a third water molecule, and the conserved amino acids Lys19, Tyr35, Thr38 and Gly63. The phosphates of the nucleotide are partially shielded by switch I residues, mainly the side chain of Tyr35. In GDP bound Rheb, the Mg^{2+}-ion is again coordinated almost octahedrally, but by four water molecules, one amino acid, Ser20, and only one oxygen of GDP. As switch I is conformationally shifted, the nucleotide is exposed to the surrounding water molecules generating multiple hydrogen bonds.[19]
In contrast to the dramatic changes in conformation of the switch regions observed for *K*-Ras, only switch I of Rheb shows a significant structural transition while switch II remains fairly stable forming no α-helix element. As a result of this unique appearance, displacement of Gln64 (corresponding to Gln61 in *K*-Ras) allows no interaction with GTP. Usually, this conserved amino acid is stabilized in the catalytic site of Ras proteins playing a significant role in the GTP hydrolysis. Additionally, Tyr35 (corresponding to Tyr32 in *K*-Ras) protects the phosphate residue of GTP preventing Rheb deactivation through intrinsic GTP hydrolysis. Consequently, it has to be concluded that the hydrolysis mechanism of Rheb differs from that of *K*-Ras and other Ras proteins.[19]

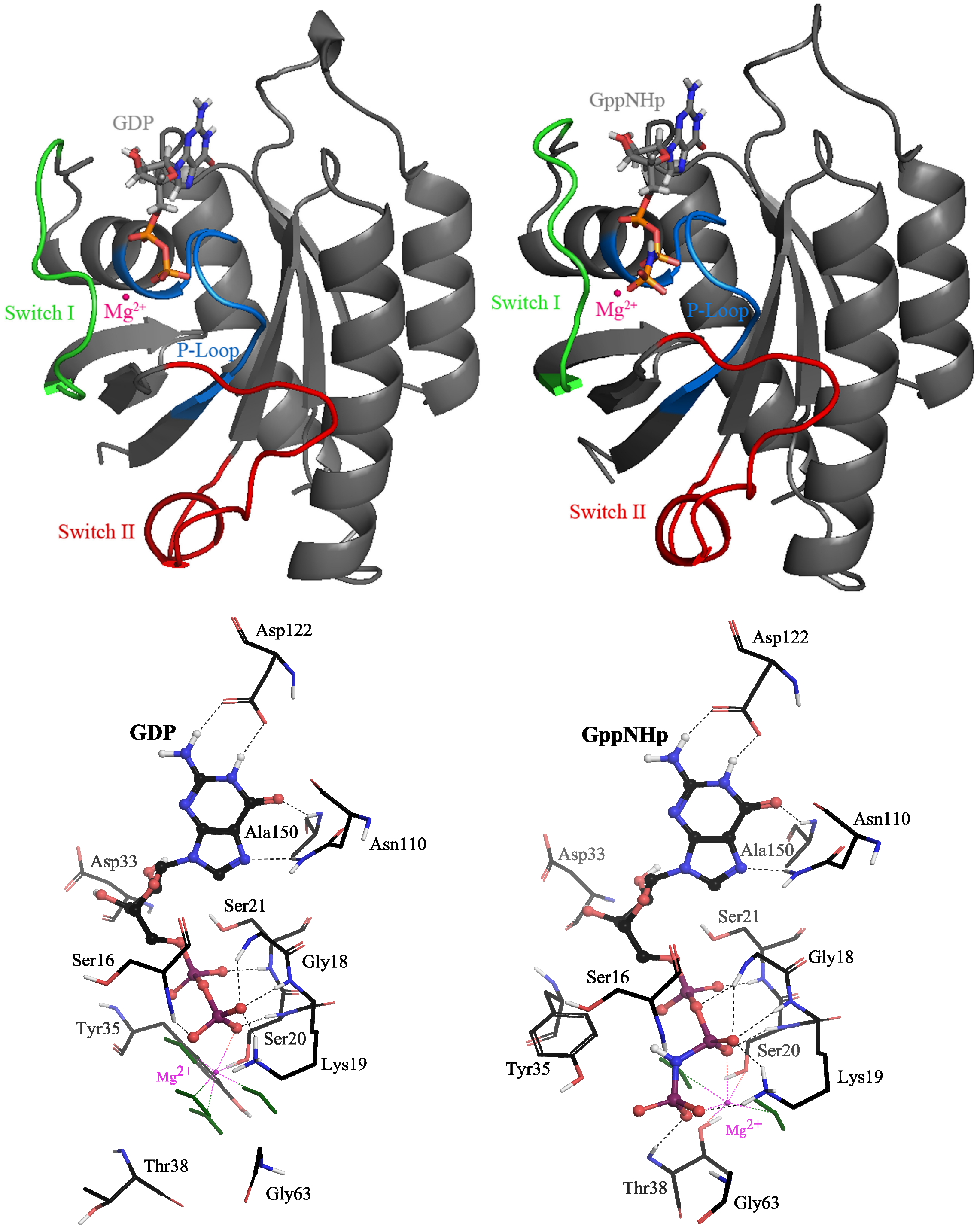

Figure 5: Top: Rheb in complex with GDP (left) and GppNHp (right). The protein is depicted in the cartoon representation while the nucleotides are shown as stick model. The magnesium ion essential for nucleotide binding is shown as a pink sphere. Highlighted are the regions most important for nucleotide binding: switch I (green), switch II (red) and P-loop (blue). Bottom: Binding mode of the nucleotides GDP (left) and GppNHp (right). The relevant amino acids and water molecules (green), which are involved in nucleotide binding, are shown. PDB IDs: 1XTQ and 1XTR.[18]

Investigations of a Tyr35Ala mutant of Rheb, which shows a 10-fold increased intrinsic hydrolysis rate, support this hypothesis. Furthermore, it has been shown that Asn65 (switch II) and Thr38 (switch I) are involved in GTP turnover. Tyr35 seems to restrict the conformation of the active site blocking access of Asn65 to the nucleotide binding pocket.[9] Structural analysis by

NMR measurement confirms that the topology of the fold is in good agreement with the one determined by X-ray crystallography. It is also identical to that for the Ras protein. As it has already been shown for *K*-Ras, NMR data clearly proves that the switch I and, to a minor degree, the switch II region of GDP-bound Rheb are flexible in solution.[11]

1.2.2. Signaling pathways of *K*-Ras and Rheb

Originally, only one linear signal transduction pathway activated by growth factor receptors was known for *K*-Ras (red pathway in Figure 7). Either EGF (epidermal growth factor) or PDGF (platelet-derived growth factor) bound to the extracellular domain of their corresponding epidermal growth factor receptors (EGFR) trigger dimerization of the receptor. Transphosphorylation of the cytoplasmic part leads to activation and structural change of the receptor to allow binding of SH2 (sarcoma homology 2) domain containing proteins. An example for those proteins is Grb2 (growth factor receptor binding), which complexes SOS (son of sevenless), a protein that has been identified as a GEF for *K*-Ras[20]. Exemplarily, the complex of *H*-Ras in complex with SOS is shown in Figure 6. The dislocation of SOS from the cell membrane increases its proximity to *K*-Ras, which is subsequently activated.

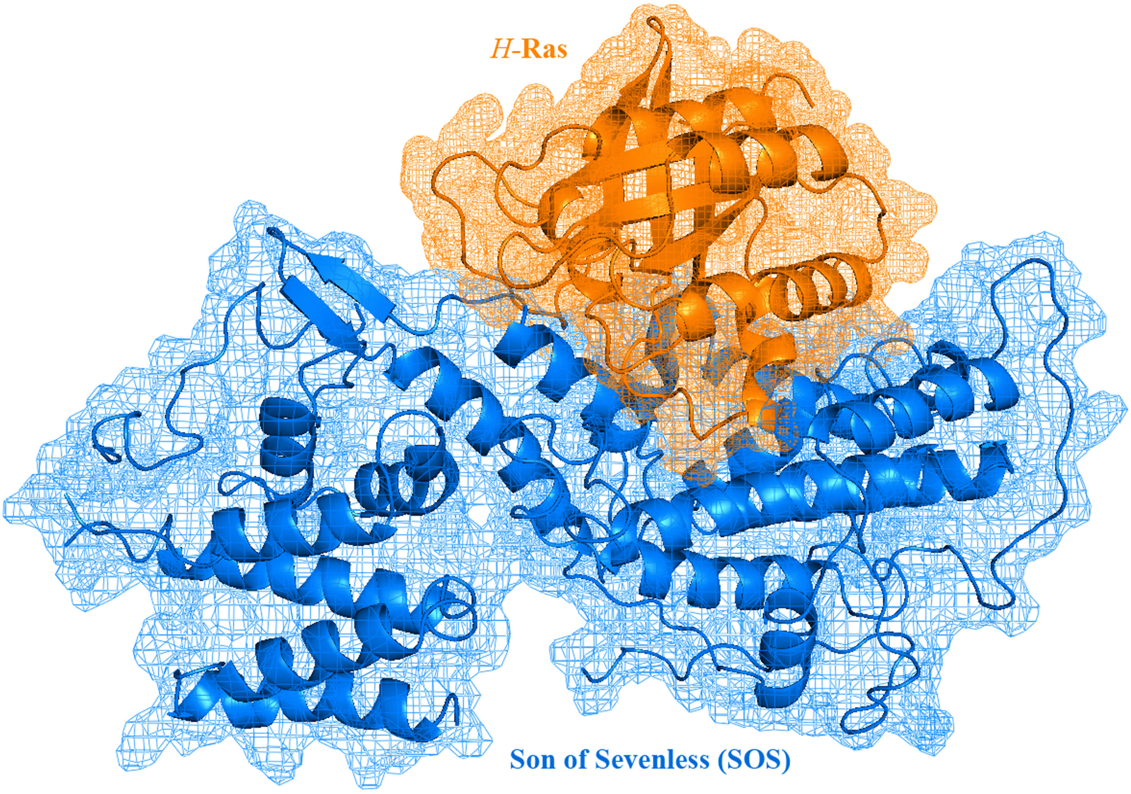

Figure 6: Complex of the GEF Son of Sevenless (SOS) and the small GTPase H-Ras. PDB ID: 1BKD.[18]

Subsequently, switched-on *K*-Ras interacts with its downstream effector, the protein kinase Raf (rapid fibrosarcoma). Dimerized Raf is translocated to the plasma membrane and activates itself to allow an interaction with the mitogen-activated protein kinase kinase (MEK). Phosphorylated MEK then activates ERK (extracellular signal-regulated kinases), a protein that is capable to enter the nucleus and activate other signal cascades. The combination of the three kinases, Raf, MEK and ERK compose a so-called MAP kinase module. Termination of the *K*-Ras signal is achieved either by interaction with a GAP protein, accelerating the hydrolysis of GTP to GDP, or phosphorylation of SOS by Raf interrupting its interaction with Grb2. As a result of this pathway, the cell-cycle progression is promoted.[4,5,7,8,21,22]

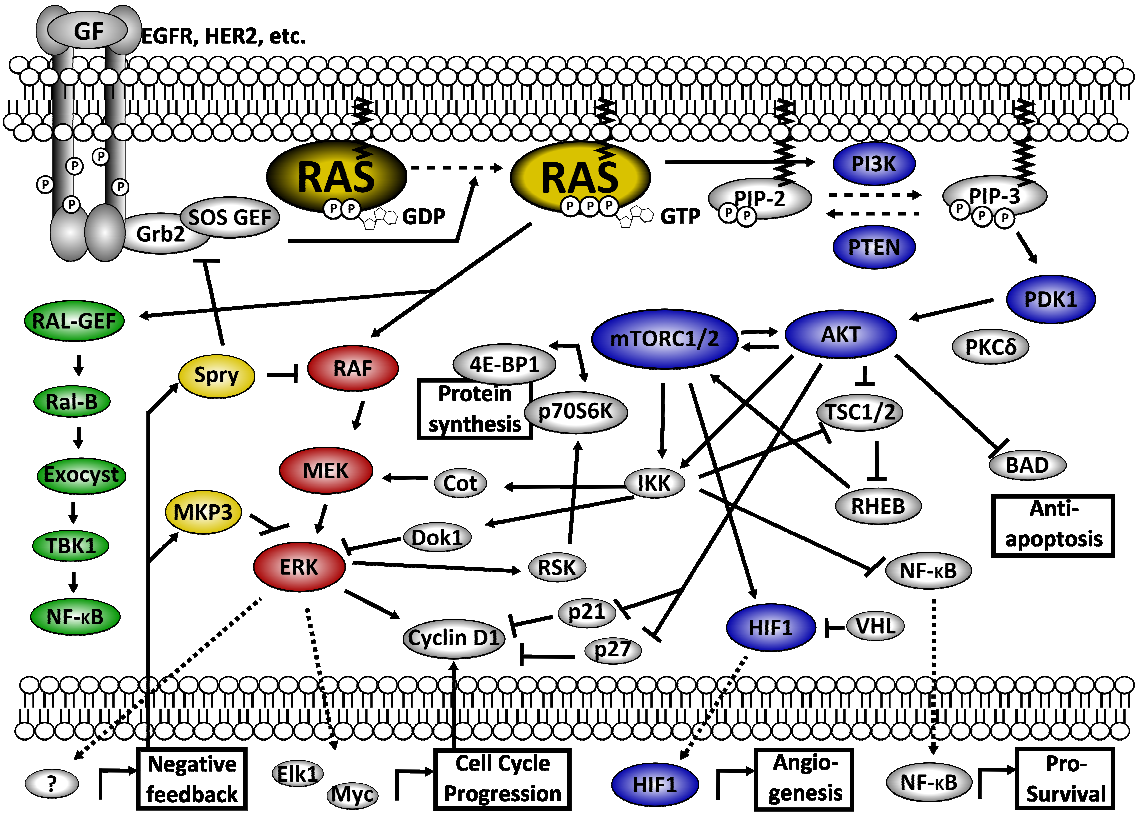

Figure 7: K-Ras activation and its various signaling pathways.[8]

Later, further downstream effectors of *K*-Ras have been found.[4,7,21] Currently, more than 10 different Ras effectors are know[4,8], of which a few will be discussed in the following section. The various isoforms of the lipid kinase PI3K (phosphatidylinositol-3'-kinase) are activated as a result of the translocation to the membrane (blue pathway in Figure 7). There, the second messenger molecule PIP2 (phosphatidylinositol-3,4-biphosphate) is phosphorylated to the corresponding triphosphate PIP3. This process can be reversed by PTEN (phosphatase and tensin homologue). PIP3 can then activate several downstream proteins such as PDK (3-phosphoinositide-dependent protein kinase-1) and AKT (also known as PKB, protein kinase B). This pathway secures the survival of the cell due to AKTs strong anti-apoptotic influence on various downstream effectors such as mTOR (mammalian target of rapamycin), which contributes significantly to initiation of DNA translation.[5,8] Further effectors of Ras belong to the RAL family as there are RALGDS

(RAL guanine nucleotide dissociation stimulator), GGL (RALGDS-like gene) and RGL2 (green pathway in Figure 7). These proteins in turn can activate RAL to trigger activation of further downstream effectors. Overall, this pathway supports the AKT signal disrupting apoptosis. Another Ras effector, Phospholipase Cε (PLCε), is believed to activate PKC (protein kinase C) and calcium mobilization.[4,21,22]

Originally, Rheb was reported to interact in the Ras signaling cascade, acting as an inhibitor for Raf. Additionally, it was believed to antagonize Ras in the activation of the MAP kinase module.[23,24] This hypothesis was later proven to be incorrect.[10] More recent literature states that Rheb is involved in arginine uptake in fungi and the insulin/TOR/S6K pathway (Figure 8). As insulin (IGF1) interacts with its receptor at the cell surface, PI3K (phosphatidylinositol-3'-kinase) is activated to phosphorylate AKT (also known as PKB, protein kinase B). This itself then phosphorylates Tsc2 (tuberous sclerosis complex 2) and therefore disables the Tsc1/Tsc2 complex from inhibiting mTORC1 (mammalian target of rapamycin complex 1, the so-called "master regulator of cell growth"). In addition, the Tsc1/Tsc2 complex has been identified to function as a GAP for Rheb, thus, restriction of the GAP results in the activation of Rheb itself and its downstream effector mTOR. As for all Ras proteins, activation of Rheb is a GEF mediated process, but a correlating protein has not yet been identified.[9,25]

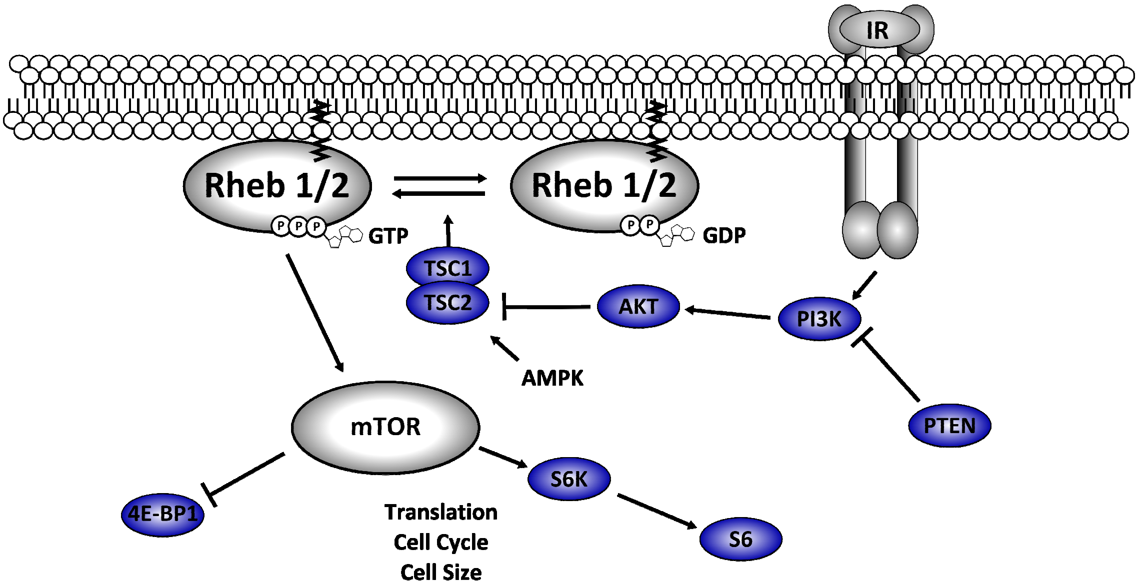

Figure 8: Involvement of Rheb in the AKT/mTOR signaling pathway.[26]

Rheb can also be activated by an increase of gene expression mediated by various growth factors, such as EGF (epithelial growth factor) or bFGF (basic fibroblast growth factor).[11] Elevated levels of expressed Rheb are sufficient to activate mTORC1 due to the already increased concentration of GTP-bound protein under basal conditions in comparison to other Ras proteins.[10,11]

Consequently, further downstream events are triggered enhancing the protein synthesis and cell cycle progression.[26] In addition to this, Ma *et al.* described that Rheb can modulate the interaction of FKBP38, an inhibitor of mTOR, and the anti-apoptotic protein Bcl-2. Active Rheb binds to FKBP38 in a competitive manner avoiding inhibition of mTORC1. This is a second pathway, by which Rheb can activate mTOR. Deactivation of Rheb enables FKBP38 to interact with proteins of the Bcl family, which inhibit programmed cell death. Remarkably, the interaction of Rheb with both, FKBP38 and Bcl proteins, is dependent on the energy level of the cell. This indicates how a single protein can mediate both, apoptotic signals and its contrary, the inhibition of programmed cell death, at the same time.[27] Another alternative pathway for indirect activation of mTORC1 via Rheb has been identified by Sun *et al.* They state that switched-on Rheb can activate PLD1 (phospholipase D1) to produce phosphatidic acid as a result of mitogen interaction, which can then activate mTORC1.[25,28]

1.2.3. Mutations of K-Ras and Rheb and their effects

The name “Ras” originates from the Harvey and Kirsten strains of retroviruses in mice (Rat sarcoma) where the mutated gene was originally found to induce cancer. Since then, it has been called a proto-oncogene.[5,7] In 1982, mutated Ras genes were first discovered in human cancers.[29] According to the Catalogue of Somatic Mutations in Cancer (COSMIC)[30], Ras point mutations occur in approximately 22% of human cancers constituting the most frequently mutated oncogene family. Although the Ras isoforms show a high structural similarity, mutations in the individual isoforms account for specific cancers (Table 1).

K-Ras mutations specifically account for about 85% of these while the other two isoforms make up only 8% (*N*-Ras) and 3% (*H*-Ras), respectively. *K*-Ras mutations are most present in pancreas adenocarcinomas and colorectal cancers while aberrant *H*-Ras is mainly found in skin and salivary gland cancers, which are known to be aggressive. Mutant *N*-Ras can be found predominantly in cancers related to the nervous system and the skin.[30] Those point mutations mainly occur on codons 12, 13 and 61 of the DNA sequence, also being specific for each of the three isoforms.[21] *K*-Ras mutations mainly occur on codon 12 (80%) while showing only very little mutation on codon 61. In contrast, more than half (60%) of all *N*-Ras mutations account for codon 61 and only one third (35%) on codon 12. Mutations of *H*-Ras are divided almost evenly between codons 12 (50%) and 61 (40%).

Table 1: Incidence of Ras isoform mutations in various cancer types.[30]

Tissue	**Point Mutations [%]**		
	K-Ras	*H*-Ras	*N*-Ras
Pancreas	56	0	1
Peritoneum	51	0	1
Large intestine	33	0	4
Small intestine	26	0	1
Biliary tract	22	0	3
Lung	16	0	1
Endometrium	15	1	2
Ovary	12	0	1
Genital tract	8	1	3
Gastrointestinal tract (site indeterminate)	6	0	0
Haematopoietic and lymphoid	5	0	10
Urinary tract	4	9	1
Penis	3	7	0
Skin	2	11	15
Salivary gland	2	12	1
Thyroid	2	4	7
Upper aerodigestive tract	2	6	1
Nervous System	2	0	20
Vulva	1	7	0
Meninges	0	0	7

Although Ras codons 12, 13 and 61 can each be transformed into 6 other amino acids by a single base substitution, more than 60% of all mutations of each isoform are evoked by only 3 distinct mutations instead of the 18 possible ones. Regarding *K*-Ras, 43% of all mutations are G→A substitutions on codons 12 and 13 resulting in Gly12Asp or Gly13Asp mutations. The majority of the remaining mutations account for G→T transitions on the second base of codon 12 leading to Gly12Val mutations. Lung cancer seems to be an exception in the mutation pattern of *K*-Ras as it shows a high percentage of G→T transitions on the first base of codon 12 resulting in Gly12Cys mutations.[6] In case of point mutations in codons 12 and 13, the GTPase activity of Ras proteins is highly impaired due to steric hindrance in the nucleotide binding side blocking interaction with the GAP. Gly12-mutants of *K*-Ras cannot form the transition-state complex with GAPs as the side chains of asparagine or valine (Figure 9 left and middle) clash with the so-called "arginine finger" of the GAP protein. The same effect can be observed for G13-mutants.[6,31] In complex with the GAP protein, Gln61 interacts directly with the γ-phosphate of the nucleotide. The amide in the side chain of Gln61 is stabilized by a hydrogen bond to the arginine finger of the GAP protein.[31] This interaction is disrupted by mutations of amino acid 61 (Figure 9 right). This renders mutated Ras proteins immune to GAP-catalyzed hydrolysis leading to the accumulation of activated Ras proteins in the cell. As it has been shown before, switched-on *K*-

Ras can interact with its effectors resulting in permanent activation of downstream pathways.[22] Uncontrolled cell proliferation, abnormal cell survival[8], invasiveness and induction of angiogenesis are the consequences of this.[32]

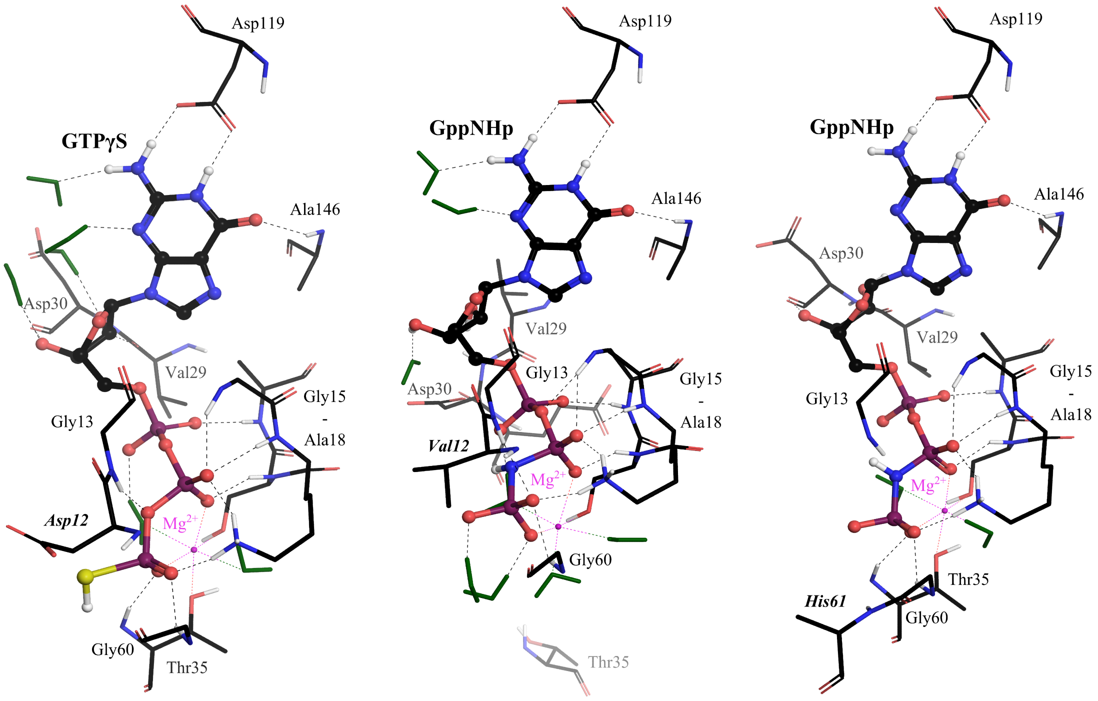

Figure 9: Binding mode of GTP analogues to K-Ras mutants. Left: K-RasGly12Val (PDB ID: 5WPL). Middle: K-RasGly12Asp (PDB ID: 4DSO). Right: K-RasGln61His (PDB ID: 3GFT).

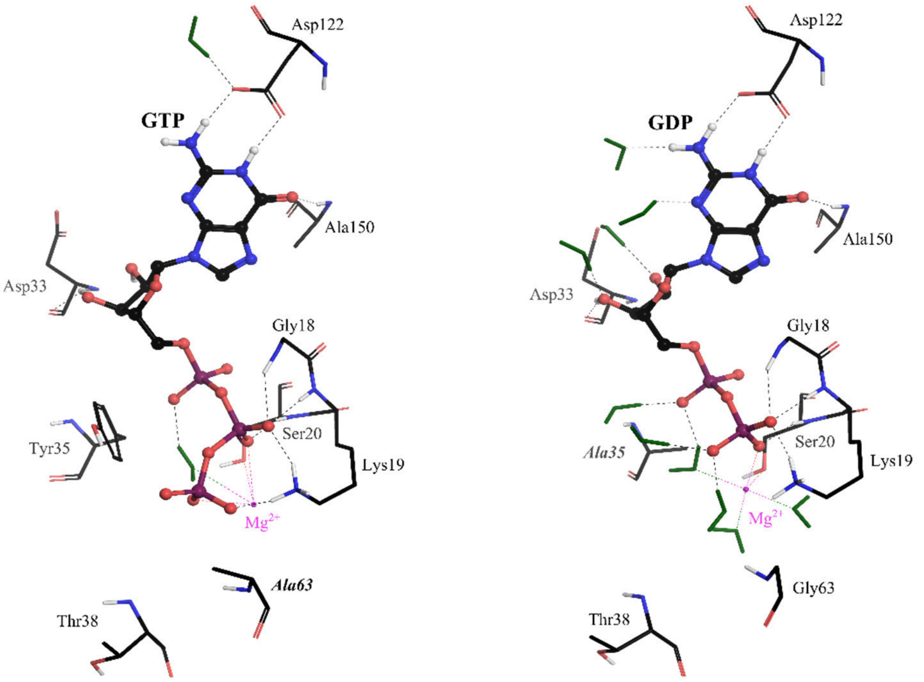

Figure 10: Binding mode of nucleotides in Rheb mutants. Left: GTP bound to RhebGly63Ala (PDB ID: 4O2L). Right: GDP bound to RhebTyr35Ala (PDB ID: 3SEA).

In contrast to *K*-Ras aberrations, mutations of Rheb are less common as can be seen from COSMIC[30]. Nevertheless, a few frequently occurring mutations such as Tyr35Asn, Glu40Lys and Gln57* (missense mutation, C→T substitution on codon 169) can be found.[30] In particular, two endometrial and three kidney clear cell cancer carry Tyr35Asn mutations, which enhance Rheb activation of mTORC1. The crystal structure of RhebTyr35Ala (Figure 10 right) clearly shows that replacement of tyrosine leads to displacement of its side chain, which then cannot interact with the Mg^{2+}-ion anymore.[9,25] Introduction of a methyl group in the side chain of Gly63 (Figure 10 left) destabilizes one of the water molecules, which bind to the Mg^{2+}-ion. Consequently, intrinsic as well as GAP-catalyzed GTP hydrolysis is highly impaired. Furthermore, this variant exchanges GDP for GTP at an accelerated rate, which leads to accumulation of the activated state of this protein. Replacement of Gly63 for valine leads to a Rheb mutant that fails to bind GTP at all. The bulkier side chain of valine interferes with the γ-phosphate of GTP.[9,33] Additionally, amplification of Rheb expression is associated with the development of several epithelial and squamous malignancies such as breast cancer, head and neck cancer and gliomas as well as prostate cancer.[25]

To identify dominant negative mutations, several groups produced Rheb variants. Thereby, it has been found that Asp60 variants (Asp60Lys/Ile/Val) lose their ability to bind GTP, culminating in the Asp60Lys variant, which also cannot bind GDP.[26] Introduction of Gly12Arg, Arg15Gly, Tyr35Ala or Gln64Leu mutations renders Rheb insensitive or even resistant to its GAP. Furthermore, it slows the intrinsic GTP hydrolysis further, thus, creating a permanently switched-on protein.[9,19] Other mutations including Ser16Asn/His, Tyr35Asn/Cys/His, Ser89Asp and Asn153Ser result in increased activation of mTORC1, while Asp36Ala, Pro37Ala, Thr38Ala and Asn51Ala mutations decrease the ability of Rheb to activate mTORC1.[9]

Although it is well established that Rheb oncogenic activity is mainly associated with its ability to activate the mTORC1 signaling pathway, several studies indicate that mTORC1-independent functions of Rheb could contribute to tumorigenesis as well.[25]

1.3. Melanoma Inhibitory Activity (MIA)

MIA (Melanoma Inhibitory Activity) belongs to a family of 4 homologous proteins (MIA, OTOR/MIA-L, MIA-2 and TANGO/MIA-3) and was identified from the tissue culture supernatant of malignant melanoma cells *in vitro* in 1994.[34] Initially, MIA was believed to possess anti-tumour activity through inhibition of the proliferation of malignant cells. Instead, further studies revealed that it is involved in metastasis by intercepting in the binding of cells to the extracellular matrix components. This protein is expressed exclusively during chondrogenesis (cartilage development), cartilage growth and in melanoma cells, but not by normal skin and melanocytes. It can therefore be used as a serum marker in patients with malignant melanoma. Increased values can be measured in the serum of all patients with metastatic melanoma (stages III and IV).[35] In contrast to MIA, its homologues MIA-2 and TANGO are downregulated or even lost in cancer.[36] The number of cases of both non-melanoma and melanoma skin cancers has increased over the past decades. Currently, 2-3 million non-melanoma skin cancers and 132 000 melanoma skin cancers occur worldwide every year.[2] Although melanoma skin cancer account only for 1% of all skin cancer cases, it represents the most fatal type of skin cancers.[37]

1.3.1. Structure of the MIA protein

The MIA protein is translated as a 131 amino acid precursor protein. It is then processed by cleavage of the first 24 residues, a hydrophobic area, responsible for the transport to the endoplasmic reticulum and subsequent secretion into the extracellular compartment. Consequently, mature MIA consists of 107 amino acids with an approximate molecular weight of 11 kDa. Structural analysis by multidimensional NMR[38] and X-ray crystallography[39] shows that MIA, as the first protein secreted into the extracellular area, adopts an Src homology (SH3)-domain like fold consisting of two perpendicular, anti-parallel three- and five-stranded β-sheets (Figure 11).

In general, SH3-domains consist of 55-70 amino acids and facilitate interactions with proline-rich peptide sequences.[36] In contrast to other proteins with an SH3-domain, MIA is a single-domain protein, which contains an additional anti-parallel β-sheet and two disulfide bonds (Cys12, 17, 35 and 106) essential for correct folding and function.[38,40] Characteristic features of SH3 domains, the disulfide loop (aa 12-18), the RT-loop (aa 32-38) and the n-Src loop (aa 53-58), have also been identified in MIA. The RT-loop is flanked by an irregular anti-parallel β-sheet structure featured by Asp29 to Met31 and Thr39 to His41, found only in a few SH3 domains. The distal hairpin/loop (aa 67-74), the most regular element of the secondary structure of SH3 domains, exhibits an extraordinarily high flexibility.[36]

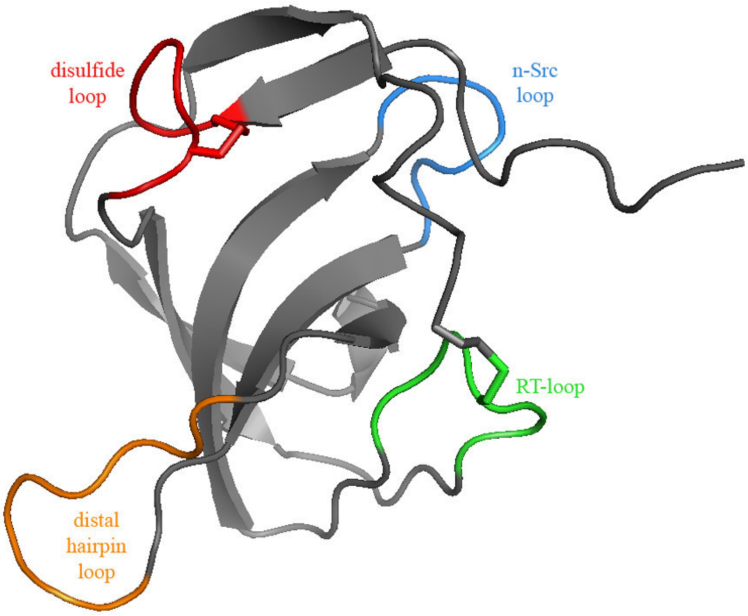

Figure 11: Crystal structure of MIA protein. PDB ID: 1I1J.[18]

For functional activity, it has been shown that MIA needs to dimerize via head-to-tail interaction. As all cysteine residues are utilized in intramolecular disulfide bonds, dimerization must be caused by noncovalent interactions between the interfaces formed by residues next to the n-Src loop and the distal loop. Most important for dimerization and functional activity of MIA are the amino acids Tyr30, Arg55 and Gly61 as has been shown by mutational studies.[41]

1.3.2. Mode of Action of MIA

As MIA has been shown to assist in the migration of cells by intercepting in the binding to the extracellular matrix, it has to be secreted first. Therefore, the protein has to be exocytosed through vesicles. The immature protein possesses an N-terminal signaling peptide that directs its transport into the endoplasmic reticulum (ER). It is then exocytosed through the ER-Golgi pathway of protein export. The MIA containing vesicles are transported along the microtubule system to the plasma membrane where it is released into the extracellular compartment. For directed migration of tumour cells, detachment from the extracellular matrix at the rear of the cell is required while providing new traction points at the front of the moving cell. Consequently, it can be proposed that MIA secretion is directed to the rear of the cell, to allow directed movement (Figure 12).[42]

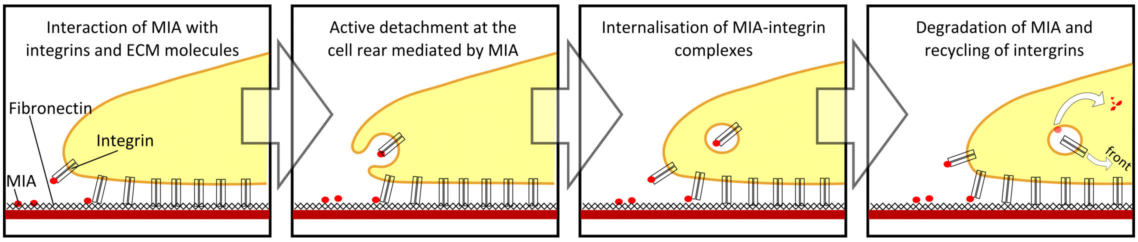

Figure 12: Directed cell migration mediated by MIA secretion.[43]

To facilitate cell detachment, MIA has been shown to interact with several extracellular matrix proteins such as laminin, tenascin and fibronectin type III repeats (Figure 13), especially FN14.

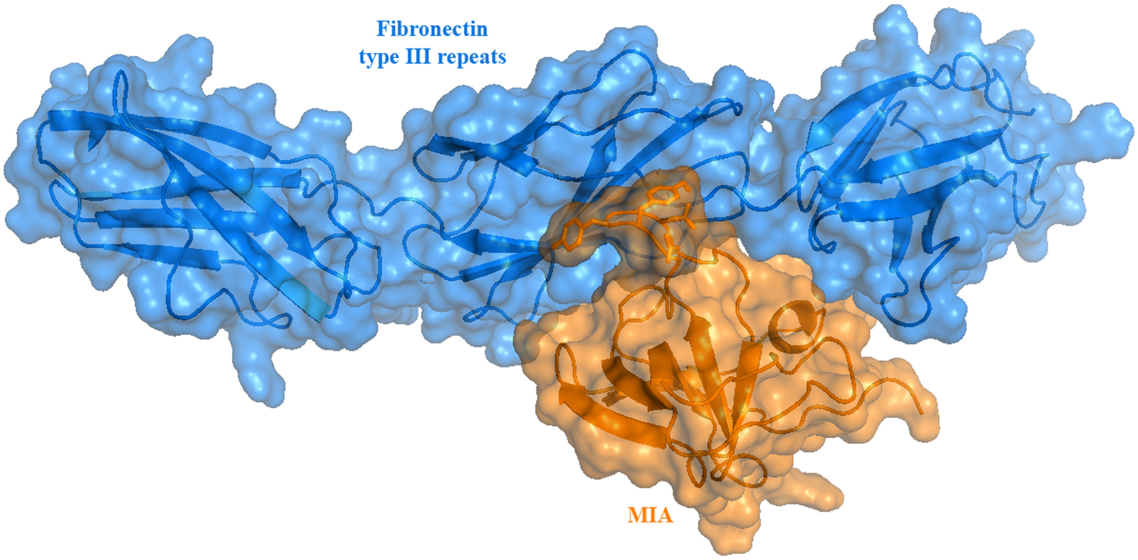

Figure 13: Model for the complex between the MIA protein and fibronectin type III repeats. PDB IDs: 1I1J and 1FNH. The structure of the complex was calculated using HADDOCK.[44]

Consequently, MIA intercepts the binding of fibronectin to the cell adhesion receptors integrin α4β1 and α5β1. Additionally, MIA itself can also bind to integrins α4β1 and α5β1 directly to achieve detachment of cells and to modulate their activity.[40] As a result, integrin signaling through the ERK1/2 (externally regulated kinases) pathway is reduced.[45] MIA-integrin-complexes are then internalized by the migrating cell. After endocytosis, the complex is dissociated and integrins are transported to the front of the cell to create new attachment points to the extracellular matrix while the MIA protein is digested in acidic vesicles of the lysosome.[42,43,46]

2. General Part

As the three proteins described above play their individual crucial role in cancer, selective inhibitors have been investigated thoroughly. Thereto, different methods can be applied, of which a few will be discussed in the following section as well as the resulting inhibitors for the cancer-related proteins *K*-Ras, Rheb and MIA.

2.1. Drugging Ras proteins

Although the *K*-Ras protein is researched for more than 30 years, no drugs have been approved for cancer treatment so far. *K*-Ras is an unrewarding therapeutic target due to its relatively smooth surface, which does not offer any deep binding pockets for potential ligands. Therefore, it is said to be "undruggable".[5,29,47,48] Nevertheless, several research groups and companies have made significant efforts in the past few years to develop drugs, which target new binding sites on the surface of the *K*-Ras protein with small molecule ligands.

There are different strategies for approaching the problem of drug development:[7,49]

- Ras proteins are inserted into the cell membrane for biological activity by farnesylation and insertion of the isoprenyl group as an anchor. Inhibition of the corresponding enzyme, the so-called farnesyl transferase, can disrupt this modification.
- Activation of the Ras proteins is facilitated by exchange of the nucleotide from GDP to GTP. Interrupting this exchange would render the protein inactive.
- In the activated state, *K*-Ras can interact with its downstream effectors as described above. Interrupting the interaction with those proteins can stop the signal transduction.
- Mutations of the Ras proteins prevent interaction with their GAPs. Thus, inactivation of the GTP-bound protein is suppressed. Development of compounds that can increase the intrinsic ability to hydrolyze GTP to GDP would deactivate the protein. As an anchor the mutated position can be targeted by covalently binding inhibitors.

The search for compounds, which have any of these effects, has been only moderately successful. Nevertheless, various molecules have been found to bind to different positions on the surface of the *K*-Ras protein (Figure 14) and will be discussed according to the targeted approach.

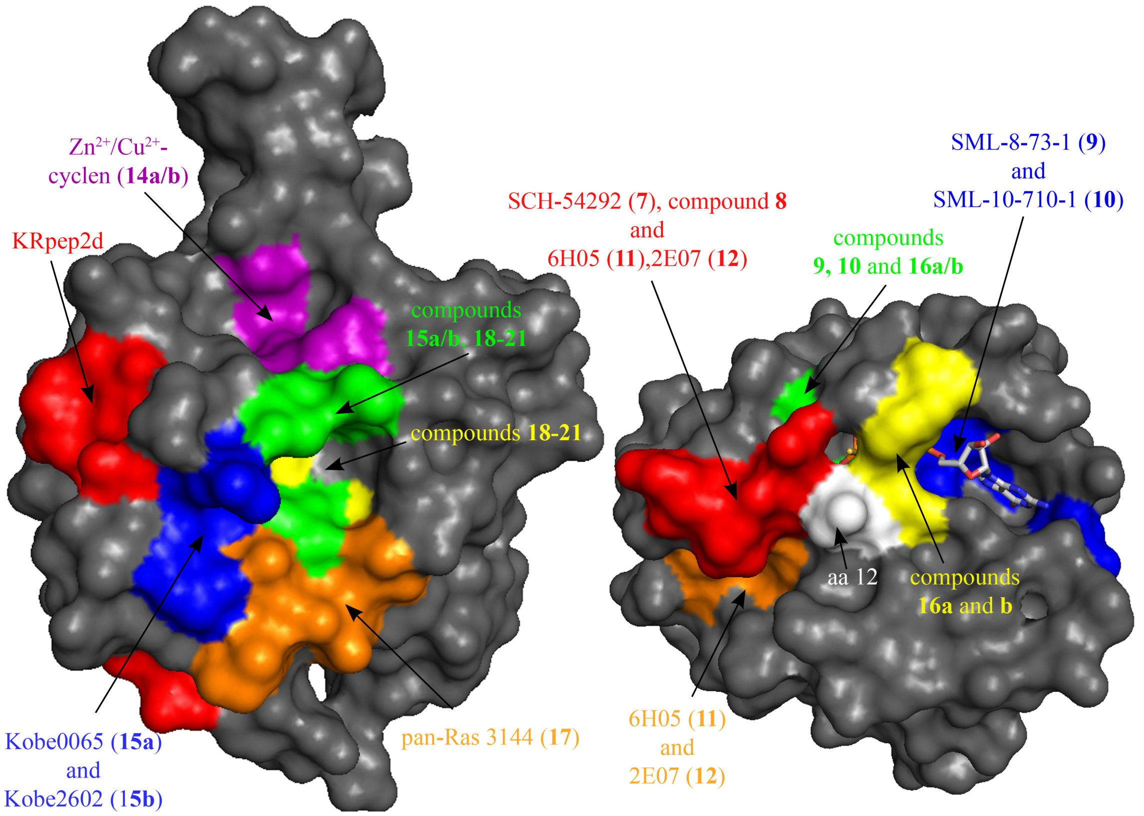

Figure 14: Side (left) and bottom (right) view of the GDP-bound K-Ras protein (PDB ID: 4DSO) with highlighted binding sides of the different compounds.

2.1.1. Farnesyl Transferase Inhibitors (FTIs)

One of the first ideas to be exploited was inhibition of *K*-Ras activity by preventing insertion into the cell membrane. In contrast to *K*-Ras itself, the farnesyl transferase is a far more grateful target. To farnesylate the C-terminus of the Ras proteins, the transferase enzyme needs to recognize the protein. Therefore, each of the Ras proteins possesses a unique C-terminal sequence, the so-called CAAX-box. Thus, one strategy was to develop peptidic (Figure 15, molecules **1-4**)[22] and non-peptidic compounds such as tipifarnib (**5**) and lonafarnib (**6**) (Figure 15)[22] to mimic the CAAX-motif and prevent the farnesyl transferase from interacting with its natural target. Another strategy utilizes so-called substrate analogues. These compounds substitute farnesyl pyrophosphate, which is transferred during the process of farnesylation. Unfortunately, the mechanism of anchoring the Ras proteins is redundant for the different isoforms, especially for *K*-Ras. Therefore, knocking out the farnesyl transferase only results in its replacement by another protein, the geranylgeranyl transferase. Consequently, all of the drugs that were developed and even entered clinical trials, failed as they had no effect due to other enzymes substituting the blocked enzyme. Blocking both enzymes with a combination of appropriate inhibitors will probably have undesirable toxic effects as other proteins also rely on isoprenylation.[7,8,21,22,29,47,50–54]

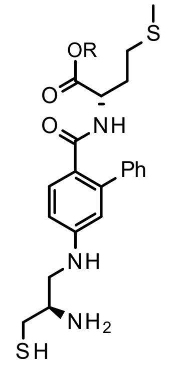
1 (FTI-276), R = H
2 (FTI-277), R = Me

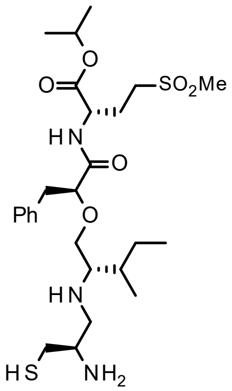
3 (L-744832)

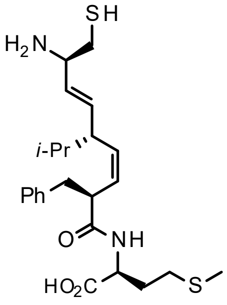
4 (B956)

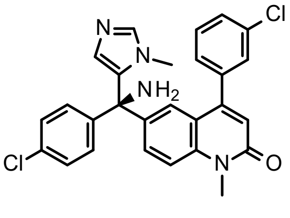
5 (Tipifarnib)

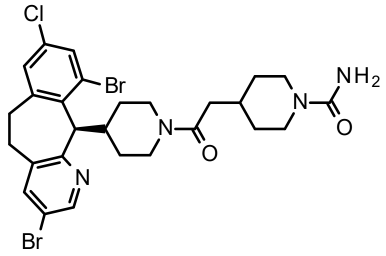
6 (Lonafarnib)

Figure 15: Structures of selected farnesyl transferase inhibitors (FTIs).[22]

2.1.2. Competing with the natural nucleotides

The second strategy, development of ligands that can replace the nucleotide, was anticipated to be rather unpromising as both, GDP and GTP, bind to the protein with k_D values in the picomolar range as stated above. Nevertheless, efforts to develop such compounds have been made using NMR spectroscopy and molecular modelling studies. By these means, Taveras *et al.*[55] identified molecules that inhibited nucleotide exchange, but were unable to compete with GDP binding. As NMR analysis showed, the ligands did not substitute GDP in the nucleotide binding pocket but interact with the surface of the protein near switch II, which is involved in the interaction with GEFs. Molecules such as SCH-54292 (**7**, Figure 16) can form non-covalent complexes with the switch II region of GDP-bound Ras inhibiting the nucleotide exchange without replacing it.[29,55] Later, Colombo and coworkers[56] improved the pharmacological and pharmacokinetic properties of one of those molecules (hydroxylamine **8**, Figure 16), while Palmioli *et al.*[57] tried to improve the selectivity of the designed compounds for Ras mutants over the wild-type protein. Also, several GTP or GDP analogues were developed, which showed higher affinities to the protein than the nucleotides.[58,59]

Nevertheless, this approach was neglected until Lim and Westover *et al.*[32] started a new attempt in 2014. They designed an inhibitor to covalently bind to Cys12 of the *K*-Ras mutant Gly12Cys, which is located close to the nucleotide binding pocket. Thereby, the nucleotide was replaced and the difficulties of competing with their high binding affinities can be overcome. As nucleotide analogues should induce the inactive state of *K*-Ras, GDP was chosen as a model for the design of a covalently binding derivative. Although SML-8-73-1 (**9**, Figure 16) could successfully substitute the nucleotide, it could not penetrate the cell membrane due to the negatively charged phosphate groups. "Caging" those groups to mask charges allows for compounds to pass through the cell membrane. The resulting derivative, SML-10-70-1 (**10**, Figure 16), can consequently overcome this barrier, but lacks target selectivity as a cytotoxicity test revealed.[5,29,60] The authors recently published optimized molecules on the basis of SML-8-73-1 (**9**) with improved chemical stability while losing slightly in affinity to the protein.[58]

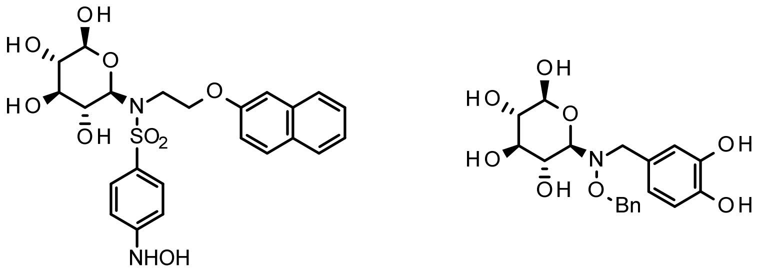

7 (SCH-54292) **8**

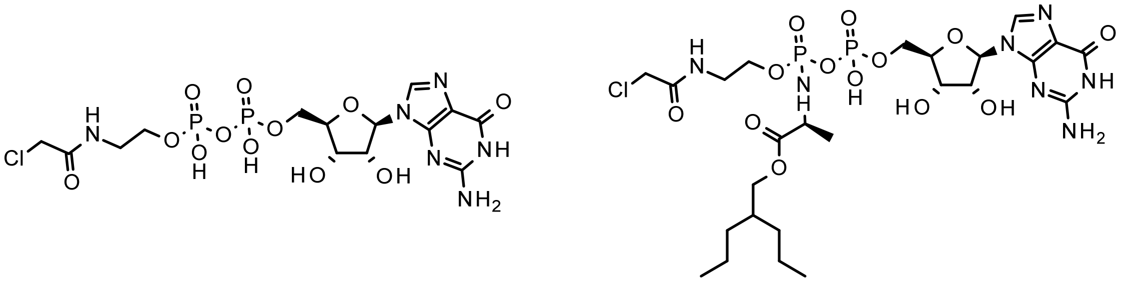

9 (SML-8-73-1) **10** (SML-10-70-1)

Figure 16: Top: Inhibitor 7 discovered by Taveras et al. and the improved ligand ***8*** *developed by Colombo and coworkers.*[56] *Bottom: Covalently binding GDP analogues designed by Lim and Westover in 2014.*[32]

Contradictory to the work of Lim and Westover[32], Müller *et al.*[61] showed that modification of the β-phosphate group by esterification leads to a dramatic loss of affinity to *K*-Ras in comparison to GDP. This is mainly due to the absence of the two negative charges on the β-phosphate group, which is involved in numerous interactions. This group interacts with Lys16 (P-loop) and the magnesium ion. Consequently, the affinity of the Mg^{2+} for the protein-nucleotide complex is reduced significantly. As a result, it is highly probable that the metal ion is not bound in the complex with the GDP analogue at physiological concentrations. Thus, it can be concluded that the binding affinity of this analogue for *K*-Ras or its mutant is lowered by at least four orders of magnitude in comparison to GDP.

2.1.3. Inhibition of *K*-Ras mutants by covalent inhibitors

In 2013 Shokat and coworkers[62] targeted the cysteine residue of the most present mutant *K*-Ras Gly12Cys for lung cancer with a covalent inhibitor. Amino acids such as cysteine can be targeted with covalent inhibitors. As those amino acids are common in many proteins, covalently binding molecules were believed to be unspecific. Therefore, this strategy was generally disfavoured in the past as it is likely to have unwanted side effects. In case of severe diseases such as cancer, application of this method is tolerated. In the past few years, this approach regained attention as it was shown to offer an elegant way for selectively addressing mutant *K*-Ras over the wild-type protein. Molecules that bind to the cysteine side chain of *K*-Ras mutant were identified using a method called "tethering".[63] This screening strategy makes use of low molecular weight ligands with a disulfide, which can react with the cysteines forming an intermediary disulfide "tether". As the reaction conditions are partially reducing to promote rapid thiol exchange, most compounds will easily be released from the protein. Weak affinities of the ligands for the protein stabilize the disulfide bond entropically shifting the equilibrium towards the protein-ligand complex. This complex can be measured via mass spectrometry and can be analysed by X-ray crystallography.[63] A small library of 480 compounds was screened by Shokat *et al.* to identify fragments, which selectively bind to a GDP bound *K*-Ras mutant. The two best compounds **11** and **12** from this library are shown in Figure 17. As an effect of covalent ligand binding, SOS-mediated nucleotide exchange as well as interaction with effectors such as Raf are decreased.[5,29,60,62]

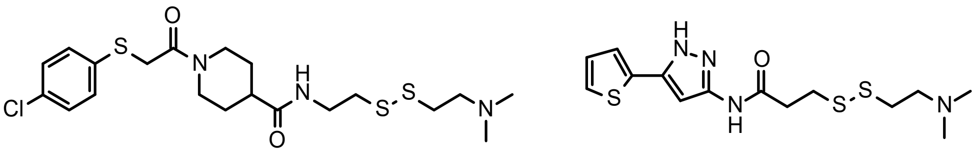

11 (6H05)

12 (2E07)

Figure 17: The two best low molecular weight fragments incorporating a disulfide moiety to covalently bind to mutant K-Ras identified by a new approach called "tethering".

2.1.4. Disrupting Protein-Protein-Interactions (PPIs)

Interfering in PPIs between *K*-Ras and its effectors is one of the most challenging approaches as the smooth surfaces of the involved proteins offer no suitable binding niche.[7,22,48,64–67] Nonetheless, efforts have been made to discover peptides derived from the Ras binding domain of Raf1, which can inhibit the Ras-Raf interaction successfully with an IC_{50} value of 7 µM. As peptides are unsuitable drugs, replacement of those structures for small non-peptidic molecules is necessary. A first attempt to realize this was made with sulindac sulfide (**13**, Figure 18), an anti-tumour agent that can inhibit the Ras-Raf binding. Unfortunately, the binding affinity of sulindac sulfide (**13**) is too low to be used as a drug so far.[7,29,48] In 2005, Kalbitzer and coworkers[68] discovered a new small molecule that can indirectly interfere in the interactions of *K*-Ras and its effectors. The ligand zinc cyclen (**14a**, Figure 18) stabilizes GTP-bound *K*-Ras in a state with 20-fold decreased effector affinity. Later, Rosnizeck *et al.*[69] used the copper analogue **14b** (Figure 18) for ^{31}P NMR studies to confirm that hypothesis.

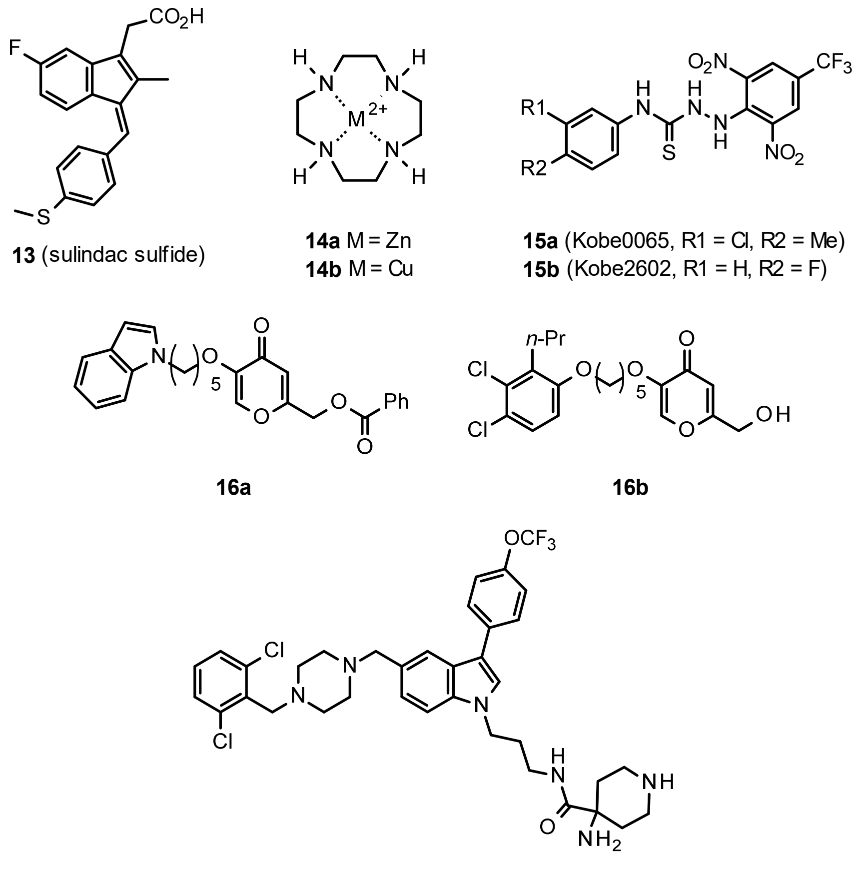
13 (sulindac sulfide)
14a M = Zn
14b M = Cu
15a (Kobe0065, R1 = Cl, R2 = Me)
15b (Kobe2602, R1 = H, R2 = F)
16a
16b
17 (3144)

Figure 18: Molecules to bind to the surface of K-Ras interrupting interactions with effector proteins in the course.

Shima and coworkers discovered the lead structures Kobe0065 (**15a**) and Kobe2602 (**15b**) depicted in Figure 18, which inhibit the Ras-Raf interaction with IC_{50} values in the low micromolar range. These compounds bind to the surface of *K*-Ras near switch II.[5,29,48,70] Very recently, Marín-Ramos and Piñar *et al.*[66] discovered a new compound, which selectively bind to the molecular surface of *K*-Ras mutants close to the nucleotide binding site extending towards switch II. A library of 1000 compounds was screened against several cancer cell lines. The initial hit structure **16a** (Figure 18) was optimized first by structural modifications of the ester group followed by replacing the indole moiety by a phenol ring. Ether **16b** (Figure 18) exhibits improved cytotoxicity in cancer cell lines compared to normal cells. In 2017, Welsch *et al.*[71]identified a multivalent small-molecules pan-Ras ligand, 3144 (**17**, Figure 18), via computational docking of fragment-like and lead-like small molecules to a binding site in the switch I region. The interaction of compound **17** with *K*-Ras mutant Gly12Asp was characterized by isothermal titration calorimetry (ITC) and heteronuclear NMR measurements. From calorimetric titration, a dissociation constant of 17.8 ± 4.5 µM for this compound was determined. NMR studies confirmed that the compound addresses amino acids Ile36-Asp38. The authors detected toxicity and off-target activity of compound **17** *in vitro*, in cells, and in mice. Consequently, further optimization is required to create a pan-Ras inhibitor with greater potency and specificity.

In 2012, two groups independently found small molecules, which can inhibit the interaction of *K*-Ras with its GEF, son of sevenless (SOS), by NMR-based fragment screening.[29] Maurer *et al.* found 25 compounds, which bind to the surface of *K*-Ras. Those ligands were identified via screening of 3300 structures using saturation transfer difference (STD) experiments followed by 2D heteronuclear NMR spectroscopy. Amongst others, DCAI (**18**, Figure 19) was identified to bind to the hydrophobic pocket located between the α-helix of switch II and the core β-sheet of the *K*-Ras protein. Thereby, it can interfere with the SOS interaction.[22,72] Fesik and coworkers identified molecules to disrupt the *K*-Ras-SOS interaction in a screening of 11000 fragments.[22,73] These first compounds such as the indole derivative **19**, phenol **20** or sulfonamide **21** (Figure 19) carry substituents such as further (hetero-)aromatic rings or aliphatic rings. Those can be connected either via a highly flexible methylene bridge or a thio- or sulfonamide. The resulting compounds exhibited only weak k_D values in the range of 1.3-2 mM. Utilizing structure-based design, the binding affinity of the lead structure **19** was optimized to reach 190 µM.[73]

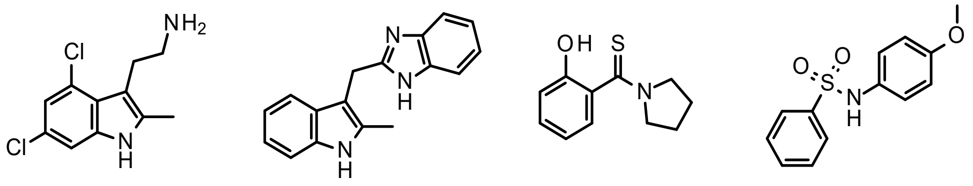

18 (DCAI) **19** **20** **21**

Figure 19: Ligands found to interfere with SOS interaction by binding to the surface of the K-Ras protein.

Recently, Sakamoto *et al.*[65] discovered a cyclic 19mer peptide called KRpep-2d (Ac-Arg-Arg-Arg-Arg-**Cys**-Pro-Leu-Tyr-Ile-Ser-Tyr-Asp-Pro-Val-**Cys**-Arg-Arg-Arg-Arg-NH$_2$). It was identified from a screening of random peptide libraries displayed on T7 phages, which is able to compete with SOS interaction. Although a crystal structure of KRpep-2d with *K*-Ras mutant Gly12Asp was measured, the inhibitory mechanism is still controversial.[67]

2.1.5. Targeting the Rheb protein

Regarding post-translational modifications, Rheb farnesylation can also be inhibited by farnesyl transferase inhibitors as described above for *K*-Ras.[54] Additionally, the strategies described for *K*-Ras can be applied to Rheb. Up to date, no specifically binding low molecular weight inhibitors for the Rheb protein are known.[20]

2.2. Drugging the MIA protein

The MIA protein was discovered in 1994 and since then the main focus of research has been on the structure and determination of physiological properties. Thus, only a small number of MIA ligands has been discovered so far. In 2001, proline-rich peptides were identified from a phage display library.[38] Later, Schmidt and Bosserhoff were able to show that a fibronectin derived peptide called AR54 (Asn-Ser-Leu-Leu-Val-Ser-Phe-Gln-Pro-Pro-Arg-Ala-Arg) inhibited MIA function in a Boyden Chamber invasion assay nearly completely at a concentration of only 1 µM while not affecting integrin activity. Whole cell assays with various cell lines showed that peptide AR54 reduced endocytosis of labeled MIA protein in a dose dependent manner. At a concentration of 2 µM, the uptake of MIA was nearly completely inhibited.[46] Five years ago, Schmidt *et al.* were able to apply a novel heterogeneous transition-metal-based fluorescence polarization (HTFP) assay to test the previously discovered peptides for their ability to stop MIA dimerization, which is crucial for MIA activity. From this essay, the dodecapeptide AR71 (Ac-Phe-His-Trp-Arg-Tyr-Pro-Leu-Pro-Leu-Pro-Gly-Glu-NH_2) was found to effectively dissociate MIA dimers. This peptide also inhibits MIA activity in a Boyden chamber invasion essay as has been shown for AR54 before. Additionally, heteronuclear multidimensional NMR experiments with the peptide were conducted to determine the exact binding location for peptide AR71. Interaction with the protein must be next to the distal loop as it can prevent dimerization. Changes in the chemical shift of protein peaks during the titration experiment clearly revealed that ligand binding with the peptide is achieved by interacting with amino acids Cys17, Ser18, Tyr47, Gly66, Asp67, Leu76, Trp102, Asp103 and Cys106 (Figure 20).[41,43]

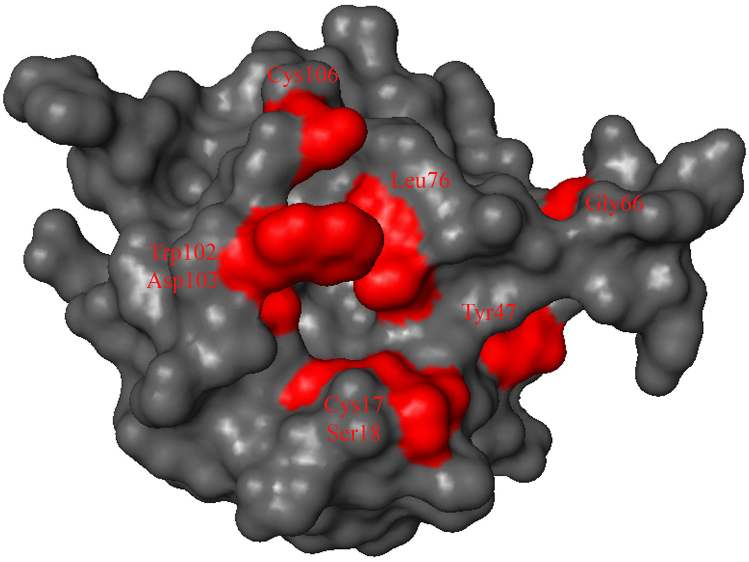

Figure 20: Surface of the MIA protein with amino acids that shift upon addition of AR71 highlighted in red.

2.3. Drug design

In the past, new drugs were usually discovered by the “trial-and-error” approach, which uses huge libraries of compounds, which are screened against a biological target. This method requires a significant amount of time and money as an appropriate high-throughput screening for the target needs to be developed and carried out. Also, the amount of data acquired needs to be reviewed and the positive hits need to be verified and then developed into lead structures.

Methods such as fragment-based drug design have been developed as the hit rate of high-throughput screenings is generally low. This approach will be described further in the upcoming section.

2.3.1. Fragment-based drug design

Fragment-based drug design (FBDD) is based on the development of small fragments, which exhibit only weak binding affinities to the targeted protein. It is also a complementary method to high-throughput screenings, which became popular over the last two decades in the pharmaceutical industry.[64,74–76]

The general process of fragment-based development consists of 3 distinct steps. At first, a library of fragments needs to be assembled. These fragments should agree with the Rule of Three: a molecular weight lower than 300 g/mol, up to three hydrogen donors and acceptors, each, and a logP (partition coefficient) value of ≤ 3. In a second step, the compound library is screened to detect interactions with the target. Finally, the fragments need to be further elaborated to increase their binding affinity in an iterative process consisting of *in silico* design of improved molecules, synthesis and (NMR-based) examination of the binding affinity of the resulting compounds.[74]

An improvement of the binding affinity of the hit fragments can be achieved through three different approaches: fragment merging, linking or growing.[74,76] The first one, fragment merging, makes use of multiple compounds, which do not overlap with each other completely while binding to the same binding site of a protein. Therefore, attaching parts of other ligands to a core fragment can enhance the binding affinity of the resulting compound. The second method, fragment linking, depends on finding and synthetically linking two fragments that bind to adjacent binding pockets on the surface of a target. The third option to improve a fragment is “growing” the molecule, also called fragment evolution, by adding additional functional groups or even larger building blocks to allow for further interaction with the target. Usually, the goal is to reach adjacent empty pockets or filling up gaps in the current binding site. The ligand efficiency is defined as $-\Delta G$ (Gibbs energy) in kcal/mol divided by the number of heavy, non-hydrogen atoms. For this method, this value reflects the effect of each group added as it increases the molecular mass of the compound.[74,76]

2.3.1.1. SAR by NMR

"SAR (structure-activity relationships) by NMR" , which was first described by Shuker, Hajduk, Meadows and Fesik in 1996[77], is based on fragment linking of small building blocks, which each bind to an individual site on the surface of the protein. One possible method to examine binding depends on chemical shift analysis in two-dimensional heteronuclear NMR spectroscopy. These shifts are caused by the addition of the ligand(s). In contrast to other methods, binding can still be detected easily even if larger excesses of ligands have to be added to the target. As the chemical shift of ^{15}N-labeled proteins are observed, no interfering signals of the ligands appear. Additionally, individual binding sites can easily be distinguished as different amino acids will be affected upon binding. A significant disadvantage of NMR-based screenings is the size-limitation of the proteins.[76,78] Only small to medium sized proteins can be investigated.[64]

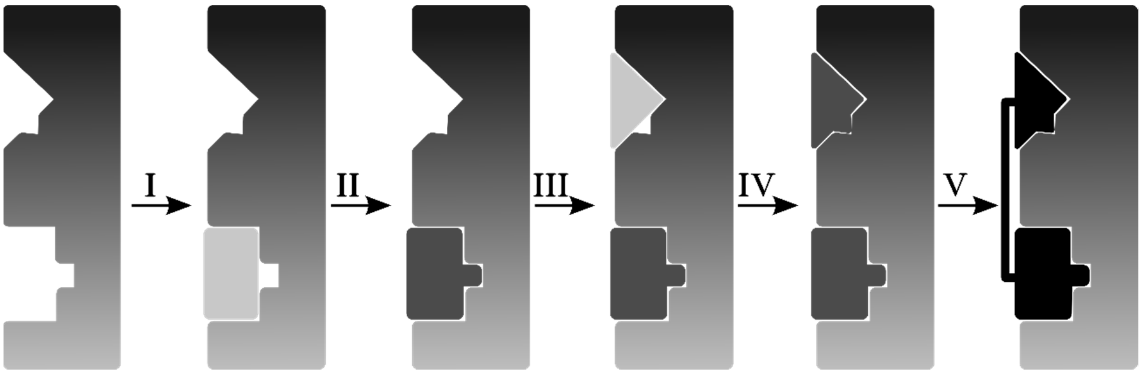

Figure 21: The process of finding a hit molecule by means of fragment linking making use of the "SAR by NMR" method. Step I: Screening for a first-site fragment. Step II: Optimization of the fragment bound to the first ligand binding pocket. Step III: Screening for a second-site binding fragment. Step IV: Optimization of the second fragment found to bind to the second binding site. Step V: Linkage of the two fragments to afford a hit compound exhibiting a k_D value that accounts approximately for the product of the dissociation constants of each of the fragments.[77]

A library of fragments (Figure 21) is screened to identify compounds interacting with the targeted binding site. These primary hits then need optimization regarding their binding affinity. After successful development of a first-site ligand, a second screening for ligands binding to a different but close-by binding pocket is performed. Sometimes, conducting a second-site screening with the first-site left unoccupied will only lead to binding of the fragments to the first binding pocket. Therefore, second-site screenings are conducted with the first site being occupied. Under such conditions, fragments can bind to a close-by binding location.[76] Data from second site screenings can be difficult to interpret as first-site ligands are usually weak binders, which cannot saturate the binding pocket.[76,79] Consequently, installing the first ligand covalently, similar to the tethering approach[63] described before, to a protein carrying a cysteine mutation close to the binding pocket can be used as an alternative approach.[79] The second-site ligands then again need optimization. Finally, both fragments are linked synthetically according to their individual binding modes. The linker has to be chosen carefully to maintain the binding affinity of the fragments to the target.

Additionally, the linker should offer favourable interactions with the protein itself. At the same time, flexibility of the linker needs to be chosen appropriately. A more rigid linker reduces the entropic costs of the linked compound while restricting the binding conformation of the fragments. In contrast, a more flexible linker favours optimal binding of the fragments, but decreases the Gibbs energy as the entropy is increased ($\Delta G = \Delta H - T \cdot \Delta S$).[74,76] Successful linkage of the fragments has to be verified again by NMR studies. This strategy takes advantage from the fact that combining two compounds with moderate binding affinities (millimolar to micromolar range) will enhance the binding affinity of the product drastically. It accounts for the product of the values of each fragment minus the entropy contributed by the linker.[76,78]

2.4. Molecular Modelling tools

In contrast to traditional “trial-and-error” approaches, modern drug development also makes use of computational methods such as molecular modelling. The software used in the thesis is introduced in the following sections.

2.4.1. Autodock/VINA

The software Autodock4[80] and its improved version VINA[81], developed at The Scripps Research Institute, can be used for molecular modelling and especially *in silico* screenings to predict the optimal bound conformations of ligands and proteins.

The software requires the three-dimensional structure of the target protein such as the X-ray or NMR structures provided by the RCSB protein data bank[18]. The binding pocket can be defined with the help of the grid box. For this purpose, a structure of the protein containing a bound ligand can be helpful. The grid box can be defined manually around the binding position of a known ligand. The software calculates the lowest energetic poses for the complex of the rigid protein and each of the ligands, provided as a pdb-file, in vacuum. Docking relies on two methods: first, a force field to evaluate the free energy of binding of the ligand-protein-complex, second, a search method to examine the conformational space available to the ligand and its target. For that, several approximations have to be made to allow docking with reasonable computational effort. The ligand is treated as flexible regarding bond rotation, but bond angles and lengths are kept rigid.[82] After successful calculation, the energetic levels of each of the compounds are given in kcal/mol for usually at most 10 poses. Integrating Autodock/VINA into PyMol 1.3, a visualization software, allows optical assessment and ranking of the calculated complexes according to the predicted binding mode. Taking the scores as well as the binding mode into account, each ligand can be rated and ranked accordingly. If the orientation of the ligand or its binding site differ from the expected binding mode, the corresponding score is disregarded.

The accuracy of free energy prediction of most computational docking techniques, including Autodock, totals to 2-3 kcal/mol standard deviation. This error should be held in mind when considering the scores of the various ligands to be calculated and judged accordingly.[82]

2.4.2. Schrödinger software package

In contrast to Autock/Vina, the Schrödinger software package is a commercial product. Using the software for molecular modelling purposes, the same requirements as for Autodock/VINA have to be met. Nevertheless, the Schrödinger software offers far more options regarding the preparation of both, the protein and the ligands.

Starting from a crystal structure obtained from the protein data bank, the protein preparation wizard[83,84] can repair the protein structure (assignment of bonds and bond orders, addition of hydrogens, filling in missing loops or side chains, capping uncapped termini, adjusting bonds and formal charges for metals, and correcting mislabeled elements). Also, water molecules, which are often present in crystal structures of proteins, can be deleted in dependence of their distance to hetero groups of the protein. This is a necessary process to enable other applications of the Schrödinger package to work with the given protein data. During an optimization step, the remaining water molecules in the protein are oriented properly and the protonation state of the protein is calculated. In the last step, the protein is minimized using the force field OPLS 2005 as by default. Other force fields such as OPLS 2001 or OPLS 2.0 are also available.

In the next step, the ligands, which can either be drawn with the incorporated 2D sketcher or imported from suitable files, have to be prepared for docking. Another subprogram called LigPrep[85] is used to minimize each ligand with a force field (OPLS 2005, by default). Subsequently, possible charged states of the ligands depending on pH (7 ± 1) can be generated and the charge distribution of the ligand is calculated. Additionally, this tool can also compute all possible stereoisomers of chiral ligands.

After successful preparation of all ligands for *in silico* screening, the software Glide (Grid-based Ligand Docking with Energetics)[86–89] is used to search for favourable interactions between the ligand and the protein. In contrast to Autodock/VINA, the Schrödinger software can compute proteins, which contain cofactors and ligands. This is especially interesting for the small GTPases *K*-Ras and Rheb as their crystal structures include GDP and a magnesium ion as ligands. As described before, a grid has to be set to define the region of the protein, the ligands will be fitted into. The Glide Grid generation tool offers the possibility to select a ligand that is already present in the given protein structure. The program then calculates a grid according to the size and location of the bound ligand. During docking, the present ligand will be removed from the protein structure. The ligands are then docked into the corresponding binding pocket. To facilitate ligand docking, Glide uses a hierarchical series of filters to search for possible locations of the ligand. First, it generates conformations of each ligand depending on the number of rotatable bonds. Then, the resulting conformations are applied to so-called “side-point” searches, to find possible locations and orientations in the ligand binding pocket. Each orientation is then evaluated for its fitting in the pocket and is skipped if too many steric clashes with the protein are recognized. Fitting orientations are subsequently scored for their capability of interacting in hydrogen bonds or ligand-metal bonds. The best rated orientations are then refined by moving the whole ligand by 1 Å in the Cartesian coordinate system to improve interaction distances. The orientations to pass this stage will then undergo energy minimization using one of the OPLS force fields. Following this final step, the scores of each orientation or pose are recalculated to give the final GlideScore in kcal/mol. As described for VINA, final ranking of the ligands depends on the orientation of the computed poses of each ligand as well as considering the calculated Glide scores.

2.4.2.1. MacroModel

MacroModel[90], a subprogram of the Schrödinger package, is a general purpose, force-field-based molecular modelling software. For minimization operations with MacroModel, a force field, usually OPLS 2005, and a solvent such as water are used. Other programs calculate “explicit solvation”, which affords extended calculation time due to each solvent molecule being handled individually. In contrast, MacroModel operates on a different basis treating the solvent as a fully equilibrated analytical continuum starting near the van der Waals surface of the protein. Here, MacroModel was used to minimize structures obtained from Glide dockings to optimize the interaction of the ligand in the binding pocket.

2.4.3. High Ambiguity Driven DOCKing (HADDOCK)

The software HADDOCK[91,92] is used to calculate protein-protein or protein-ligand interactions. In contrast to the programs described above, HADDOCK makes use of chemical shift perturbation data previously obtained from NMR titration experiments of the ligand with the corresponding protein. The information on the residues involved is provided as so-called “ambiguous interaction restraints” (AIRs) to drive the docking. Similar to both Autodock/VINA and Glide, the structures are ranked according to their intermolecular energy (electrostatic, van der Waals and AIR energy terms) after calculation. Like other docking software, HADDOCK requires the pdb-file of the free protein(s) or the ligand. Additionally, designation of the ambiguous interaction constraints is needed, which are obtained from the shifts resulting from NMR titration experiments. Shifting amino acids are defined as “active” residues while non-shifting or weakly shifting residues belong to the list of “passive” amino acids. Then, the docking protocol passes through three stages: first, randomization of orientations and rigid body energy minimization (EM), second, semi-rigid simulated annealing in torsion angle space (TAD-SA, molecular dynamics-based refinement) and third, final refinement in Cartesian space with explicit solvent, usually water. What makes HADDOCK special in comparison to other docking software is the semi-rigid optimization step during which side-chains as well as the backbone of “active” residues of the involved protein(s) are allowed to move.[91] HADDOCK runs can be operated as a Linux stand-alone program or a more user-friendly Web browser interface.[44]

2.5. Preliminary studies

In preliminary studies towards this project, small molecules (Figure 22) for the cancer-related proteins Rheb, *K*-Ras and MIA have been identified.

A library of small molecules incorporating acidic, basic, and neutral compounds was screened against the targeted proteins *K*-Ras and Rheb. The interaction of each of the compounds was investigated by multidimensional heteronuclear NMR spectroscopy and chemical shift perturbation analysis. In case of Rheb, the linear molecule 4,4'-Biphenol (**22**) was identified as the first small molecule to bind to a binding cleft on the surface of the protein. The dissociation constant (k_D) was calculated to be 1.54 ± 0.23 mM.[20] For *K*-Ras, the same library of compounds was also investigated. Bisphenol A (**23**) was found to bind (k_D 600 ± 200 µM) to a binding pocket identified before by Fesik and coworkers.[20,73] It was also shown that Bisphenol A (**23**) intercepts the SOS-mediated nucleotide exchange in *K*-Ras. This keeps the protein in the inactivated state, in which it cannot interact with effectors.[20]

4,4'-Biphenol (**22**) Bisphenol A (**23**)

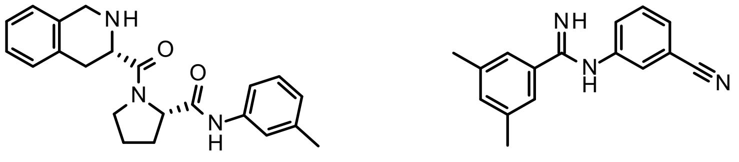

ZINC05203919 (**24**) ZINC01400183 (**25**)

Figure 22: Small molecules identified as ligands for the cancer-related proteins K-Ras, Rheb and MIA.

In case of the MIA protein, the ZINC database[93,94] was searched for compounds similar to fibronectin, one of the natural binding partners of MIA. The resulting 5000 compounds were examined using the *in silico* high throughput screening approach implemented in AutoDock Vina. The 30 most promising hits were purchased and investigated using a NMR-based saturation transfer difference (STD) assay. Two compounds, ZINC05203919 (**24**) and ZINC01400183 (**25**), were identified as weak binders of the MIA protein. The dissociation constants were calculated from further NMR-based titration experiments to be 328 ± 84 µM in case of ZINC05203919 (**24**) and 320 ± 76 µM for ZINC01400183 (**25**), respectively.[95]

3. Objectives

The goal of this thesis is the elucidation of structure-activity-relationships of inhibitors for the cancer-related proteins Rheb, *K*-Ras and MIA. The structures given in Figure 22 can be regarded as lead structures. Additionally, the compounds will be examined for their binding affinity to the corresponding protein. The strategies to vary substituents and achieve improvements of the ligand affinity will be explained for each of the targeted proteins independently in the following.

Rheb: In case of the Rheb protein, improvement of the lead structure 4,4’-Biphenol (**22**) can be achieved using the fragment-based drug design approach. Two strategies to improve the binding affinity of the compound with the Rheb protein and to gather SAR information will be performed in parallel: fragment growth and removal of one hydroxy groups. Starting with an *in silico* screening of analogues of 4,4’-Biphenol (**22**), the most promising compounds will be synthesized. The effect of each derivatisation then needs to be evaluated by NMR measurements with the ^{15}N-labeled protein performed by our collaboration partners at the Ruhr Universität Bochum. Based on the result of this investigation, the alterations will either be neglected or incorporated in the molecule (iterative optimization).

***K*-Ras:** The lead structure Bisphenol A (**23**), a bulk chemical, which is used as plasticizer and for polymer synthesis, is believed to imitate the hormone estrogen. Consequently, this compound is inappropriate as a potential drug. On one hand, optimization of the binding affinity of the lead structure is one of the envisaged strategies. On the other hand, BPA derivatives, which do not bind to *K*-Ras, are also promising targets as less toxic substitutes of BPA (**23**) for polymer synthesis. Information on the SAR of Bisphenol A (**23**) is collected. Derivatization of this compound is based on molecular modelling of derivatives of the lead structure **23**. Promising hits resulting from the *in silico* screening will be synthesized and investigated for their binding affinity to the ^{15}N-enriched protein via heteronuclear NMR studies.

MIA: Two molecules were found to bind to the same binding cleft of the MIA protein. In a first step, thorough investigation of the SAR of amidine **25** is intended. In the next step, a hybrid molecule of ZINC molecules **24** and **25** following the fragment-merging approach will be developed. According to the overlap of the two ZINC compounds **24** and **25**, hybrid molecules will be investigated utilizing molecular modelling techniques. Promising hybrid structures will be synthesized and the interaction with the MIA protein will be evaluated by heteronuclear NMR studies.

4. Results and Discussion

4.1. Protein preparation of Rheb in an internship at the RUB

The ^{15}N-enriched protein Rheb was expressed and purified. This was completed during an internship with our collaboration partners at the RUB in Bochum. Genetically modified *Escherichia coli* bacteria were cultured with ^{15}N-labeled minimal medium. Following protein expression induction, the cells were harvested and lysed. The obtained lysate was purified chromatographically, concentrated and rebuffered for NMR spectroscopy. The concentration of the protein solution was measured by UV spectroscopy and subsequently diluted (0.25 - 0.30 M), aliquoted and stored at -20 °C until use.[11,20]

4.2. Screening and synthesis of novel compounds binding to the Rheb protein

As described in Chapter 2.5, 4,4'-Biphenol (**22**) was among a group of molecules found to bind weakly to the Rheb protein.[20] Since it exhibits the best dissociation constant (k_D 1.54 ± 0.23 mM), it was chosen as a lead structure for optimization. Therefore, the binding mode of 4,4'-biphenol (**22**) was calculated using HADDOCK based on the chemical shifts of the NMR titration experiment (Figure 23, top).

In general, a titration experiment consists of several steps: At first, the NMR spectrum of the pure protein is measured to verify the correct fold of the protein as well as sufficient isotopic labeling. The resulting spectrum can be used as reference for the titration experiment. In the next step, substoichiometric amounts of ligand are added followed by adjustment of the pH value of the aqueous buffer solution. In case that the pH is not kept constant throughout the titration experiment, pseudo shifts of amino acid peaks might be observed. Then, an NMR spectrum of the protein-ligand mixture is measured. Addition of ligand, adjustment of the pH and measurement of an NMR spectrum are repeated until the saturation point for the ligand-protein complex is reached if possible. To decide whether a titration experiment is needed, an NMR spectrum with an excess amount of ligand is measured first. If no significant shifts are observed, the ligand is classified as non-active.

The shift range of each of the affected amino acids can be obtained from the titration spectra (Figure 23, bottom). Amino acids with a shift exceeding twice the standard deviation (2σ) are set as the active amino acids, which directly interact with the ligand. The remaining residues are defined as passive. The software HADDOCK then calculates possible binding modes for the ligand with the target protein. The resulting pose for 4,4’-biphenol (**22**) is shown in Figure 24.

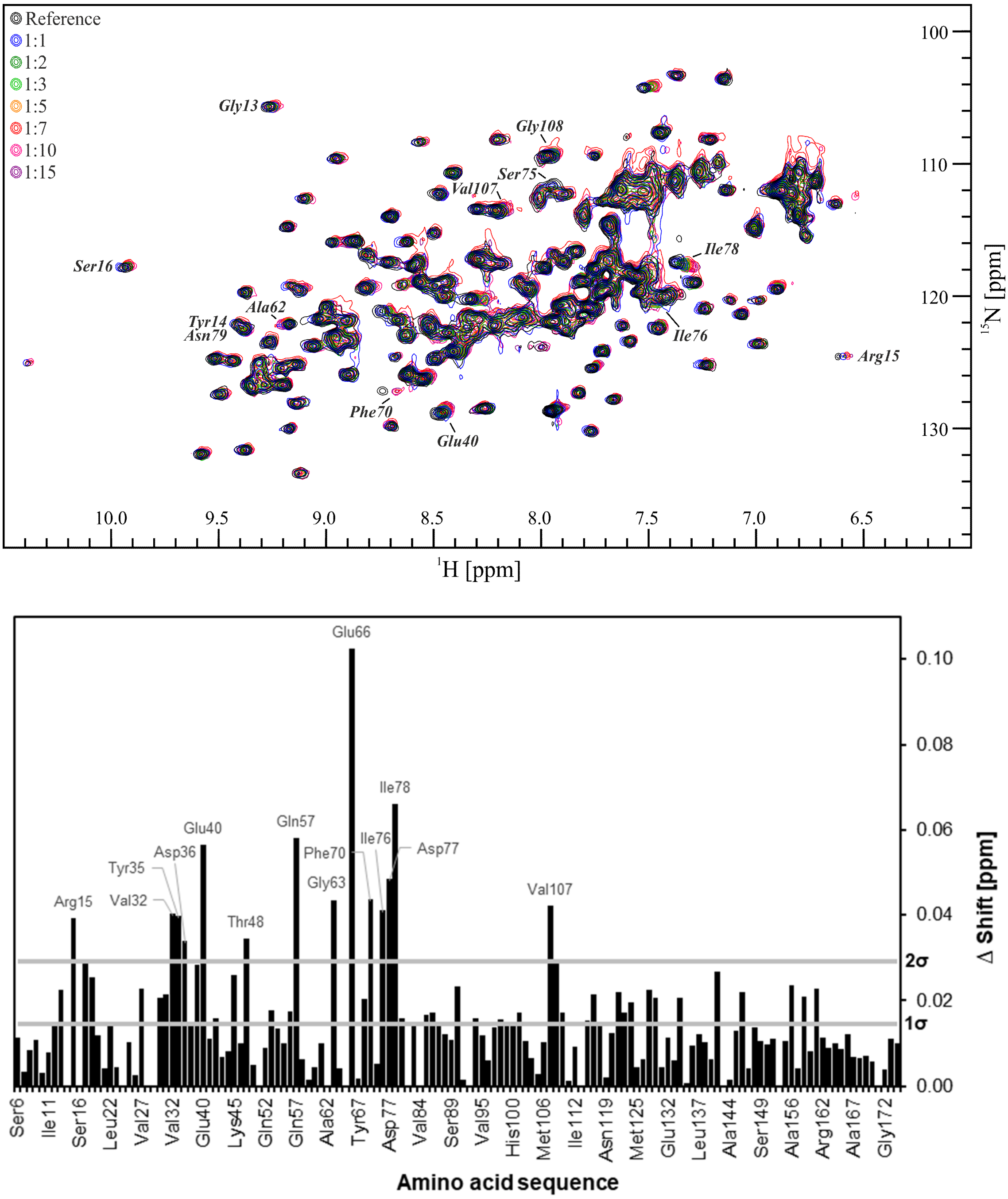

*Figure 23: Top: ^{1}H,^{15}N-SOFAST NMR overlay of the titration steps of 4,4’-biphenol (**22**) to the Rheb protein.[96] Bottom: Shift ranges for the amino acids of the Rheb protein.*

The HADDOCK model (Figure 24) predicts that 4,4’-biphenol (**22**) interacts with the protein via three hydrogen bonds. One hydroxy group of biphenol **22** forms two hydrogen bonds to the residues Ile78 and Lys109 while the other one is involved in a hydrogen bridge with Ile69. The binding pocket is formed by the residues Ser75, Ile76, Ile78 and Asn79 of the flexible switch II region to one side and Val107 and Gly108 on the other side according to the chemical shifts in the NMR spectrum (Figure 23). Phe70 appears to be in the wrong position to interact with the ligand. Nevertheless, this residue belongs to the highly flexible switch II region and can therefore fold back into the binding pocket to facilitate interactions with the ligand.[20]

Chemical shifts observed for switch I residues Glu40 and Ala62 (orange) and P-loop residues Gly13, Tyr14, Arg15 and Ser16 (red), constituting the nucleotide binding pocket, are caused by allosteric effects. Consequently, binding of the ligand indirectly causes conformational changes on the opposite side of the protein.

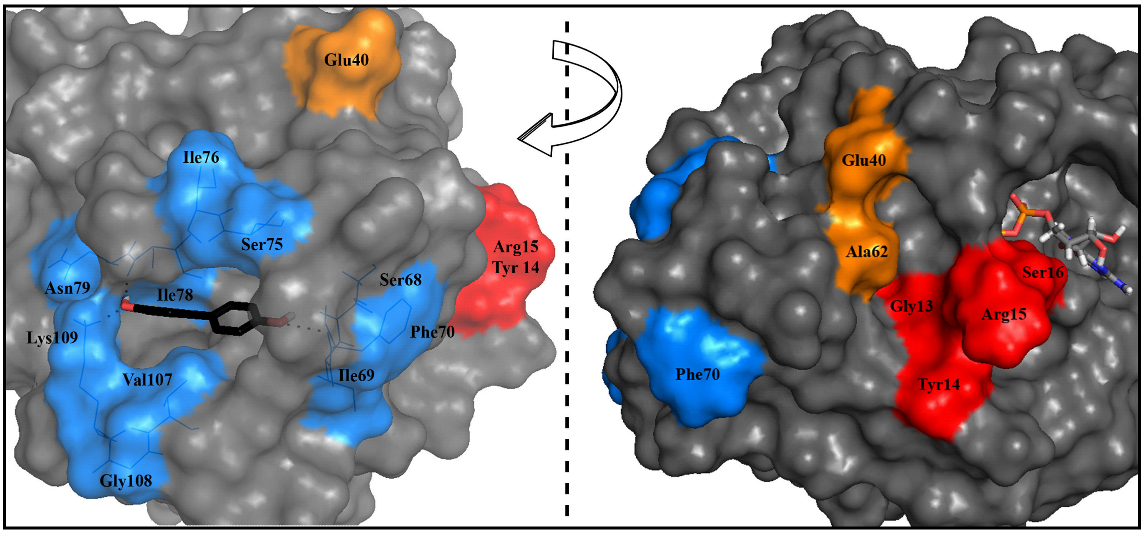

*Figure 24: 4,4'-Biphenol (**22**) in the binding pocket (blue) of the Rheb protein identified by chemical shifts in the NMR measurement. Residues near the nucleotide (red, orange) experience chemical shifts as a result of allosteric effects.*

4.2.1. Attachment of additional hydroxy groups via a spacer

As described above, the hydroxy groups of 4,4'-biphenol (**22**) are involved in hydrogen bonds, which stabilize the ligand-protein complex. Additional hydroxy groups can be introduced into the molecule to form further hydrogen bonds. Those hydroxy groups could either be directly attached to the biphenol core or via a flexible spacer such as a methylphenyl or ethylphenyl moiety. These spacers would also provide additional hydrophobic interactions. Therefore, the biphenol analogues **26-29** (Table 2) were designed and modeled into GDP-free Rheb (PDB ID: 2L0X) using Glide (Schroedinger Software) and Autodock/VINA. The Glide score values (max to min) result from different protonation states as well as variations in the exact orientation of each ligand in the binding pocket of the protein (see also Chapter 2.4.2).

The scores obtained for the designed molecules are higher in comparison to that of 4,4'-biphenol (**22**). The best two molecules are highlighted in grey in Table 2. While 3-(4-hydroxyphenyl)ethyl-4,4'-biphenol (**27**) exhibits the strongest VINA score, 2-(4-hydroxyphenyl)methyl-4,4'-biphenol (**28**) reaches the highest score in the Glide docking.

Table 2: First iteration of biphenol derivatives 26-29 applied to molecular modelling with Glide and Autodock/VINA using 4,4'-biphenol (22) as reference.

Substance	Structure		Glide Score		VINA Score	
			max	min	max	min
4,4'-Biphenol (22) (lead structure)	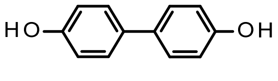 **22**		-5.60		-6.0	-4.6
3-(4-Hydroxy-phenyl)methyl-4,4'-biphenol (26)	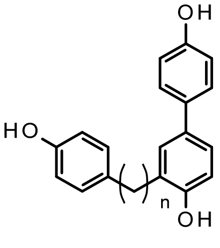 **26** (n = 1) **27** (n = 2)	n = 1	-5.69	-5.56	-6.9	-5.5
3-(4-Hydroxy-phenyl)ethyl-4,4'-biphenol (27)		n = 2	-6.17	-5.29	-7.1	-6.5
2-(4-Hydroxy-phenyl)methyl-4,4'-biphenol (28)	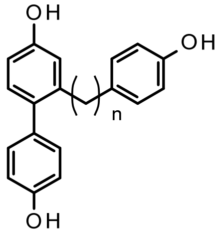 **28** (n = 1) **29** (n = 2)	n = 1	-6.91	-5.30	-6.3	-5.6
2-(4-Hydroxy-phenyl)ethyl-4,4'-biphenol (29)		n = 2	-6.25	-4.72	-6.7	-5.2

Regarding the positioning of those two molecules in comparison to 4,4'-biphenol (**22**) predicted by Glide (Figure 25), 2-(4-hydroxyphenyl)methyl-4,4'-biphenol (**28**) adopts a similar binding mode in the binding pocket. It provides an additional hydrogen bond via the newly attached side chain to Ser75 or Met106 depending on the orientation of the methyl(hydroxyphenyl) residue. In contrast, 3-(4-hydroxyphenyl)ethyl-4,4'-biphenol (**27**) can insert the side chain into the binding pocket instead of the biphenyl core. In both cases, it does not provide any additional hydrogen bonds to the protein.

In comparison, none of the ten best structures predicted by Autodock/VINA (Figure 25) for 2-(4-hydroxyphenyl)methyl-4,4'-biphenol (**28**) fit into the binding pocket as calculated for 4,4'-biphenol (**22**). Therefore, no preferential orientation of the side chain can be deduced. In case of 3-(4-hydroxyphenyl)ethyl-4,4'-biphenol (**27**), VINA also predicts a binding mode different from that of 4,4'-biphenol (**22**). One of the phenol rings of the biphenyl core is replaced for the side chain. The replaced phenyl ring is oriented towards amino acids forming a polar region to one side of the binding pocket including Leu103 and Met106 to Lys109.

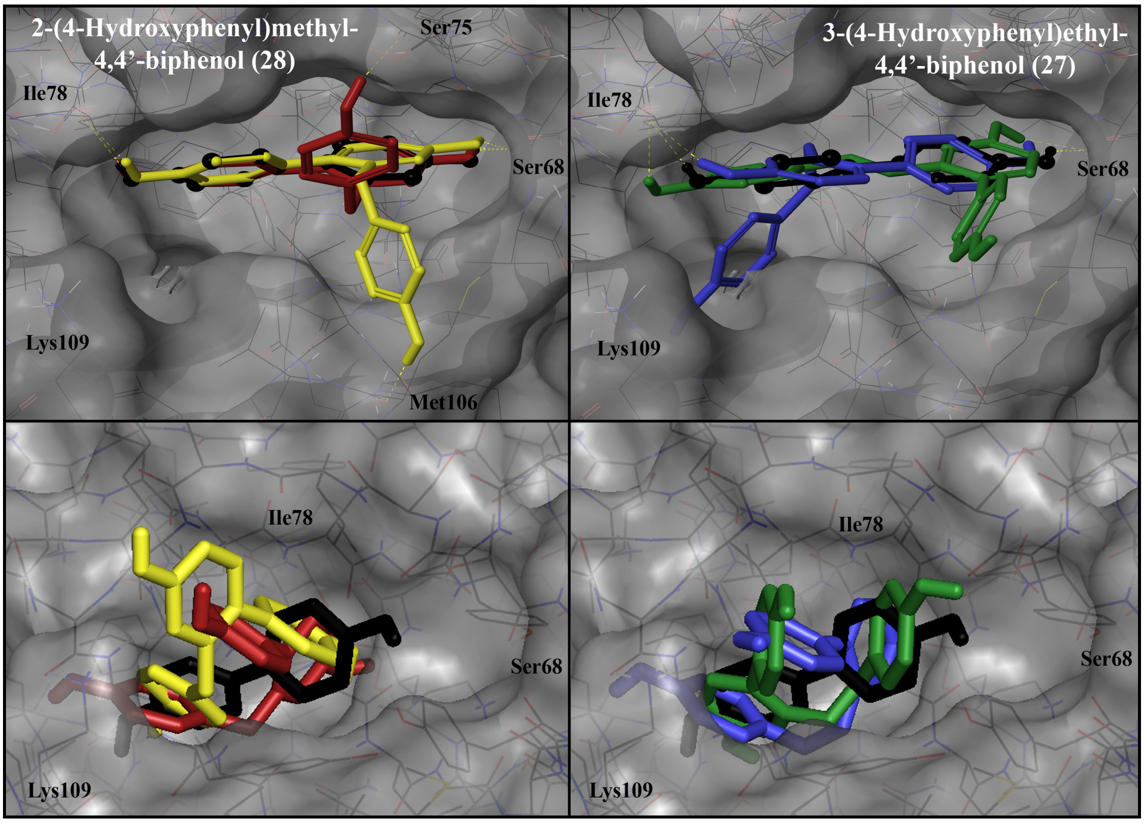

*Figure 25: Comparison of the binding modes predicted by Glide (top) and Autodock/VINA (bottom) of 2-(4-hydroxyphenyl)methyl-4,4'-biphenol (**28**, red and yellow structures on the left side) and 3-(4-hydroxyphenyl)ethyl-4,4'-biphenol (**27**, green and blue structures on the right side) in the binding pocket of the Rheb protein with 4,4'-biphenol (**22**, black) as reference.*

Since both structures show interesting binding modes compared to 4,4'-biphenol (**22**), they represent promising targets for synthesis. A literature search revealed no suitable straight-forward synthesis strategy for 2-(4-hydroxyphenyl)methyl-4,4'-biphenol (**28**), especially, since the required *meta*-substitution pattern for the side chain cannot be generated easily. Consequently, only 3-(4-hydroxyphenyl)ethyl-4,4'-biphenol (**27**) was selected for synthesis, because the side chain attachment is readily available through a Wittig type or Heck reaction.

The synthesis of biphenols was accomplished through Suzuki coupling reactions in all cases. This reaction uses less toxic reagents in comparison to tin- or zinc-organometallics and mild reaction conditions. Also, a large variety of boronic acids is commercially available. The side chain can be attached via a Wittig reaction. The newly introduced C=C-double bond can be reduced to the corresponding saturated system. As a hydrogenation step is required to reduce the double bond, benzyl groups were chosen as protecting group for the hydroxy moieties. Removal of the benzyl groups can be achieved during the reduction of the alkene. This shortens the synthesis by one step in comparison to the usage of any other non-hydrogenable protecting group.

The hydroxy group of 5-bromosalicylaldehyde (**30**) was protected as a benzyl ether using benzyl bromide and potassium carbonate in DMF (Scheme 1).[97] The reaction gave the desired product in an excellent yield of 99% after precipitation. The Suzuki coupling with 4-benzyloxyphenylboronic acid was carried out under standard conditions[98] to afford biphenol **32** in good yield (81%).

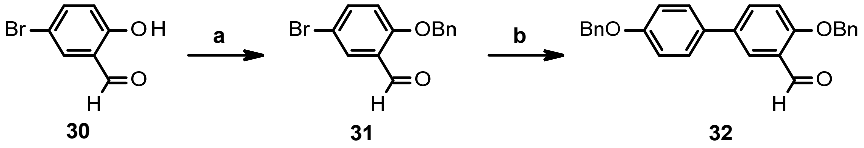

Scheme 1: Synthesis of biphenol ***32*** *via Suzuki coupling. Reaction condition: (a)* K_2CO_3*, benzyl bromide, DMF, r.t., 23 h, 99%, (b) 4-benzyloxyphenylboronic acid,* Na_2CO_3*,* $Pd(PPh_3)_4$*, LiCl, DME/*H_2O*, 80 °C, 16 h, 81%.*

Benzyl alcohol **33** was subsequently transformed into benzyl bromide **34** with phosphorous tribromide (Scheme 2).[99] The Wittig reagent **35** was obtained in quantitative yield by substitution of the benzylic bromide with triethyl phosphine.[100]

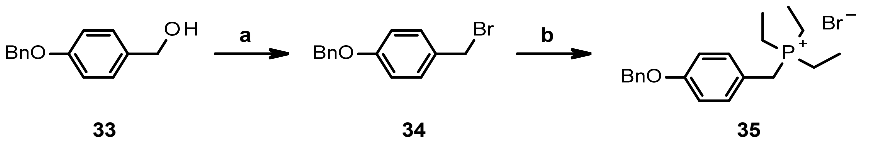

Scheme 2: Synthesis of Wittig reagent ***35****. Reaction condition: (a)* PBr_3*, DCM, 0 °C → r.t., 2h, 98%, (b) 10%* PEt_3 *in hexane, DCM, 0 °C → r.t., 17.5 h, quant.*

The Wittig reaction between biphenol **32** and phosphonium salt **35** was carried out as described by McNulty *et al.*[100] with aqueous sodium hydroxide as base (Scheme 3). After chromatographic purification, the pure alkene **36** could only be obtained in 29% yield due to incomplete conversion. A first attempt to simultaneously remove the benzyl groups and hydrogenate the alkene resulted in the fully protected alkane **37**.[101] The benzyl groups could not be removed by further hydrogenation using either palladium(0) or palladium(II)hydroxide. Therefore, ether cleavage with boron tribromide was carried out giving the desired biphenol **27** in low yield of 35%.

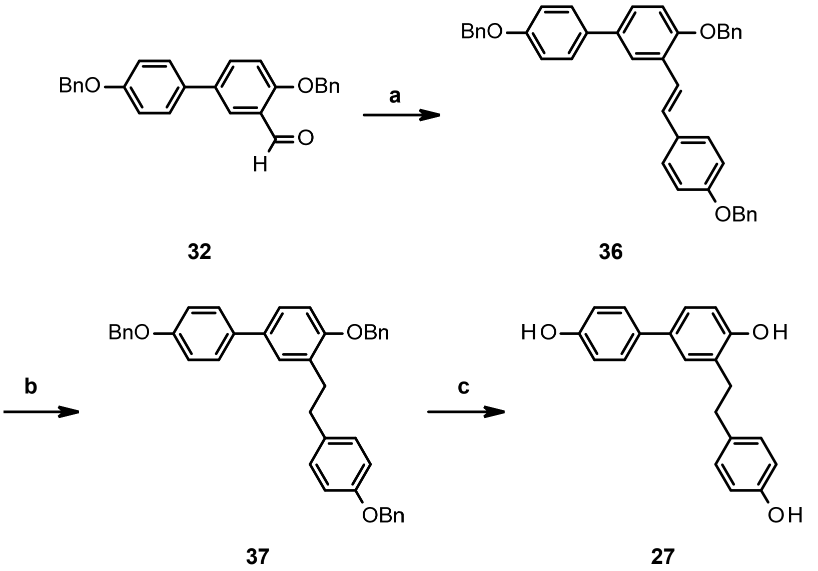

*Scheme 3: First route to synthesize biphenol **27**. Reaction conditions: (a) phosphonium bromide **35**, NaOH, H_2O, 70 °C, 6 h, 29%, (b) 10% Pd/C, methanol/EtOAc, 1 bar H_2, r.t., 24 h, 97%, (c) 1 M BBr_3 in DCM, DCM, -78 °C → r.t., 23 h, 35%.*

Instead of a Wittig reaction, a Horner-Wadsworth-Emmons reaction was attempted to increase the yield of alkene **36**. Unfortunately, phosphonate **38** was not obtained from benzyl bromide **34** by heating in neat triethyl phosphonate (Scheme 4).

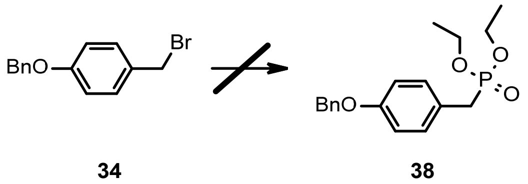

*Scheme 4: Synthesis of phosphate **38** for reaction with aldehyde **32** in a Horner-Wadsworth-Emmons reaction.*

In a second attempt, the order of reaction steps of the Suzuki coupling and the Wittig reaction was interchanged as can be seen from Scheme 5. As described above, the Wittig reaction between aldehyde **31** and phosphonium salt **35** was carried out with sodium hydroxide in water.[100] In this case, the conversion of the starting material was complete. The alkene **39** precipitated from the reaction mixture in excellent yield (96%). Subsequent Suzuki reaction gave biphenol **36** in moderate yield of 44% due to the low solubility of the compound during purification. Nevertheless, it has to be emphasized that the conversion of the reaction is complete and purification of the alkene **36** is simplified in comparison to the reaction described above. Deprotection and reduction of the double bond was done in one step by increasing the hydrogen pressure. Under 5 bar hydrogen pressure, alkene **36** was converted into the desired biphenol **27** in good yield of 86% using 10% palladium(0) on charcoal.

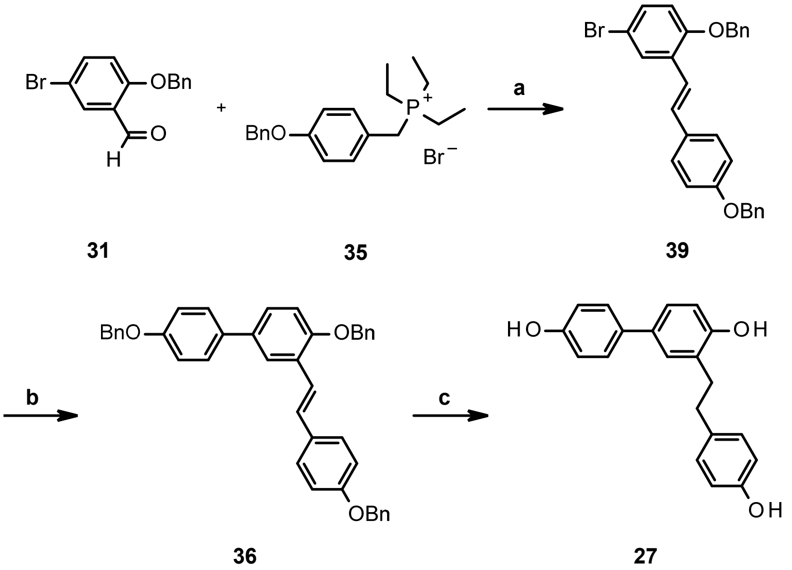

*Scheme 5: Optimized reaction sequence towards biphenol **27** by interchanging two reaction steps. Reaction conditions: (a) NaOH, H_2O, 70 °C, 6 h, 97%, (b) 4-benzyloxyphenylboronic acid, Na_2CO_3, $Pd(PPh_3)_4$, LiCl, DME/H_2O, 80 °C, 19 h, 44%, (c) 10% Pd/C, 5 bar H_2, r.t., 20 h, 86%.*

Comparing the two synthetic pathways for biphenol **27**, the first pathway is less convenient due to purification issues resulting from the incomplete conversion of the Wittig reaction. Still, an overall yield of 8% was achieved over 8 reaction steps. The optimized route towards the final product results in an overall yield of 36% over 6 reaction steps.

Biphenol derivative **27** was dissolved in DMSO (100 µM). This solution was added portionwise to the GDP-bound Rheb protein dissolved in an aqueous buffer solution as described in Chapter 4.1. During the titration, a colorless precipitate was observed. This either implies denaturation of the protein or precipitation of the ligand. The measurement showed that the protein was unimpaired. Consequently, the ligand had precipitated from the aqueous solution. This can be explained with the unpolar character of 3-(4-hydroxyphenyl)ethyl-4,4’-biphenol (**27**), which consists of three phenol rings. The substance is not soluble in water although it contains three hydroxy groups. Consequently, the excess shown in Figure 26 for each of the titration steps does not correlate with the amount of compound in solution, which can interact with the protein. As a consequence, the k_D value calculated from the NMR measurement (1.4 ± 0.6 mM) undervalues the actual efficacy of the compound.

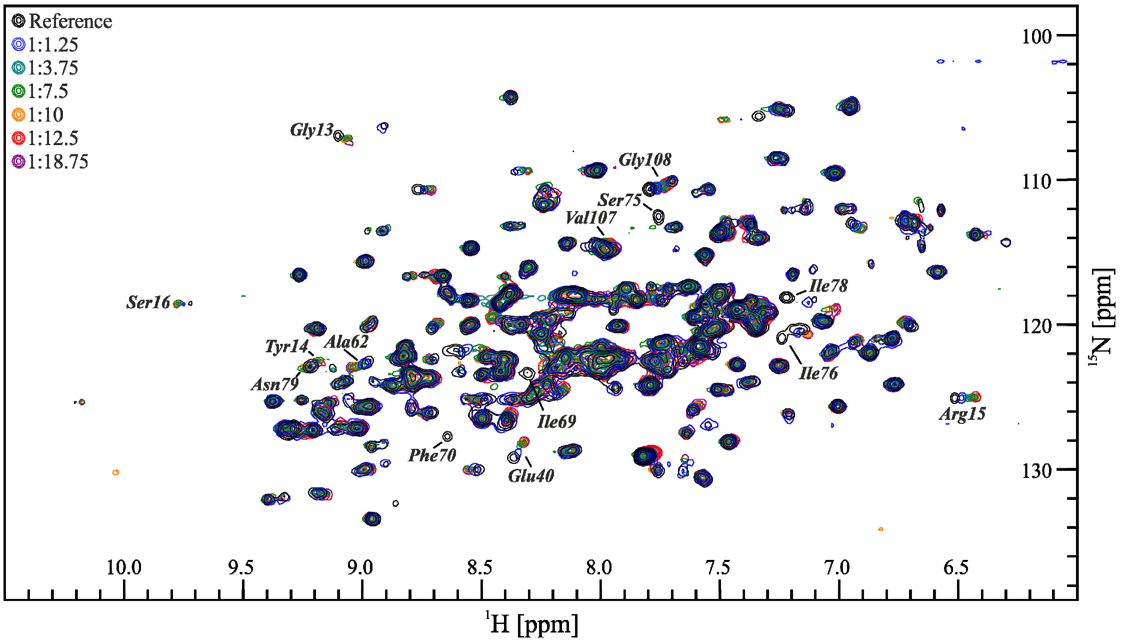

*Figure 26: ^{1}H,^{15}N-TROSY NMR overlay of the titration steps of biphenol derivative **27** to the Rheb protein.*[102]

The binding mode of the compound in comparison to 4,4'-biphenol (**22**) can be deduced from the shifts in the NMR measurement shown in Figure 26. As has been shown for the lead compound (**22**), the ligand binding pocket is strongly affected by ligand interaction. Additionally, allosteric effects cause shifts of amino acids in the nucleotide binding pocket. Those shifts indicate the intensity of the interaction with the protein as they depend on the strength of the direct effect of the ligand. Important shifts of the ligand binding pocket, which were used for the HADDOCK calculation, include residues Ile78 and Gly108 while other peaks get extinct by ligand addition (Ile69, Phe70, Ser75 and Ile76).

This makes interpretation of the NMR measurement difficult, as the disappearance of those peaks can have different causes. One possible explanation is a slow or intermediate exchange mechanism for ligand binding in case of 3-(4-hydroxyphenyl)ethyl-4,4'-biphenol (**27**). This leads to line broadening of the original peak upon ligand addition. A new peak arises increasing in intensity as the protein is close to saturation with the ligand. The saturated state has probably not been reached, because biphenol derivative **27** precipitates from the aqueous buffer solution. This leaves the peaks in the "line-broadened" state.[103] Another explanation is that the peaks shift by such a large range that identification of the shifted peaks is impossible. Consequently, it can be concluded that 3-(4-hydroxyphenyl)ethyl-4,4'-biphenol (**27**) interacts with the protein, although the k_D value is in the low millimolar range. Both, the shifting and the missing peaks indicate a binding mode similar to 4,4'-biphenol (**22**). In contrast, none of the conformations of the HADDOCK model (Figure 27) are in accordance with that. The biphenyl core is not inserted deeply into the pocket as shown for 4,4'-biphenol (**22**). Instead, the biphenyl core interacts with the upper edge (Ile69, Ser75 and Ile76) of the binding cleft while the hydroxy group of the side chain is inserted deeply. Additionally, the compound is poorly soluble in water due to the extended aryl-/alkyl-system. Summed up, attachment of a (4-hydroxyphenyl)ethyl side chain did not lead to an improvement of the binding affinity of the ligand **27**. Consequently, a different approach for improving the binding affinity of the biphenol derivative was envisaged.

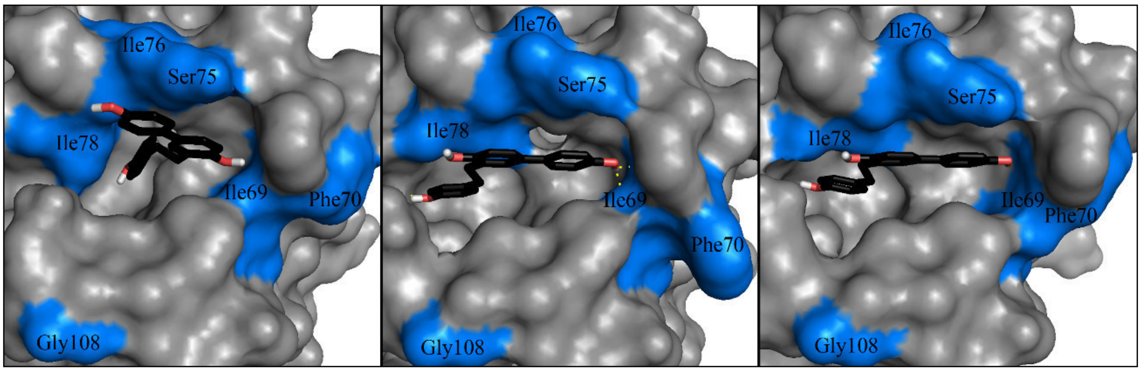

Figure 27: Conformations of 3-(4-hydroxyphenyl)ethyl-4,4'-biphenol (27) predicted by HADDOCK.[44] The residues of the protein, which were used for the calculation, are highlighted in blue.

4.2.1.1. Interpretation of HADDOCK output

After successful completion of a HADDOCK run, the refined structures are automatically sorted into clusters. Although it often applies, the different clusters are not in accordance with the various binding sites. In the web interface, the ten best clusters are sorted by their corresponding HADDOCK score starting with the best cluster. Cluster 1 always contains the most structures, but it is not necessarily the cluster with the highest HADDOCK score.

In case of the HADDOCK run performed for 3-(4-hydroxyphenyl)ethyl-4,4'-biphenol (**27**), Cluster 1 contains 101 of 400 refined structures with the highest HADDOCK score of 38.1 ± 2.7. The HADDOCK score of the second best cluster (30.9 ± 4.0) does unfortunately not lie within the margin of error of the best cluster. Another criteria for the quality of the calculation is the distribution of the refined structures. Figure 28 **A** shows that the structures are scattered over the surface of the protein. Only part of the molecules occupy the targeted binding pocket, which is highlighted by one structure shown in blue and as ball-and-stick model. A large number of structures is located to the left of the targeted binding cleft.

Additionally, HADDOCK automatically prepares diagrams, which show the statistics of the calculation. Figure 28 **B** correlates the calculated HADDOCK score for each structure and each cluster with the interface-ligand RMSDs (Root-Mean-Square Deviation). Figure 28 **C** shows the AIR energy term plotted against the mean interface deviation (i-RMSD). In both cases, the energy terms as well as the deviation should be as low as possible. This indicates strong interaction with the protein. The clusters (indicated in colour in the graphs) are calculated based on the interface-ligand RMSDs calculated by HADDOCK, with the interface defined automatically based on all observed contacts. In case of Figure 28, Cluster 1 clearly contains the best structures.

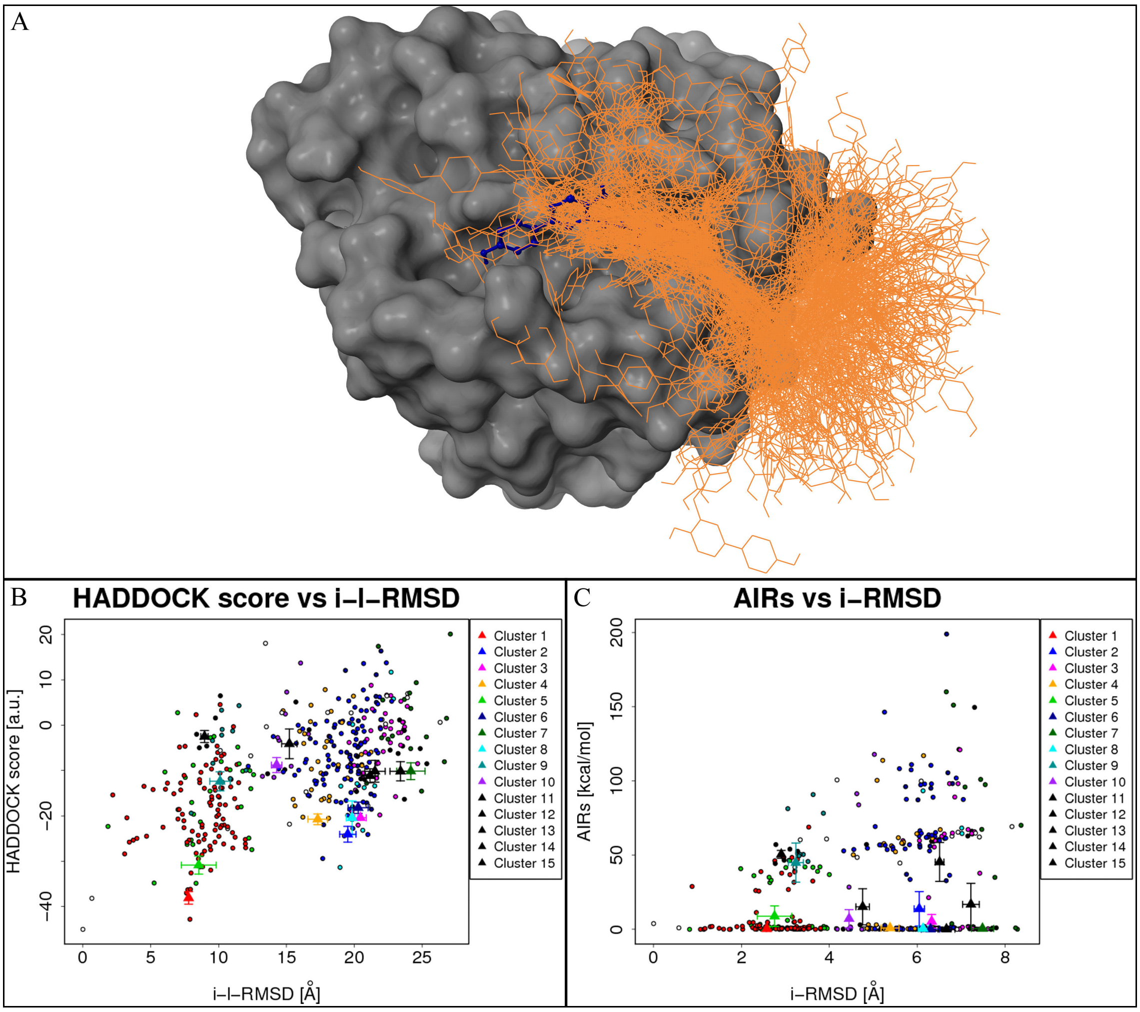

Figure 28: ***A****: Distribution of all 400 refined structures of 3-(4-hydroxyphenyl)ethyl-4,4'-biphenol (27), which were docked to the Rheb protein by HADDOCK. One structure is shown in blue and as ball-and-stick model to highlight the targeted binding pocket.* ***B+C****: Structural analysis is made with respect to the HADDOCK model with the lowest HADDOCK score. The cluster averages and standard deviations are indicated by coloured dots with associated error bars. The average values are calculated on the best 4 structures of each cluster (based on the HADDOCK score).*

4.2.2. Direct attachment of additional hydroxy groups

The first approach to improve the binding affinity of biphenol **22** by introducing a hydroxyphenyl group failed. Direct attachment of further hydroxy groups onto the biphenol core was chosen for the next attempt. These should be able to form further hydrogen bonds to the surrounding amino acids depending on the orientation of the higher substituted phenyl ring. Therefore, biphenol derivatives **40-47** with up to two additional hydroxy groups were docked into a GDP-free form of the Rheb protein by both Glide and Autodock/VINA.

*Table 3: Second iteration of biphenol derivatives 40-47 applied to molecular modelling with Glide and Autodock/VINA using 4,4'-biphenol (**22**) as reference.*

Substance	**Structure**	**Glide Score**		**VINA Score**	
		max	min	max	min
4,4'-Biphenol (22)		-5.60		-6.0	-4.6
3-Hydroxy-4,4'-biphenol (40)	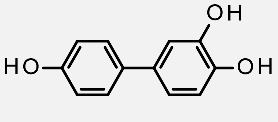 **40**	-7.78	-6.05	-6.4	-5.1
2-Hydroxy-4,4'-biphenol (41)	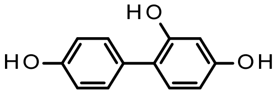 **41**	-6.57	-6.39	-6.2	-5.6
2,2'-Dihydroxy-4,4'-biphenol (42)	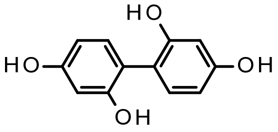 **42**	-6.49	-6.44	-6.1	-5.3
3,3'-Dihydroxy-4,4'-biphenol (43)	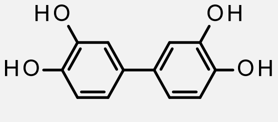 **43**	-8.32	-7.58	-6.5	-5.3
2,3'-Dihydroxy-4,4'-biphenol (44)	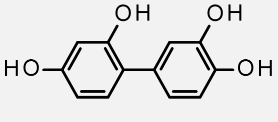 **44**	-7.79	-7.52	-6.4	-5.3
2,5-Dihydroxy-4,4'-biphenol (45)	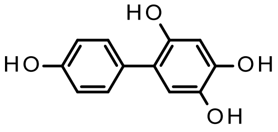 **45**	-6.37	-5.62	-6.3	-5.4
3,5-Dihydroxy-4,4'-biphenol (46)	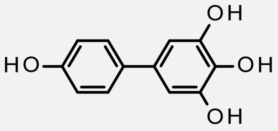 **46**	-7.21		-6.2	-5.4
2,6-Dihydroxy-4,4'-biphenol (47)	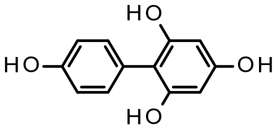 **47**	-6.59	-5.43	-5.7	-5.1

As can be seen from Table 3, most of the *in silico* hits (except for 2,6-dihydroxy-4,4'-biphenol (**47**) regarding the VINA score) show increased scores both in Glide and VINA docking compared to 4,4'-biphenol (**22**). Remarkably, biphenols carrying at least one additional hydroxy group in *ortho*-position such as compounds **40**, **43**, **44** and **46** **(**highlighted in grey in Table 3**,** depicted in Figure 29) show the highest scores. In contrast, introducing a hydroxy group in *meta*-position is not as effective as in *ortho*-position.

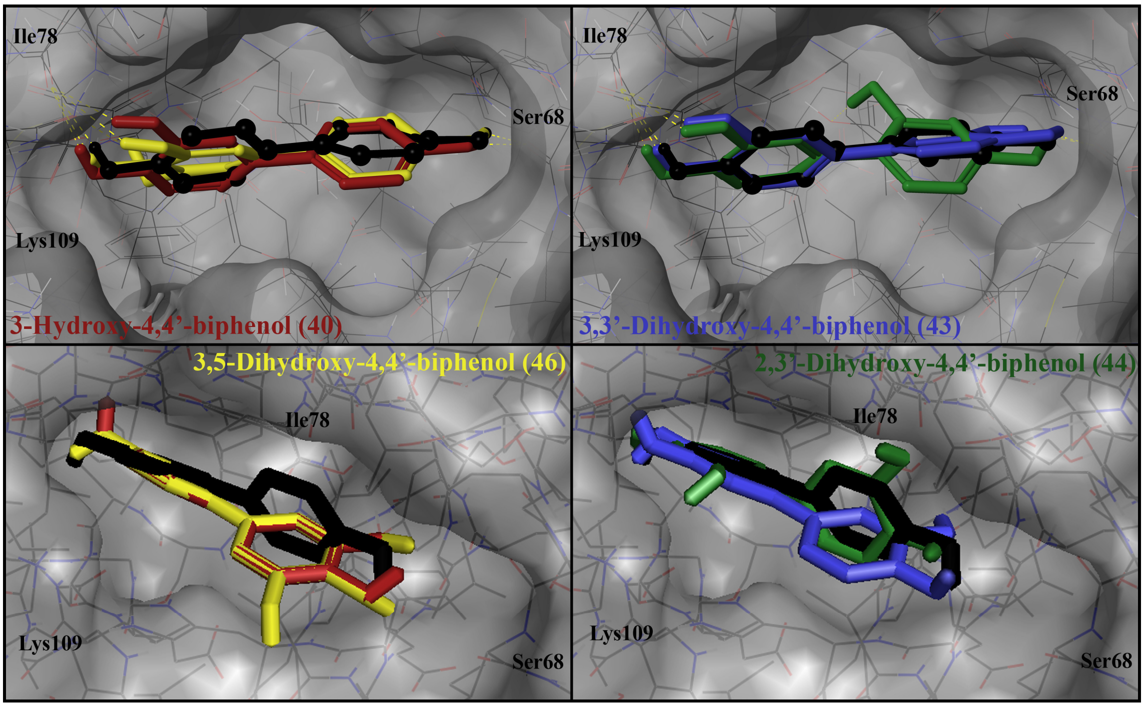

*Figure 29: Comparison of the binding modes predicted by Glide (top) and Autodock/VINA (bottom) of 3-hydroxy-4,4'-biphenol (**40**, red), 3,3'-dihydroxy-4,4'-biphenol (**43**, blue), 2,3'-dihydroxy-4,4'-biphenol (**44**, green) and 3,5-dihydroxy-4,4'-biphenol (**46**, yellow) in the binding pocket of the Rheb protein with 4,4'-biphenol (**22**, black) as reference.*

3,3'-Dihydroxy-4,4'-biphenol (**43**) and 2,3'-dihydroxy-4,4'-biphenol (**44**) together with 3-hydroxy-4,4'-biphenol (**40**) show the highest scores both in VINA and Glide. Although 3-hydroxy-4,4'-biphenol (**40**) does not exhibit the best docking score, it constitutes the most reasonable compound to be synthesized as it requires the least structural modifications in comparison to the lead structure 4,4'-biphenol (**22**). To collect SAR information, stepwise introduction of additional functional groups is required. Additionally, the other two structures, 3,3'-dihydroxy-4,4'-biphenol (**43**) and 2,3'-dihydroxy-4,4'-biphenol (**44**), were also selected for synthesis as they incorporate the core structure of 3-hydroxy-4,4'-biphenol (**40**).

In contrast to the synthesis described before, methoxy groups have been chosen as protecting group for the hydroxy moieties due to the availability of the corresponding boronic acid and anisole derivatives. Although this protecting group offers the best atom economy, it requires harsh deprotection conditions. These are difficult especially for more sensitive organic compounds.

As described before, Suzuki coupling[104] of the two phenol rings was carried out using palladium on charcoal, the phase transfer catalyst 18-crown-6 and potassium carbonate (Scheme 6). After chromatographic purification, the protected biphenol **50** was obtained in 73% yield. Cleavage of the methoxy groups was achieved by addition of the Lewis acid boron tribromide at -78 °C.[105]

The reaction gave the desired 3-hydroxy-4,4’-biphenol (**40**) in good yield of 83%. For the two-step synthesis of biphenol **40** an overall yield of 61% was obtained.

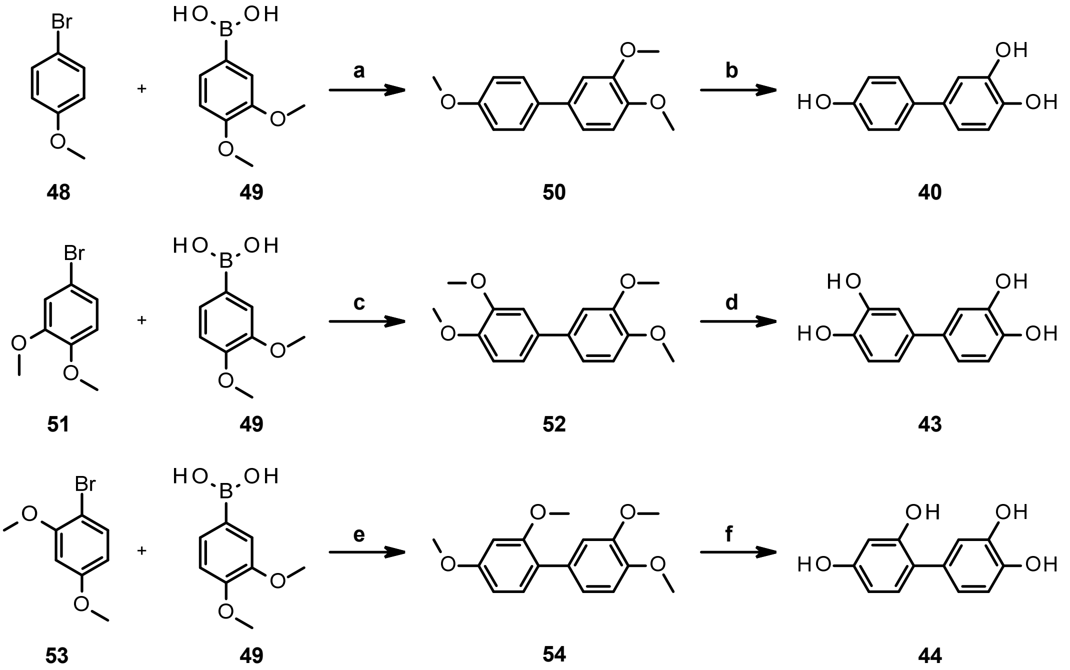

Scheme 6: Reaction sequence to biphenol derivatives ***40****,* ***43*** *and* ***44****. Reaction conditions: (a) K_2CO_3, 10% Pd/C, 18-crown-6, MeOH/H_2O, 45 °C, 1.5 h, 73%, (b) 1 M boron tribromide in DCM, DCM, -78 °C → r.t., 19 h, 81%, (c) K_2CO_3, 10% Pd/C, 18-crown-6, MeOH/H_2O, 45 °C, 3 h, 65% (d) 1 M boron tribromide in DCM, DCM, -78 °C → r.t., 20 h, 91%, (e) K_2CO_3, 10% Pd/C, 18-crown-6, MeOH/H_2O, 45 °C, 5 h, 69%, (f) 1 M boron tribromide in DCM, DCM, -78 °C → r.t., 20 h, 44%.*

Similarly, the Suzuki reaction[104] of boronic acid **49** with 2,4-dimethoxybromobenzene (**53**) or 3,4-dimethoxybromobenzene (**51**), respectively, gave the desired biphenyl compounds **52** and **54** in good yields. Subsequent deprotection of the methoxy groups with boron tribromide afforded phenols **43** (91%) and **44** (44%).[105] The overall yield of the symmetric biphenol derivative **43** was 59%, while the asymmetric analogue **44** was obtained in 30% overall yield.

3-Hydroxy-4,4’-biphenol (**40**), 3,3’-dihydroxy-4,4’-biphenol (**43**) and 2,3’-dihydroxy-4,4’-biphenol (**44**) were titrated to the GDP-bound Rheb protein as shown in Figure 30. The relevant shifting residues are labeled in the NMR spectra. The three molecules induce the same amino acids to shift as 4,4’-biphenol (**22**). Comparing the spectra, it has to be noted that 3-hydroxy-4,4’-biphenol (**40**) obviously induces the largest shifts throughout the whole spectrum for example on Ile76 and Ile78 (Figure 30 **A**). Those two residues are also affected by 3,3’-dihydroxy-4,4’-biphenol (**43**) and 2,3’-dihydroxy-4,4’-biphenol (**44**) as can be seen from Figure 30 **B** and **C**, but to a smaller extent.

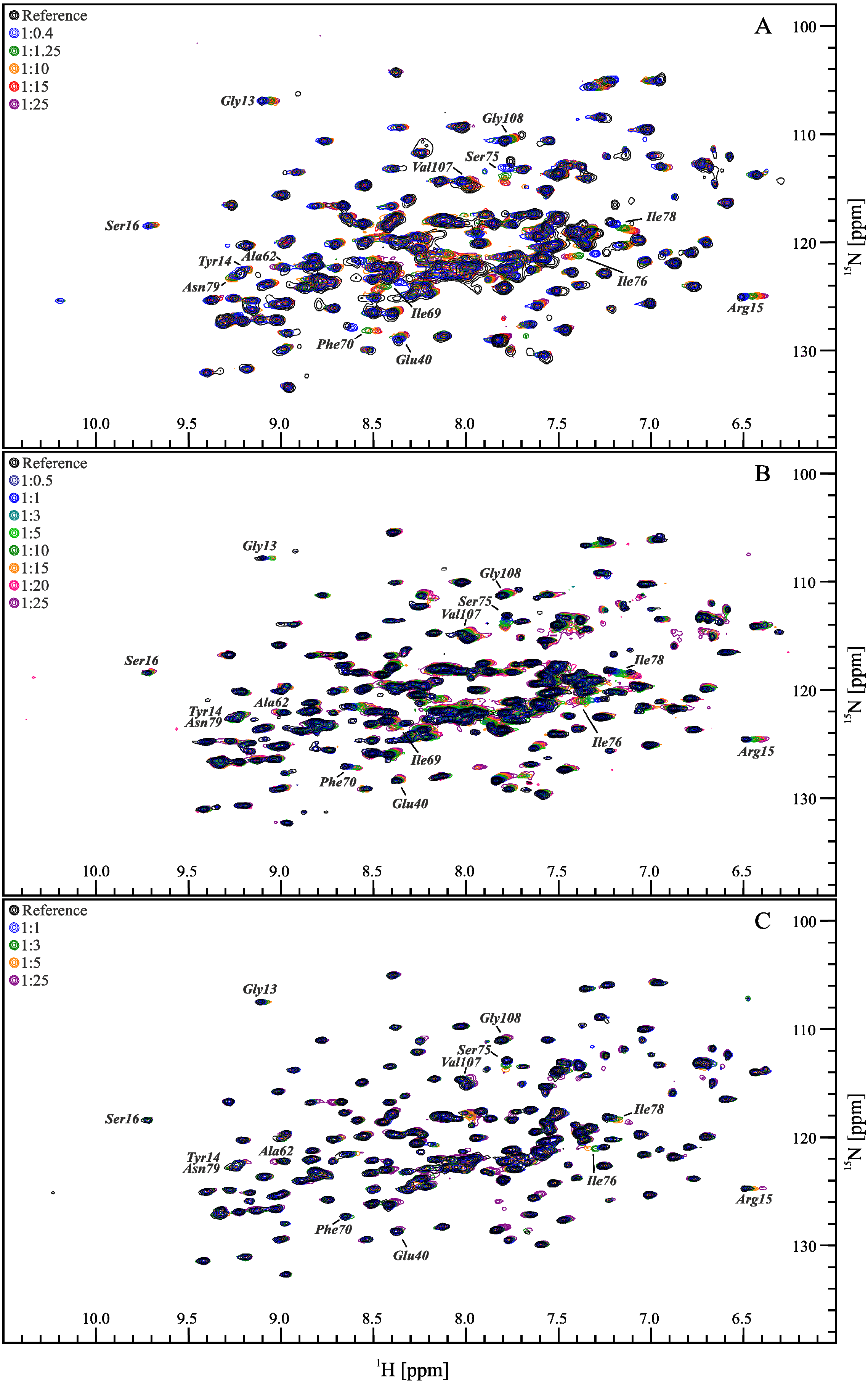

*Figure 30: ^{1}H,^{15}N-TROSY NMR overlay of the titration steps of biphenols **A: 40**[102], **B: 43** and **C: 44**[106].*

This observation hints towards a weaker k_D value for the two higher substituted biphenols in comparison to 3-hydroxy-4,4'-biphenol (**40**). The spectra show significant shifts for amino acids Ile69, Phe70, Ser75, Ile76 and Ile78 as well as Gly108 confirming that the compounds bind to the designated binding pocket. Furthermore, a shift can be observed for Val107, although the effect on this residue located in the binding pocket of the ligand is less significant. Due to allosteric effects, residues next to the nucleotide binding pocket (Gly13, Tyr14, Arg15, Ser16, Glu40 and Ala62) are also affected by the interaction with these ligands. Unfortunately, the hydrogen bond to Lys109 cannot be confirmed by the NMR measurements as the peak for this residue is located in an area of low resolution. Nevertheless, comparing the shift mode of the three biphenols, the shifts caused by biphenol **40** are more distinct than those of the two other compounds. This indicates a higher affinity to the protein. This assumption is confirmed by the k_D values (229 ± 16 µM (**40**), 2.18 ± 1.07 mM (**43**), 2.55 ± 1.17 mM (**44**)) determined from the NMR measurements.

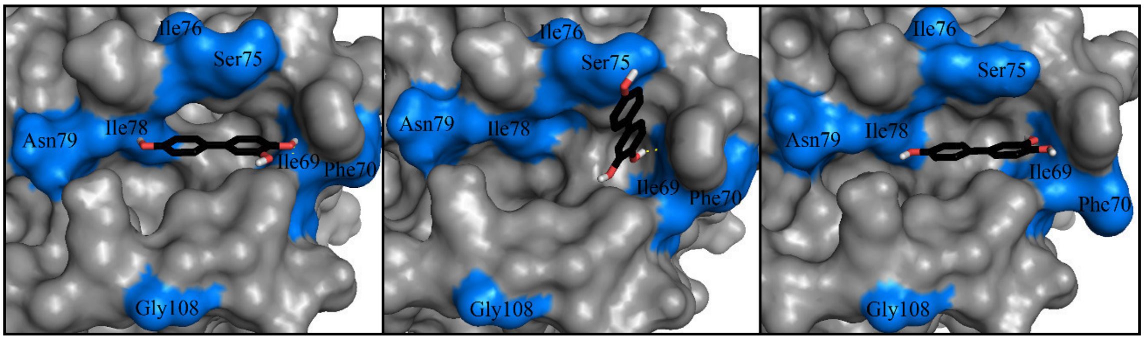

*Figure 31: Conformation of 3-hydroxy-4,4'-biphenol (**40**) predicted by HADDOCK.*[44] *The residues of the protein, which were used for the calculation, are highlighted in blue.*

The HADDOCK models (Figure 31 - Figure 33) show that mainly a similar binding mode as described for biphenol **22** can be adopted by these molecules. For each of the compounds, HADDOCK predicts conformations where the biphenyl core is inserted deeply into the pocket. Additionally, the biphenyl core can be inserted vertically into the ligand binding pocket. In case of 3-hydroxy-4,4'-biphenol (**40**), an interaction with Ile69 (Figure 31) to the right of the binding pocket is predicted while 3,3'-dihydroxy-4,4'-biphenol (**43**) interacts with Ile78 (Figure 32).

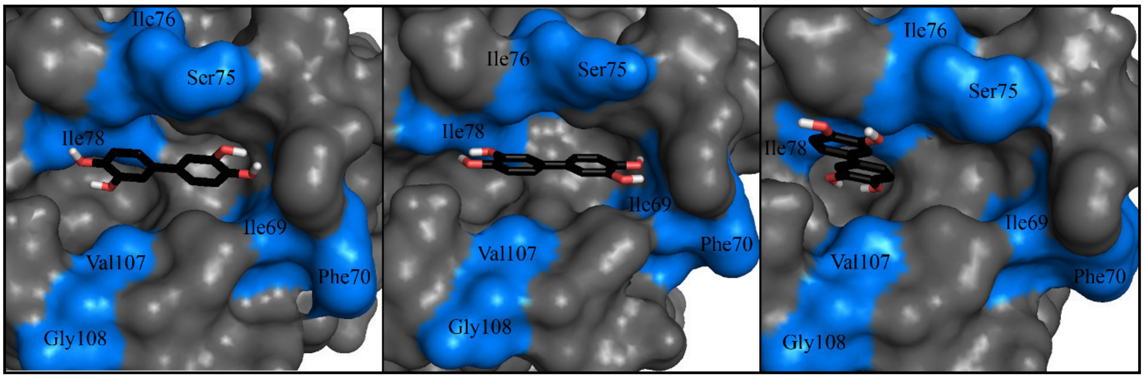

*Figure 32: Conformation of 3,3'-dihydroxy-4,4'-biphenol (**43**) predicted by HADDOCK.[44] The residues of the protein, which were used for the calculation, are highlighted in blue.*

The prediction of the binding mode of 2,3'-dihydroxy-4,4'-biphenol (**44**) is more inconsistent (Figure 31). Also, the molecule cannot be inserted into the binding pocket as deeply as the other two. This observation is also reflected in the weaker dissociation constant of this compound.

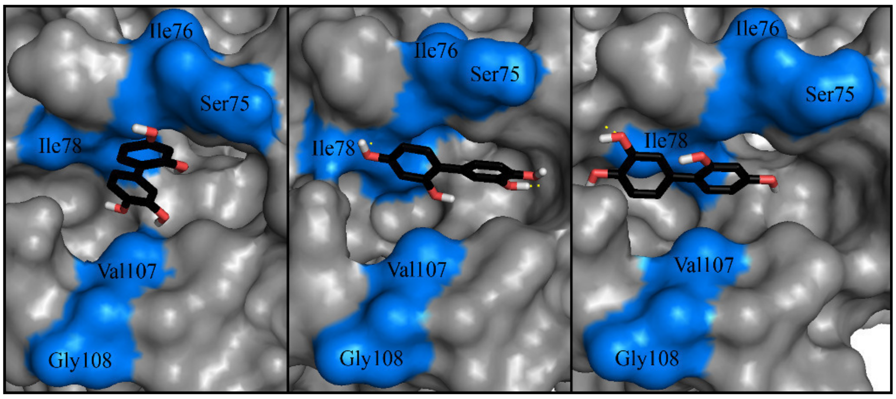

*Figure 33: Conformation of 2,3'-dihydroxy-4,4'-biphenol (**44**) predicted by HADDOCK.[44] The residues of the protein, which were used for the calculation, are highlighted in blue.*

Consequently, the prediction via molecular modelling has been verified by NMR experiments and the resulting dissociation constants for the complex of the Rheb protein with biphenols **40**, **43** and **44**. Significant differences can be noticed for the three ligands rendering 3-hydroxy-4,4'-biphenol (**40**) the best compound found in this iteration also with regard to the ligand efficiency.

4.2.3. Installation of further hydroxy groups via a methylene moiety

Improvement of the interaction of the lead structure 4,4'-biphenol (**22**) with Rheb was achieved by the introduction of a third hydroxy group to form an additional hydrogen bond to Ile78. As the second docking (Table 3) has shown, a further hydroxy group increases the score of the compounds significantly. Although, 3,3'-dihydroxy-4,4'-biphenol (**43**) exhibits a comparatively high docking score, it only forms three hydrogen bonds as does 3-hydroxy-4,4'-biphenol (**40**). This consideration also reveals that elongating the hydroxy group towards the protein with a spacer group such as a methylene residue might enable the ligand to form further hydrogen bonds to the protein. Therefore, ligands containing up to two hydroxymethyl groups were screened. The results of this third docking iteration are shown in Table 4.

Table 4: Third iteration of biphenol derivatives 55-59 applied to molecular modelling with Glide and Autodock/VINA using 4,4'-biphenol (22) as reference.

Substance	Structure	Glide Score		VINA Score	
		max	min	max	min
4,4'-Biphenol (22)		-5.60		-6.0	-4.6
3-Hydroxy-3'-hydroxymethyl-4,4'-biphenol (55)	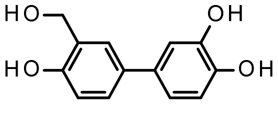 **55**	-7.51		-6.7	-5.3
3-Hydroxy-2'-hydroxymethyl-4,4'-biphenol (56)	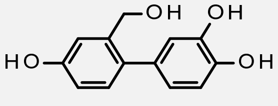 **56**	-7.88		-6.7	-5.5
3-Hydroxy-2',5'-dihydroxymethyl-4,4'-biphenol (57)	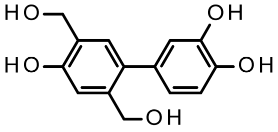 **57**	-7.26	-6.59	-6.3	-5.5
3-Hydroxy-3',5'-dihydroxymethyl-4,4'-biphenol (58)	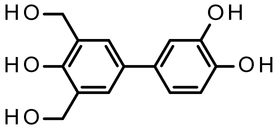 **58**	-7.55		-6.1	-5.3
3-Hydroxy-2',6'-dihydroxymethyl-4,4'-biphenol (59)	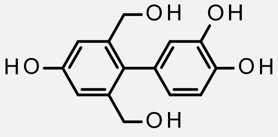 **59**	-8.03	-6.49	-6.1	-5.2

Both mono-substituted hydroxymethylbiphenols **55** and **56** show good docking scores with Glide in the same range as 3-hydroxy-4,4'-biphenol (**40**) while the VINA scores are even slightly increased. Also, the compounds show an additional hydrogen bond to either Tyr74 or Tyr67. Regarding the orientation of the phenyl rings, 2-hydroxymethylbiphenol **56** and 3-hydroxy-2',6'-dihydroxymethyl-4,4'-biphenol (**59**) adopt the same positioning as 3-hydroxy-4,4'-biphenol (**40**) in Glide (Figure 34), orienting the dihydroxy substituted phenyl ring towards Ile78. In contrast, 3-hydroxymethylbiphenol **55** is predicted to form two hydrogen bonds to Ser68 instead. This might be an explanation for the minute difference in docking scores. Nevertheless, 3-hydroxy-2',6'-dihydroxymethyl-4,4'-biphenol (**59**) only exhibits a weaker VINA score, excluding it as a potential compound for the third iteration. Consequently, 3-hydroxy-3'-hydroxymethyl-4,4'-biphenol (**55**) and 3-hydroxy-2'-hydroxymethyl-4,4'-biphenol (**56**) were chosen as they allow for a straightforward synthesis.

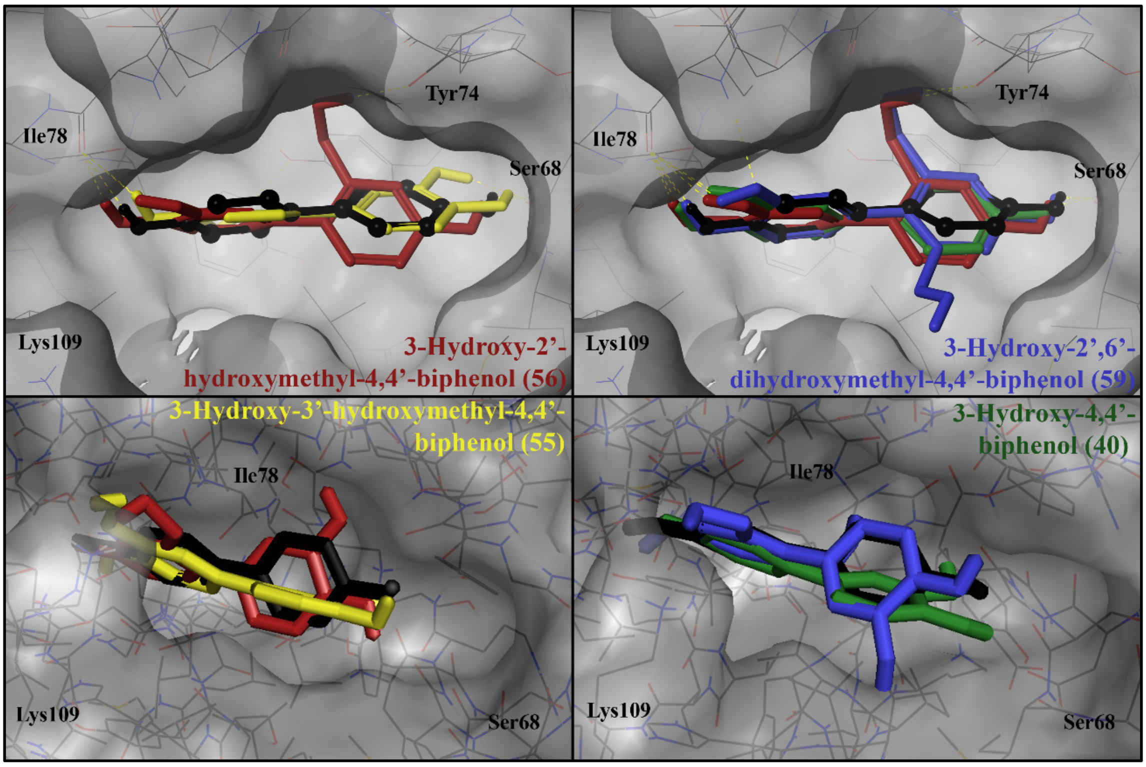

*Figure 34: Comparison of the binding modes predicted by Glide (top) and Autodock/VINA (bottom) of 3-hydroxy-3'-hydroxymethyl-4,4'-biphenol (**55**, yellow), 3-hydroxy-2'-hydroxymethyl-4,4'-biphenol (**56**, red) and 3-hydroxy-2',6'-dihydroxymethyl-4,4'-biphenol (**59**, blue) in the binding pocket of the Rheb protein with 3-hydroxy-4,4'-biphenol (**40**, green) and 4,4'-biphenol (**22**, black) as reference.*

Synthesis of benzyl alcohol **56** was achieved starting from the corresponding ester **63**, which can be obtained from the Suzuki coupling of anisole derivative **62** with boronic acid **49**. Ester **62** has to be synthesized from 5-hydroxyanthranilic acid (**60**) in a two-step procedure as described by Aoyama *et al.*[107] as it is not commercially available. Therefore, aniline **60** was converted to the corresponding iodide **61** via a Sandmeyer reaction (Scheme 7) in a good yield of 84%. In the next step, the acid and hydroxy functionalities were protected as methyl ester or ether, respectively, using dimethyl sulfate. The desired ester **62** was obtained in excellent yield of 98% after chromatographic purification. Suzuki coupling was carried out following the procedure by Mamane *et al.*[98] using tetrakis(triphenylphosphine) palladium(0), sodium carbonate and lithium chloride as reagents. Biphenol **63** was obtained in good yield of 89% after purification. Reduction of ester **63** to the corresponding benzyl alcohol **64** was accomplished by addition of lithium aluminum hydride giving the desired product in excellent yield (96%).[108] Subsequent deprotection of the hydroxy groups to afford alcohol **56** failed due to decomposition of the starting material during the reaction.

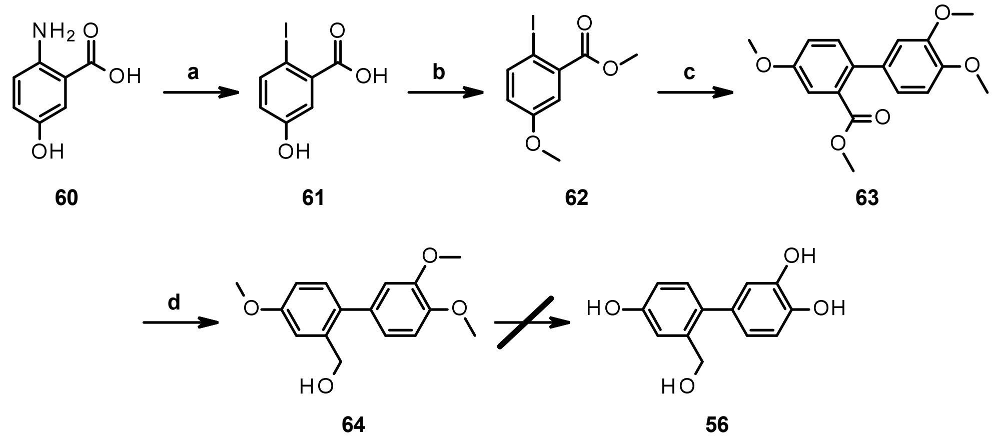

Scheme 7: First attempted route for the synthesis of biphenol ***56****. Reaction conditions: (a) conc. HCl, $NaNO_2$, KI, H_2O, 0 °C → 90 °C, 1.5 h, 84%, (b) K_2CO_3, dimethyl sulfate, acetone, reflux, 5 h, 98%, (c) 3,4-dimethoxybenzeneboronic acid* ***49****, $Pd(PPh_3)_4$, LiCl, Na_2CO_3, DME/H_2O, 80 °C, 15 h, 89%, (d) $LiAlH_4$, THF, 0 °C → r.t., 21 h, 96%.*

As an alternative route to benzyl alcohol **56**, the last two steps of the synthesis were interchanged (Scheme 8). The first cleavage reaction with boron tribromide[105] for the removal of all four methyl groups led to decomposition of the starting material. Therefore, other Lewis acids were applied to accomplish the desired deprotection. While aluminum trichloride[109] led to decomposition of the starting material**,** aluminum tribromide[110] gave the demethylated ester **65**. After chromatographic purification to afford ester **65** in 63% yield, reduction of the ester functionality to the corresponding benzyl alcohol **56** was conducted with lithium aluminum hydride (63%).[111] The overall yield for the synthesis of benzyl alcohol **56** amounts to 28% over 5 steps.

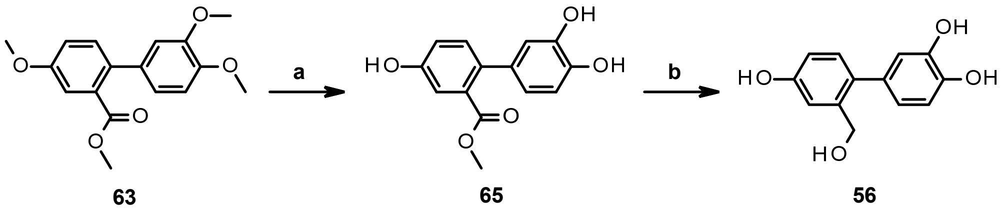

Scheme 8: Expedient routes to benzyl alcohol ***56****. Reaction conditions: (a) $AlBr_3$, toluene, 80 °C, 24 h, 63%, (b) $LiAlH_4$, THF, reflux, 18 h, 63%.*

The synthesis of the regioisomer **55** was first designed to follow a pathway equivalent to triphenol **56** (Scheme 9). Therefore, the corresponding ester **67** had to be synthesized from salicylic acid **66**. The acid and hydroxy functionalities were protected following the procedure applied before.[107] The pure ester **67** was obtained in excellent yield of 99%. Subsequent coupling was achieved under the same reaction conditions as used for the coupling of ester **62**. The Suzuki coupling of iodide **67** with boronic acid **49** gave the ester **68** in good yield of 90%. Reduction of the ester functionality to the corresponding benzyl alcohol **69** was accomplished by addition of lithium aluminum hydride as described before (90%).[108] Unfortunately, deprotection of benzyl alcohol **69** failed as described before for benzyl alcohol **64**.

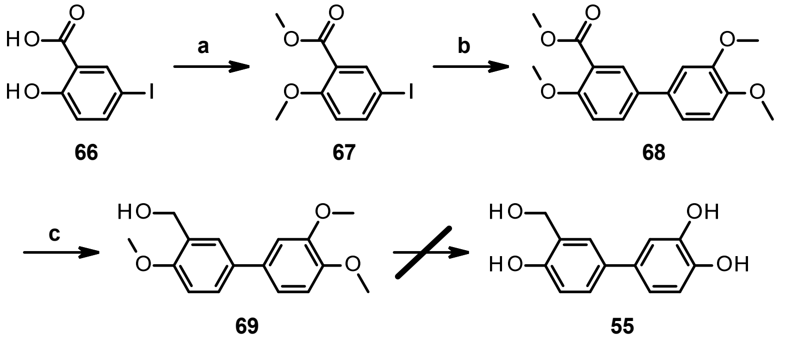

*Scheme 9: First attempt towards triphenol **55**. Reaction conditions: (a) dimethyl sulfate, K_2CO_3, acetone, reflux, 3 h, 99%, (b) 3,4-dimethoxybenzeneboronic acid **49**, $Pd(PPh_3)_4$, LiCl, Na_2CO_3, DME/H_2O, 80 °C, 19 h, 90%, (c) $LiAlH_4$, THF, r.t., 16.5 h, 90%.*

According to the synthesis of the regioisomer **56**, the order of reaction steps was interchanged. Deprotection of the methyl groups was achieved either by addition of boron tribromide solution[105] to afford the corresponding free acid **70** or by adding aluminum tribromide[110] to give ester **71** (Scheme 10). Free acid **70** (quant. yield) was used as obtained after work-up due to the high polarity of the compound, which impedes column chromatography on silica gel. In contrast, ester **71** could be purified chromatographically (76% yield). The subsequent reduction of the carbonyl groups of either acid **70** or ester **71** was carried out using lithium aluminum hydride.[111] In case of the free acid **70**, the desired benzyl alcohol **55** was obtained in a low yield of 22% while reduction of ester **71** led to a better yield of 36%. The yields are fairly low in both cases due to the high polarity of the target compound leading to massive tailing during chromatography. In conclusion, the desired benzyl alcohol could be synthesized utilizing two different pathways. The synthetic route passing through ester **71** was more convenient due to the easier chromatographic purification of the intermediate product. The overall yields differ only slightly with 18% via the free acid **70** and 22% via the ester **71**.

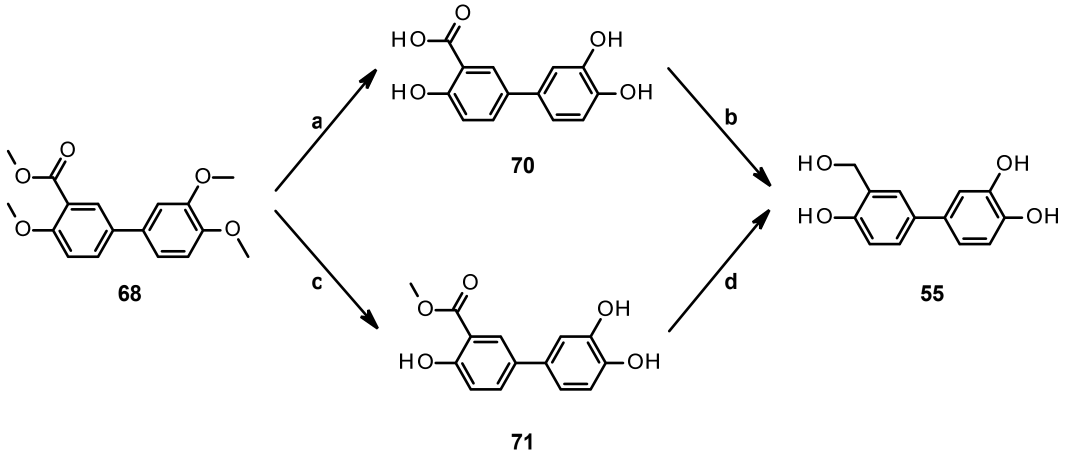

*Scheme 10: Two alternative routes towards the synthesis of benzyl alcohol **55**. Reaction conditions: (a) 1 M BBr_3 in DCM, DCM, -78 °C → r.t., 17 h, quant., (b) $LiAlH_4$, THF, reflux, 18.5 h, 22% (c) $AlBr_3$, toluene, 80 °C, 3 h, 76%, (d) $LiAlH_4$, THF, reflux, 14 h, 36%.*

Addition of an excess of biphenol **56** did not result in significant peak shifts of the Rheb protein in the NMR spectrum (Figure 36). The residues of the designated binding pocket, Ile76, Ile78 and Val107, only show minor shifts while other residues such as Phe70, Ser75 and Gly108 are not affected by ligand addition at all. Consequently, no allosteric effects on the residues forming the nucleotide binding pocket can be observed. In contrast to the prediction by both Glide and VINA, biphenol **56** only binds weakly to the protein. The HADDOCK model in Figure 35 shows that the ligand enters the binding pocket but is then not stabilized in the same way as has been observed for 3-hydroxy-4,4’-biphenol (**40**) and 4,4’-biphenol (**22**). In contrast, the molecule cannot be positioned in the centre of the binding pocket either losing interaction with Ile78 to one side or Phe70 to the other. This leads to a different orientation of the compound, which allows less interaction with the protein.

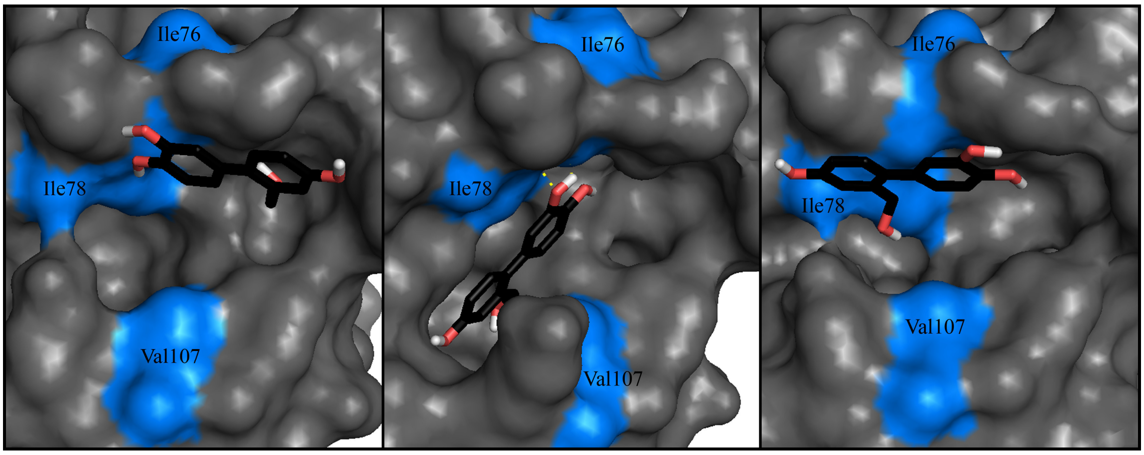

*Figure 35: Conformations of 3-hydroxy-2’-hydroxymethyl-4,4’-biphenol (**56**) predicted by HADDOCK.[44] The residues of the protein, which were used for the calculation, are highlighted in blue.*

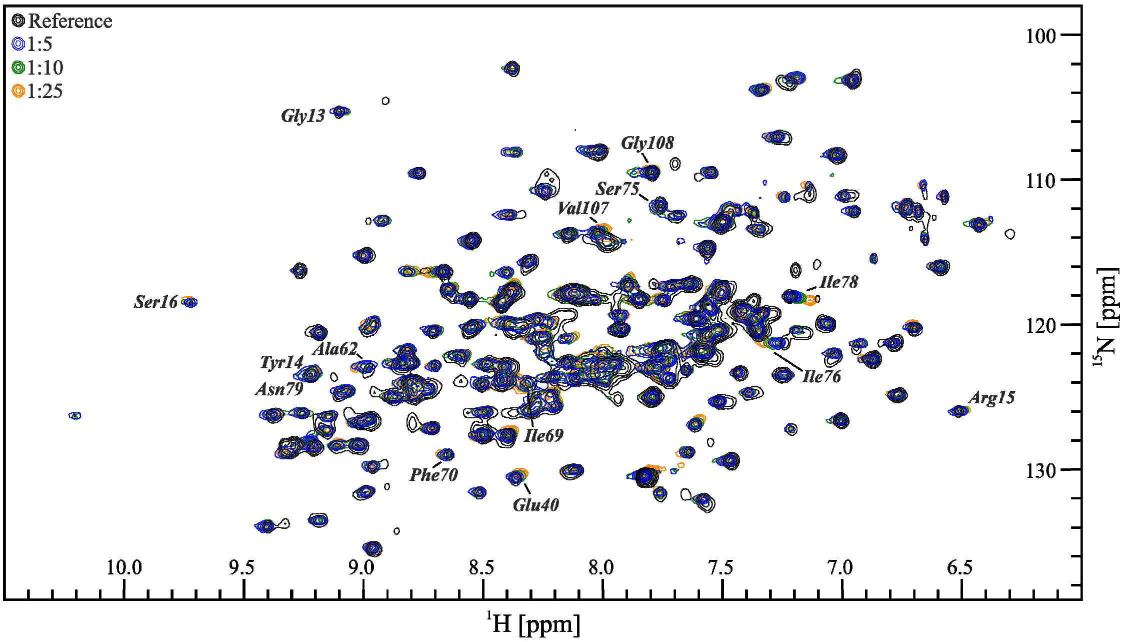

*Figure 36: ^{1}H,^{15}N-TROSY NMR overlay of the titration steps of benzyl alcohol **56** to the Rheb protein.[102]*

While VINA and Glide predicted benzyl alcohol **55** to bind to Rheb less strong than biphenol **56,** the titration experiment (Figure 38) proved otherwise. In contrast to biphenol **56**, benzyl alcohol **55** binds to Rheb as expected. Shifts of the amino acids Phe70, Ser75, Ile76, Ile78, Asn79, Val107 and Gly108 suggest a similar binding mode of benzyl alcohol **55** as has been shown for 4,4'-biphenol (**22**).

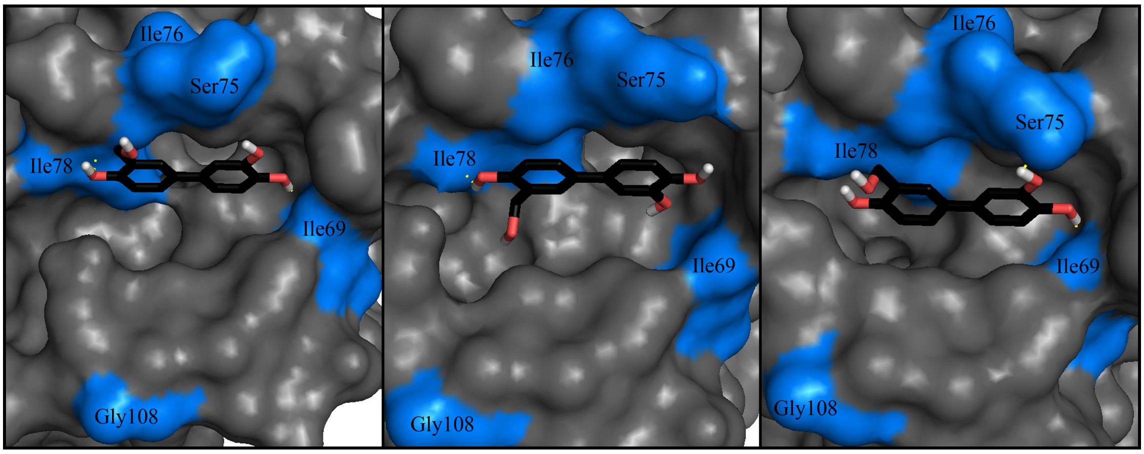

*Figure 37: Conformations of 3-hydroxy-3'-hydroxymethyl-4,4'-biphenol (**55**) predicted by HADDOCK.*[44] *The residues of the protein, which were used for the calculation, are highlighted in blue.*

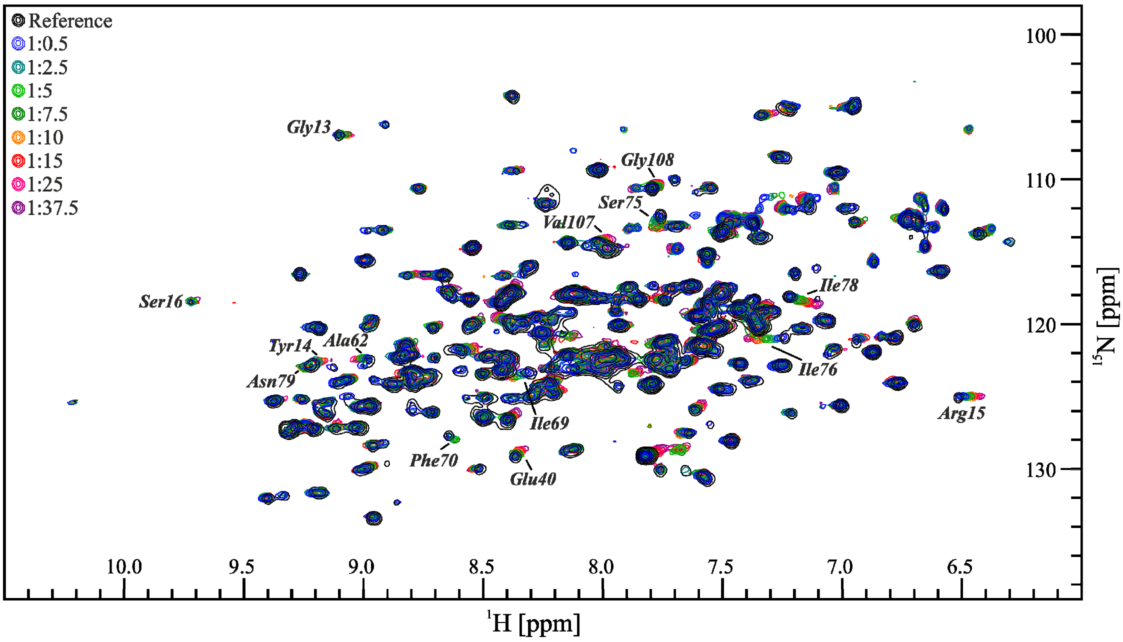

*Figure 38: ^{1}H,^{15}N-TROSY NMR overlay of the titration steps of benzyl alcohol **55** to the Rheb protein.*[102]

This is clearly confirmed by the HADDOCK model (Figure 37), which shows that the biphenyl core is inserted horizontally into the binding pocket. This allows for a hydrogen bond to Ile78 to be formed. Interaction with Ile69 depends on the orientation of the hydroxymethyl group. From the HADDOCK prediction, orientation towards Ile78 seems favourable to inserting it into the binding pocket. Nevertheless, a comparison of the shift range of the amino acids to the shifts caused by biphenol **40** (Figure 30) shows that the interaction of benzyl alcohol **55** with the protein is weaker. Interaction with Ile76 and Ile78 can be maintained by 3-hydroxy-3'-hydroxymethyl-4,4'-biphenol (**55**) as the HADDOCK model shows. In contrast, interaction with the other side (Ile69, Phe70) is weakened in comparison to 3-hydroxy-4,4'-biphenol (**40**). The k_D value (4.5 ± 0.5 mM) calculated from the NMR measurement clearly confirms this observation. Weak allosteric effects on the nucleotide binding pocket can also be observed (Gly13, Tyr14, Arg15, Ser16, Glu40, and Ala62), because the adopted binding mode is comparable to that of 4,4'-biphenol (**22**).

As the only structural difference between those two compounds is the hydroxymethyl group in 3-position, the loss in activity can be ascribed to this change. Thus, it can be assumed that the hydroxymethyl group is unable to form an additional hydrogen bond as confirmed by HADDOCK. Consequently, the structural change of compounds 3-hydroxy-2'-hydroxymethyl-4,4'-biphenol (**56**) and 3-hydroxy-3'-hydroxymethyl-4,4'-biphenol (**55**) has to be reconsidered as it did not result in an improved interaction with the protein.

4.2.4. Attachment of benzylaminomethyl residues as an alternative to hydroxy groups

As a result of the weaker interaction of the hydroxymethyl compounds **55** and **56** with Rheb, no additional hydroxymethyl derivatives of 4,4'-biphenol (**22**) have been synthesized. For further hydrogen bond formation, amines can also be introduced. Consequently, benzylaminomethyl residues were chosen as a new substituent for the biphenol lead structure **22** given that this group is a good hydrogen bond acceptor while unprotonated. Additionally, they offer the possibility to get partially protonated under physiological conditions to function as a hydrogen bond donor as well. The benzene ring can further interact through π,π-interactions with surrounding aromatic amino acid side chains such as Tyr67, Tyr74 or Tyr81 forming the bottom of the binding pocket. The results of the Glide and VINA docking of the various benzylaminomethyl derivatives **72**-**80** are shown in Table 5.

*Table 5: Fourth iteration of biphenol derivatives **72-80** applied to molecular modelling with Glide and Autodock/VINA using 4,4'-biphenol (**22**) as reference.*

Substance	Structure	Glide Score		VINA Score	
		max	min	max	min
4,4'-Biphenol (22)		-5.60		-6.0	-4.6
3-Hydroxy-3'-benzylaminomethyl-4,4'-biphenol (72)	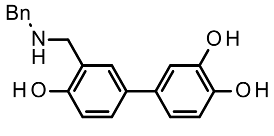 **72**	-6.85	-4.04	-6.9	-6.1

3-Hydroxy-2'-benzylaminomethyl-4,4'-biphenol (73)	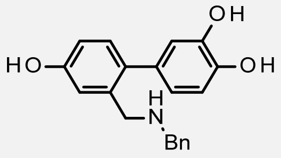 **73**	-7.94	-7.58	-6.8	-5.7
3-Hydroxy-2',5'-dibenzylaminomethyl-4,4'-biphenol(74)	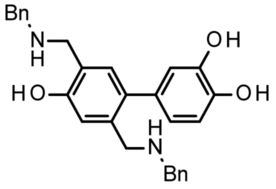 **74**	-7.12	-2.37	-7.1	-6.1
3-Hydroxy-3',5'-dibenzylaminomethyl-4,4'-biphenol (75)	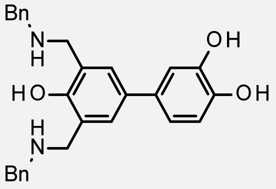 **75**	-9.96	-1.61	-6.6	-5.9
3-Hydroxy-2',6'-dibenzylaminomethyl-4,4'-biphenol (76)	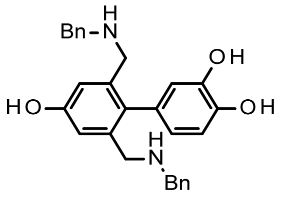 **76**	-8.07	-6.82	-6.8	-5.7
3-Hydroxy-2'-hydroxymethyl-5'-benzylaminomethyl-4,4'-biphenol (77)	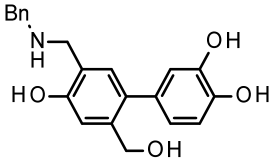 **77**	-5.05	-4.70	-6.6	-5.7
3-Hydroxy-2'-benzylaminomethyl-5'-hydroxymethyl-4,4'-biphenol (78)	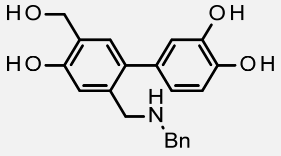 **78**	-8.94	-5.71	-7.1	-5.7
3-Hydroxy-3'-benzylaminomethyl-5'-hydroxymethyl-4,4'-biphenol (79)	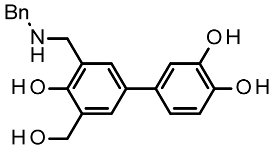 **79**	-8.02	-5.59	-7.0	-6.3
3-Hydroxy-2'-benzylaminomethyl-6'-hydroxymethyl-4,4'-biphenol (80)	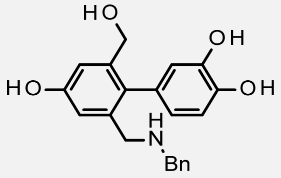 **80**	-8.24	-6.07	-7.1	-6.0

Derivatives **72** and **73** show good scores. Remarkably, the 2-position is again distinctly favoured, a fact that has already been disproven for hydroxymethyl derivative **56**. Introduction of two benzylaminomethyl groups into the biphenol structure yields 3-hydroxy-3’,5’-dibenzylaminomethyl-4,4’-biphenol (**75**), which exhibits the highest score obtained for any Glide docking so far. In contrast, an unsymmetrical combination of benzylaminomethyl groups in *ortho*- and *meta*-position results only in a minor improvement of the docking score in comparison to 3-hydroxy-3’-benzylaminomethyl-4,4’-biphenol (**72**). The combinations of one hydroxymethyl and one benzylaminomethyl group introduced into 3-hydroxy-4,4’-biphenol (**40**) show that the *meta*-position is significantly favoured for the benzylaminomethyl group in agreement with the result for 3-hydroxy-2’-benzylaminomethyl-4,4’-biphenol (**73**). In contrast to the binding mode adopted by the other biphenol derivatives, benzylaminomethyl substituted compounds are positioned differently in the ligand binding pocket to some extent (Figure 39). Usually the biphenol structure is inserted horizontally deeply into the binding cleft. The docking of the benzylaminomethyl derivatives predicts that, in most cases, only one phenyl ring will be vertically occupying the binding pocket while the rest of the space is filled with the benzylaminomethyl group. The amino group forms a hydrogen bond either to Ile76 or Tyr74 depending on the exact orientation.

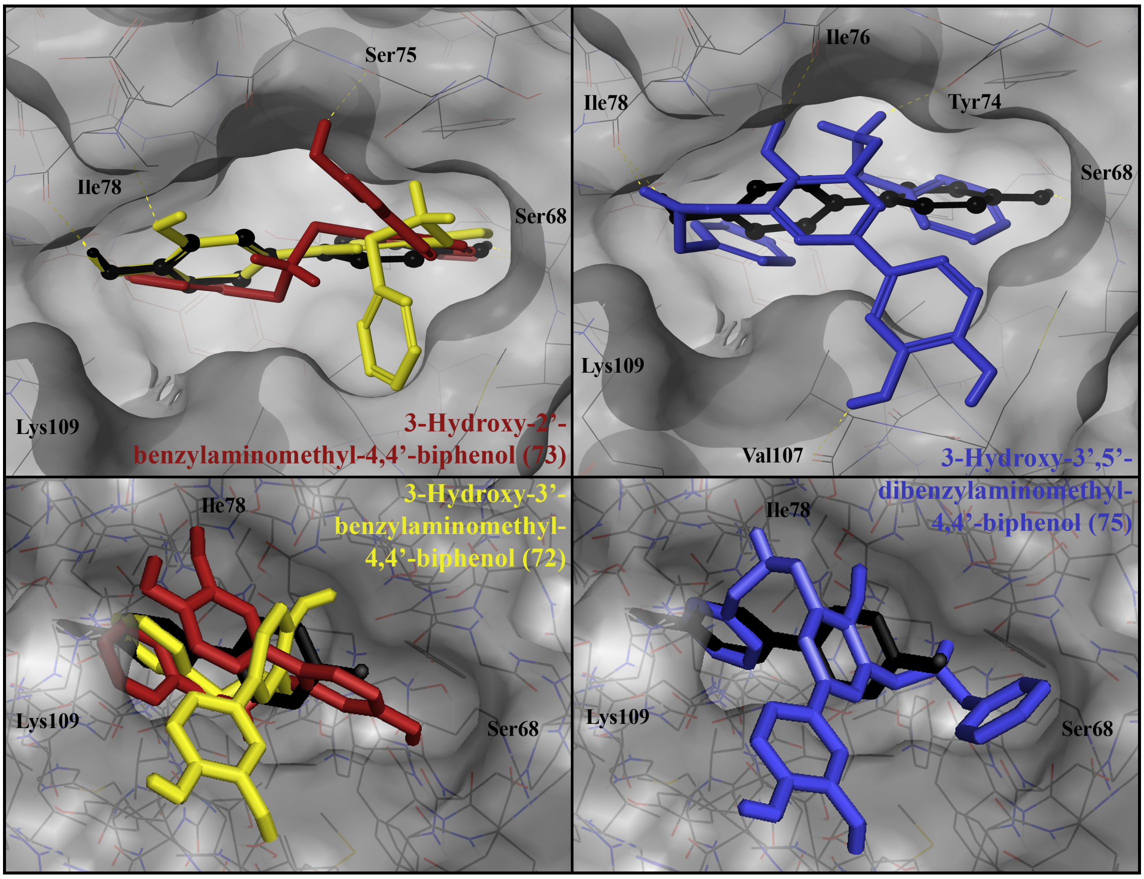

*Figure 39: Comparison of the binding modes predicted by Glide (top) and Autodock/VINA (bottom) of 3-hydroxy-3’-benzylaminomethyl-4,4’-biphenol (**72**, yellow), 3-hydroxy-2’-benzylaminomethyl-4,4’-biphenol (**73**, red) and 3-hydroxy-3’,5’-dibenzylaminomethyl-4,4’-biphenol (**75**, blue) in the binding pocket of the Rheb protein with 4,4’-biphenol (**22**, black) as reference.*

Taking into account that the docking has at least been questionable about the positioning of the hydroxymethyl group, both benzylaminomethyl-4,4'-biphenols **72** and **73** should be synthesized. From the results it can be deduced if compounds with one hydroxymethyl and one benzylaminomethyl group offer preferential binding properties. In addition to that, the different binding mode of the benzylaminomethyl compounds limits the access of the hydroxy groups to the amino acid residues, which have been included in hydrogen bonds so far, resulting in an overall less active compound.

The protecting group scheme was changed for this synthesis due to the issues with the cleavage of the methoxy groups of biphenols **55** and **56**. MEM ((2-methoxyethoxy)methyl) groups were chosen instead, because of the milder deprotection conditions (diluted HCl). In case of 3-benzylaminomethylbiphenol **72**, the synthesis proceeds from iodosalicylic acid **66** while 2-benzylaminomethylbiphenol **73** can be obtained from 5-hydroxyanthranilic acid **60**. Boronic acid **87** was synthesized according to Lin *et al.* and Kaller *et al.* from 5-bromo-2-hydroxybenzaldehyde (**30**) as it was not commercially available.[112,113]

Preparation of iodobenzene **82** (Scheme 11) proceeded from acid **66** by amide formation with benzylamine and EDC hydrochloride as coupling reagent.[114] The corresponding amide **81** was obtained in a good yield of 82% after chromatographic purification.

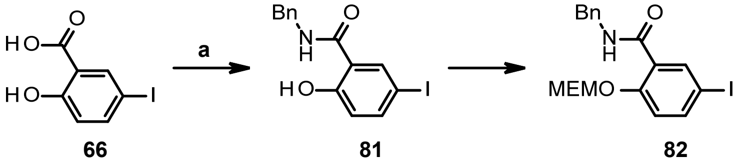

*Scheme 11: Synthesis of MEM protected iodobenzamide **82** from 4-iodosalicyclic acid (**66**). Reaction conditions: (a) benzylamine, EDC hydrochloride, HOBt, DCM, r.t., 19 h, 82%.*

Similarly, benzamide **83** was prepared from acid **61** (Scheme 12), which can be easily obtained from anthranilic acid derivative **60** as described above. Amide coupling was conducted in accordance to the synthesis of amide **81** by coupling with benzylamine using EDC hydrochloride.[114] The desired product was obtained in moderate yield of 67% after purification.

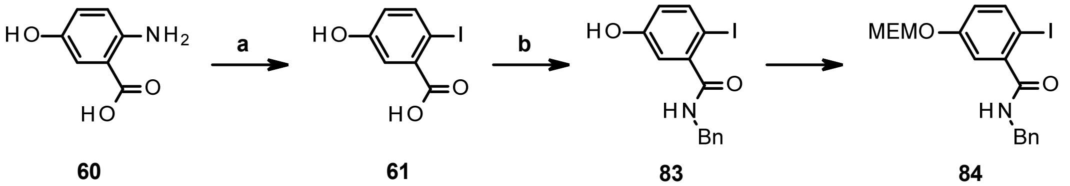

*Scheme 12: Synthesis of MEM protected iodobenzamide **84** from 4-hydroxyanthranilic acid (**60**). Reaction conditions: (a) conc. HCl, $NaNO_2$, KI, H_2O, 0 °C → 90 °C, 1.5 h, 84%, (b) benzylamine, EDC hydrochloride, HOBt, DCM, r.t., 19 h, 67%.*

For the synthesis of boronic acid **87** (Scheme 13), bromide **30** was chosen as starting material as bromide **85** is not commercially available due to its high sensitivity.[112] It was synthesized according to Kaller *et al.* from benzaldehyde **30** in a Dakin oxidation.[113] Diol **85**, which was obtained in 93% yield, was protected immediately using the procedure described by Lin *et al.*[112] MEM protection was carried out by addition of methoxyethoxymethyl chloride and DIPEA. The reaction gave the desired diether **86** in good yield of 90%. To convert bromide **86** into the desired boronic acid **87**, the benzene ring was lithiated using *n*-BuLi. The partially negatively charged carbon atom can then attack the boron atom of trimethyl borate to form boronic acid **87**. Unfortunately, the reaction only gave a black polymeric residue. The syntheses of 3-hydroxy-3'-benzylaminomethyl-4,4'-biphenol (**72**) and 3-hydroxy-2'-benzylaminomethyl-4,4'-biphenol (**73**) were aborted due to the failure of this reaction.

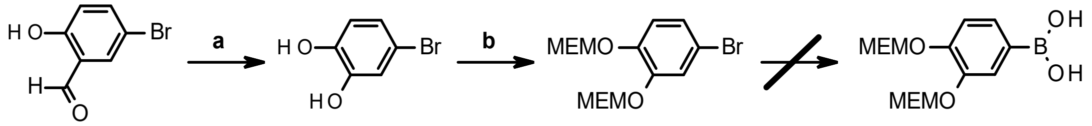

30 **85** **86** **87**

*Scheme 13: Synthesis of MEM protected boronic acid **87** through the conversion of 5-bromo-2-hydroxybenzaldehyde (**30**). Reaction conditions: (a) H_2O_2, NaOH, water, r.t., 2h, 93%, (b) methoxyethoxymethyl chloride, DIPEA, DCM, 0 °C → r.t., 4.5 d, 90%.*

4.2.5. Design of a mono-ring-substituted biphenyl derivative

In contrast to the approach described above, optimization of the lead structure 4,4'-biphenol (**22**) can also be achieved by removal of one of the hydroxy groups. To form all hydrogen bonds, the molecules have to position themselves in the centre of the binding pocket to interact with the amino acids Lys109 and Ile78 to one side and Ser68 to the other side. It was assumed that the length of each hydrogen bond can be shortened by removing the hydroxy group, which forms a hydrogen bond to Ser68. The length of the hydrogen bonds between the Rheb protein and 4,4'-biphenol (**22**) or 3-hydroxy-4,4'-biphenol (**40**) can be measured from the Glide structures minimized using MacroModel[90] as depicted in Figure 40.

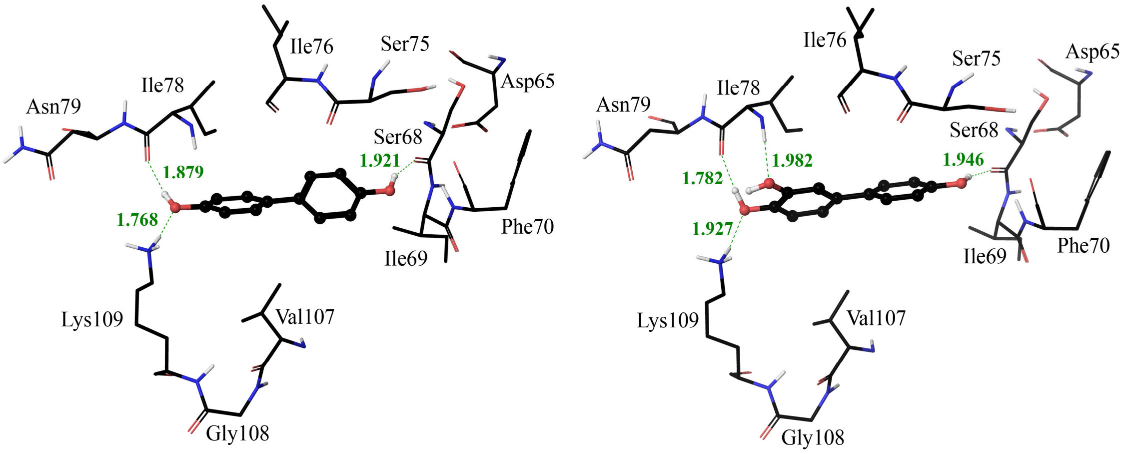

*Figure 40: Comparison of the binding mode of 4,4'-biphenol (**22**) and 3-hydroxy-4,4'-biphenol (**40**). The residues shifted in the NMR measurement are shown. The hydrogen bonds formed between the ligand and the corresponding amino acids of the protein are depicted in green.*

By decreasing the distance to Ile78 and Lys109, the hydrogen bonds formed to those residues will be strengthened as shown in Figure 41. Consequently, biphenyl-4-ol (**88**, Glide score: -4.55) was obtained from a commercial vendor and examined by NMR measurement.

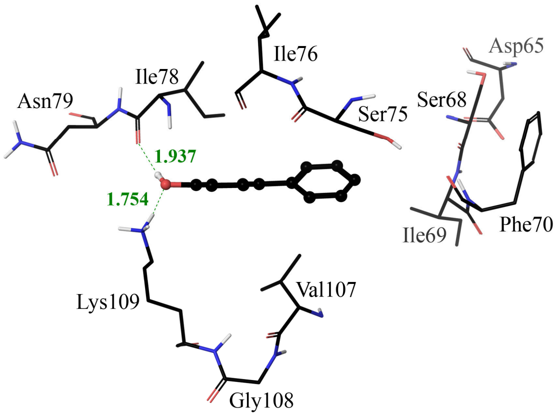

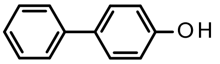

Biphenyl-4-ol (**88**)

*Figure 41: Orientation of biphenyl-4-ol (**88**) in the binding pocket of the Rheb protein indicating the predicted hydrogen bonds formed with the amino acids Lys109 and Ile78.*

The titration experiment in Figure 42 clearly shows that the simplified molecule is able to bind to the Rheb protein strongly. The overlay depicts significant shifts for amino acids belonging to the ligand binding site such as Ile69, Phe70, Ser75, Ile76, Ile78, Asn79, Val107 and Gly108. Also, the nucleotide binding pocket is affected through allosteric effects by ligand addition as can be seen from residues Gly13, Tyr14, Arg15 and Ser16.

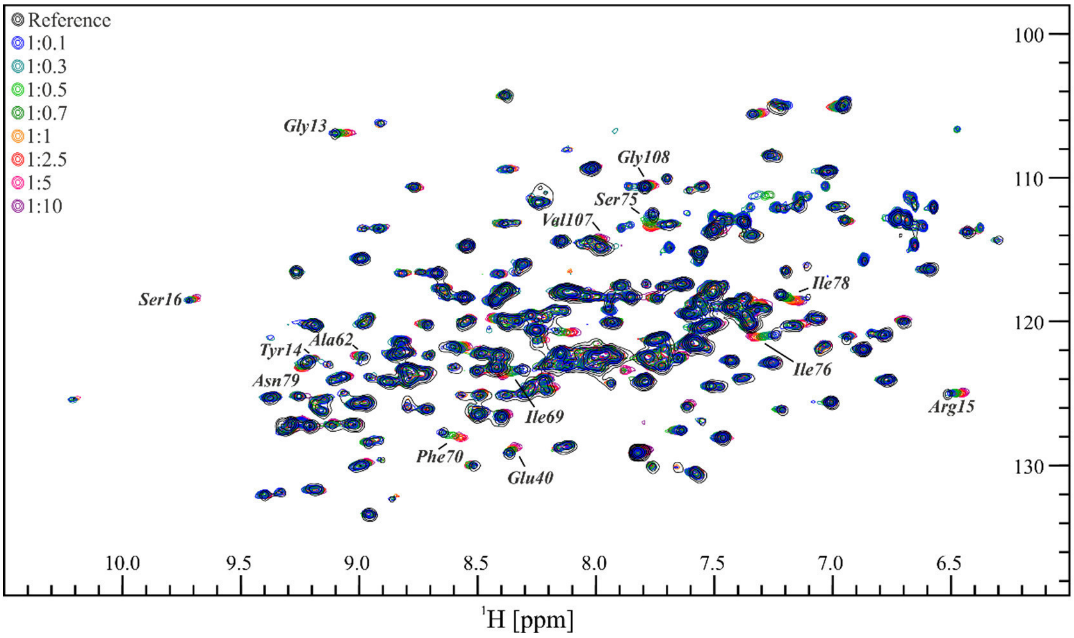

*Figure 42: ^{1}H,^{15}N-TROSY NMR overlay of the titration steps of biphenyl-4-ol (**88**) to the Rheb protein.*[102]

As those amino acids coincide with the residues shifted for 4,4'-biphenol (**22**) as well as 3-hydroxy-4,4'-biphenol (**40**), it is assumed that the binding mode of those molecules has also been adopted by biphenyl-4-ol (**88**). This assumption is confirmed by the HADDOCK model depicted in Figure 43. The biphenyl core is inserted deeply into the ligand binding pocket either interacting with Ile69 or Ile78. The best conformation shows a hydrogen bond of the hydroxy group with Ile69 while the other models validate an interaction with the other side of the ligand binding pocket (Ile78).

The k_D value calculated from the NMR measurement conforms to 259 ± 33 µM. In comparison to 4,4-biphenol (**22**, 1540 ± 230 µM), the NMR measurement and the k_D value clearly show an improvement of the binding affinity of the compound in the same range of 3-hydroxy-4,4'-biphenol (**40**, 229 ± 16 µM). Consequently, the prediction made for the biphenol structure shortened by one hydroxy group was verified.

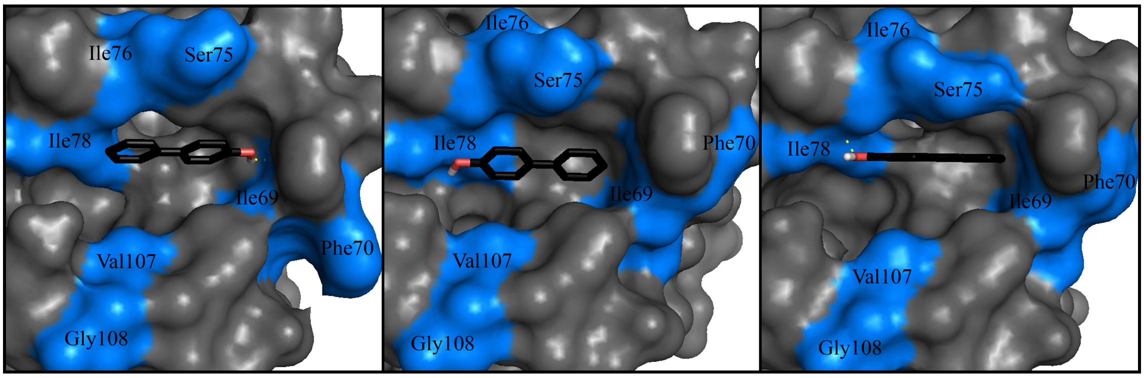

*Figure 43: Conformations of biphenyl-4-ol (**88**) predicted by HADDOCK.*[44] *The residues of the protein, which were used for the calculation, are highlighted in blue.*

4.2.6. Synthesis of a hybrid molecule derived from biphenols 88 and 40

According to the synthesis of 3-hydroxy-4,4’-biphenol (**40**), a Suzuki coupling was used to fuse the two phenyl rings. Bromobenzene (**89**) was coupled to boronic acid **49** (Scheme 14). The coupling conditions applied before in the synthesis of 3-hydroxy-4,4’-biphenol (**40**) afforded the desired dimethoxy compound **90** in good yield (78%).[104] Cleavage of the methoxy groups was done with boron tribromide to afford biphenyl-3,4-diol (**91**) in excellent yield (95%).[105] The overall yield for the two-step-synthesis of biphenol **91** amounts to 74%.

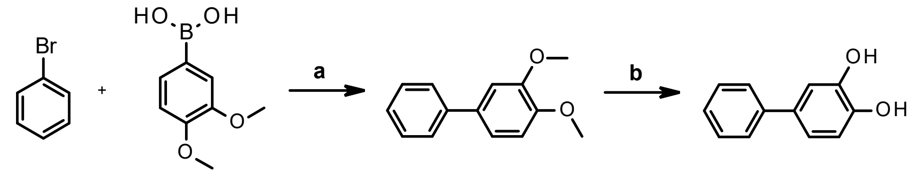

89 **49** **90** **91**

*Scheme 14: Reaction sequence to biphenol **91**. Reaction conditions: (a) K_2CO_3, 10% Pd/C, 18-crown-6, MeOH/H_2O, 45 °C, 2 h, 78%, (b) 1 M boron tribromide in DCM, DCM, r.t., 19 h, 95%.*

Biphenyl-3,4-diol (**91**) was used for a titration experiment with the ^{15}N-labeled Rheb protein. An overlay of the spectra of the titration steps, depicted in Figure 45, shows significant shifts similar to those observed for biphenyl-4-ol (**88**) and 3-hydroxy-4,4’-biphenol (**40**). This supports the assumptions made before. From the shifts in Figure 45, a similar binding mode of the compound can be deduced because several residues, which belong to the ligand binding pocket, such as Ser75, Ile76 and Ile78 are affected. Additionally, the spectra show allosteric effects on residues farther away from the binding site of biphenyl-3,4-diol (**91**).

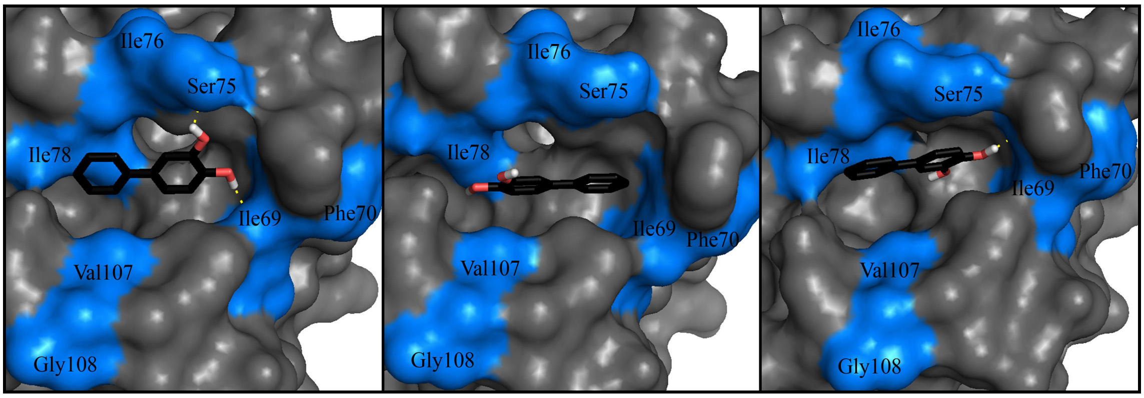

*Figure 44: Conformations of biphenyl-3,4-diol (**91**) predicted by HADDOCK.[44] The residues of the protein, which were used for the calculation, are highlighted in blue.*

The HADDOCK model (Figure 44), which was calculated from these shifts, depicts that the binding mode of biphenyl-3,4-diol (**91**) is in accordance with that of 4,4’-biphenol (**22**) as well as biphenyl-4-ol (**88**). Orientation of the substituted phenyl ring again is predicted to vary. Two models show interactions with the right side of the binding cleft (Ser75, Ile69) while only one predicts orientation of the hydroxy groups towards Ile78. This is in contradiction to the HADDOCK model for biphenyl-4-ol (**88**), which mainly orients the hydroxy group towards Ile78.

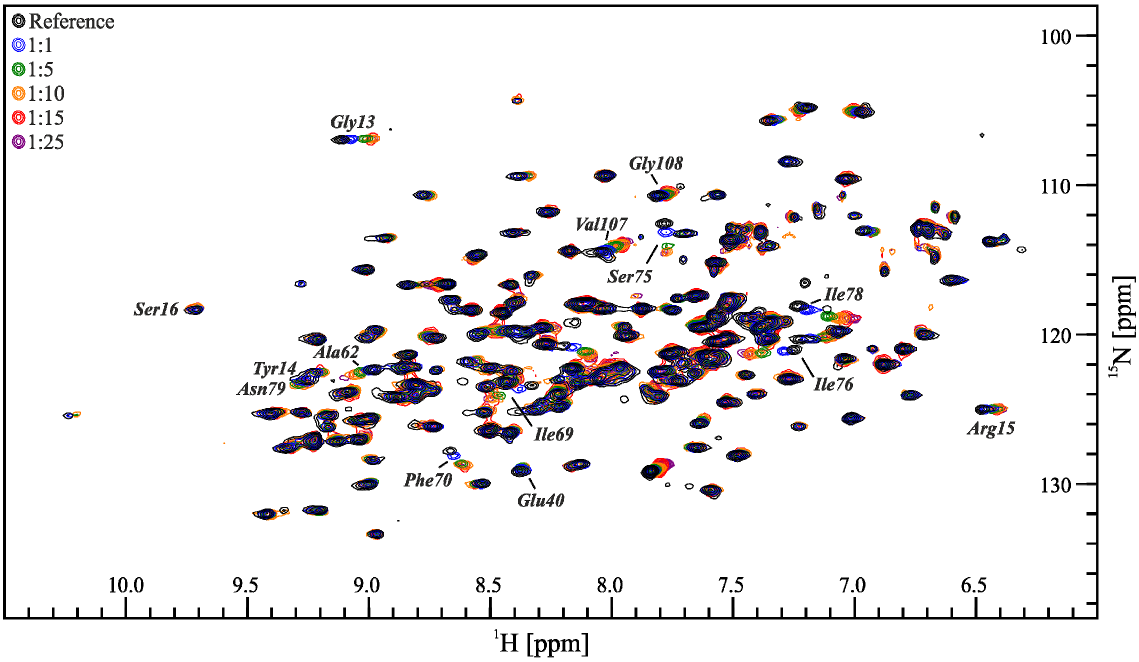

*Figure 45: ^{1}H,^{15}N-TROSY NMR overlay of the titration steps of biphenyl-3,4-ol (**91**) to the Rheb protein.*[106]

In comparison to biphenols **40** and **88**, the k_D value of biphenyl-3,4-diol (**91**) is calculated to be inferior (1090 ± 270 µM). Consequently, the expected enhancement of the dissociation constant was not achieved. One possible explanation for this finding is the removal of the wrong hydroxy group from the hybrid molecule. This resulted from a misleading impression regarding the orientation of the two compounds deduced from the predictions made by Glide and improved by MacroModel (Figure 40 and Figure 41). According to Glide, the di-substituted phenyl ring interacts with Lys109 and Ile78. In contrast to that, VINA predicts that the di-substituted phenyl ring of 3-hydroxy-4,4'-biphenol (**40**) is oriented towards Ser68 as shown in the bottom left picture of Figure 29. This is also supported by the corresponding HADDOCK model (Figure 31 **A**).

In comparison to 4,4'-biphenol (**22**, 1540 ± 230 µM), which is a regioisomer of biphenyl-3,4-diol (**91**), a minor improvement of the binding affinity to Rheb was achieved.

4.3. Screening and synthesis of novel compounds binding to the *K*-Ras protein

Bisphenol A (BPA, **23**) was found to bind (600 ± 200 µM)[20] to the *K*-Ras4B protein. BPA (**23**) was therefore chosen as a lead structure, which requires structural modification to improve the interaction with the protein. The binding mode of BPA (**23**) was investigated on the basis of the NMR titration experiment shown in Figure 46, top. The shifts of each of the protein peaks are also shown in the diagram below. The shift range needs to exceed twice the standard deviation (2σ) to be relevant for HADDOCK calculations.

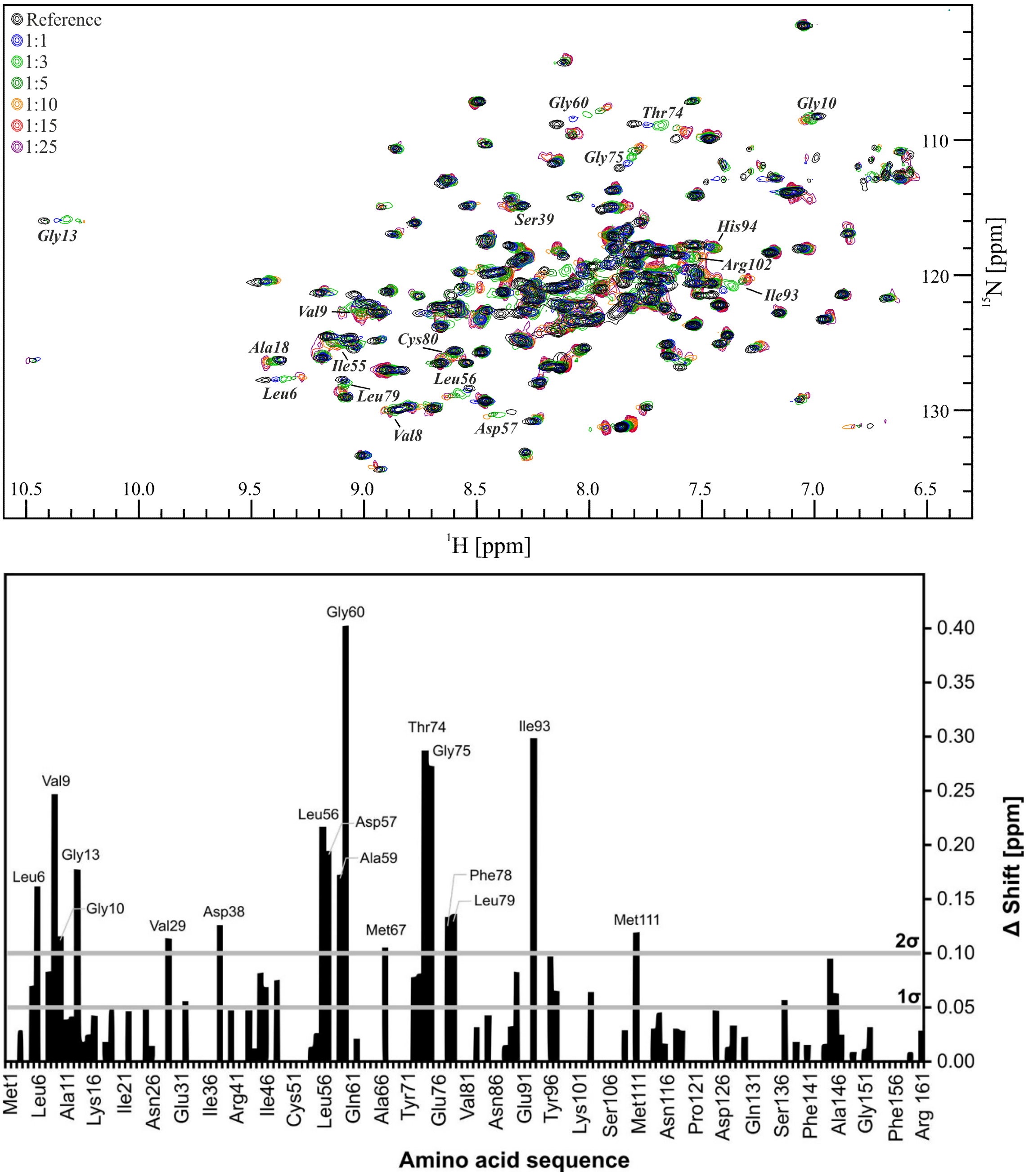

*Figure 46: Top: $^{1}H,^{15}N$-TROSY NMR overlay of the titration steps of bisphenol A (**23**) to the K-Ras4B protein.[102] Bottom: Shift ranges for the amino acids of the K-Ras4B protein.*

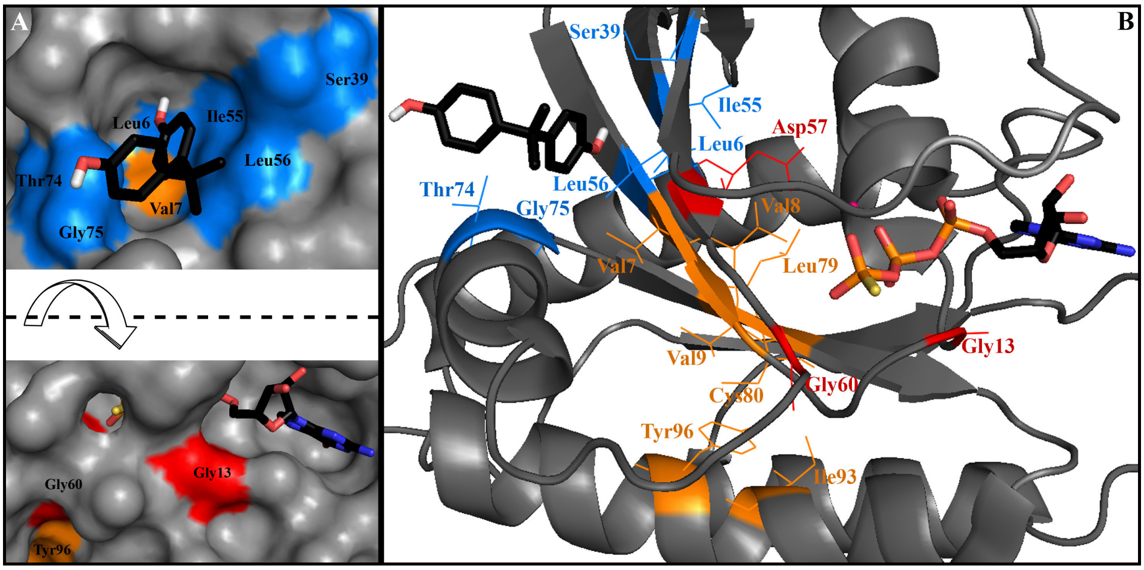

Figure 47: HADDOCK model of bisphenol A (23) in the binding pocket (blue) of the K-Ras4B protein (PDB ID: 4DSO) identified by chemical shifts in the NMR measurement. Residues throughout the protein (orange) and near the nucleotide (red) experience chemical shifts as a result of allosteric effects.

The NMR overlay shows significant shifts for amino acid residues, which belong to the ligand binding pocket (Leu6, Ser39, Ile55, Leu56, Gly60, Thr74 and Gly75). From these shifts, a HADDOCK model (Figure 47), which predicts the binding situation of BPA (**23**) in the ligand binding pocket, was calculated. As Figure 47 **A** shows, only one phenyl ring of the ligand can be inserted into the binding cleft, which is considerably smaller than the binding site identified for the Rheb protein. The other phenyl ring interacts with amino acids on the surface such as Gly75 and Leu56. Additionally, interaction with the ligand results in allosteric effects, which influence the nucleotide binding pocket (Gly13, Asp57 and Gly60). The effect on Leu6 also implies a chain reaction of shifts in amino acids Val8 and Val9 where the latter is influenced also by Thr96. Again, the change in environment of these amino acids causes chemical shifts for residues Leu79, Cys80 and Ile93. This cascade can be easily tracked from Figure 47 **B**. Unfortunately, the resolution of the NMR spectra does not always allow interpretation of the peak shifts of all those amino acids.

4.3.1. Bisphenol A substitutes as new lead structures

Bisphenol A (**23**) is a bulk chemical, which is used as a monomer for polymer synthesis such as polycarbonates and epoxy resins. Additionally, it was used for food and beverage packaging as well as a developer in thermal papers. The production of bisphenol A (**23**) was increased drastically over the past decades.[115] From sources, which provide bisphenol A (**23**) as a monomer, the chemical was shown to enter our environment as well as the human body. Today, significant BPA (**23**) levels can be measured in various animals such as fish and insects.[116] A vast number of studies proves the uptake of bisphenol A (**23**) by the consumption of canned food. While most of the BPA ingested is excreted rapidly, it is still not clear if BPA (**23**) absorbed through non-food exposure routes can accumulate in human tissues.[116]

In the human body, BPA (**23**) can mimic hormones of the endocrine system, which are essential for reproduction and development. Particularly endangered are pregnant women and children exposed to this chemical.[117] In the past, BPA (**23**) was considered to be only a weak estrogen mimic with significantly lower binding affinities for the receptors ERα and ERβ (estrogen receptor) than its natural activator estradiol. Newer studies have shown that BPA can promote estrogen-like activities with a higher potency than estradiol itself via non-classical estrogen signaling pathways.[118]

Due to its high impact on the human hormone system, the production of BPA-containing drinking bottles for babies is prohibited in the European Union since 2011. At the beginning of 2017, bisphenol A (**23**) was considered as toxic to reproduction by the European Commision.[119,120]

Consequently, substitutes for bisphenol A (**23**) were developed, which were also considered as alternatives for BPA (**23**) in this study. Therefore, the following BPA substitutes summarized in Table 6 were applied to molecular modelling with Glide and then tested for their binding affinity to *K*-Ras4B in NMR measurements except for bisphenol S (**107**), which was already tested before (k_D: 5.8 ± 0.7 mM).[121] In the following, only the most relevant NMR data, which was provided by Miriam Schöpel[122], will be shown.

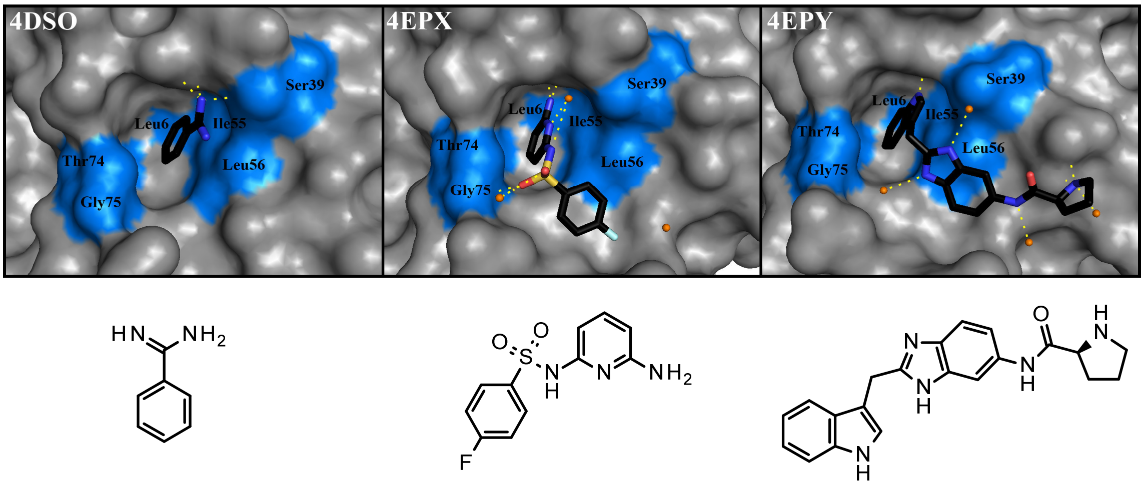

92 **93** **94a**

Figure 48: Binding modes of the compounds ***92-94a*** *discovered by Maurer (4DSO) and Fesik (4EPX, 4EPY). Water molecules are shown as orange spheres. Amino acids relevant for interaction with BPA (23) are highlighted in blue.*

For molecular modelling of bisphenol A (**23**) analogues, three different crystal structures of *K*-Ras4B mutant Gly12Asp (PDB ID: 4DSO) and *K*-Ras4B mutant Gly12Val, Cys118Ser (PDB IDs: 4EPY, 4EPX) were used for the predictions via Glide. These structures differ in their three-dimensional surface as a result of co-crystallisation with inhibitor molecules **92-94a** discovered by Maurer *et al.*[72] and Fesik *et al.*[73] as shown in Figure 48. In case of the Maurer structure (4DSO), the binding pocket retains its shape while it is opened in two different ways in the structures obtained by Fesik and coworkers (4EPY and 4EPX). 4EPX and 4EPY contain inhibitors **93** and **94a** found by Fesik. Both compounds show interactions with the protein via water molecules (Figure 48). These different binding modes have to be considered when applying molecular modelling strategies to the *K*-Ras4B protein. The most relevant crystal structure 4DSO resembles the *K*-Ras4B structure, which is used for NMR experiments, the best.

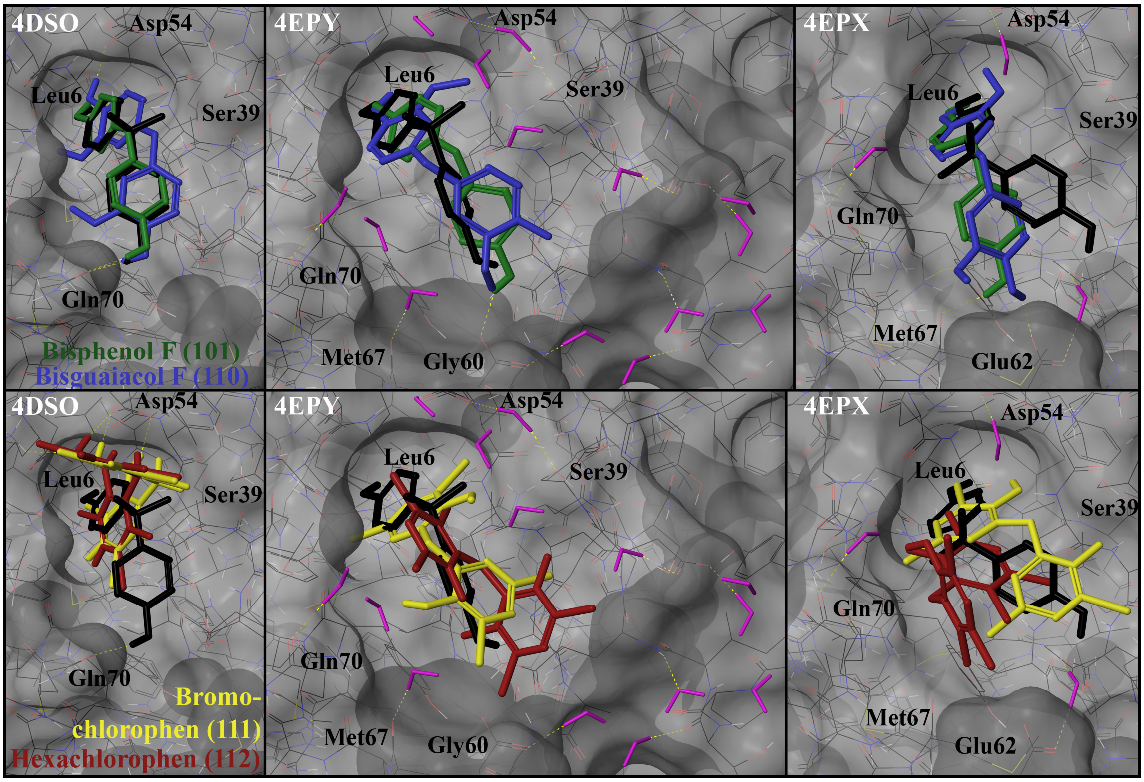

*Figure 49: Comparison of the binding modes of bisphenol F (**101**, green), bisguaiacol F (**110**, blue), bromochlorophen (**111**, yellow) and hexachlorophen (**112**, red) in the binding pocket of the crystal structures 4DSO, 4EPY and 4EPX of the K-Ras protein predicted by Glide with bisphenol A (**23**, black) as reference. Water molecules are shown in purple as a stick model.*

From the data in Table 6, it can be seen that substitutes such as bisguaiacol F (**110**), bromochlorophen (**111**) and hexachlorophen (**112**) exhibit increased Glide scores compared to bisphenol A (**23**). In contrast to these predictions, it was already shown that a conformationally non-restricted sp^3-carbon bridging the two phenol residues provides less active compounds.[20] The required angle between the two residues cannot be adjusted. The same conclusion can be drawn for bisphenol F (**101**). The Glide score of this analogue is comparable to the score of bisphenol A (**23**). An overview of the binding modes of the best structure of bisphenol F (**101**), bisguaiacol F (**110**), bromochlorophen (**111**) and hexachlorophen (**112**) in comparison to bisphenol A (**23**) is shown in Figure 49. Bisguaiacol F (**110**) and BPF (**101**) resemble the binding mode of bisphenol A (**23**) in the binding pocket of 4DSO. In contrast, the second phenyl ring of bromochlorophen (**111**) and hexachlorophen (**112**) is oriented in a different direction. The hydroxy group interacts with Asp54 at the upper rim of the binding cleft instead of Gln70. 4,4’-Biphenol (**22**), which was also tested before, did not show any interaction with *K*-Ras4B due to its linear structure.[20]

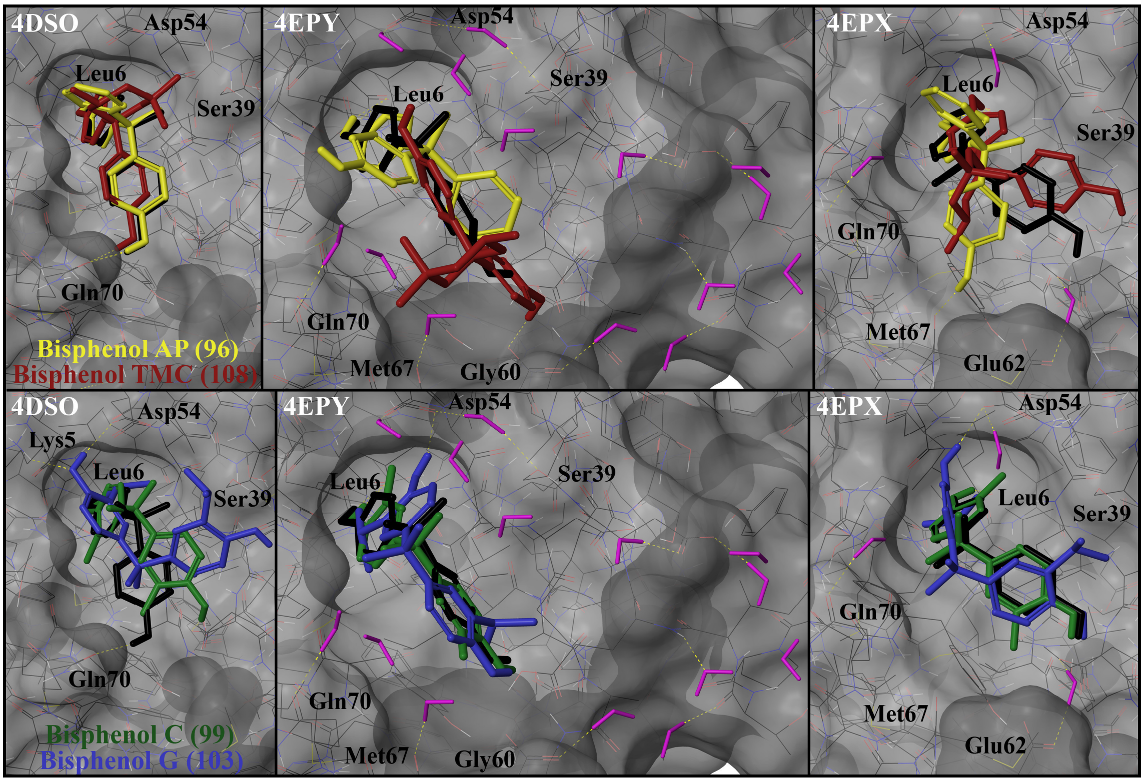

*Figure 50: Comparison of the binding modes of BPAP (**96**, yellow), BPC (**99**, green), BPG (**103**, blue) and BPTMC (**108**, red) in the binding pocket of the crystal structures 4DSO, 4EPY and 4EPX of the K-Ras protein predicted by Glide with bisphenol A (**23**, black) as reference. Water molecules are shown in purple as a stick model.*

The Glide scores of analogues **96**, **98** and **102**, which incorporate an aromatic substituent at the central C-atom, are lower in comparison to bisphenol A (**23**). In contrast, analogues with a sterically more demanding alkyl substituent such as BPB (**97**), BPTMC (**108**), and BPZ (**109**) show slightly increased Glide scores. Compounds with additional substituents at the phenyl rings show lower Glide scores. This effect increases with the size of the substituent. The score of BPC (**99**), which carries a methyl group, is only slightly decreased while the Glide value of BPG (**103**) with an isopropyl group is significantly lower. Exemplarily, the binding modes of BPAP (**96**), BPC (**99**), BPG (**103**) and BPTMC (**108**) are depicted in Figure 50. Compounds **96** and **108** overlap perfectly with bisphenol A (**23**) while the binding mode of BPC (**99**) differs slightly. In contrast, bisphenol G (**103**) is oriented in the wrong way in the binding pocket of 4DSO. It forms a hydrogen bond to Lys5 at the upper left rim of the binding pocket instead of interacting with Leu6 at the bottom of the binding pocket. Additionally, interaction with Gln70 via the hydroxy group of the second phenyl ring is lost.

Table 6: Glide scores of Bisphenol A substitutes ***95-112*** *in comparison to BPA (**23**) as reference. In case of 4DSO, all water molecules were removed prior to docking experiments. For 4EPX, three water molecules are included for docking experiments while 4EPY contains a total of 14 water molecules surrounding the ligand binding pocket.*

Substance	Structure	4DSO		4EPY		4EPX	
		max	min	max	min	max	min
Bisphenol A (23)	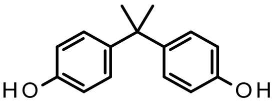 **23**	-3.24	-2.30	-1.36	-1.00	-1.67	3.02
Bisphenol AF (95)	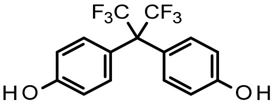 **95**	-3.13		1.56		0.18	
Bisphenol AP (96)	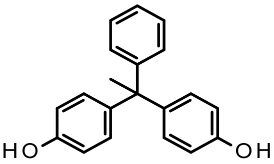 **96**	-2.87	-1.36	-1.57	2.90	-1.48	1.22
Bisphenol B (97)	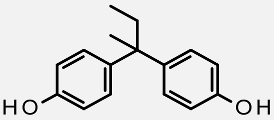 **97**	-3.51	-2.51	-4.42	-1.17	-1.80	3.19
Bisphenol BP (98)	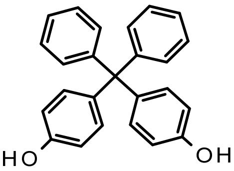 **98**	-2.55	-0.88	-0.15	2.57	0.12	1.07
Bisphenol C (99)	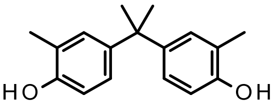 **99**	-2.91		-1.58	-1.07	-0.11	
Bisphenol E (100)	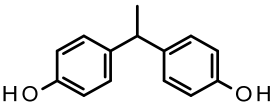 **100**	-3.02	1.44	-1.25	-0.28	-3.32	2.84
Bisphenol F (101)	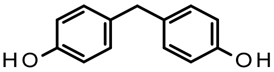 **101**	-3.04	0.64	-1.34	-0.03	-1.72	2.79
Bisphenol FL (102)	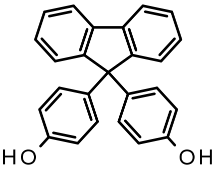 **102**	-2.95	-0.99	2.24	2.60	0.41	5.02

Bisphenol G (103)	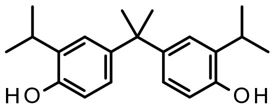 **103**	-1.94	-1.38	-0.21	0.24	-0.82	1.05
Bisphenol M (104)	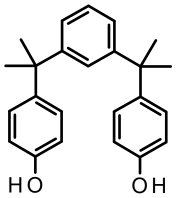 **104**	-3.29	-2.35	-1.06	-0.98	-0.83	1.45
Bisphenol P (105)	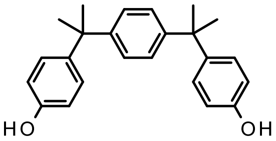 **105**	-2.33	-1.20	-1.22	0.14	-3.08	-1.50
Bisphenol PH (106)	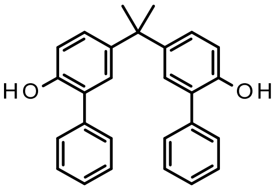 **106**	-2.12	1.12	-3.98	-0.56	0.22	2.12
Bisphenol S (107)	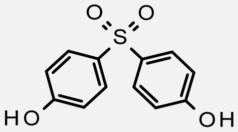 **107**	-3.32		-4.86	-1.01	-1.67	
Bisphenol TMC (108)	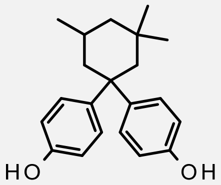 **108**	-3.70	-2.21	-2.05	2.20	-3.19	0.42
Bisphenol Z (109)	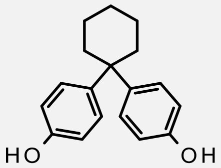 **109**	-3.60	1.24	-2.63	1.16	-3.72	2.05
Bisguaiacol F (110)	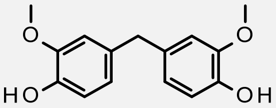 **110**	-4.01	-3.46	-3.85	-1.02	-1.46	2.09
Bromochlorophen (111)	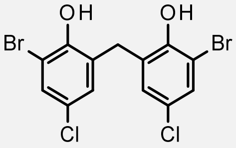 **111**	-3.86	-2.09	0.46	3.29	-2.37	0.80

Hexachlorophen (112)	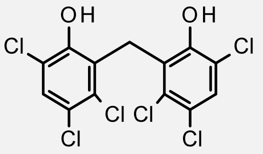 **112**	-3.34	1.46	-1.73	4.48	-2.30	2.65

A selection of the compounds shown in Table 6 was obtained from commercial vendors and examined by NMR experiments.[122] Some compounds, which incorporate the required restricted sp^3-carbon atom, were either too insoluble to be tested via NMR spectroscopy (BPAP (**96**), BPBP (**98**), BPFL (**102**)) or led to denaturation of the protein (BPC (**99**), BPM (**104**), BPP (**105**), BPZ (**109**)).[122] The most interesting compound investigated was bisphenol AF (BPAF, **95**), which shows a significantly improved binding affinity (k_D: 346 ± 9 µM) to *K*-Ras4B as calculated from the NMR titration shown in Figure 52.[122]

Noticeably, the prediction by Glide did not identify BPAF (**95**) as a strong binder for the *K*-Ras4B protein. The scores for the crystal structures 4EPY and 4EPX with an opened ligand binding pocket even show positive Glide scores. This is a rather deterring finding as the Glide score depicts the ligand binding free energy, which should be as negative as possible to identify a strong binding affinity with the protein. Figure 51 shows the binding modes of BPAF (**95**) and BPS (**107**) in comparison to BPA (**23**). Most remarkably, the positioning of the three compounds coincides for 4DSO and 4EPX while BPAF (**95**) is significantly misplaced in 4EPY. BPAF (**95**) is not inserted into the biding pocket. Instead, it forms a hydrogen bond to Glu63. This explains the significantly decreased Glide score of BPAF (**95**) for 4EPY. In contrast, the prediction by Autodock/VINA clearly shows that BPAF (**95**, VINA score: -7.0 to -5.0) should be a better binder than BPA (**23**, VINA score: -6.2 to -4.2). This most probably results from the difference in docking environment: while Autodock/VINA calculates the binding affinity of the ligand and the protein in vacuum, Glide uses water as the surrounding solvent for the computations.

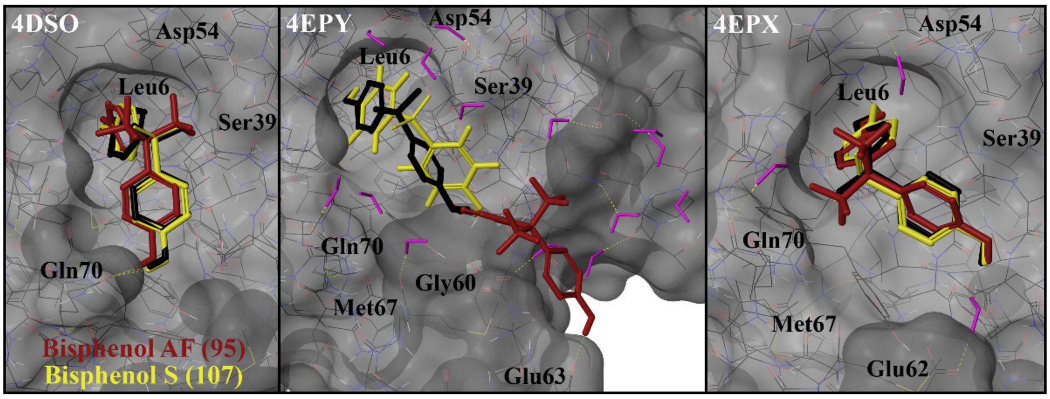

*Figure 51: Comparison of the binding modes of BPAF (**95**, red) and BPS (**107**, yellow) in the binding pocket of the crystal structures 4DSO, 4EPY and 4EPX of the K-Ras protein predicted by Glide with bisphenol A (**23**, black) as reference. Water molecules are shown in purple as a stick model.*

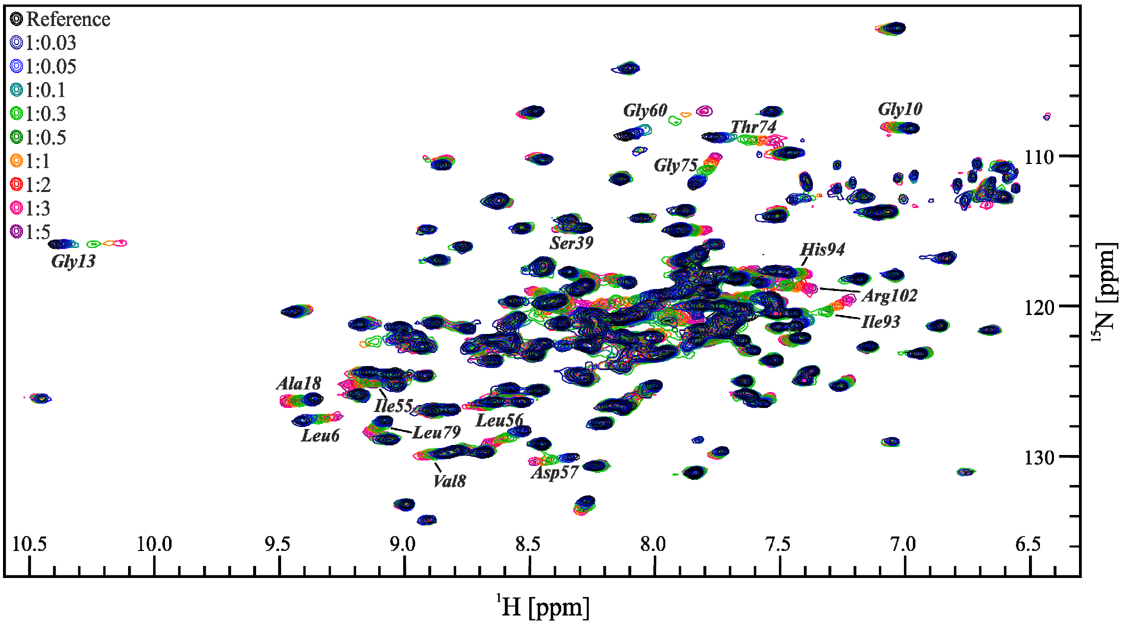

*Figure 52: ^{1}H,^{15}N-TROSY NMR overlay of the titration steps of Bisphenol AF (**95**) to the K-Ras protein.*[102]

The overlay of the different spectra from the titration experiment of BPAF (**95**) with *K*-Ras4B[122] shows wide shifts for the relevant amino acids. Besides the ligand binding pocket, residues of the nucleotide binding pocket are also shifted by allosteric effects that cascade throughout half of the protein. Remarkably, a significantly lower excess of BPAF (**95**) was added during this titration in comparison to bisphenol A (**23**) to accomplish the same range of peak shifts (1:5 for BPAF (**95**) in comparison to 1:25 for BPA (**23**)). This also indicates a stronger interaction with the protein when compared with the relatively low binding affinity of BPA (**23**).

The HADDOCK model in Figure 53 shows that bisphenol AF (**95**) enters the ligand binding pocket with a phenol ring in most predictions. In contrast to bisphenol A (**23**), the analogue can also insert one of the highly unpolar CF$_3$-groups into the ligand binding cleft instead. This prediction clearly proves that the bisphenol A analogue BPAF (**95**) adopts the same conformation in the binding pocket of *K*-Ras4B as bisphenol A (**23**). The strength of the interaction with the protein cannot be measured from the HADDOCK calculation as no additional hydrogen bonds are observed.

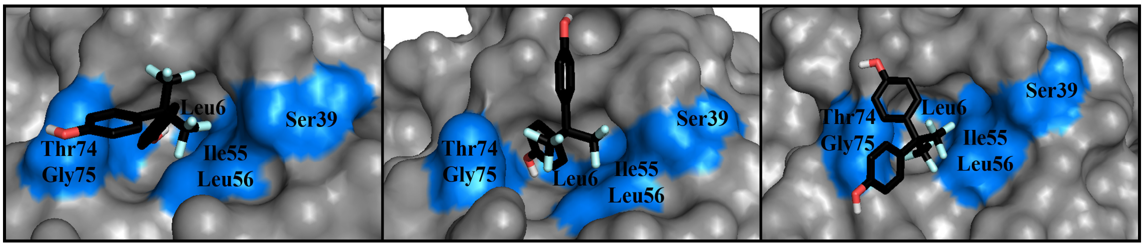

*Figure 53: Different conformations of bisphenol AF (**95**) in the binding pocket of K-Ras4B (PDB ID: 4DSO) predicted by HADDOCK.*[44] *The amino acids, which were defined as active residues for the HADDOCK calculation are highlighted in blue.*

Regarding structure-activity relationships, bisphenol AF (**95**) clearly shows that the more lipophilic CF_3-groups allow a better interaction with the *K*-Ras4B protein. This compound can also be used as a new lead structure for the development of inhibitor compounds. Nevertheless, it should be considered that BPAF (**95**) was shown to have a comparable or even higher toxicity and teratogenic effect in zebrafish embryo-larvae as bisphenol A (**23**).[115] Additionally, BPAF (**95**), BPB (**97**), BPF (**101**), and BPS (**107**) have been shown to exhibit estrogenic and/or antiandrogenic activities similar to or even greater than that of BPA (**23**).[123]

4.3.2. Structural modifications of bisphenol A (23) and bisphenol AF (95)

BPA (**23**) and BPAF (**95**) consist of three structural motifs that can be used for functionalization: the (trifluoro-)methyl groups, the phenol rings and the hydroxy groups.

As a first attempt, modification of one of the hydroxy groups was targeted. The resulting compounds cannot be used for polymer synthesis. Instead, these compounds are interesting as analogues of bisphenol A, which will show either increased binding affinities to the protein or decreased toxicity due to inactivity towards *K*-Ras4B. In both cases, relevant structure activity relationship data will be obtained.

In a second approach, derivatization of the phenol rings for heteroaromatic rings was attempted. The resulting compounds are also unsuitable for polymer synthesis as the compounds lack the hydroxy groups. As described above, the results from the NMR measurement of these analogues will provide significant information on the structure activity relationship of bisphenol A (**23**) and bisphenol AF (**95**).

The third motif, the methyl groups of bisphenol A (**23**), can be used to attach further substituents to the bisphenol core. For these modifications, only the bisphenol A motif will be used. In contrast to the analogues described above, the resulting analogues can still be used for polymer synthesis. Additionally, the NMR results of these compounds will contribute to the SAR data.

4.3.2.1. Modification of the hydroxy groups of bisphenol A (**23**) and bisphenol AF (**95**)

The hydroxy moiety can be used as an anchor group for structural modifications. Formation of an ester, for instance, allows introduction of a large variety of different residues, which are attached to the corresponding carboxylic acid.

4.3.2.1.1. First iteration

To elucidate the influence of a mono-derivatisation of one of the hydroxy groups, the acetate derivative **113** was chosen. The Glide value obtained for acetate **113** decreased expectedly, because a hydrogen bond between the ligand and the protein is broken (Figure 54). Thus, different side chains such as an amino group were chosen to provide new interaction points.

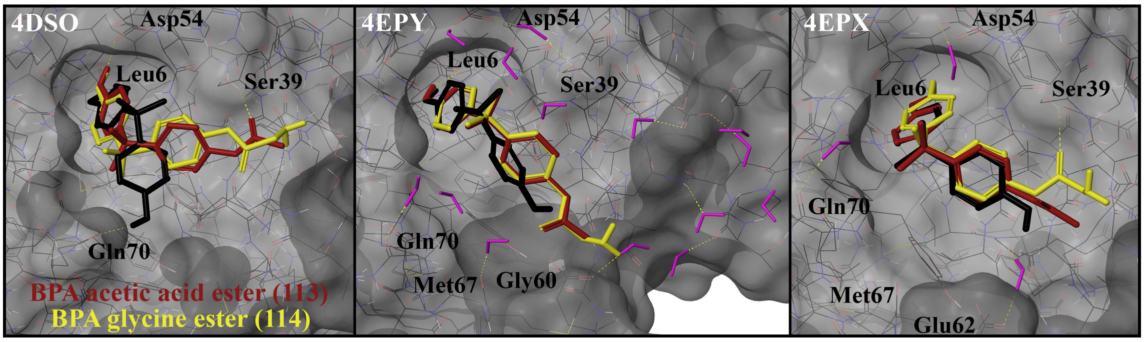

*Figure 54: Comparison of the binding modes of BPA acetic acid ester (**113**, red) and BPA glycine ester (**114**, yellow) in the binding pocket of the crystal structures 4DSO, 4EPY and 4EPX of the K-Ras protein predicted by Glide with bisphenol A (**23**, black) as reference. Water molecules are shown in purple as a stick model.*

This structural modification can be introduced by an amino acid such as glycine, which led to the desired effect on the Glide scores for derivative **114**. According to the binding modes depicted in Figure 54, derivative **114** cannot form a hydrogen bond to Ser39 in 4DSO in comparison to ester **113**. For 4EPX, the situation of glycine ester **114** allows the formation of a hydrogen bond with Ser39 while acetate **113** is unable to orient its side chain appropriately. As a result, more complex structures such as proline and lysine or indolyl acids carrying further amino groups were tested.

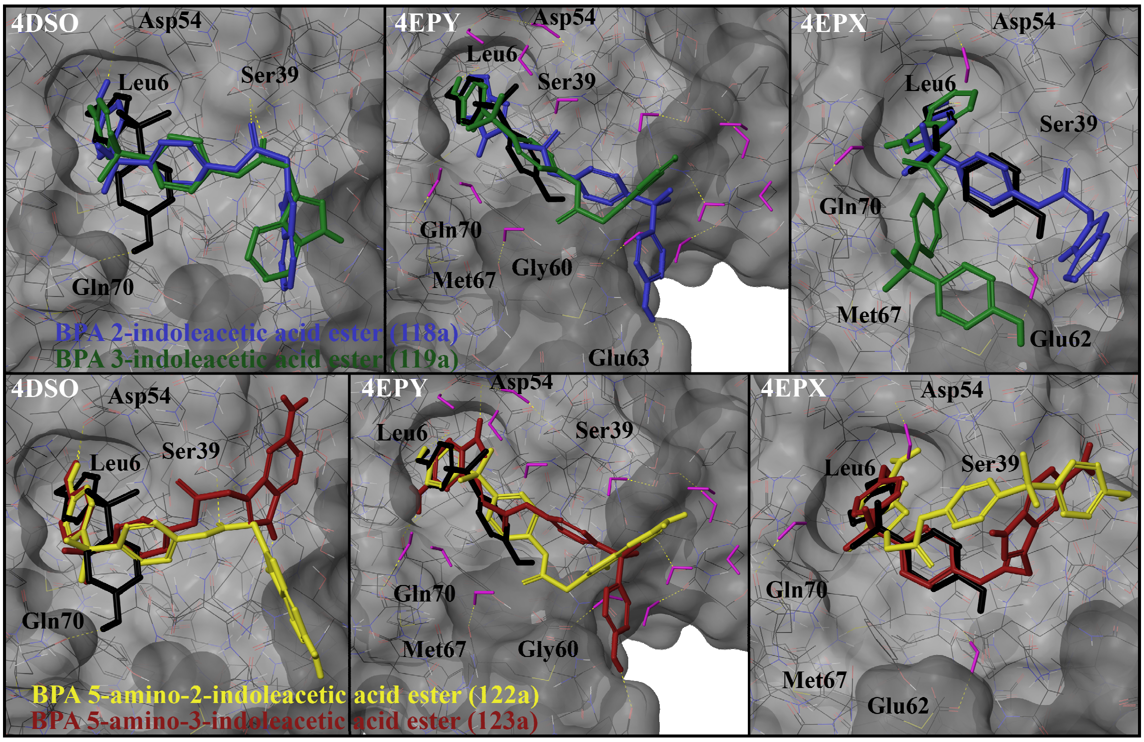

*Figure 55: Comparison of the binding modes of BPA 2-indoleacetic acid ester (**118a**, blue), BPA 2-indoleacetic acid ester (**119a**, green), BPA 5-amino-2-indoleacetic acid ester (**122a**, yellow) and BPA 5-amino-2-indoleacetic acid ester (**123a**, red) in the binding pocket of the crystal structures 4DSO, 4EPY and 4EPX of the K-Ras protein predicted by Glide with bisphenol A (**23**, black) as reference. Water molecules are shown in purple as a stick model.*

Most compounds displayed in Table 7 show positive Glide scores, which indicates repellent instead of attractive interactions with the protein. As a result, these compounds such as proline esters **115** and **116** or histidine esters **129** and **130** are not further considered. In addition, only few compounds exhibit improved Glide scores in comparison to bisphenol A (**23**). It can therefore be expected that attachment of a substituent to one of the hydroxy groups of BPA (**23**) leads to a significantly decreased binding affinity.

Regarding their potential for further modifications, the indole derivatives were chosen for synthesis. In case of the unsubstituted indole derivatives **118a** and **119a**, the 2-substituted indole ester **118a** exhibits the better Glide scores, especially for the most relevant crystal structure 4DSO. In contrast, the amino substituted esters **122a** and **123a** show the opposite effect. As Figure 55 shows, the indole esters are oriented towards Ser39.

In 4DSO, esters **118a**, **119a** and **122a** form a hydrogen bond to Ser39. In contrast to BPA (**23**), the esters are inserted not as deep into the pocket. Therefore, the hydrogen bond to Leu6 cannot be formed. Instead, the hydroxy group of each of the esters interacts with Asp54. In case of the other two crystal structures, the positioning of the compounds in the binding cleft is inconsistent. While esters **118a** and **123a** insert the indole ring into the binding pocket of 4EPY, a similar orientation is observed for the other two compounds in 4EPX. Only the 3-substituted analogue **119a** was chosen for synthesis, because the corresponding 2-substituted indole acid is not commercially available.

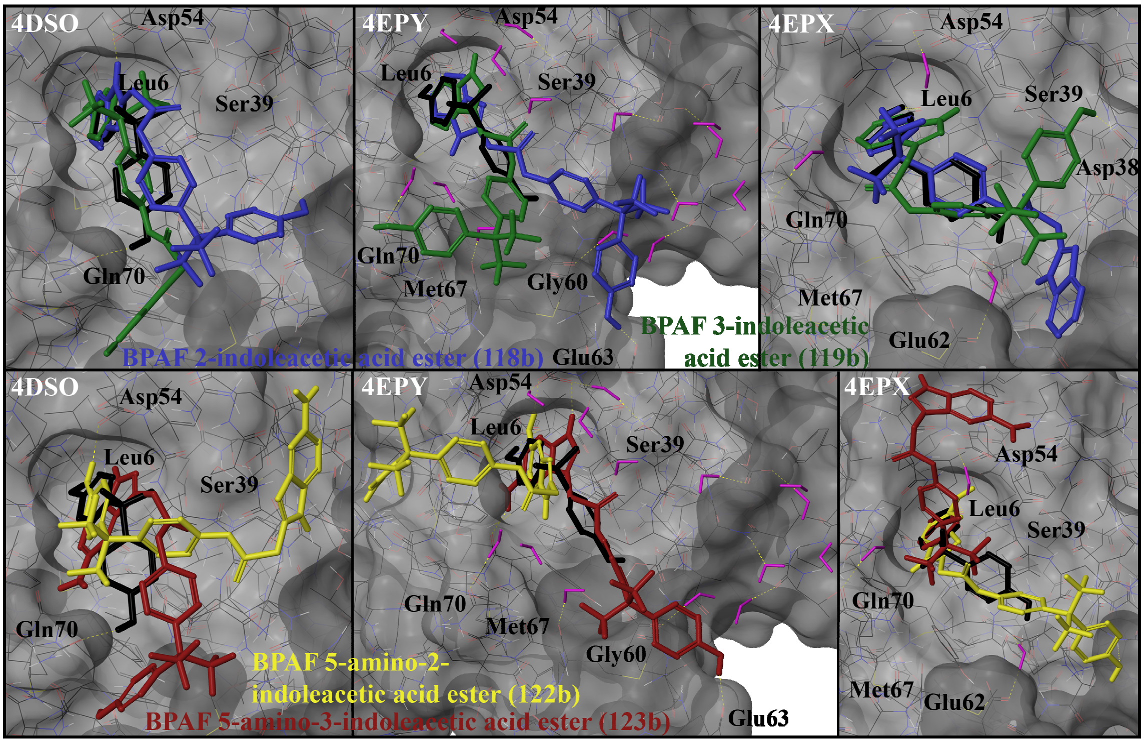

*Figure 56: Comparison of the binding modes of BPAF 2-indoleacetic acid ester (**118b**, blue), BPAF 2-indoleacetic acid ester (**119b**, green), BPAF 5-amino-2-indoleacetic acid ester (**122b**, yellow) and BPAF 5-amino-2-indoleacetic acid ester (**123b**, red) in the binding pocket of the crystal structures 4DSO, 4EPY and 4EPX of the K-Ras protein predicted by Glide with bisphenol A (**23**, black) as reference. Water molecules are shown in purple as a stick model.*

It is expected that the effects of the substituents computed for BPA (**23**) can be transferred to BPAF (**95**). Therefore, only the indole derivatives **118b**, **119b**, **122b** and **123b** of BPAF (**95**) were modelled. As expected, the Glide values of those compounds show the same effect as the BPA derivatives, especially for 4DSO. In contrast to the BPA derivatives, only derivatives **119b** and **122b** are oriented in the desired way. Additionally, esters **122b** and **123b** are inserted into the binding pocket in a different position (Figure 56).

*Table 7: Glide scores of bisphenol A derivatives **113-134** in comparison to BPA (**23**) and bisphenol AF (**95**) as reference. In case of 4DSO, all water molecules were removed prior to docking experiments. For 4EPX, three water molecules are included for docking experiments while 4EPY contains a total of 14 water molecules surrounding the ligand binding pocket.*

Substance	**Structure**	**4DSO**		**4EPY**		**4EPX**	
		max	min	max	min	max	min
Bisphenol A (23)		-3.24	-2.30	-1.36	-1.00	-1.67	3.02
Bisphenol AF (95)		-3.13		1.56		0.18	
	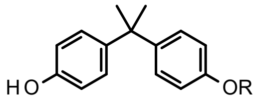						
BPA acetic acid ester (113)	R = 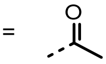 **113**	-1.91		-1.04	-0.49	1.77	8.09
BPA glycine ester (114)	R = 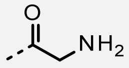 **114**	-3.57	-2.27	-1.47	-0.02	-1.10	-0.11
BPA S-proline ester (115)	R = 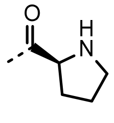 **115**	-2.80	4.30	-1.21	5.61	-3.22	8.03
BPA R-proline ester (116)	R = 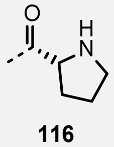 **116**	-3.89	6.67	-1.91	8.42	-2.08	12.69
BPA 2-indole acid ester (117)	R = 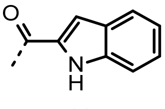 **117**	-1.68		-0.89	2.06	-1.11	3.79
BPA 2-indoleacetic acid ester (118a)	R = 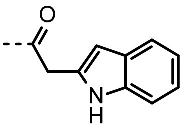 **118a**	-2.13	-1.09	-0.65	-0.57	-2.01	2.50
BPA 3-indoleacetic acid ester (119a)	R = 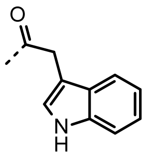 **119a**	-1.20	-0.60	0.49	0.60	0.28	9.68

BPA 6-amino-2-indoleacetic acid ester (120)	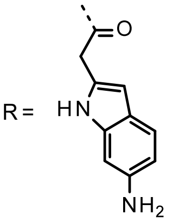 **120**	-1.62	5.04	0.81	4.94	-3.49	0.48
BPA 6-amino-3-indoleacetic acid ester (121)	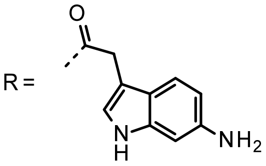 **121**	-1.65		-0.27	11.20	0.01	1.97
BPA 5-amino-2-indoleacetic acid ester (122a)	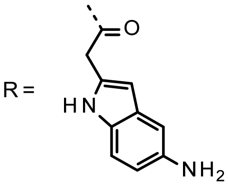 **122a**	-0.43	4.62	-0.76	0.67	-0.67	8.12
BPA 5-amino-3-indoleacetic acid ester (123a)	 **123a**	-3.07	5.43	-3.54	0.92	0.07	1.74
BPA 5,6-diamino-2-indoleacetic acid ester (124)	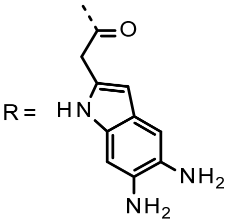 **124**	-2.92	-1.25	-0.67		1.52	
BPA 4,6-diamino-2-indoleacetic acid ester (125)	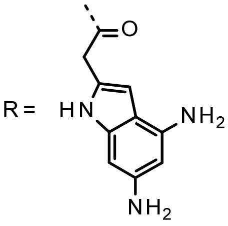 **125**	-2.14	1.27	0.71	2.56	0.31	3.78
BPA 4,6-diamino-2-indole-propionic acid ester (126)	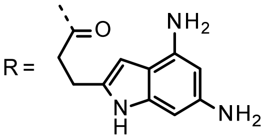 **126**	1.35		-0.51		-0.72	4.90

BPA S-lysine ester (127)	R = 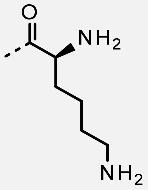 **127**	-3.46	0.87	-1.25	2.66	-5.56	-4.35
BPA R-lysine ester (128)	R = 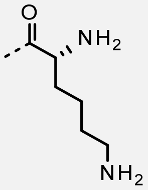 **128**	-4.74	-3.39	-1.89		-5.62	-5.52
BPA S-histidine ester (129)	R = 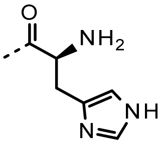 **129**	-2.31	6.70	-1.89	2.08	-6.24	1.86
BPA R-histidine ester (130)	R = 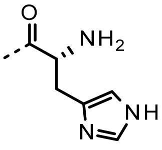 **130**	-2.63	7.13	-1.44	5.16	-5.55	1.25
BPA 4-imidazolepropionic acid ester (131)	R = 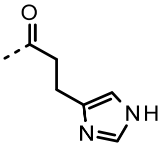 **131**	-2.07	3.24	-1.94	1.45	-5.52	-0.43
BPA 4-imidazoleacetic acid ester (132)	R = 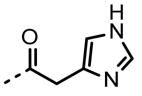 **132**	-3.14	5.63	-2.18	3.99	-3.87	6.37
BPA 4-imidazolebutanoic acid ester (133)	R = 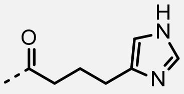 **133**	-4.06	4.53	-1.85	3.25	-3.21	5.47
BPA 6-amino-2-benzimidazole-acetic acid ester (134)	R = 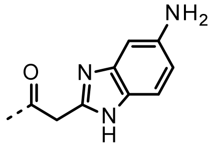 **134**	-0.72	9.10	-3.01	3.25	-2.62	0.23
BPAF 2-indoleacetic acid ester (118b)	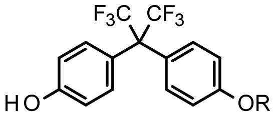 R = 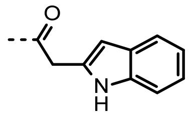 **118b**	-1.40	-1.39	-0.97		1.45	4.81

BPAF 3-indoleacetic acid ester (119b)	R = 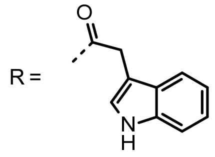 **119b**	-0.91		9.07		2.93	4.21
BPAF 5-amino-2-indoleacetic acid ester (122b)	R = 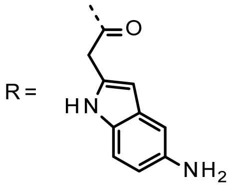 **122b**	-1.41	-0.58	-0.27	5.13	1.25	5.96
BPAF 5-amino-3-indoleacetic acid ester (123b)	R = 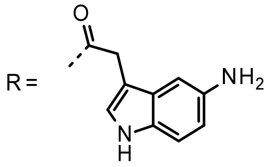 **123b**	-2.04	7.51	3.53	3.57	-0.14	0.90

Ester formation between bisphenol A (**23**) or bisphenol AF (**95**), respectively, and 3-indoleacetic acid (**135**) was performed without protecting groups to shorten the reaction sequence to one step. BPA (**23**) or BPAF (**95**) were coupled with the corresponding acid **135** (Scheme 15) using DCC and catalytic amounts of DMAP.[124–126] The acid was added slowly over 24 h to afford BPA ester **119a** in 21% and BPAF ester **119b** in 14% yield, respectively. The low yields are due to diester formation. Also, separation from unreacted starting material proved difficult due to significant tailing of BPA (**23**) and BPAF (**95**).

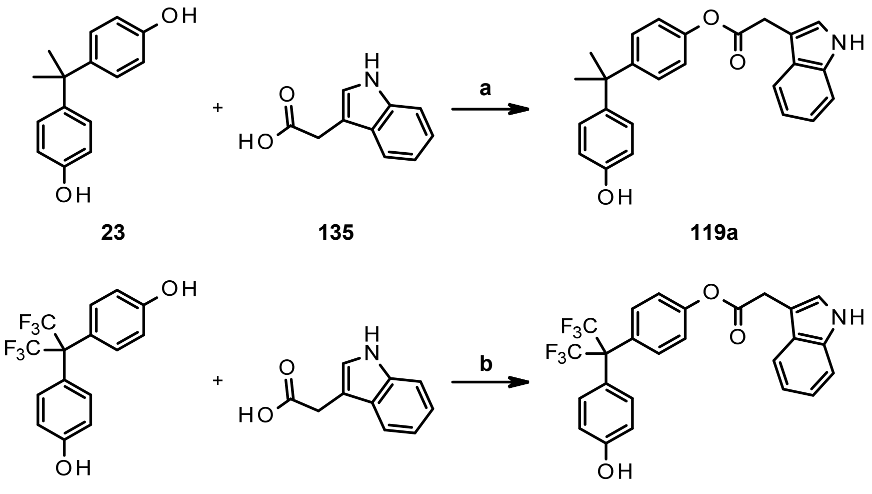

*Scheme 15: Synthesis of bisphenol A ester **119a** and bisphenol AF ester **119b** from indoleacetic acid **135**. Reaction conditions: (a) DCC, DMAP, DCM, r.t., 3 d, 21%, (b) DCC, DMAP, DCM, r.t., 2 d, 14%.*

As expected, the NMR measurements (Figure 57) of *K*-Ras4B with an excess (1:25) of indole derivatives **119a** and **119b** did not reveal any significant interactions of the compounds with the protein. Additionally, the histidine-tag (His-Tag), which is attached during expression of the protein and used for affinity chromatography with a Ni-NTA column, also shifts. Consequently, the minor effects do not necessarily indicate an interaction of the molecule with the protein.

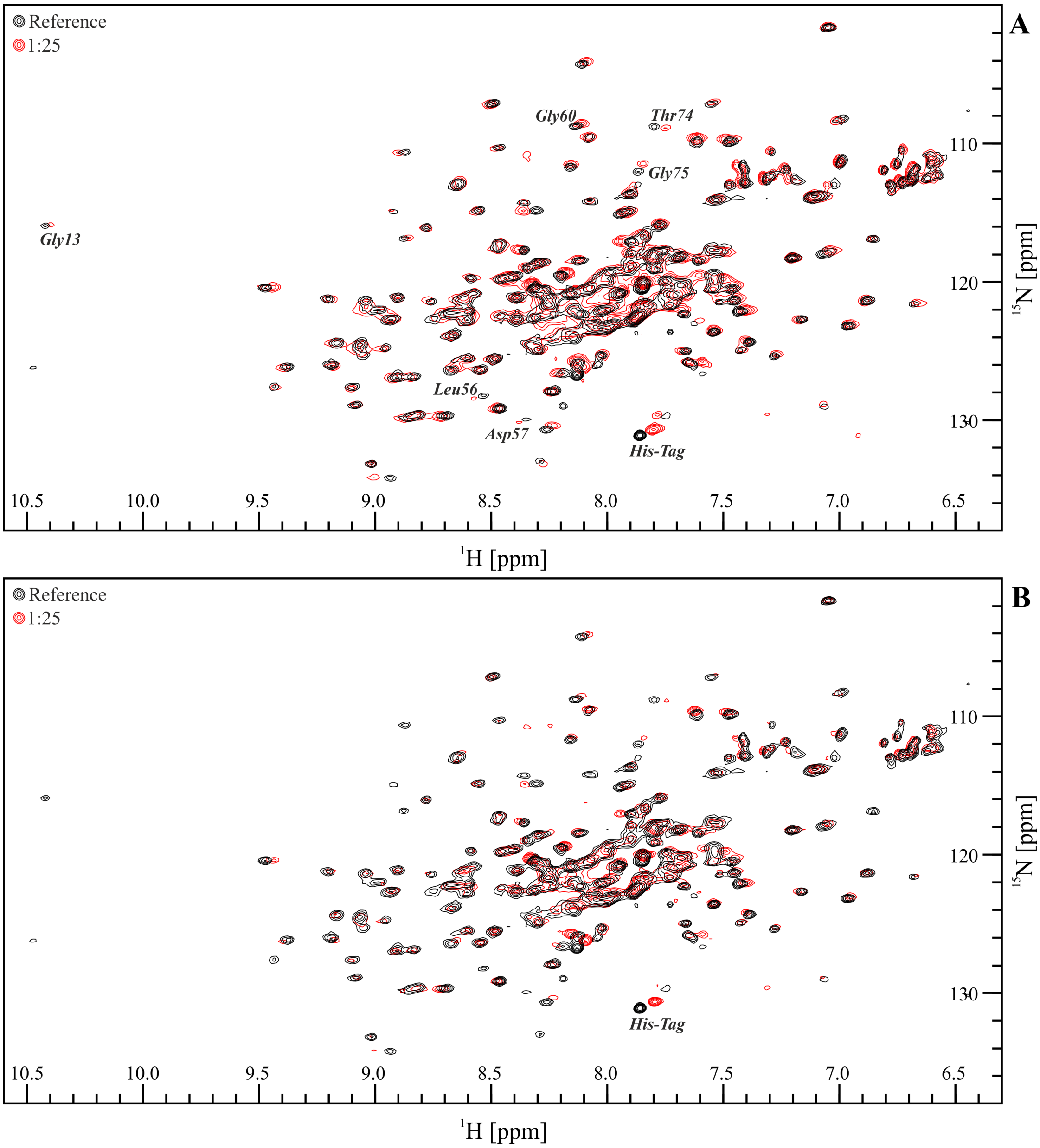

*Figure 57: NMR measurements of BPA esters **119a** (A) and **119b** (B) in excess to the protein K-Ras showing minor shifts for only a few of the relevant peaks.*

The HADDOCK model in Figure 58 clearly supports the thesis that the second phenol ring contributes significantly to ligand binding. BPA ester **119a** cannot enter the ligand binding pocket in any of the predicted conformations. BPAF ester **119b** is predicted to insert the indole moiety into the binding pocket instead of a phenol ring. Both compounds are obviously unable to interact with the protein in the desired way. Consequently, it has to be deduced that the second hydroxy group contributes significantly to the interaction with the surface of *K*-Ras4B as the predicted conformations of esters **119a** and **119b** show.

Additionally, steric hindrance of the residue attached to the hydroxy group needs to be considered. This effect might prevent the compounds from interacting with the ligand binding pocket in the desired way. This assumption is supported by the HADDOCK model for ester **119b**, which shows that the indole moiety can occupy the binding cleft.

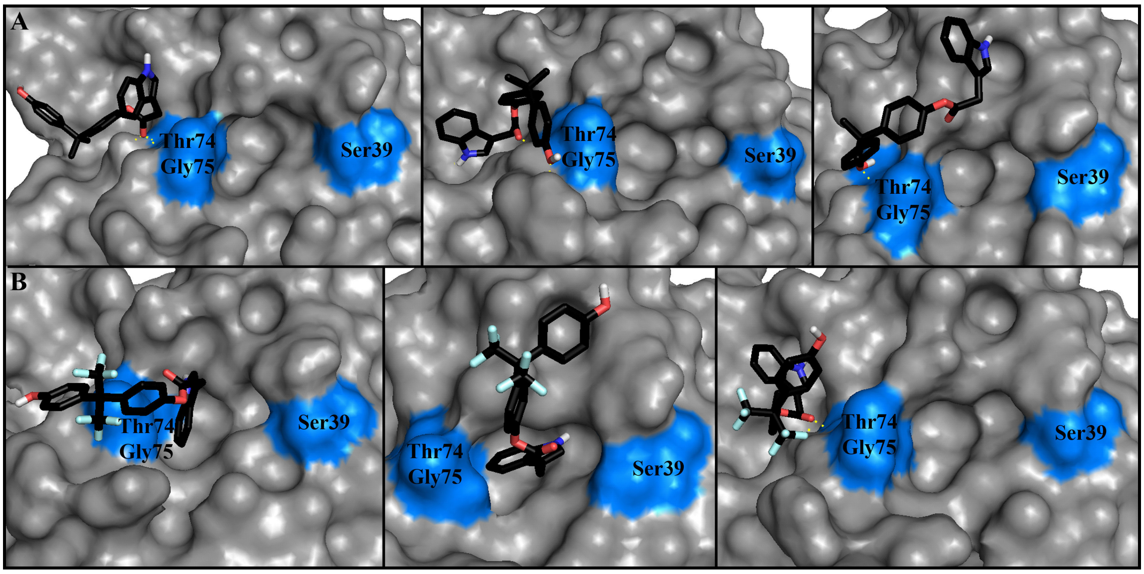

*Figure 58: Different conformations of BPA esters **119a** (**A**) and **119b** (**B**) in the binding pocket of K-Ras4B (PDB ID: 4DSO) predicted by HADDOCK.[44] The amino acids, which were defined as active residues for the HADDOCK calculation are highlighted in blue.*

4.3.2.1.2. Second iteration

To prove the finding that derivatization of one of the hydroxy groups of bisphenol A (**23**) and bisphenol AF (**95**) is not tolerable, derivatives **136a** and **136b** carrying one or two methyl groups were screened *in silico* (Table 8). The scores for the different crystal structures of *K*-Ras4B show that protection of the hydroxy groups leads to less active compounds. The methoxy derivatives are unable to form the same number of hydrogen bonds to the amino acids of the protein. In contrast to dimethoxy BPA (**136b**), the monomethoxy derivative **136a** maintains the hydrogen bond to Leu6 in 4DSO. Both methoxy derivatives are rotated away from Glu70 due to a repellent interaction. Dimethoxy BPA (**136b**) is also turned away from Leu6 to form a hydrogen bond to Ser39 instead (Figure 59). In case of 4EPY, bisphenol A (**23**) and monomethoxy BPA (**136a**) overlap perfectly, because both compounds form a hydrogen bond to Leu6. In contrast, the dimethoxy derivative is inserted less deeply into the binding pocket due to no attractive interaction with Leu6. The prediction for 4EPX shows no difference in positioning for the three compounds although only bisphenol A (**23**) forms a hydrogen bond to Leu6.

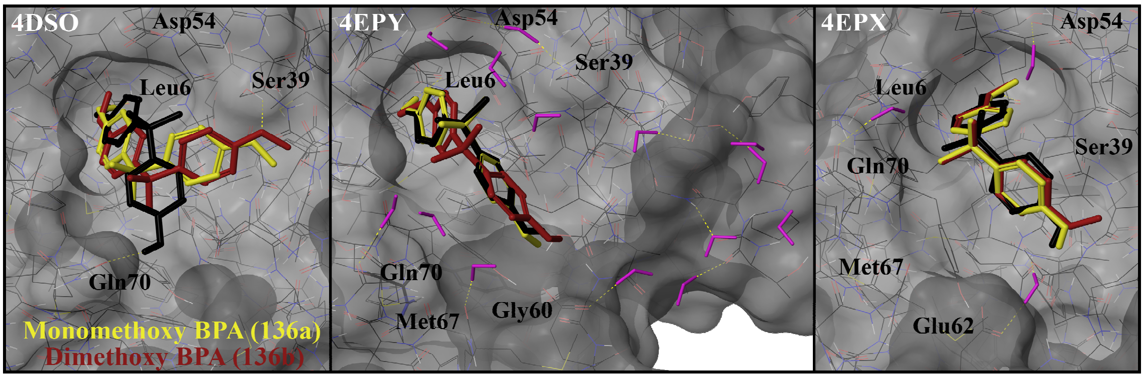

*Figure 59: Comparison of the binding modes of monomethoxy BPA (136a, yellow) and dimethoxy BPA (136b, red) in the binding pocket of the crystal structures 4DSO, 4EPY and 4EPX of the K-Ras protein predicted by Glide with bisphenol A (**23**, black) as reference. Water molecules are shown in purple as a stick model.*

The Glide scores of crystal structures 4DSO and 4EPY decrease successively with an increasing number of methoxy groups. For 4EPX, the Glide score of the monomethoxy derivative **136a** is increased in comparison to bisphenol A (**23**). Dimethoxy BPA (**136b**) then again even shows positive Glide values as expected.

*Table 8: Glide scores of mono- and dimethoxy derivatives **136a** and **136b** in comparison to BPA (**23**) as reference. In case of 4DSO, all water molecules were removed prior to docking experiments. For 4EPX, three water molecules are included for docking experiments while 4EPY contains a total of 14 water molecules surrounding the ligand binding pocket.*

Substance	Structure	4DSO		4EPY		4EPX	
		max	min	max	min	max	min
Bisphenol A (23)		-3.24	-2.30	-1.36	-1.00	-1.67	3.02
Monomethoxy BPA (136a)	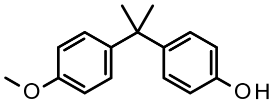 **136a**	-2.47	-1.76	-1.26		-3.65	
Dimethoxy BPA (136b)	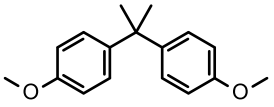 **136b**	-1.91		1.36	1.79	0.20	3.57

Ethers **136a** and **136b** are easily accessible through reaction of Bisphenol A (**23**) with potassium carbonate and dimethylsulfate (Scheme 16).[107] As both hydroxy groups can react with the reagent, a mixture of the starting material, the monoether and the diether were obtained. Due to the significant difference in polarity, the compounds were easily separated giving monoether **136a** in 38% yield and diether **136b** in 45% yield, respectively.

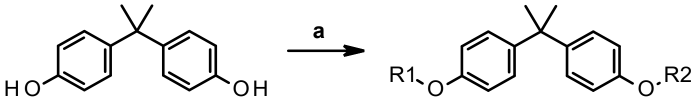

23

136a R1 = Me, R2 = H
136b R1 = Me, R2 = Me

*Scheme 16: Synthesis of bisphenol A ethers **136a** and **136b**. Reaction conditions: (a) K_2CO_3, dimethylsulfate, acetone, reflux, 7 h, 38% (**136a**), 45% (**136b**).*

As expected, the NMR experiment for dimethoxy BPA derivative **136b** does not show any interaction of the ligand with the protein. That finding confirms the assumption that blocking of both hydroxy groups of bisphenol A (**23**) is not tolerated. In contrast, the monomethoxy derivative **136a** was expected to bind to *K*-Ras4B via the unmethylated phenol ring. The affinity was predicted to be weakened as the probability to insert the unmethylated ring into the binding pocket is 50%. However, the monomethoxy derivative **136a** does also not bind to the protein. This result shows that both hydroxy groups are obviously required for binding to the *K*-Ras4B protein.

As no significant shifts can be identified from the NMR experiments, no HADDOCK model can be computed. The calculation requires the definition of active residues, which are not available in these cases. Therefore, the conclusion that both phenol rings are contribute significantly to ligand binding can only be supported by the results of the Glide docking. The Glide scores as well as the conformations depicted in Figure 59 clearly prove that derivatisation of the hydroxy groups leads to a loss of affinity to the protein. The ability to form hydrogen bonds as a hydrogen bond donor is lost. Consequently, interaction with the protein is significantly weakened, which results in no significant shifts in the NMR measurement.

4.3.2.1.3. Examination of fragments of the bisphenols **23** and **95**

To examine the exact binding mode of bisphenol A (**23**) and bisphenol AF (**95**) further, two different fragments of the lead structures were investigated: 4-*tert*-butylphenol (**137**) and 4-(trifluoromethyl)phenol (**138**, Figure 60).

137 **138**

*Figure 60: Fragments of the lead structures BPA (**23**) and BPAF (**95**).*

Figure 62 shows the titration experiment of the bisphenol A fragment 4-*tert*-butylphenol (**137**). As can be seen from the overlay of the spectra, the compound interacts with the protein in a similar way as bisphenol A (**23**). Shifts of the amino acids belonging to the ligand binding pocket (Leu6, Leu56, Thr74 and Gly75) can be observed. Additionally, allosteric effects on amino acids throughout the protein reaching even the nucleotide binding pocket (Gly13, Asp57 and Gly60) appear. Furthermore, a minor shift of the peak of Ser39 is observable. Strong interaction with this amino acid is considered to be unfavourable as it orients the ligand towards the wrong side of the binding pocket away from Thr74 and Gly75. The k_D value calculated from the NMR titration experiment amounts to 6.26 ± 1.66 mM. The HADDOCK model (Figure 61) clearly proves that the compound enters the ligand binding pocket deeply. In contrast to bisphenol A (**23**), phenol **137** can be inserted into the pocket with the *tert*-butyl group first. The hydroxy group then interacts with the surface of the protein instead of Leu6 at the bottom of the binding pocket.

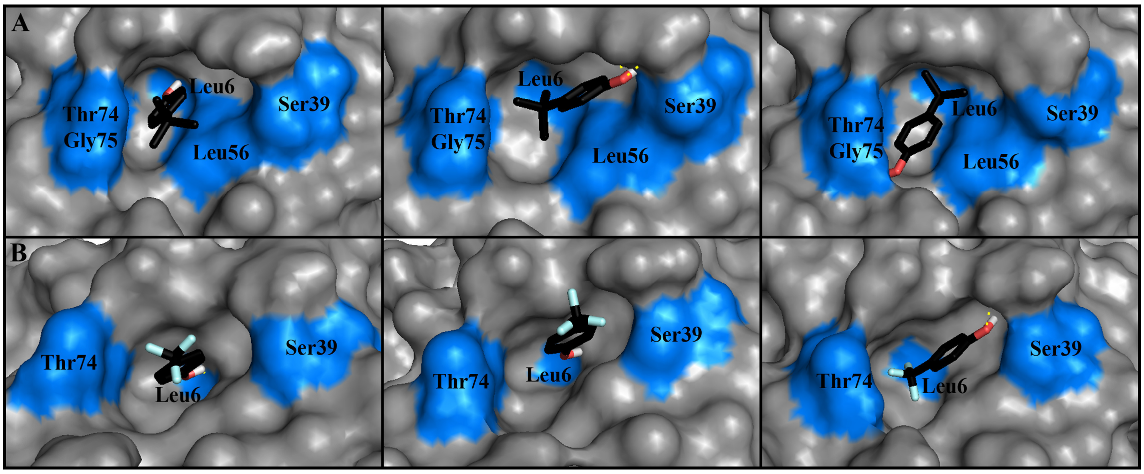

*Figure 61: Different conformations of 4-tert-butylphenol (**137**, **A**) and 4-(trifluoromethyl)phenol (**138**, **B**) in the binding pocket of K-Ras4B (PDB ID: 4DSO) predicted by HADDOCK.[44] The amino acids, which were defined as active residues for the HADDOCK calculation are highlighted in blue.*

The bisphenol AF fragment 4-(trifluoromethyl)phenol (**138**) exhibits a significantly weaker interaction (k_D>15 mM) with the protein as the NMR titration shows (Figure 63). The peak shifts induced by phenol **138** are weak in comparison to bisphenol AF (**95**). The compound is able to address the ligand binding pocket similar to BPA (**23**) and BPAF (**95**) as the HADDOCK model shows (Figure 61). The measurement of these two small fragments of bisphenol A (**23**) and bisphenol AF (**95**) reveal that the second phenyl ring, which interacts with the surface of the protein, contributes significantly to the binding affinity to the protein.

In conclusion, this moiety may not be derivatised in order to maintain good interaction with the protein. On the contrary, preventing the bisphenol A analogues from interacting with the *K*-Ras4B protein can be achieved by derivatisation of the hydroxy groups.

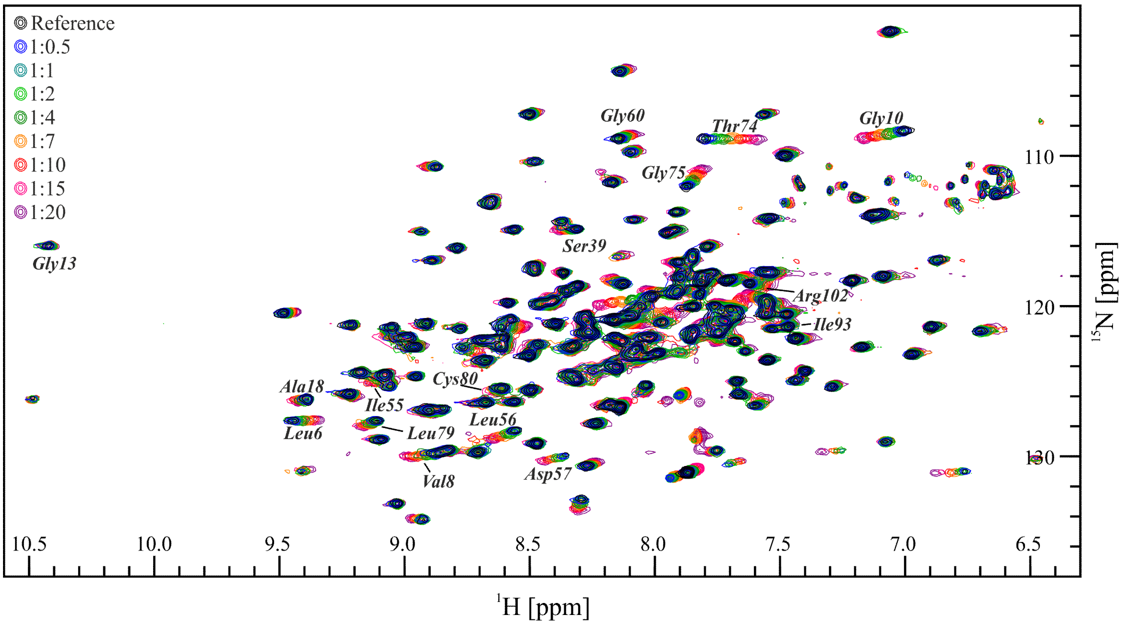

*Figure 62: ^{1}H,^{15}N-TROSY NMR overlay of the titration steps of 4-tert-butylphenol (**137**) to the K-Ras protein.*[106]

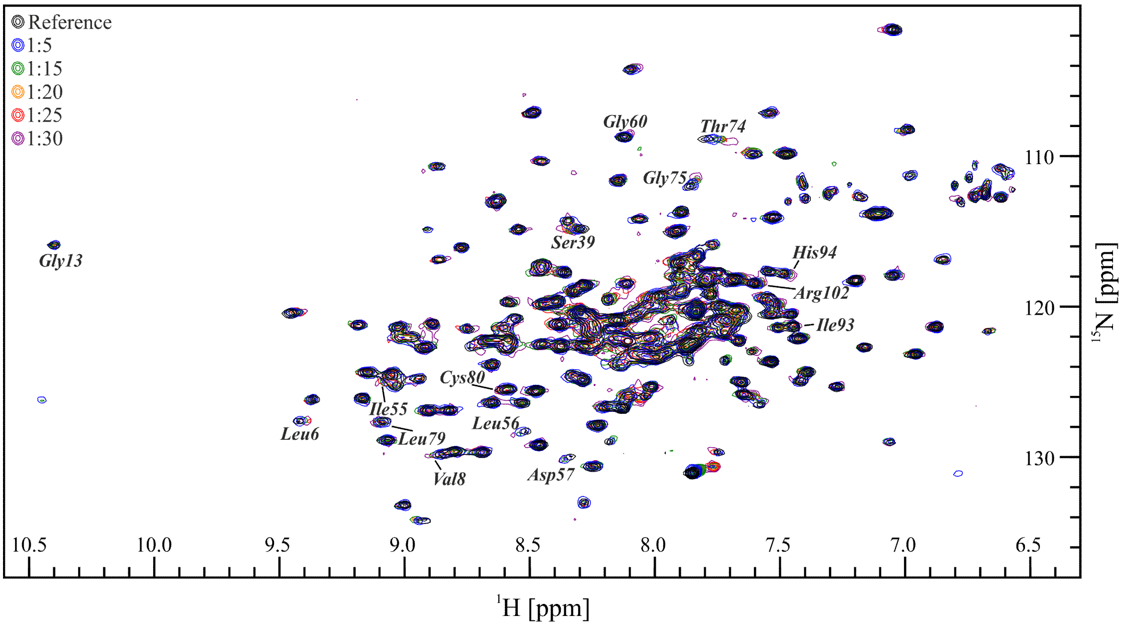

*Figure 63: ^{1}H,^{15}N-TROSY NMR overlay of the titration steps of 4-(trifluoromethyl)phenol (**138**) to the K-Ras protein.*[102]

4.3.2.2. Modification of the phenol rings of bisphenol A (**23**)

Fesik and coworkers[73] showed that the ligand binding pocket of *K*-Ras4B can also be occupied by an indole moiety (inhibitors **19** and **94a**). As a second approach, the phenol rings of bisphenol A (**23**) are replaced by heteroaromatic rings. The heteroatoms need to recreate the interaction of the hydroxy groups of bisphenol A (**23**) and bisphenol AF (**95**) with the protein.

As shown in the first section of Table 9, five-membered rings with a nitrogen atom exhibit the best docking scores. In comparison to bisphenol A (**23**), none of the compounds **139-143** exhibits an improved Glide score. In case of 4DSO, the pyrrole derivatives **139** and **140** can facilitate a hydrogen bond to the side chain of Asp54 to interact with the protein (Figure 64). Additionally, bis-3-pyrrol A (**140**) forms a hydrogen bond to the side chain of Glu37. In contrast, heteroaromatic compounds with either an oxygen or a sulfur atom cannot act as a hydrogen donor the same way. In case of 4EPX and 4EPY, the pyrrole analogue **140** forms hydrogen bonds either to Tyr71 or to the side chain of Glu37 (Figure 64). Overall, heteroaromats incorporating a nitrogen atom especially in 3-position seems favourable.

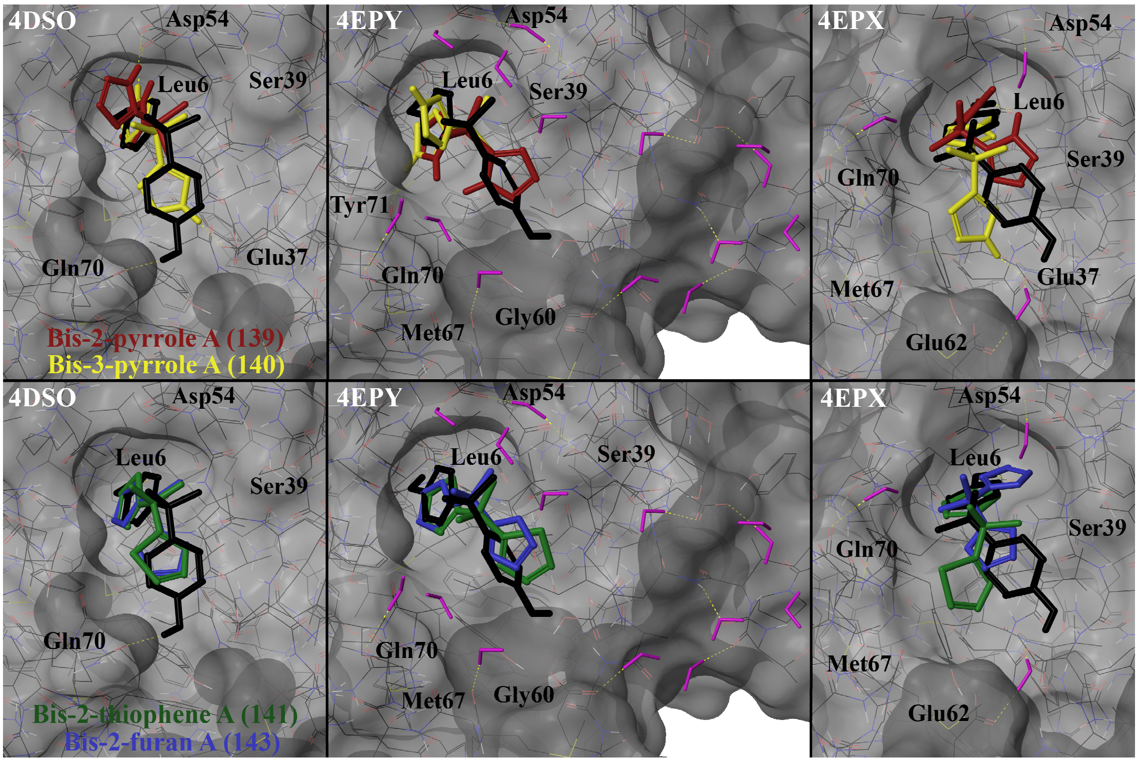

*Figure 64: Comparison of the binding modes of bis-2-pyrrole A (**139**, red), bis-2-pyrrole A (**140**, yellow), bis-2-thiophene A (**141**, green) and bis-2-furan A (**143**, blue) in the binding pocket of the crystal structures 4DSO, 4EPY and 4EPX of the K-Ras protein predicted by Glide with bisphenol A (**23**, black) as reference. Water molecules are shown in purple as a stick model.*

Introduction of a second nitrogen atom has a positive effect on the Glide score of the resulting imidazole or pyrazole derivatives **144-149** (Table 9). Both, imidazole as well as pyrazole nitrogen atoms can be included in an additional hydrogen bond with the backbone of Asp54 regarding 4DSO (Figure 65). Furthermore, Lys5 can be addressed by the second heteroaromatic ring. In case of 4EPX and 4EPY, Tyr71 and Glu37 are involved in hydrogen bonds instead of Asp54.

An annulated pyrrole ring seems to be a favourable structure, since it allows the nitrogen atom to be inserted deeper into the binding pocket depending on its position. Bis-indoles **150-155** mainly feature good Glide scores, especially the 2- and 3-substituted bis-indoles **150** and **151**. These compounds show that the nitrogen atom preferably interacts with the top of the ligand binding pocket such as Asp54 (Figure 66). In case of bis-3-indole A (**151**), the nitrogen atom of the second indole ring can interact with Gln70 similar to bisphenol A (**23**).

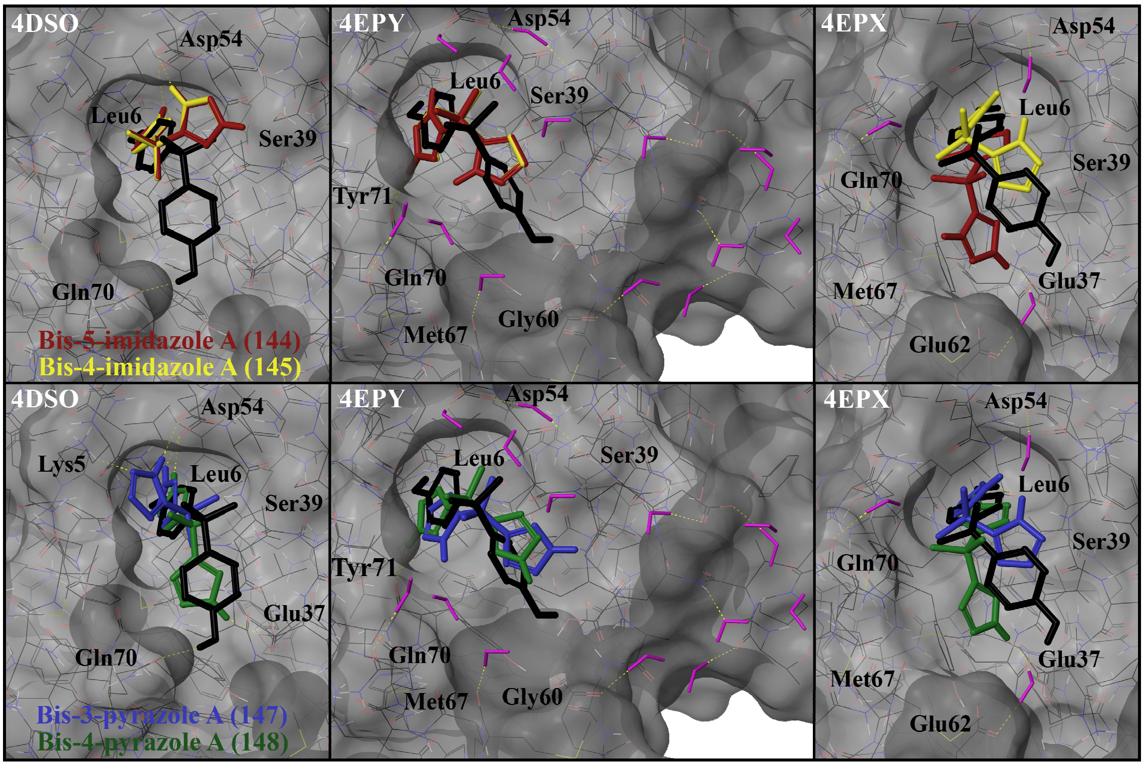

*Figure 65: Comparison of the binding modes of bis-5-imidazole A (**144**, red), bis-6-imidazole A (**145**, yellow), bis-3-pyrazole A (**147**, green) and bis-4-pyrazole A (**148**, blue) in the binding pocket of the crystal structures 4DSO, 4EPY and 4EPX of the K-Ras protein predicted by Glide with bisphenol A (**23**, black) as reference. Water molecules are shown in purple as a stick model.*

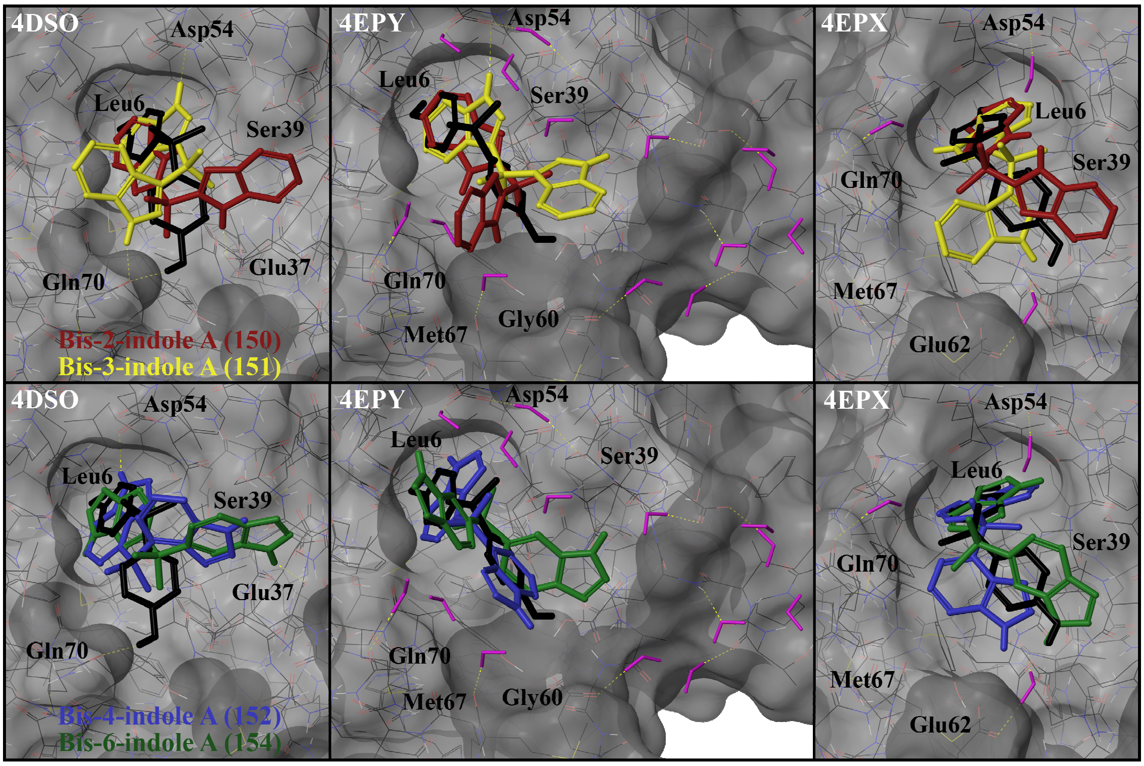

*Figure 66: Comparison of the binding modes of bis-2-indole A (**150**, red), bis-3-indole A (**151**, yellow), bis-4-indole A (**152**, blue) and bis-6-indzole A (**154**, green) in the binding pocket of the crystal structures 4DSO, 4EPY and 4EPX of the K-Ras protein predicted by Glide with bisphenol A (**23**, black) as reference. Water molecules are shown in purple as a stick model.*

The 2- and 3-substituted bis-indoles **150** and **151** seem favourable according to the predictions by Glide. Additionally, it is known from the Fesik inhibitors **19** and **94a** that an indole moiety binds to the ligand binding pocket of *K*-Ras4B. Thus, indole **151** was chosen for synthesis in analogy to the compounds found by Fesik and coworkers[73]. The 2-substituted indole **150** was also chosen for comparison with the 3-substituted analogue.

*Table 9: Glide scores of heteroaromatic analogues **139-155** in comparison to BPA (**23**) as reference. In case of 4DSO, all water molecules were removed prior to docking experiments. For 4EPX, three water molecules are included for docking experiments while 4EPY contains a total of 14 water molecules surrounding the ligand binding pocket.*

Substance	Structure	4DSO		4EPY		4EPX	
		max	min	max	min	max	Min
Bisphenol A (23)		-3.24	-2.30	-1.36	-1.00	-1.67	3.02
Bis-2-pyrrole A (139)	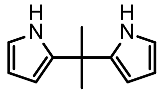 **139**	-2.45	-1.79	-1.22		-0.75	0.14
Bis-3-pyrrole A (140)	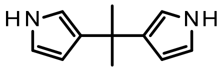 **140**	-3.15		-0.83	1.64	-2.44	-0.17
Bis-2-thiophene A (141)	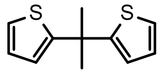 **141**	-2.28	-1.97	-3.42	-0.31	-2.66	-0.26
Bis-3-thiophene A (142)	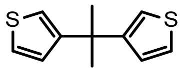 **142**	-2.00	-1.58	-0.16	0.22	-2.84	0.03
Bis-2-furan A (143)	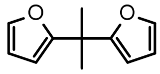 **143**	-1.18	-0.95	-0.22		-0.37	-0.25
Bis-5-imidazole A (144)	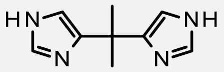 **144**	-3.65	-2.19	-1.18	-0.28	-3.36	-3.05
Bis-4-imidazole A (145)	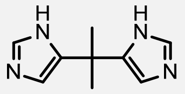 **145**	-3.49	-2.17	-1.78	2.04	-3.51	0.61
Bis-2-imidazole A (146)	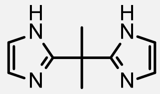 **146**	-3.26	-1.62	-4.80	-1.03	-0.94	0.35
Bis-3-pyrazol A (147)	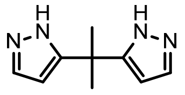 **147**	-3.22	-1.75	-1.20	-0.33	-3.23	0.87
Bis-4-pyrazol A (148)	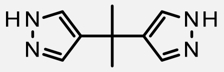 **148**	-3.30		-1.19		-2.84	

Bis-5-pyrazol A (149)	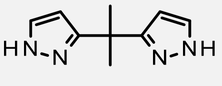 **149**	-3.47	-2.58	-0.97	-0.67	-4.09	-0.53
Bis-2-indole A (150)	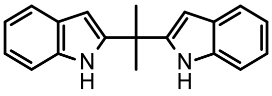 **150**	-3.13	-2.79	-4.39	-1.23	-2.21	0.17
Bis-3-indole A (151)	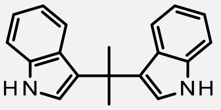 **151**	-3.62		-3.99	-0.39	-0.52	0.77
Bis-4-indole A (152)	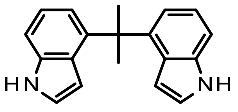 **152**	-2.89	-1.38	-0.87		-1.97	
Bis-5-indole A (153)	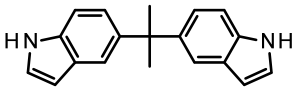 **153**	-2.88	-2.52	-0.85	0.68	-1.79	
Bis-6-indole A (154)	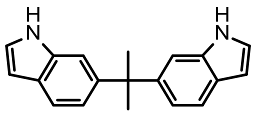 **154**	-3.03	2.17	-0.11	0.54	-3.68	-3.26
Bis-7-indole A (155)	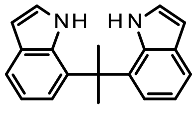 **155**	-2.62	-1.90	-0.37		-0.81	1.54

Bis-indoles **150** and **151** were synthesized similar to BPA (**23**) using indole (**156**) instead of phenol (**161**) in the dehydration reaction with acetone. In case of indole (**156**), two different compounds can be synthesized as shown in Scheme 17. As the 3-position of indole (**156**) is favoured in electrophilic aromatic substitution reactions, the conversion to the bis-3-indole A derivative **151**[127–129] can easily be accomplished with catalytic amounts of aluminum trichloride.

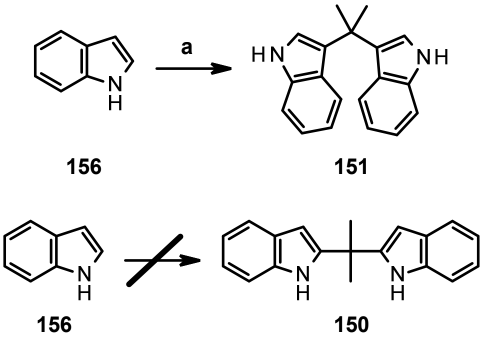

Scheme 17: Synthesis of bis-3-indole A derivative ***151*** *and bis-2-indole A derivative* ***150****. Reaction conditions: (a) acetone, AlCl*$_3$*, ACN, r.t., 20 min, 11%.*

In contrast, the 2-position of indole (**156**) is disfavoured in the indole system, which makes this conversion more challenging. According to Smithen *et al.*[130], indole (**156**) and acetone were mixed with TFA in DCM. Unfortunately, the desired compound could not be found in the resulting mixture. Instead, bis-3-indole A derivative **151** was obtained in minor amounts.

As no further literature was available on this reaction, the synthesis of the 3-methyl analogue of bis-2-indole A **158** was attempted according to Das *et al.* (Scheme 18).[131] For this reaction, an ionic liquid was required, which is readily available from di-*n*-propylamine and sulfuric acid. Catalytic amounts of the ionic liquid (di-*n*-propylammonium hydrogensulfate) were mixed with skatole (**157**) and acetone and subsequently irradiated in a microwave oven at 100 °C for 7 min. The temperature was increased to 130 °C for 30 min as almost no conversion was observed. This resulted in two reaction products as observed by thin-layer-chromatography (TLC). The starting material was still not consumed completely. Therefore, the mixture was reacted at 160 °C for another 30 min. According to TLC, the compound that was first formed in the reaction had disappeared. Examination of the reaction mixture revealed that the desired product was not obtained. To isolate the product formed first, the reaction was repeated with a temperature of 120 °C and a reaction time of 30 min. The products formed were separated chromatographically. Unfortunately, again none of the fractions contained the desired product.

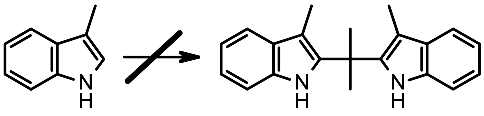

*Scheme 18: Failed synthesis of 3,3'-dimethyl-bis-2-indole A **158**.*

Bis-indole **151** shows no significant interaction with the protein in the NMR measurement. Minor shifts can be observed for Ser39, Thr74 and Gly75, which were used for the HADDOCK computation in Figure 67. According to the best model provided by HADDOCK, molecule **151** does not enter the ligand binding pocket, but interacts with the surface of the protein instead. One possible explanation for this finding could be a wrong attaching point between the bridging C-atom and the indole rings. The 3-substitution of the indole moiety requires the aromatic ring to enter the binding pocket in a twisted manner as can be seen from Figure 67. The binding pocket is known to be of limited size not even tolerating a methyl substituent as the examination of the bisphenol A analogue **99**[122] has shown. The ligand might therefore not be able to penetrate the binding cleft as deeply as bisphenol A (**23**) and bisphenol AF (**95**) to interact with Leu6.

It can therefore be deduced that replacing the phenol moieties for heteroaromatic rings results in compounds, which are unable to interact with the *K*-Ras4B protein to the same extend as bisphenol A (**23**) and bisphenol AF (**95**). This again underlines the importance of the phenyl rings in general and the hydroxy groups in particular. Ligands, which lack this structural motif, do not bind to the protein. This knowledge can be used for the development of ligands, which selectively bind to the protein, as well as compounds that cannot interact with the protein.

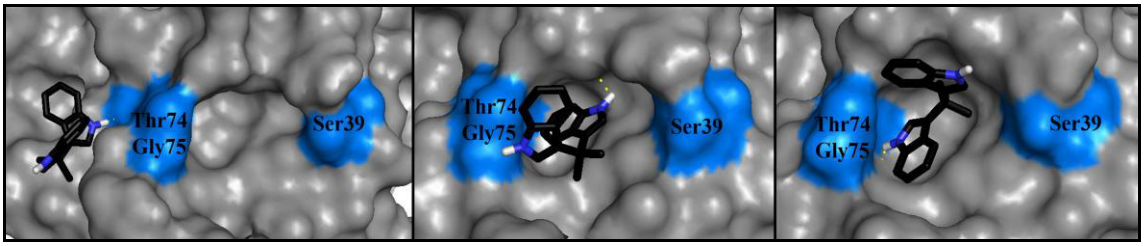

Figure 67: Different conformations of bis-3-indole derivative ***151*** *in the binding pocket of K-Ras4B (PDB ID: 4DSO) predicted by HADDOCK.*[44] *The amino acids, which were defined as active residues for the HADDOCK calculation are highlighted in blue.*

4.3.2.3. Modification of the methyl groups of bisphenol A (**23**)

To increase the binding affinity of the lead structure bisphenol A (**23**), hit evolution by fragment growth was attempted to enable further interactions with the protein. Therefore, elongation of the molecule from one of the methyl groups was attempted.

4.3.2.3.1. First iteration

As an anchor group for the attachment of building blocks, an acid functionality was chosen. This group can either substitute or be attached to one of the CH_3-groups as shown in Table 10. In the first case, the methyl group would be formally oxidized to the corresponding acid. The second case seemed preferable as this directly extends the molecule. Additionally, it allows more flexibility for further building blocks to be attached in a later optimization step.

Table 10: Glide scores of BPA derivatives ***159*** *and* ***160*** *in comparison to BPA (****23****) as reference. In case of 4DSO, all water molecules were removed prior to docking experiments. For 4EPX, three water molecules are included for docking experiments while 4EPY contains a total of 14 water molecules surrounding the ligand binding pocket.*

Substance	**Structure**	**4DSO**		**4EPY**		**4EPX**	
		max	min	max	min	max	min
Bisphenol A (23)		-3.24	-2.30	-1.36	-1.00	-1.67	3.02
BPA formic acid (159)	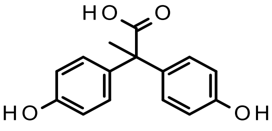 **159**	-3.53	-2.74	-1.58	-1.01	-1.15	
BPA acetic acid (160)	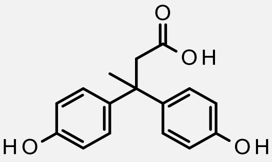 **160**	-4.35	-2.56	-1.55	-1.40	-2.43	-1.98

As displayed in Table 10, acid derivative **160** exhibits the better Glide score in comparison to both, BPA and the other acid derivative **159**. As expected, the acid functionality is predicted to form an additional hydrogen bond to Lys5 in case of crystal structure 4DSO while it interacts with water molecules in the binding pocket in case of 4EPY and 4EPX (Figure 68). In all cases, the hydrogen bond to Leu6, which fixates the ligands deep into the pocket, is maintained. The structures predicted for BPA acetic acid (**160**) can more frequently form these hydrogen bonds while the acid moiety of BPA formic acid (**159**) points in the wrong direction in several structures. Thus, BPA acetic acid (**160**) was chosen for synthesis as the more promising derivative.

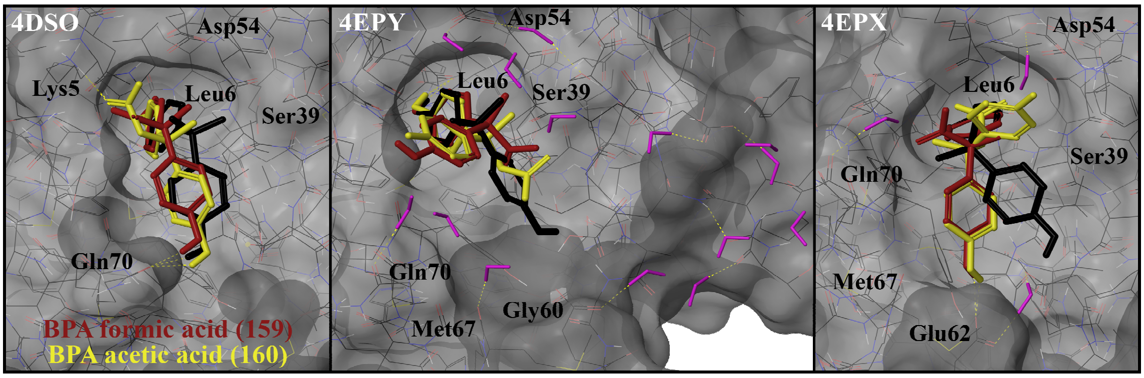

*Figure 68: Comparison of the binding modes of BPA formic acid (**159**, red) and BPA acetic acid (**160**, yellow) in the binding pocket of the crystal structures 4DSO, 4EPY and 4EPX of the K-Ras protein predicted by Glide with bisphenol A (**23**, black) as reference. Water molecules are shown in purple as a stick model.*

The synthesis of bisphenol A acid derivative **160** follows the route described by Seward *et al.* and Carta *et al.*[132,133] The reaction (Scheme 19) did not give the desired compound regardless of the ester functionality of ketone **162**.

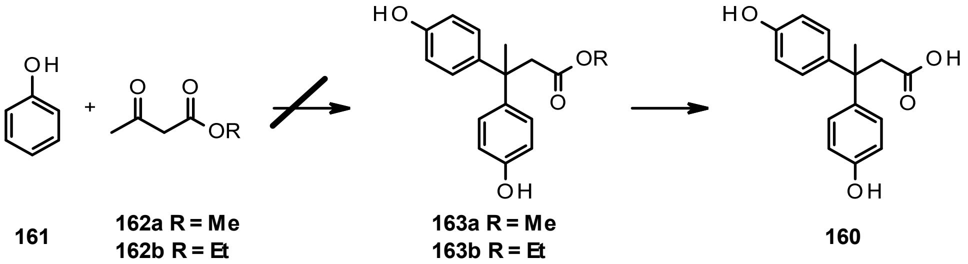

*Scheme 19: Synthesis of Bisphenol A acid derivative **160** through the dehydration reaction of phenol (**161**) with β-ketoester **162** to afford Bisphenol A ester derivative **163**.*

As the first reactions with phenol (**161**) as reaction partner failed, the reaction was repeated using anisole (**164**) to afford the protected bisphenol A derivative **165a** in a moderate yield of 55% (Scheme 20).[132,133] Depending on the water content of the sulfuric acid, free acid **165b** can be observed in varying amounts as a side product of the dehydration reaction. Cleavage of the methoxy residues as well as the ethyl ester is accomplished through reaction with the Lewis acid boron tribromide to yield bisphenol A 2-acid derivative **160** (76%).[105] This route afforded the desired bisphenol A acid derivative **160** in an overall yield of 42%.

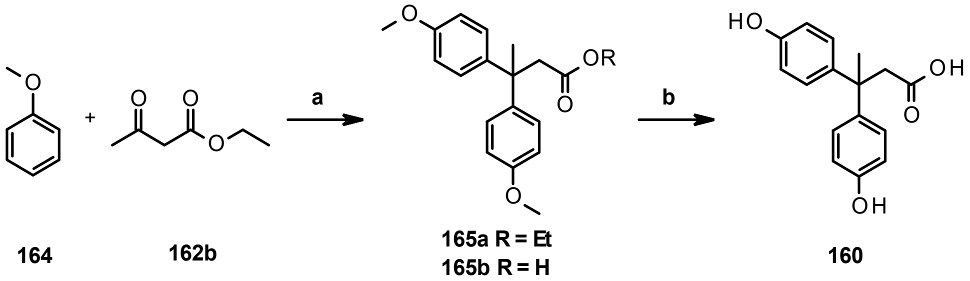

*Scheme 20: Synthesis of Bisphenol A acid derivative **160** through the dehydration reaction of anisole (**164**) with β-ketoester **162b** to afford Bisphenol A ester derivative **165**. Reaction conditions: (a) conc. H_2SO_4, 0 °C → r.t., 22 h, 55%, (b) 1 M BBr_3, DCM, -78 °C → r.t., 19 h, 76%.*

Upon addition of BPA derivative **160** to the aqueous buffer solution of the protein, the compound precipitated. Under physiological conditions, the acid functionality is deprotonated. A proton NMR proves that the compound was available for interaction with the protein. Minor shifts of Leu6, Leu56, Thr74 and Gly75 can be observed in the NMR measurement, which can be found in the Appendix (Chapter 7). These amino acids were then used for a HADDOCK computation. Figure 69 shows that acid **160** cannot penetrate the ligand binding pocket as was expected from the Glide dockings. Instead, the molecule interacts with the surface of the protein, especially Thr74 and Gly 75 via the acid residue. This interaction prevents the molecule from inserting a phenol ring into the ligand binding pocket and the affinity for the protein is weakened.

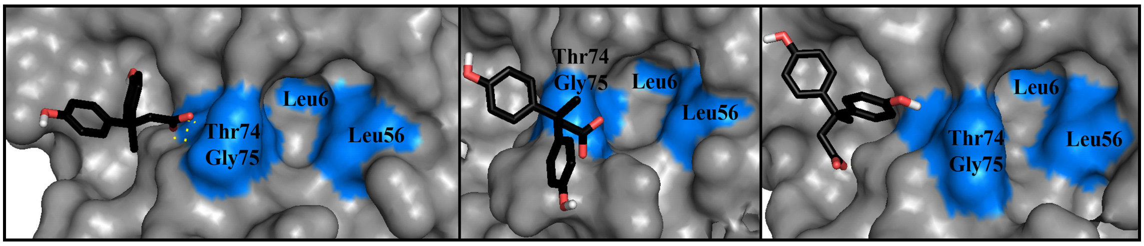

*Figure 69: Different conformations of acetic acid derivative **160** in the binding pocket of K-Ras4B (PDB ID: 4DSO) predicted by HADDOCK.[44] The amino acids, which were defined as active residues for the HADDOCK calculation are highlighted in blue.*

4.3.2.3.2. Second iteration

The free acid **160** precipitated partially from the aqueous protein buffer solution as a result of its highly polar character. Therefore, the acid functionality was masked either as a methyl ester or an amide to obtain less polar compounds.

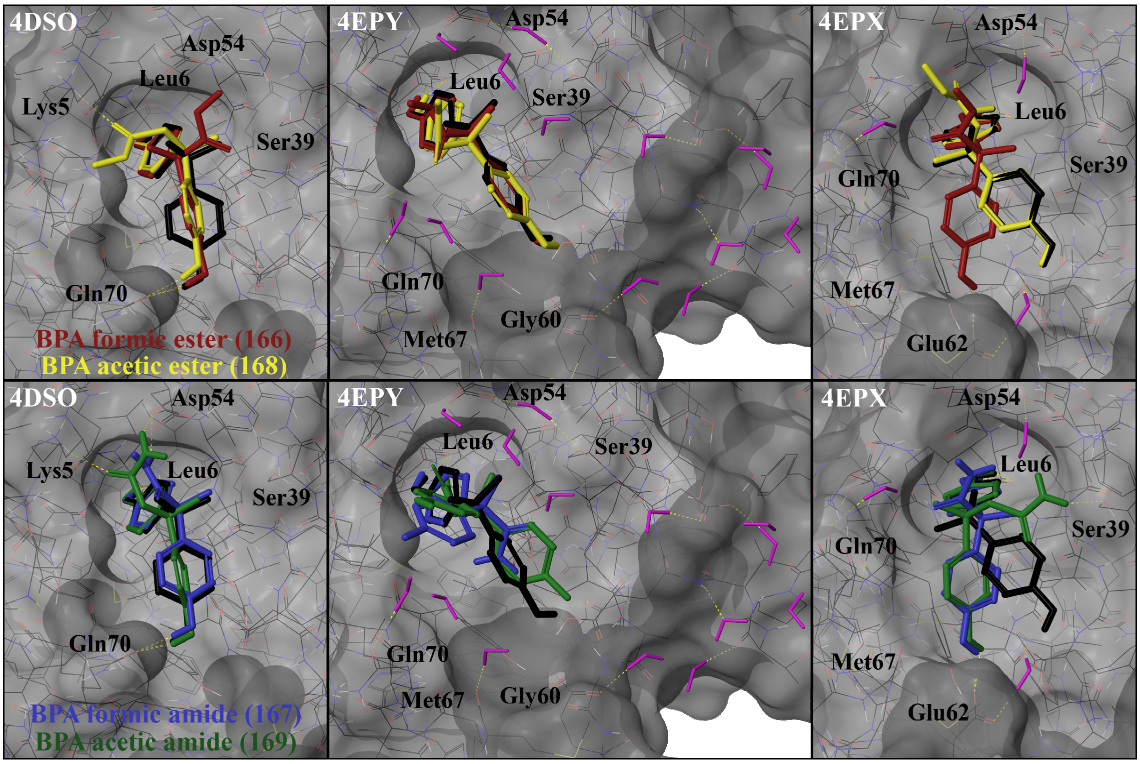

*Figure 70: Comparison of the binding modes of BPA formic ester (**166**, red), BPA formic amide (**167**, blue), BPA acetic ester (**168**, yellow) and BPA acetic amide (**169**, green) in the binding pocket of the crystal structures 4DSO, 4EPY and 4EPX of the K-Ras protein predicted by Glide with bisphenol A (**23**, black) as reference. Water molecules are shown in purple as a stick model.*

The methyl ester was chosen in order to reduce the polarity and prevent deprotonation of the compound. The amide moiety offers additional hydrogen bond acceptor and donor functionalities to increase the interaction with the protein.

As Table 11 shows, the best Glide scores can be obtained when incorporating an amide functionality. In case of 4DSO, hydrogen bonds to Lys5, Asp54 and Gln70 are predicted for BPA acetic amide (**169**) as depicted in Figure 70. In contrast, the more restricted amide functionality of BPA formic amide (**167**) cannot reach two amino acids simultaneously to form two hydrogen bonds although it adopts a similar orientation. Interaction with the protein is less strong than in case of BPA acetic amide (**169**).

In case of crystal structure 4EPY, the ester functionality of BPA formic ester (**166**) cannot interact with the protein. In contrast, BPA acetic ester (**168**) forms a hydrogen bond to a nearby water molecule. The corresponding amides form up to two hydrogen bonds to reach two water molecules as expected. BPA formic amide (**167**) has to adopt a binding mode differing from that of BPA (**23**) breaking the hydrogen bond to Leu6. The prediction for 4EPX gives a similar result for the amide derivatives. The prediction for BPA acetic ester (**168**) disagrees with the other two computations as no hydrogen bond can be formed between the surrounding water molecules and the ester group.

Taking these considerations into account, the amides are preferred over the ester derivatives. BPA acetic amide (**169**) is able to orient the amide group in a more beneficial way to form the desired hydrogen bonds than the conformationally more restricted BPA formic amide (**167**).

*Table 11: Glide scores of BPA derivatives **166-169** in comparison to BPA (**23**) as reference. In case of 4DSO, all water molecules were removed prior to docking experiments. For 4EPX, three water molecules are included for docking experiments while 4EPY contains a total of 14 water molecules surrounding the ligand binding pocket.*

Substance	**Structure**	**4DSO**		**4EPY**		**4EPX**	
		max	Min	max	min	max	min
Bisphenol A (23)		-3.24	-2.30	-1.36	-1.00	-1.67	3.02
BPA formic ester (166)	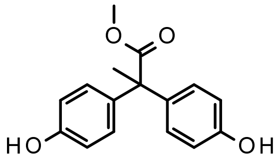 **166**	-2.89	-2.80	-1.34	-1.03	-1.58	4.85
BPA formic amide (167)	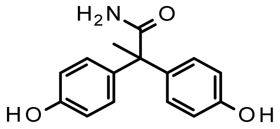 **167**	-3.56	-2.50	-2.52	-2.31	-1.96	2.20
BPA acetic ester (168)	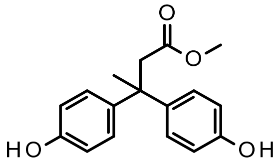 **168**	-3.69	-1.80	-1.55	2.60	-1.69	-0.27
BPA acetic amide (169)	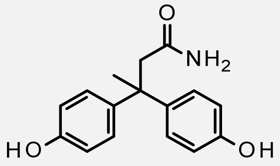 **169**	-4.47	-2.33	-2.37	1.67	-1.90	2.19

Amide derivative **169** can be synthesized from the deprotected bisphenol A derivative **160** in two steps by amide coupling and subsequent cleavage of the benzyl group (Scheme 21). Amide coupling of derivative **160** with benzylamine afforded amide **170** under standard conditions. Cleavage of the benzyl group to afford free amide **169** was unsuccessful under the conditions described by Nemmara *et al.* or Thirumalai Rajan *et al.*[134,135] Instead, substituted amide derivatives **170** and **173** were chosen for NMR studies. These analogues should still be able to form at least one hydrogen bond by donating the remaining proton in the interaction.

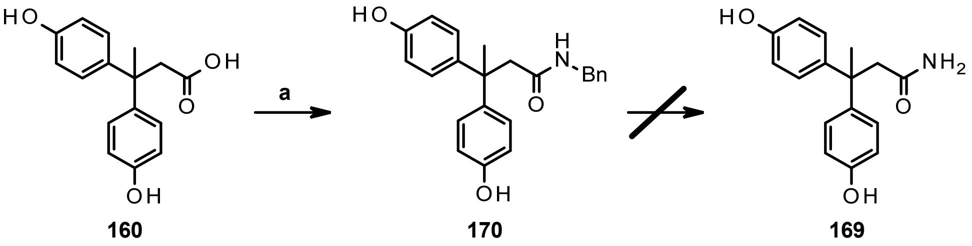

*Scheme 21: Synthesis of benzylamide **170** proceeding from acid derivative **160** to afford free amide **169** through cleavage of the benzyl residue. Reaction conditions: (a) benzylamine, HATU, DIPEA, DMF, r.t., 16 h, 77%.*

To improve the coupling yield, amide **173** was synthesized from the protected BPA acid derivative **165b** (Scheme 22). The amide coupling of acid **165b** with aniline under standard reaction conditions gave amide **171** in good yield of 82%. Unfortunately, even after 4.5 days reaction time no fully deprotected amide **173** was obtained with boron tribromide.[105] Instead, the mono-deprotected amide **172** was obtained in 13% yield. As the deprotection of the methoxy groups is difficult, the amide coupling was conducted with bisphenol A acid derivative **160** under the same reaction conditions as before to directly afford amide **173** in moderate yield of 56%.

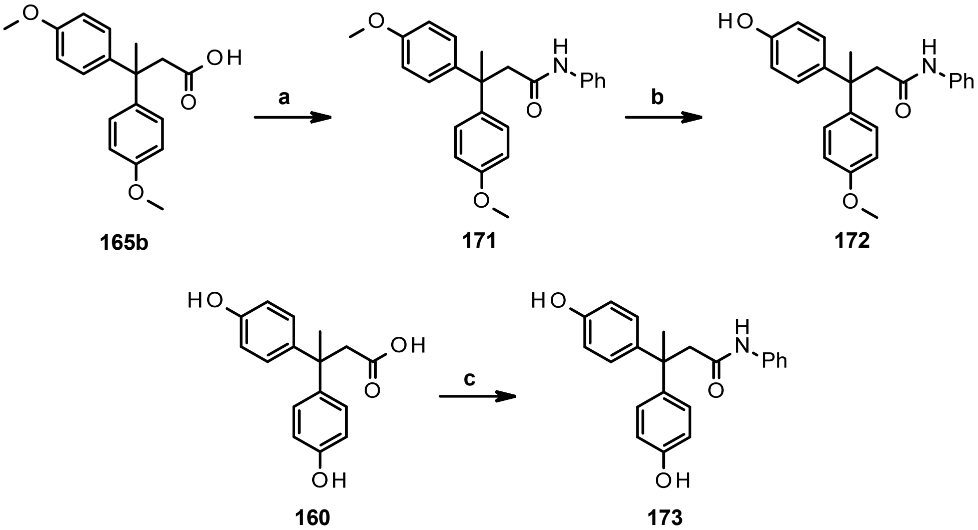

*Scheme 22: Synthesis of Bisphenol A benzamide derivative **173**. The first attempt starting from protected Bisphenol A acid derivative **165b** failed due to incomplete deprotection of the methoxy groups affording amide **172** instead. In the second attempt proceeding from acid derivative **160**, the desired amide was successfully obtained. Reaction conditions: (a) aniline, HATU, DIPEA, DMF, r.t., 16 h, 82%, (b) 1 M BBr_3, DCM, -78 °C → r.t., 4.5 d, 13%, (c) aniline, HATU, DIPEA, DMF, r.t., 15 h, 56%.*

Amide **172**, a side product of the synthesis of amide **173**, was examined as well due to its asymmetric substitution pattern regarding the two phenyl rings. Unfortunately, all three amides **170**, **172** and **173** precipitated partially from the protein solution. The proton spectrum indicates only minor amounts of the compounds in solution. None of the compounds shows a significant interaction with the protein. The corresponding NMR overlays can be found in the Appendix (Chapter 7). The minor shifts observed for amides **170** and **173** were used for HADDOCK computations. In comparison, no shifts could be identified from the NMR measurement of **172**. Thus, no HADDOCK model can be calculated for this compound.

The HADDOCK models in Figure 71 shows that both amides **170** and **173** cannot interact with the ligand binding pocket of the *K*-Ras4B protein in the anticipated way. Instead of inserting a phenol ring into the binding cleft, the molecule is located on the surface of the protein. Amide **170** can form hydrogen bonds to amino acids close to the binding pocket, amide **173** can only interact with residues farther away from the targeted binding site.

Consequently, it can be deduced that introduction of a large substituent to one of the methyl groups leads to compounds, which cannot interact with the protein. In contrast to other analogues before, there substances can be used for polymer synthesis as both hydroxy groups are preserved.

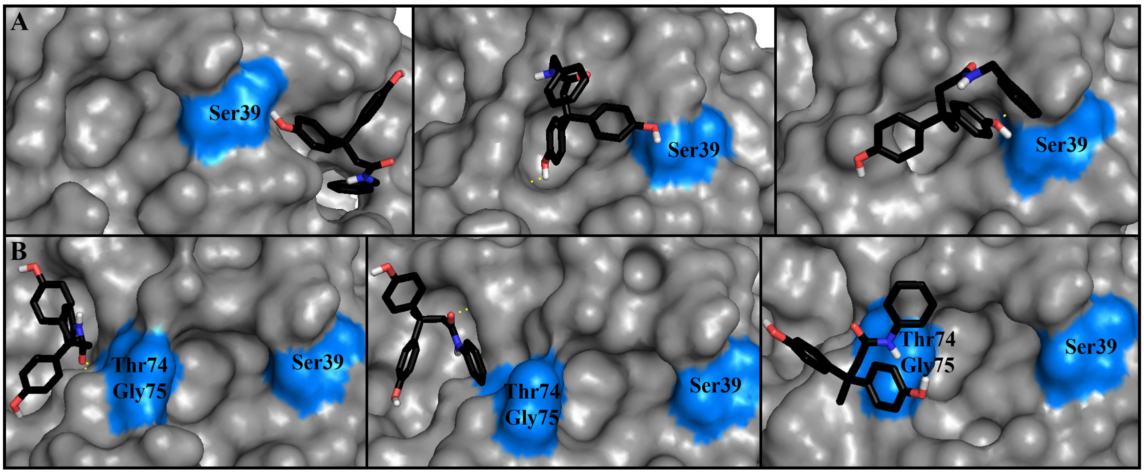

*Figure 71: Different conformations of amides **170** (A) and **173** (B)in the binding pocket of K-Ras4B (PDB ID: 4DSO) predicted by HADDOCK.[44] The amino acids, which were defined as active residues for the HADDOCK calculation are highlighted in blue.*

4.3.2.3.3. Third iteration

As mentioned before, Prof. S. W. Fesik and coworkers screened thousands of small molecules to discover potential binders[73] for the binding pocket addressed by bisphenol A (**23**) and bisphenol AF (**95**) at the interface of *K*-Ras4B and SOS. All these compounds incorporate an aromatic or heteroaromatic ring, which can be inserted into the ligand binding pocket.

Optimization of the NMR hits led to the compounds shown in Figure 72. The crystal structure (4EPY) obtained from proline derivative **94a** shows that the indole ring enters the ligand binding pocket, while the rest of the molecule interacts with the surface of the protein (Figure 19). The ligand **94a** can induce the formation of an opened conformation, which strengthens the interaction with the protein.

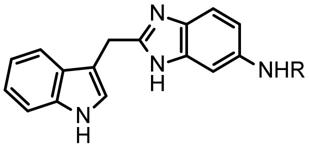

94a-e

Compound	R	K_D [µM]
94b	H	≈ 1300
94c	Gly	420
94a	Pro	340
94d	Val	240
94e	Ile	190

*Figure 72: Left: Optimized structure of the small fragment **19** shown above. Right: Dissociation constants of the core structure depending on the attached amino acid. The values were obtained from the chemical shifts observed in a heteronuclear NMR titration experiment with the ^{15}N-labeled protein.*

Combining structural elements of the Fesik ligand **94e** and bisphenol A (**23**) or bisphenol AF (**95**) seems promising, because all three structures address the same ligand binding pocket. As a reference for NMR studies of the hybrid molecules, the Fesik inhibitor **94e** was synthesized.

According to the literature procedure reported by Sun *et al.*[73], the synthesis of inhibitor **94e** proceeds from 3-indoleacetic acid (**135**) and 4-nitro-*ortho*-phenylenediamine (**174**) as shown in Scheme 23.[i] The synthesis of amine **177** was carried out in three subsequent steps (amide coupling with carbonyldiimidazole (CDI), cyclization, hydrogenation of the nitro group) without purification of the intermediates. Unfortunately, the literature procedure could not be reproduced as the amide coupling failed repeatedly. Therefore, the coupling reagent was changed from CDI to HATU or EDC hydrochloride. In both cases, the reaction successfully gave the desired regioisomeric mixture of amides **175a** and **175b**. As this mixture results in the same product during the cyclization step, the mixture was not separated. With EDC hydrochloride, a low yield of 30% was obtained while HATU gave an excellent yield of 92%. Subsequent cyclization of the regioisomers **175a** and **175b** was carried out according to the literature conditions. Acid catalysed dehydration reaction gave benzimidazole **176** in an almost quantitative yield of 98% after chromatographic purification.

Hydrogenation of the nitro group to the corresponding amine **177** was achieved with palladium on charcoal and 1 bar hydrogen pressure. After filtration of the heterogenic catalyst, the amine **177** was obtained in excellent yield of up to 98%. Amide coupling of acid **135** with diamine **174** gave an excellent yield with HATU as coupling reagent. Accordingly, amine **177** was reacted with Boc-isoleucine under the same reaction conditions to afford Boc-protected amide **178** in a very good yield (93%). Deprotection of the Boc group was carried out with trifluoroacetic acid in DCM as described by Sun *et al.* For NMR studies, amine **94e** was resalted from a trifluoroacetate to the hydrochloride in a yield of 97%. The overall yield of the optimized reaction sequence amounts to 59% compared to 38% achieved by Sun *et al.*[73] Although the reaction sequence for

---

[i] The synthesis was carried out by Dario Wetterling and Isabell Geisler in the course of their bachelor theses.

the synthesis of amine **94e** requires additional purification steps in comparison to the pathway described in the literature[73], the overall yield was increased.

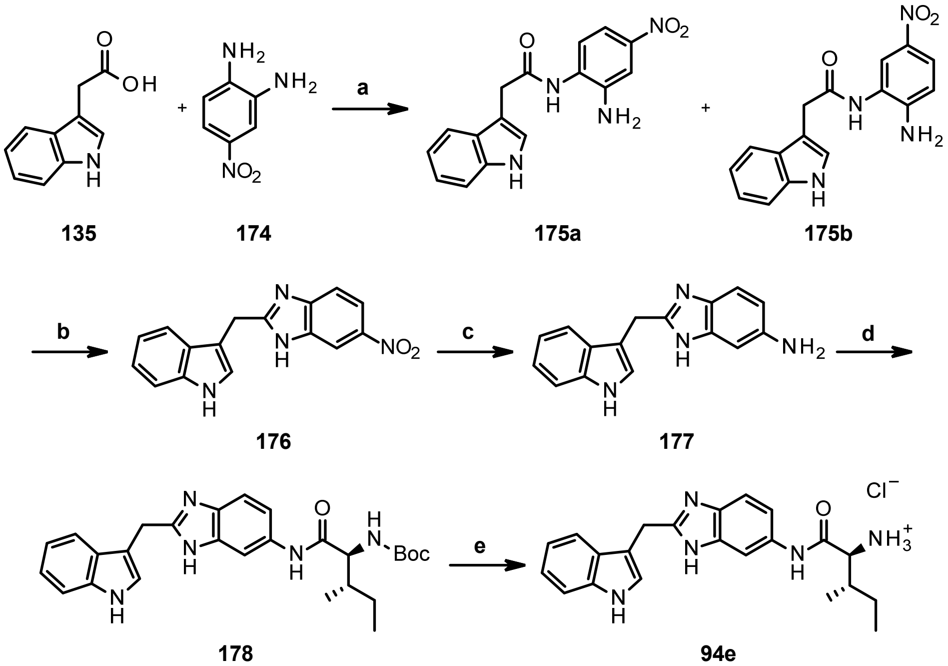

Scheme 23: Synthesis of the best inhibitor ***94e*** *found by Fesik et al. Reaction conditions: (a) HATU, DIPEA, DMF, r.t., 16 h, 92%, (b) AcOH, 120 °C, 30 min, 72%, (c) 10% Pd/C, H_2, EtOAc, r.t., 4 d, 98%, (d) Boc-L-isoleucine, HATU, DIPEA, DMF, r.t., 20 h, 93%, (e) TFA, TIPS, DCM, 0 °C, 1.5 h, 97%.*

At first glance, the NMR titration experiment in Figure 73 shows only minor interaction of the ligand with the protein as no significant shifts can be observed. This can be a result of the strong interaction of the ligand with the protein, which makes the peaks broaden and consequently vanish in the noise of the spectrum. The k_D value for the Fesik inhibitor **94e** can only be estimated roughly from the NMR data. It is in the same range as bisphenol A (**23**). Since Fesik determined the k_D value (190 µM) for the *K*-Ras4B mutant Gly12Asp, it is not directly comparable with the k_D value estimated from the measurements with wild-type *K*-Ras4B shown in Figure 73.

The shifting and vanishing amino acids can be used for a HADDOCK calculation, which is depicted in Figure 74 The HADDOCK model predict conformations of the Fesik inhibitor **94a**, which either insert the indole moiety or the amino acid residue into the ligand binding pocket. The rest of the molecule either points towards Glu3 and Leu52 or Tyr64. This prediction is in distinct contrast to the crystal structure for the proline derivative **94a**. The crystal structure in Figure 48 clearly shows an opened conformation of the protein. The binding pocket is enlarged by ligand binding. It can be deduced that the Fesik inhibitor **94e** has a similar effect on the protein. Such conformational changes cannot be predicted by HADDOCK as the protein is mainly kept rigid throughout the calculation. The HADDOCK model in Figure 74 does therefore not necessarily depict the actual conformation of ligand **94e** in the binding cleft of *K*-Ras4B.

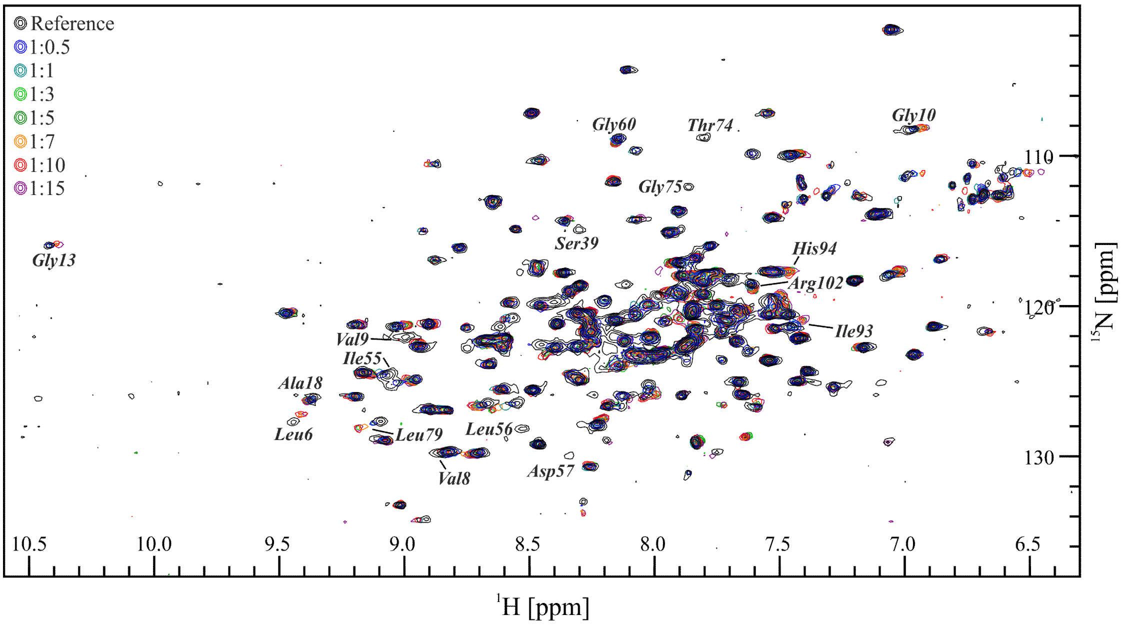

Figure 73: ^{1}H,^{15}N-TROSY NMR overlay of the titration steps of Fesik inhibitor ***94e*** *to the K-Ras protein.*[102]

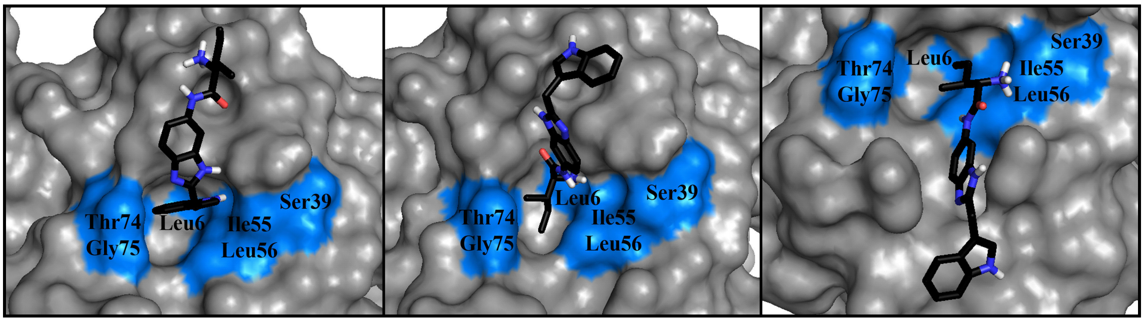

Figure 74: Different conformations of the Fesik inhibitor ***94e*** *in the binding pocket of K-Ras4B (PDB ID: 4DSO) predicted by HADDOCK.*[44] *The amino acids, which were defined as active residues for the HADDOCK calculation are highlighted in blue.*

4.3.2.3.4. Fourth iteration

It has been shown that both phenol rings are required for binding of bisphenol A (**23**) to the *K*-Ras4B protein. For the hybrid molecule, the indole moiety of the Fesik inhibitor **94e** was consequently replaced for the bisphenol A (**23**) structure. Accordingly, linkage of both fragments was only possible via one of the CH_3-groups of bisphenol A (**23**). Table 12 shows that a minor improvement of the Glide score of hybrid molecule **179** in comparison to bisphenol A (**23**) is achieved. The compound was therefore chosen for synthesis.

*Table 12: Glide scores of the hybrid molecule **179** in comparison to BPA (**23**) and the Fesik inhibitor **94e** as reference. In case of 4DSO, all water molecules were removed prior to docking experiments. For 4EPX, three water molecules are included for docking experiments while 4EPY contains a total of 14 water molecules surrounding the ligand binding pocket.*

Substance	Structure	4DSO		4EPY		4EPX	
		max	min	max	min	max	Min
Bisphenol A (23)		-3.24	-2.30	-1.36	-1.00	-1.67	3.02
Fesik inhibitor 94e	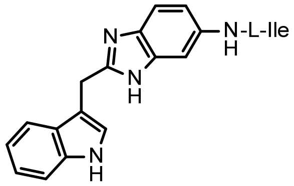 **94e**	-5.93	-5.60	-4.14	-3.79	-5.35	-0.80
BPA hybrid molecule 179	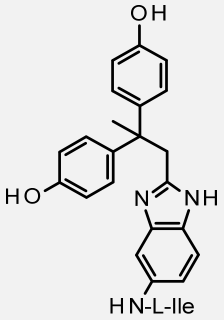 **179**	-3.51	-1.28	-5.59	-1.67	-3.09	0.95

The different crystal structures (Figure 75) show hydrogen bonds for the Fesik ligand **94e** to amino acids Glu37, Ser39 and Asp54. In case of both, 4EPY and 4EPX, additional hydrogen bonds are formed with the water molecules located in the ligand binding pocket and Asp38. These interactions fix the molecule properly in the binding pocket. In comparison, the hybrid molecule **179** is oriented towards the other side of the protein, interacting with Glu3 instead of Glu37 and Ser39. This observation is only made for 4DSO and thus explains the lower Glide score. The orientation of the hybrid molecule **179** docked to 4EPX and 4EPY is identical with that of the Fesik ligand **94e**. It should be noted that the best structure predicted for hybrid molecule **179** bound to 4EPY inserts the amino acid L-Ile into the binding pocket instead of the bisphenol moiety. This residue interacts with Asp38 and Glu63 instead of Leu6.

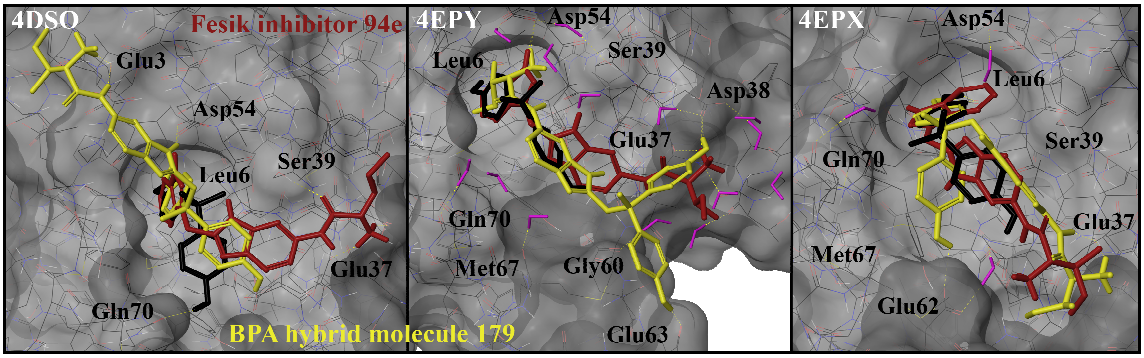

*Figure 75: Comparison of the binding modes of Fesik inhibitor (**94e**, red) and BPA hybrid molecule (**179**, yellow) in the binding pocket of the crystal structures 4DSO, 4EPY and 4EPX of the K-Ras protein predicted by Glide with bisphenol A (**23**, black) as reference. Water molecules are shown in purple as a stick model.*

The synthesis of the hybrid molecule **179** follows the reaction pathway that was developed for benzimidazole **94e** (Scheme 24). The synthesis proceeds from bisphenol A acid derivative **160** and 4-nitro-*ortho*-phenylenediamine (**174**).[i]

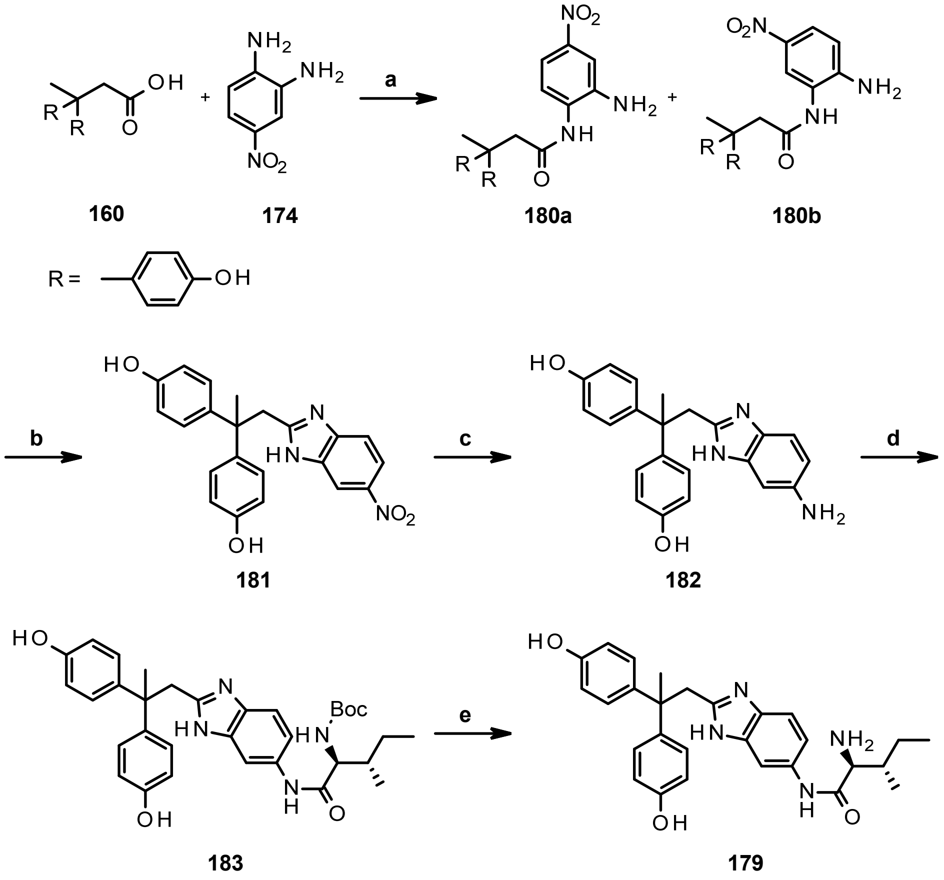

*Scheme 24: Synthesis of a hybrid molecule **179** of Bisphenol A (**23**) and the Fesik inhibitor **94e**. Reaction conditions: (a) HATU, DIPEA, DMF, r.t., 29 h, 13%, (b) AcOH, 120 °C, 30 min, 25%, (c) Pd/C, H_2, EtOAc, r.t., 26 h, 56%, (d) Boc-L-isoleucine, HATU, DIPEA, DMF, r.t., 19 h, 74%, (e) TFA, TIPS, DCM, 0 °C, 1.5 h, 99%.*

---

[i] The synthesis was carried out by Dario Wetterling and Isabell Geisler in the course of their bachelor theses.

Following the procedure described above, the amide coupling was carried out using HATU to afford a regioisomeric mixture of amide **180**, which was not separated, because both isomers give the same product during cyclization. After chromatographic purification, the desired amide was obtained in 13% yield. The low yield resulted from purification issues caused by a side product and remaining diamine **174** in the mixture. The side product was formed by a reaction between two molecules of acid **160** and one molecule of diamine **174**. Since two structures with the same mass are probable, an unambiguous structure determination was not possible. The structures of the side products **184** and **185** are shown in Figure 76.

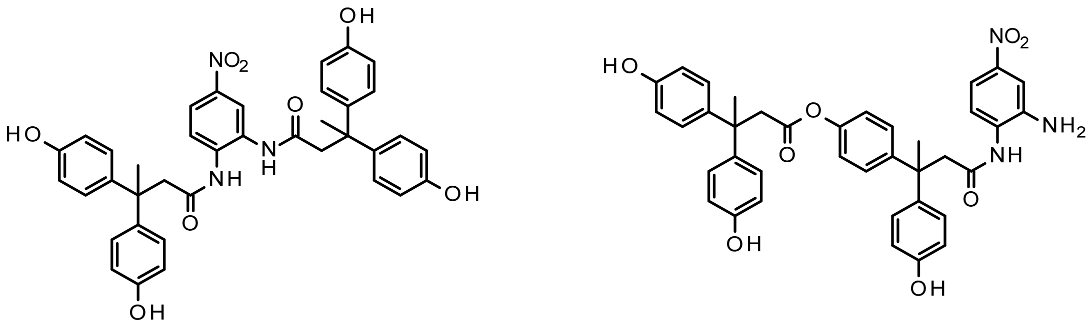

184 **185**

*Figure 76: Possible side products obtained in the amide coupling between acid **160** and diamine **174**.*

Amide **180** was then cyclized to the corresponding benzimidazole **181** using the reaction conditions described above. The yield for this reaction was low (25%) due to purification issues. Subsequent hydrogenation of the nitro group with palladium on charcoal afforded amine **182** was achieved. After filtration of the catalyst, the pure product was obtained in moderate yield of 56%. Coupling of amide **182** with Boc-L-isoleucine was carried out with HATU as coupling reagent. The pure product **183** was obtained after chromatographic purification in a low yield of 26%. The low yield results from a side reaction of the product with the coupling reagent, which forms a uronium salt. Thus, the amino acid was pre-activated with the coupling reagent, which was also used as limiting reagent. The yield of the Boc-protected amide **183** was increased drastically to 74%. The final reaction step, Boc-deprotection with trifluoroacetic acid and triisopropysilane in DCM, afforded the desired hybrid molecule **179** as the corresponding TFA salt in 99% yield. This was resalted as described above to the corresponding hydrochloride. The overall yield of this reaction sequence amounts to 1% over 5 reaction steps.

In addition to the hybrid molecule, the precursor molecule **182** was tested for its interaction with the protein. The NMR experiments for the precursor **182** and the final hybrid molecule **179** show no significant interaction with *K*-Ras. In case of the precursor amine **182** weak shifts for Leu6, Leu56, Thr74 and Gly75 are observed. These can be used for HADDOCK calculations, which are shown in Figure 77. The prediction shows that the compound is unable to enter the ligand binding pocket. The benzimidazole ring as well as the phenol moiety can only interact with the surface amino acids of the binding cleft, but cannot reach deeply into the pocket to form a hydrogen bond to Leu6. This result is in accordance with the prediction made by Glide especially for crystal structure 4DSO. The Glide score of the hybrid molecule **179** shows only a minor improvement in comparison to bisphenol A (**23**) while the Glide score of the Fesik ligand **94e** is significantly higher. A possible explanation for the inactivity of both compounds is their high sterical demand at the central C-atom. This impedes interaction with the protein, especially accessing the ligand binding pocket with one of the phenyl rings as can be seen from the HADDOCK results.

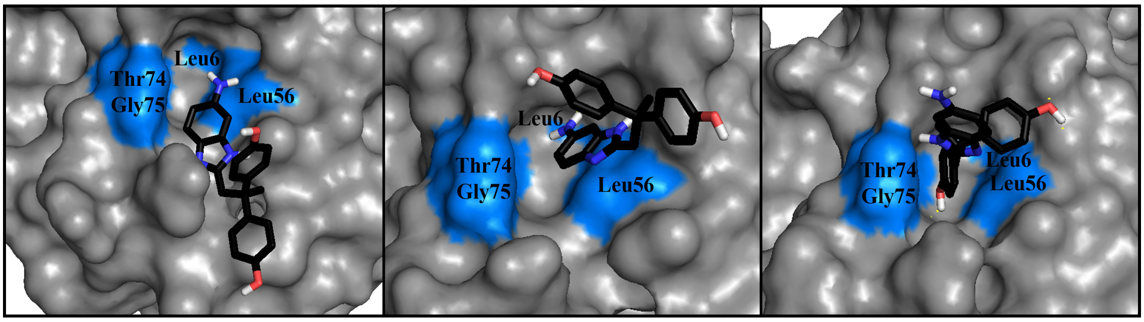

*Figure 77: Different conformations of amine **182** in the binding pocket of K-Ras4B (PDB ID: 4DSO) predicted by HADDOCK.[44] The amino acids, which were defined as active residues for the HADDOCK calculation are highlighted in blue.*

4.3.2.3.5. Fifth iteration

In the next step, hybrid molecules with only two aromatic rings were planned. While compound **186** carries a dimethyl group for higher resemblance to bisphenol A (**23**), hybrid **187** contains a methylene bridge in accordance with the Fesik ligand **94e**. Additionally, these compounds are less sterically demanding than hybrid **179**.

The Glide scores of the calculated compounds (Table 13) are again in the range of the Fesik ligand for the most relevant protein structure 4DSO. Since the differences of the scores are insignificant, both compounds **186** and **187** were selected for synthesis. In 4DSO, the overlay of the docked structures of the Fesik ligand **94e** and the hybrid molecule **186** carrying two methyl groups shows that the hybrid can adopt the exact same binding mode (Figure 78). Interactions with the residues Glu37, Asp38, Ser39 and Asp54 are observed. The same observation can be made for the docking results with 4EPX and 4EPY. Here, the ligand interacts with Leu6, Glu37 and Asp38. The hybrid molecule **187** can adopt exactly the same binding mode as described above for the more sterically demanding analogue **186**. Both compounds are highly interesting as they can mimic the binding mode of the Fesik ligand **94e** while adding some of the interactions characteristic for bisphenol A (**23**) as can be seen from Figure 78. Also, it possesses a sterically hindered C-atom to allow for correct positioning in the ligand binding pocket.

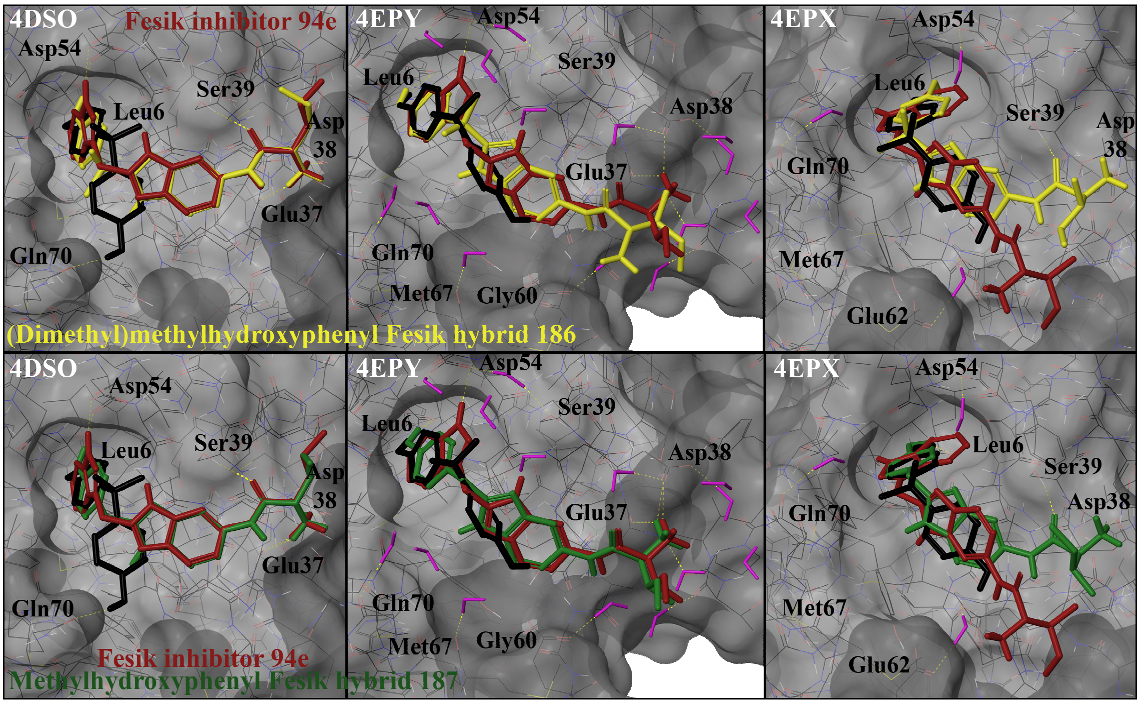

*Figure 78: Comparison of the binding modes of Fesik inhibitor (**94e**, red), (Dimethyl)methylhydroxyphenyl Fesik hybrid (**186**, yellow) and Methylhydroxyphenyl Fesik hybrid (**187**, green) in the binding pocket of the crystal structures 4DSO, 4EPY and 4EPX of the K-Ras protein predicted by Glide with bisphenol A (**23**, black) as reference. Water molecules are shown in purple as a stick model.*

*Table 13: Glide scores of sterically less hindered derivatives **186** and **187** in comparison to BPA (**23**) and the Fesik inhibitor **94e** as reference. In case of 4DSO, all water molecules were removed prior to docking experiments. For 4EPX, three water molecules are included for docking experiments while 4EPY contains a total of 14 water molecules surrounding the ligand binding pocket.*

Substance	**Structure**	**4DSO**		**4EPY**		**4EPX**	
		max	min	max	min	max	Min
Bisphenol A (23)		-3.24	-2.30	-1.36	-1.00	-1.67	3.02
Fesik inhibitor 94e		-5.93	-5.60	-4.14	-3.79	-5.35	-0.80
(Dimethyl)methyl hydroxyphenyl Fesik hybrid 186	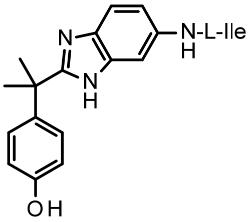 N-L-Ile H N N H OH **186**	-5.94	-4.49	-5.60	-4.28	-4.42	-4.39
Methylhydroxy-phenyl Fesik hybrid 187	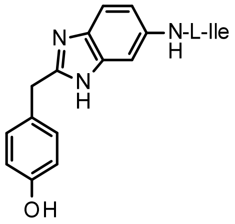 N-L-Ile H N N H OH **187**	-5.33	-2.73	-6.16	-5.67	-4.38	-3.06

The syntheses of both compounds follow the route that was developed for the synthesis of inhibitor **94e** and bisphenol A derivative **179**. The synthesis of the α-unsubstituted methylphenol analogue **187** started from 4-methoxyphenylacetic acid (**188**), which was coupled to diamine **174** using HATU as reagent (Scheme 25). At first, the reaction was conducted in DMF as solvent. The product was obtained in only 41% yield. Instead, the reaction was performed in DCM, from which the product precipitated. This also accelerated the reaction drastically. Collecting and washing gave the desired amide **189** after only 2.5 h in a good yield of 65%. Subsequent cyclization in acetic acid did not afford the desired benzimidazole **191** in contrast to similar reactions performed before. Analogous reactions described by Banoglu *et al.* (1,2-phenylenediamine and 4-isopropylphenylacetic acid) and Salikov *et al.* (1,2-phenylenediamine and various substituted cyclopropanecarboxylic acids) successfully gave the desired benzimidazoles.[136,137]

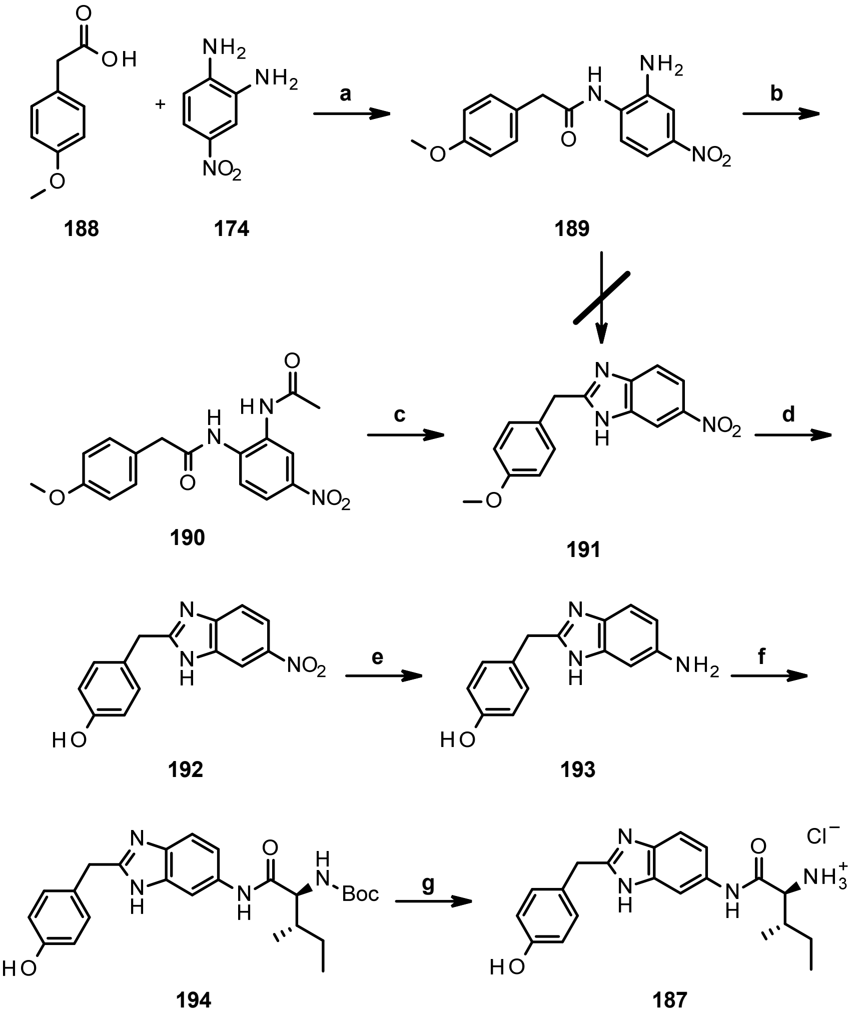

*Scheme 25: Synthesis of methylphenol derivative **187** of the inhibitor **94e** invented by Fesik and coworkers. (a) HATU, DIPEA, DCM, r.t., 2.5 h, 65%, (b) acetic anhydride, r.t., 24 h, 81%, (c) pTsOH, toluene, reflux, 17 h, 80%, (d) 1 M BBr_3, DCM, -78 °C → r.t., 21 h, 93%, (e) 10% Pd/C, H_2, methanol, r.t., 4.5 h, 85%, (f) Boc-L-isoleucine, HATU, DIPEA, DMF, r.t., 19.5 h, 29%, (g) TFA, TIPS, DCM, 0 °C, 2 h, 91%.*

Repetition of the reaction at room temperature in dry acetic acid only gave the acetylated amide **190** even after 3 days. A literature research revealed that such mixed diacylated diamines can be converted into the corresponding benzimidazoles by refluxing with *para*-toluenesulfonic acid in toluene.[138] This procedure afforded the desired benzimidazole **191** in a good yield of 70% over two steps. Reactions in polyphosphoric or sulphuric acid at high temperatures to obtain benzimidazole **191** in a one-step procedure were unsuccessful. An improved yield of 81 % was obtained by stirring amide **189** in neat acetic anhydride for 24 h. Cyclisation of diamide **190** in refluxing toluene with *para*-toluenesulfonic acid gave the desired benzimidazole **191** (80%).[138] Subsequent deprotection of the methoxy group was performed in accordance to the cleavage of the methoxy groups of ester **165a** with the Lewis acid boron tribromide.[105] This procedure gave the desired phenol **192** in excellent yield of up to 93%. Following the procedure described for the hydrogenation of the nitro group of benzimidazole **176**, reduction of phenol **192** to amine **193** was achieved (85%). The solvent was changed from ethyl acetate to methanol to dissolve the starting material. This also accelerated the reaction significantly. Coupling of amine **193** with Boc-L-isoleucine in DMF yielded amide **194** after 19.5 h in a low yield of 29%. Boc-deprotection of the amino acid was performed using trifluoroacetic acid and triisopropylsilane in DCM as described before. The compound was purified by column chromatography due to minor impurities. The free amine was obtained in 62% yield. As only a part of the crude product was applied to purification, the total yield of this reaction step can be extrapolated to approximately 91%. The overall yield for the synthesis of α-unsubstituted methylphenol derivative **187** proceeding from 4-methoxyphenylacetic acid (**188**) over seven reaction steps accounts to 9%.

For the synthesis of α-dimethyl-substituted methylphenol **186**, α-dimethyl substituted phenylacetic acids **195** or **196** were required. These were synthesized from 4-methoxyphenylacetic acid (**188**) as described by Palkowitz *et al.* and Coterón *et al.* (Scheme 26).[139,140] Acid **188** was alkylated with LDA and iodomethane to afford α-dimethyl-substituted acid **195** in a low yield of 23%. Thus, a different pathway towards acids **195** and **196** was developed. The corresponding dimethylated ester **198** can be obtained by dialkylation of the methylester using lithium hexamethyldisilazide as described by Rousseaux *et al.* or from the corresponding *tert*-butylester as shown by Chaumontet *et al.*[141,142] Alternatively, potassium *tert*-butoxide can be used as a base for this conversion as described by Baloglu and coworkers.[143,144] The methylester was chosen as it is readily available from phenylacetic acid **188** as described by Trieu and coworkers[145]. Acid **188** was dissolved in methanol and thionyl chloride was added to afford the desired ester **197** in excellent yield (99%). The crude product was directly used for subsequent dialkylation using lithium hexamethyldisilazide as base.[141] Unfortunately, the reaction showed no conversion. Therefore, the second method applying potassium *tert*-butoxide as base was carried out to afford the desired α-dialkylated ester **198** in a good yield of 88% after chromatographic purification. Subsequent cleavage of the methyl ether and ester of compound

198 was attempted in a one-pot reaction using the Lewis acid boron tribromide.[143] Unfortunately, this mainly led to decomposition of the starting material. Obviously, deprotection had to be done stepwise by first cleaving the ester functionality with aqueous sodium hydroxide followed by ether cleavage with boron tribromide.[144] Ester cleavage with excess of sodium hydroxide gave the desired free acid **195** in an excellent yield of 94%. In contrast to the literature, a mixture of methanol and THF was used as the starting material aggregated into a separate oily phase when methanol was used. This increased the reaction time considerably. Subsequent ether cleavage of acid **195** with boron tribromide in DCM afforded the fully deprotected α-dimethyl-substituted acid **196** in good yield of 63% after purification.

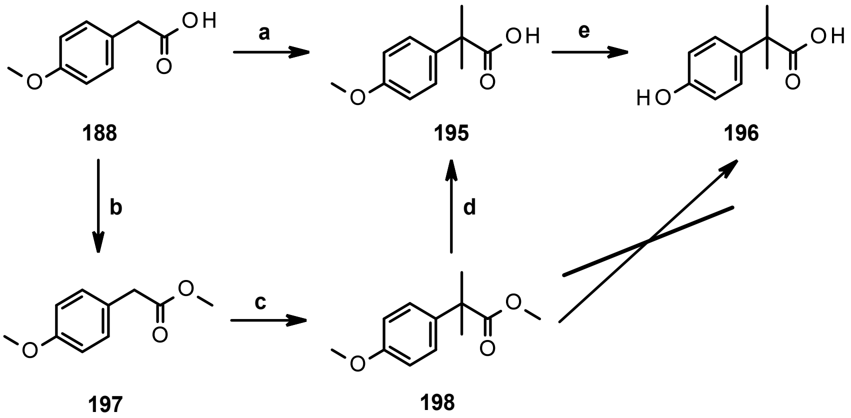

Scheme 26: Synthesis of dimethyl-substituted 4-hydroxyphenylacetic acid ***196****. (a) DIPA, n-BuLi, iodomethane, THF, -10 °C → r.t., 19 h, 23%, (b)* $SOCl_2$*, methanol, 0 °C → reflux, 4 h, 99%, (c)* KO^tBu*, iodomethane, THF, -78 °C → r.t., 3.5 h, 88%, (d) NaOH, THF/methanol, r.t., 18 h, 94%, (e) 1 M* BBr_3*, DCM, -78 °C → r.t., 1.5 h, 63%.*

Acid **196** was then coupled with diamine **174** with HATU as coupling reagent as described before (Scheme 27). Unfortunately, amide **199** could not be purified by column chromatography due to its low solubility. To circumvent this problem, the methoxy-protected acid **195** was used.

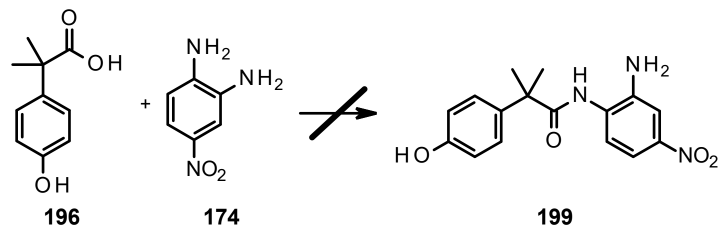

Scheme 27: Synthesis of amide ***199*** *from hydroxyphenylacetic acid* ***196*** *and diamine* ***174****.*

Coupling of acid **195** with diamine **174** under the same reaction conditions afforded amide **200** in a yield of 68% after purification (Scheme 28). Unfortunately, all attempts to cyclize this amide to the corresponding benzimidazole **202**, either following the procedure successfully applied by Sun and coworkers or by the procedure used for the α-unsubstituted methylphenol derivative **187** via a diacylated intermediate, failed.

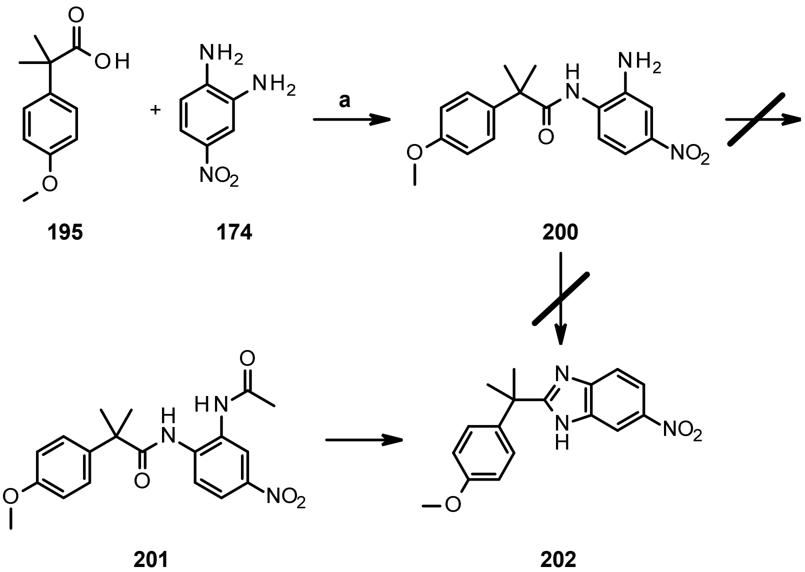

*Scheme 28: First attempt towards the synthesis of benzimidazole **202**. (a) HATU, DIPEA, DMF, r.t., 19 h, 68%.*

Direct cyclization of amide **200** using various acids such as acetic acid, *para*-toluenesulfonic acid[146] or polyphosphoric acid led to decomposition of the starting material. The proton NMR as well as the HPLC spectrum prove that acid **195** was retrieved as the amide bond was broken. The same observation was made when amide **200** was acetylated to give intermediate **201**. The different reaction conditions tested are summarized in Table 14.

*Table 14: Reaction conditions used for the conversion of amide **200** to either diamide **201** or benzimidazole **202**.*

entry		reaction conditions	result
1	benzimidazole **202**	AcOH, 120 °C, 30 min (microwave)	decomposition to acid **195**
2		AcOH (dried over P_2O_5), reflux, 3 h	decomposition to acid **195**
3		AcOH (dried with Ac_2O), reflux, 3 h	decomposition to acid **195**
4		pTsOH, toluene, reflux, 6 h	decomposition to acid **195**
5		phosphoric acid, r.t., 17 h	decomposition to acid **195**
6	mixed diamide **201**	Ac_2O, TEA, DMAP, DCM, r.t., 2 d	remaining starting material and decomposition to acid **195**
7		Ac_2O, TEA, DMAP, THF, r.t., 4 d	unidentified product
8		Ac_2O, r.t., 22 h, 50 °C, 7 d	remaining starting material and decomposition to acid **195**
9		Ac_2O, DIPEA, DMAP, DCM, 5 d	decomposition to acid **195**
10		AcCl, TEA, DMF, r.t., 17 h	decomposition to acid **195**
11		AcCl, toluene, r.t., 22 h	remaining starting material and unidentified product

As an alternative route towards diamide **201**, diamine **174** was acetylated following the procedure by Sherman and coworkers[147] using acetic anhydride and trimethylamine. Acetylated diamine **203** was obtained in a moderate yield of 43% (Scheme 29). Unfortunately, the subsequent coupling to acid **195** was not successful regardless of the reaction conditions. Using HATU as coupling reagent and triethylamine in either DCM or DMF did not give the desired product. Instead, the starting materials as well as diacetylated diamine were found. Applying EDC hydrochloride instead as coupling reagent resulted in the same outcome of the reaction.

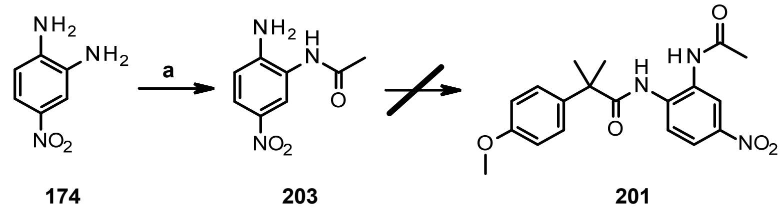

*Scheme 29: Second attempt towards the synthesis of benzimidazole **202** failing in the preparation of acetylated amide **201**. (a) Ac_2O, TEA, DCM, 0 °C → r.t., 4 d, 43%.*

It is known that substitution reactions in neopentyl position are significantly hindered due to the high sterical demand of the *tert*-butyl group in β-position. A similar situation is given for the cyclisation of amide **200** as well as the coupling of amine **203** and acid **195**. The neopentyl-like situation of acid **195** might prevent that amine **203**, which is sterically more demanding than diamine **174**, can substitute the hydroxy group of the acid functionality. Similarly, it can also prohibit that the mechanism shown in Scheme 30 can be followed. Instead the amide bond between acid **195** and amine **174** is broken in the course of the reaction.

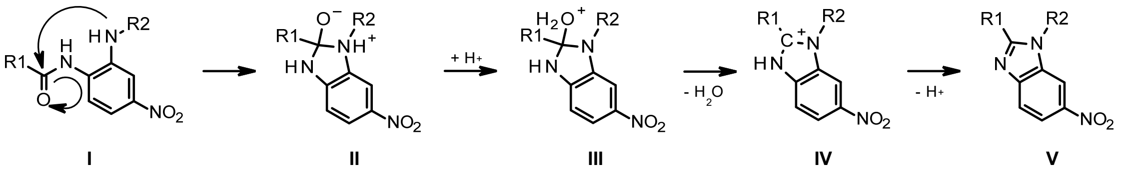

Scheme 30: Mechanism of the cyclisation of acetylated diamines to the corresponding benzimidazoles under acidic conditions.

The titration experiment depicted in Figure 79 shows significant interactions of the unsubstituted hybrid molecule **187** with *K*-Ras. Amino acids Ser39, Leu56, Thr74 and Gly75 are clearly affected by ligand addition. Unfortunately, other residues belonging to the ligand binding pocket such as Leu6 and Ile55 only shift weakly. This faint interaction also impacts the strength of the allosterically shifted peaks such as Gly13, Asp57 and Gly60, which belong to the nucleotide binding pocket. The k_D value calculated from the NMR titration experiment (4.14 ± 0.07 mM) is considerably weaker than that of bisphenol A (**23**) or the Fesik ligand **94e**.

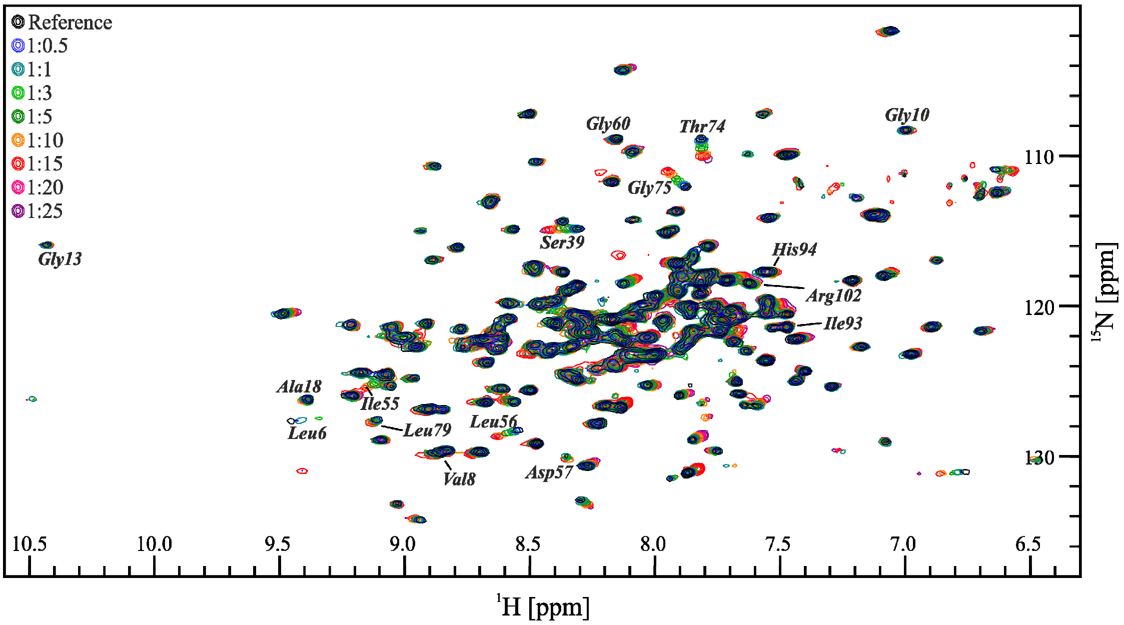

*Figure 79: ^{1}H,^{15}N-TROSY NMR overlay of the titration steps of α-unsubstituted methylphenol derivative **187** to the K-Ras protein.*[106]

The shifts observed in the NMR can be used to define active residues for the corresponding HADDOCK computation (Figure 80). In accordance with the HADDOCK results obtained for the Fesik ligand **94e**, the ligand **187** is predicted to insert the amino acid residue into the ligand binding pocket instead of the phenol moiety. From the crystal structure 4EPY, it is known that the Fesik ligand **94a** can open the ligand binding pocket. The same effect can be expected for its analogue **94e** although the HADDOCK computation suggests otherwise. In contrast, it is unknown if the same applies to amide **187**.

The interaction with the protein is dominated by hydrogen bonds with Ile55, Leu56 and Ser 39 according to the prediction. As the prediction shows, the amino acid residue cannot be inserted into the binding pocket deeply enough to interact with Leu6. Although the interaction with the protein is considerably weaker in comparison to amide **94e**, this result clearly proves that substitution of the indole moiety of the Fesik ligand for a phenol ring is possible.

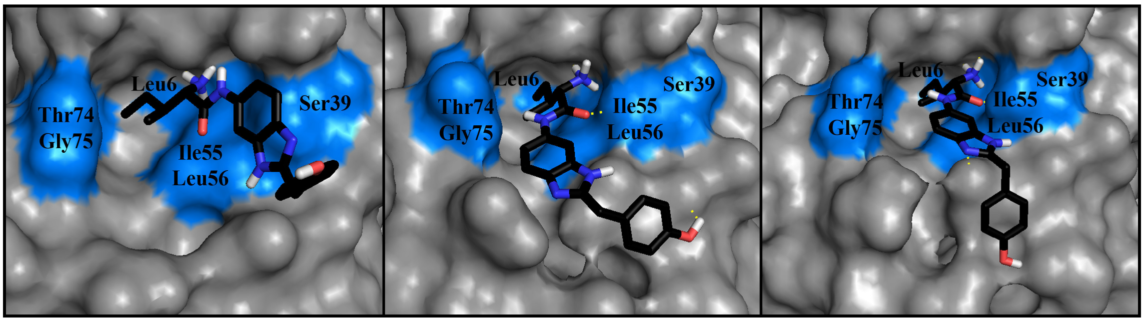

*Figure 80: Different conformations of α-unsubstituted methylphenol derivative **187** in the binding pocket of K-Ras4B (PDB ID: 4DSO) predicted by HADDOCK.*[44] *The amino acids, which were defined as active residues for the HADDOCK calculation are highlighted in blue.*

4.3.2.3.6. Sixth iteration

In a third step, the dimethyl moiety, which could not be incorporated into the hybrid molecule, was substituted for a cyclopropyl group. The resulting derivative **204a** (Table 15) shows docking scores comparable to the Fesik ligand **94e** for 4DSO and 4EPX and a significantly better score for 4EPY.

In case of 4DSO and 4EPY, the overlay of the Fesik ligand **94e** and the cyclopropyl derivative **204** are in perfect accordance interacting with the protein in the same way (Figure 81). In contrast, the orientation of the amino acid of the ligand differs slightly for 4EPX providing an explanation for the lower docking score in comparison to the Fesik inhibitor **94e** itself. As a result of this findings, the cyclopropyl analogue **204a** was chosen for synthesis. Its docking score can compete with the score of the Fesik ligand **204a** and the overlays of the compounds in the ligand binding pocket of each crystal structure of *K*-Ras4B are promising.

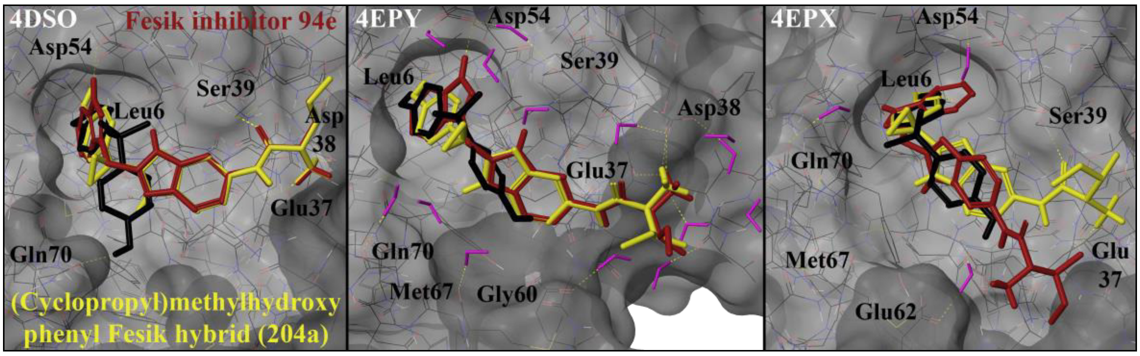

*Figure 81: Comparison of the binding modes of Fesik inhibitor (**94e**, red) and (Cyclopropyl)methylhydroxy phenyl Fesik hybrid (**204a**, yellow) in the binding pocket of the crystal structures 4DSO, 4EPY and 4EPX of the K-Ras protein predicted by Glide with bisphenol A (**23**, black) as reference. Water molecules are shown in purple as a stick model.*

*Table 15: Glide scores of the cyclopropyl derivative **204a** in comparison to BPA (**23**) and the Fesik inhibitor **94e** as reference. In case of 4DSO, all water molecules were removed prior to docking experiments. For 4EPX, three water molecules are included for docking experiments while 4EPY contains a total of 14 water molecules surrounding the ligand binding pocket.*

Substance	**Structure**	**4DSO**		**4EPY**		**4EPX**	
		max	min	max	min	max	Min
Bisphenol A (23)		-3.24	-2.30	-1.36	-1.00	-1.67	3.02
Fesik inhibitor 94e		-5.93	-5.60	-4.14	-3.79	-5.35	-0.80
(Cyclopropyl) methylhydroxy phenyl Fesik hybrid (204a)	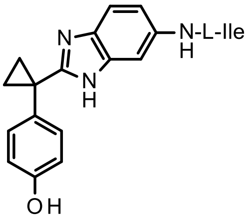 **204a**	-5.54	-5.50	-6.01	-5.63	-4.42	

The synthesis of phenol **204a** follows the route developed for the synthesis of α-unsubstituted derivative **187** as shown in Scheme 31. In the first step, α-cyclopropylacetic acid (**205**) was coupled with diamine **174** to the corresponding amide **206**, which was obtained in moderate yield of 57% after column chromatography. Acetylation of amide **206** was achieved by stirring in neat acetic anhydride to afford diamide **207** in 89% yield. Subsequently, cyclization was performed in refluxing toluene with *para*-toluenesulfonic acid. After purification, benzimidazole **208** was obtained in excellent yield of 94%. Deprotection of the methoxy group of benzimidazole **208** was done using boron tribromide as described above to afford phenol **209** in good yield (82%). Hydrogenation of benzimidazole **209** to the corresponding amine **210a** was conducted using palladium on charcoal (99%). Unfortunately, this hydrogenation reaction generated a side product (approx. 20%). According to LC-MS, the molecule has a higher molecular mass (+ 2 Da) than the desired product.

It is known for a long time that cyclopropane rings can be opened reductively.[148,149] Since the two compounds could not be separated by normal phase column chromatography, the mixture was analysed by NMR. The NMR data revealed that the cyclopropane ring was opened in a 1,2- or 1,3-manner. An ethyl residue coupling with a single proton was observed. This finding is underlined by various literature articles. Phenyl-substituted cyclopropane rings are always opened in a 1,2- or 1,3-manner depending on other substituents of the cyclopropane ring.[149] In case of an acceptor substituent, one of the vicinal C-C-bonds is broken forming an ethyl-group while a donor substituent weakens the distal C-C-bond of the cyclopropane ring establishing a dimethyl moiety.[148] As the 1-position of the cyclopropane residue in benzimidazole **209** is activated by two aromatic rings, the ring opening reaction is even more favoured. Additionally, both, a 1,2- and a 1,3-opening, lead to the same compound **210b** as the cyclopropane ring does not carry any further substituents.[150–154]

The mixture of amines **210a** and **210b** was coupled with Boc-L-isoleucine using the standard coupling conditions described above to afford a mixture of the amides **211a** and **211b** in 42% yield. Also on this stage, the two products could not be separated chromatographically. Thus, the mixture was used for the next step. In the last step, the Boc-group was removed using TFA and triisopropylsilane in DCM at 0 °C. The resulting TFA salts were converted into the corresponding hydrochloride salts of amines **204a** and **204b** in quantitative yield.

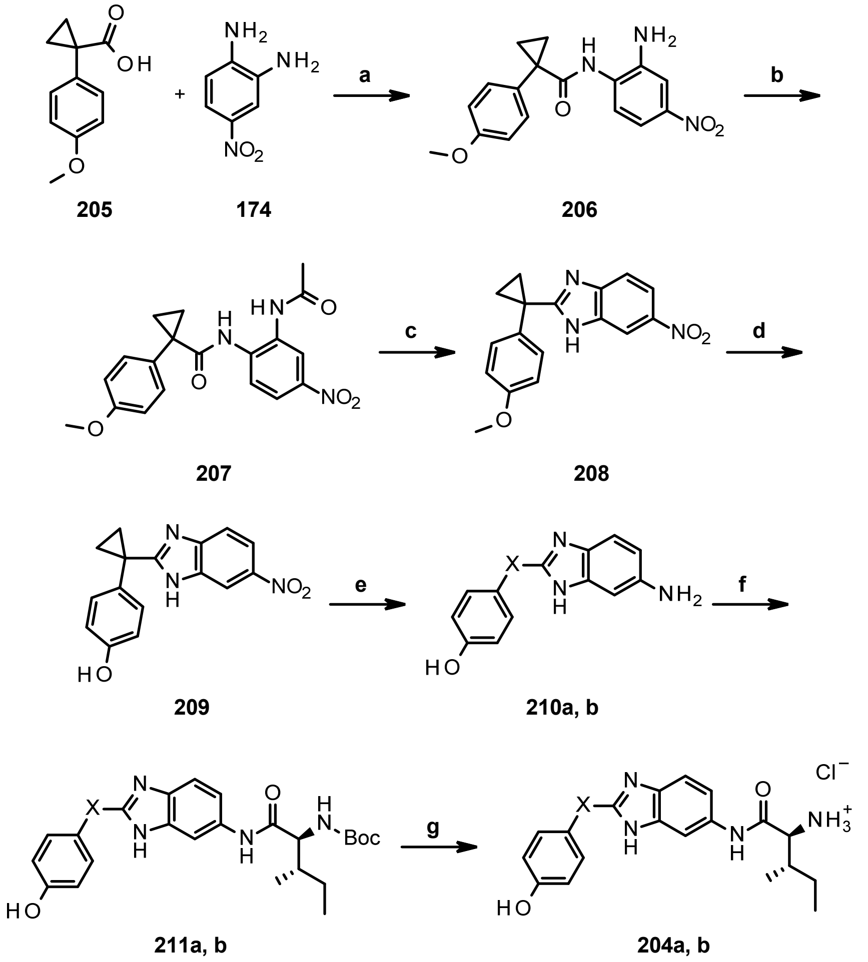

a X = cyclopropyl
b X = CHEt

Scheme 31: Synthesis of α-cyclopropyl-substituted methylphenyl derivative ***204a*** *of the inhibitor* ***94e*** *invented by Fesik and coworkers. (a) HATU, DIPEA, DCM, r.t., 16 h, 57%, (b)*Ac_2O*, r.t., 7 h, 89%, (c) pTsOH, toluene, reflux, 23 h, 94%, (d) 1 M* BBr_3*, DCM, -78 °C → r.t., 3.25 h, 82%, (e) 10% Pd/C,* H_2*, methanol, r.t., 1.5 h, 99%, (f) HATU, DIPEA, DMF, r.t., 15 h, 42%, (g) TFA, TIPS, DCM, 0 °C, 2.5 h, quant.*

To synthesize pure cyclopropyl-substituted amide **204a** (Scheme 32), the hydrogenation step was investigated thoroughly. Instead of a classical reduction using hydrogen gas and a palladium catalyst, the conversion can also be achieved using tin chloride hydrate in methanol[155] or ethyl acetate[156,157]. Refluxing the reaction mixture for 1 h gave the desired pure amine **210a** in a good yield of 83%. Additionally, the original procedure was reconsidered. Hydrogenation at 0 °C for 1.5 h afforded amide **210a** in quantitative yield.

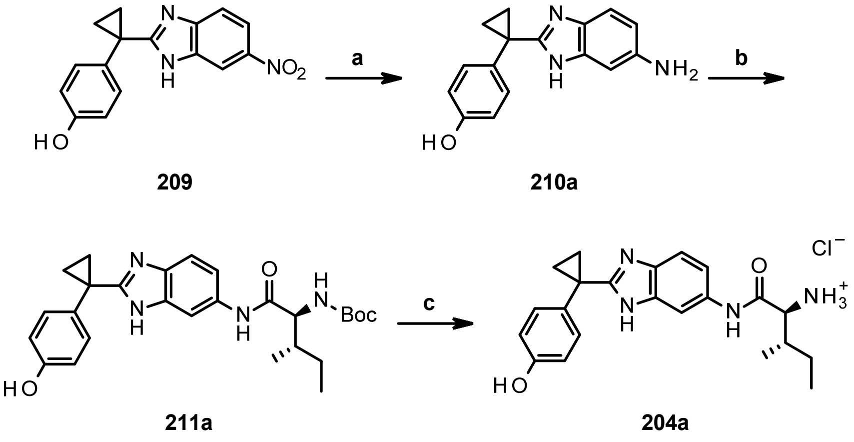

*Scheme 32: Synthesis of pure α-cyclopropyl-substituted methylphenyl derivative **204a** following optimized reaction conditions for the reduction of nitrobenzmidazole **209**. Reaction conditions: (a) $SnCl_2$ hydrate, methanol, reflux, 1 h, 83% or 1 bar H_2, 10% Pd/C, methanol, 0 °C , 1.5 h, quant., (b) HATU, DIPEA, DMF, r.t., 20 h, 45% , (c) TFA, TIPS, DCM, 0 °C, 2.5 h, 82%.*

Subsequent coupling with Boc-L-isoleucine as well as Boc-deprotection of the amino acid were done according to the procedures described above for the mixture. Boc-protected amide **211a** was obtained in moderate yield of 45%. Deprotection with trifluoroacetic acid and TIPS gave the desired TFA salt of amine **204a**, which was resalted to the corresponding hydrochloride, in a good yield of 82%. Overall, amine **204a** was synthesized in a yield of 14% over seven reaction steps.

As can be seen from Figure 83, the pure amine **204a** does not induce significant shifts of the protein peaks. Moreover, a distinct shift of the His-Tag, which is used for purification of the protein, can be observed. This renders other shifts less significant as both effects are probably a result of DMSO addition. Nevertheless, slight shifts for amino acids belonging to the ligand binding pocket such as Ser39, Thr74 and Gly75 can be observed. Other peaks such as Leu6 or Gly13 vanish instead of shifting. Consequently, amine **204a** does not evoke the same shifts in the NMR measurement as bisphenol A (**23**) or the Fesik ligand **94e**. Additionally, the precursor amine **210a** was also examined by an NMR measurement. This experiment also showed no interaction of the compound with the labeled protein.

Utilizing the weak shifts in the NMR measurement, a HADDOCK computation was performed. The predicted conformations of amine **204a** in the ligand binding pocket of *K*-Ras4B are shown in Figure 82. According to the HADDOCK model, the ligand is unable to enter the binding cleft to interact with Leu6. Instead, the compound interacts with the surface of the binding pocket (Leu56, Thr74 and Gly75). Similar to the Fesik ligand **94e** and amine **187**, the amino acid residue is oriented towards the binding pocket instead of the phenol ring. In contrast to the amides **94e** and **187**, which show significant shifts in the NMR measurement, this compound cannot interact with the protein in the desired way. It can therefore be deduced that a cyclopropyl substituent at the central C-atom leads to a loss in activity. This result is contradictory to the finding that compounds incorporating a highly substituted C-atom are favoured.

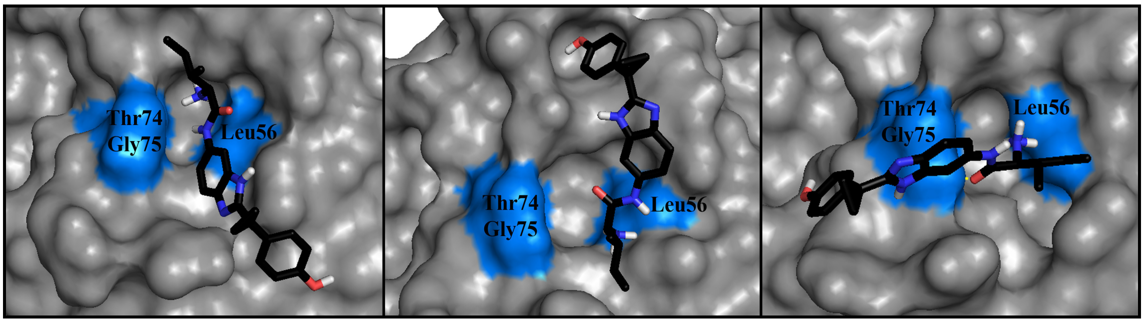

*Figure 82: Different conformations of amine **204a** in the binding pocket of K-Ras4B (PDB ID: 4DSO) predicted by HADDOCK.[44] The amino acids, which were defined as active residues for the HADDOCK calculation are highlighted in blue.*

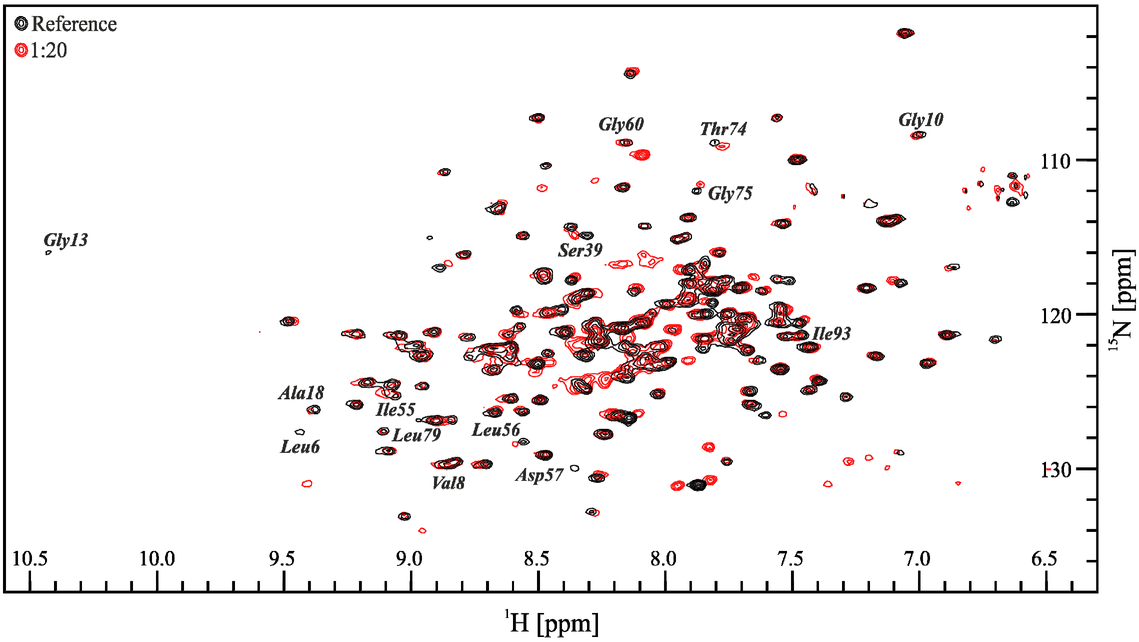

*Figure 83: ^{1}H,^{15}N-TROSY NMR overlay of the excess measurement of pure amine **204a** to the K-Ras4B protein.[106]*

In contrast, Figure 84 shows that the mixture interacts with the protein in the expected way. As described before for the unsubstituted derivative **187**, the shifts of the relevant peaks are less strong. Only a few residues belonging to the ligand binding pocket shift at all such as Leu56, Thr74 and Gly75 while others (Leu6, Ile55, and Gly60) are not affected significantly. This reduced interaction with the protein also affects the strength of the allosteric effect on residues such as Val8, Leu79 or Ile93. Nevertheless, a k_D value (4.74 ± 0.27 mM) can be calculated from the shifts of the NMR titration experiment. Though it is noticeably weaker than that of both, bisphenol A (**23**) and the Fesik ligand **94e**, it has to be taken into consideration that a mixture of two compounds was measured.

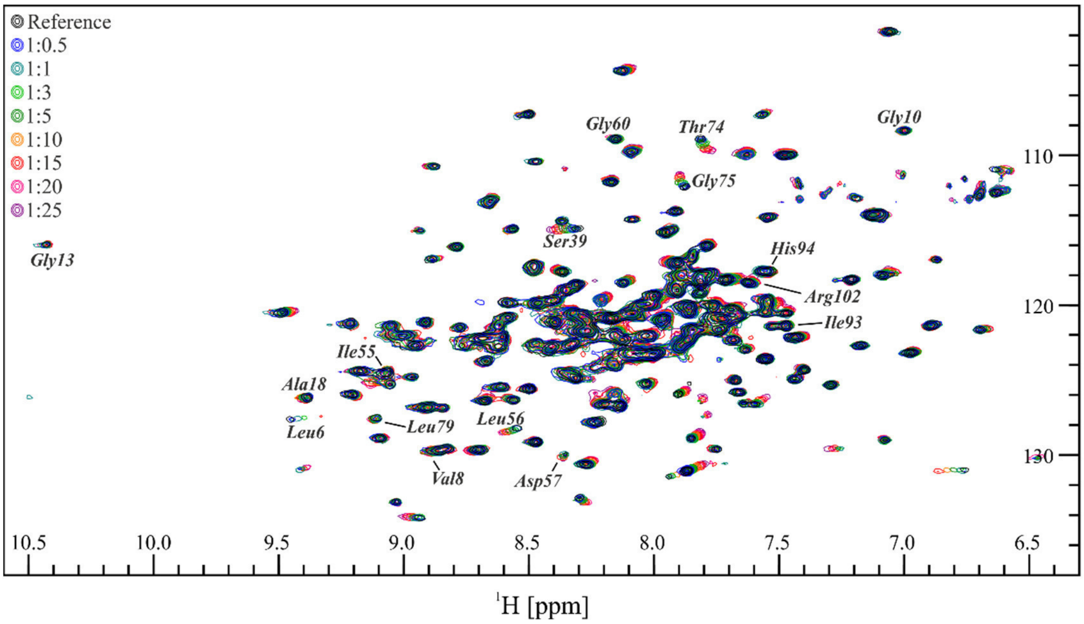

*Figure 84: ^{1}H,^{15}N-TROSY NMR overlay of the titration steps of a mixture of methylphenol derivatives **204a** and **204b** to the K-Ras protein.*[106]

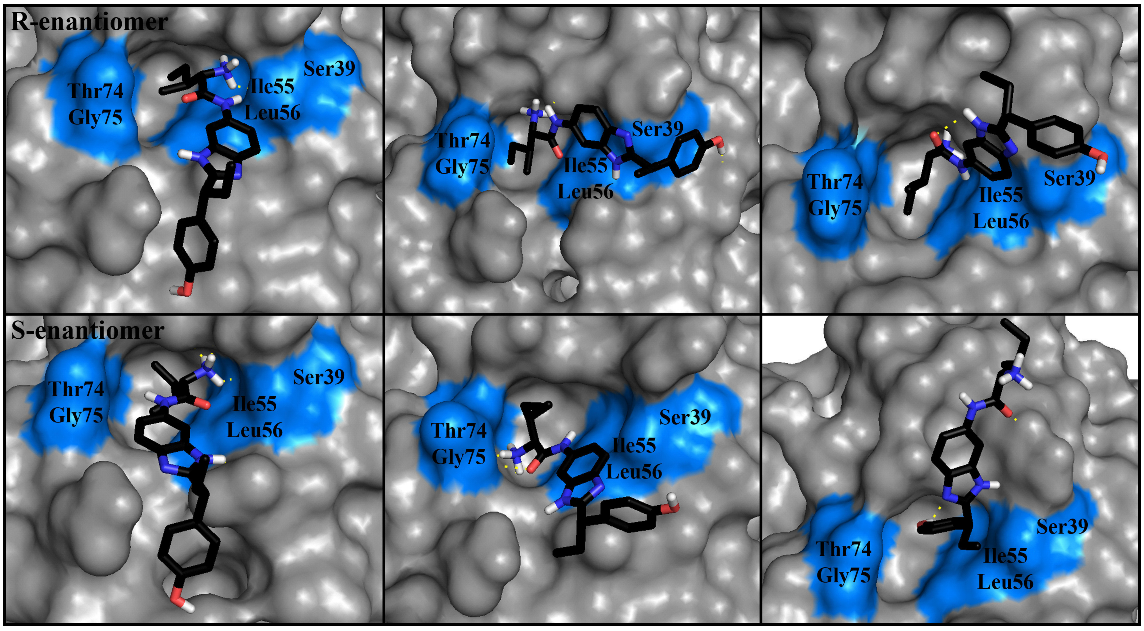

*Figure 85: Different conformations of the enantiomers of amine **204b** in the binding pocket of K-Ras4B (PDB ID: 4DSO) predicted by HADDOCK.*[44] *The amino acids, which were defined as active residues for the HADDOCK calculation are highlighted in blue.*

The NMR studies clearly prove that the ethyl derivative **204b** interacts with the labeled protein. This means that the k_D value calculated for the mixture of both amides **204a** and **204b** needs to be reconsidered. The calculation was made based on the assumption that the major compound **204a** and not the minor compound **204b** was responsible for the observed shifts. Additionally, the ethyl derivative contains a stereocenter. Only one of the enantiomers in the racemate of **204b** will interact with the *K*-Ras4B protein leading to a 50% lower concentration of the active compound. Table 16 shows the Glide scores of the two enantiomers calculated for the three different crystal structures. From the prediction, it can be concluded that the R-enantiomer is slightly favoured over the S-enantiomer. To evaluate the k_D value for amide **204b**, both enantiomers need to be synthesized and examined by NMR measurement.

Additionally, a HADDOCK model (Figure 85) of each of the enantiomers was calculated based on the shifts in the NMR measurement of the mixture. The prediction shows that both enantiomers prefer to insert the amino acid residue into the ligand binding pocket instead of the phenol ring similar to the predictions for the Fesik ligand **94e** and the hybrid molecule **187**. The HADDOCK computation also shows that the S-enantiomer can insert the phenol ring into the ligand binding cleft instead of the amino acid. This supports the prediction made by Glide, which slightly favours the S-enantiomer over the R-enantiomer.

*Table 16: Comparison of the Glide scores of the enantiomers of the ethyl derivative **204b** to BPA (**23**) and the Fesik inhibitor **94e**. In case of 4DSO, all water molecules were removed prior to docking experiments. For 4EPX, three water molecules are included for docking experiments while 4EPY contains a total of 14 water molecules surrounding the ligand binding pocket.*

Substance	**Structure**	**4DSO**		**4EPY**		**4EPX**	
		max	**min**	**max**	**min**	**max**	**Min**
Bisphenol A (23)		-3.24	-2.30	-1.36	-1.00	-1.67	3.02
Fesik inhibitor 94e		-5.93	-5.60	-4.14	-3.79	-5.35	-0.80
(R)-(Ethyl) methylhydroxy phenyl Fesik hybrid ((R)-204b)	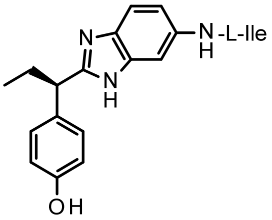 **(R)-204b**	-5.71	-4.78	-5.92		-4.00	
(S)-(Ethyl) methylhydroxy phenyl Fesik hybrid ((S)-204b)	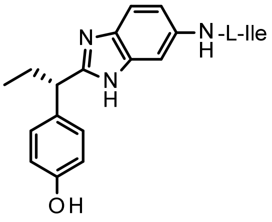 **(S)-204b**	-5.76	-2.50	-5.73	-4.29	-4.14	-2.17

From the results of the hybrid molecules of bisphenol A (**23**) and the Fesik ligand **94e**, it can be concluded that substitution of the indole moiety of the Fesik ligand **94e** for the bisphenol core leads to a sterically too demanding compound. Decreasing the sterical demand and therefore the number of substituents at the central C-atom led to a weak interaction of amine **187** with the protein. Increasing the number of substituents again to secure the desired angle at the bridging carbon-atom by introducing a cyclopropyl residue failed. In the process, the enantiomeric mixture of amine **204b** was obtained. This mixture shows a weak interaction with the protein. This indicates that three substituents at the central C-atom are tolerated. The actual dissociation constant for each of the enantiomers of amine **204b** therefore needs to be evaluated in future work.

4.4. Search for ligands of the secondary binding site of the K-Ras4B protein

As described in Chapter 2.3.1, the fragment-based drug design offers the possibility to improve the binding affinity by combining two fragments to a larger molecule.

Bisphenol A (**23**) and bisphenol AF (**95**) are known to bind to *K*-Ras4B with moderate affinity. Since optimization of those compounds was unsuccessful so far, a fragment linking approach was applied. According to Fesik and coworkers[79], the first ligand binding site needs to be fully occupied and saturated as i.e. by a covalently bound ligand. From a mutation experiment, the *K*-Ras4B Ser39Cys mutant with covalently bound benzimidazolethiomethane (Figure 86 **A**) was found to be suitable for second site screening. This binding site is created in equilibrium by a conformational change. The "opened" conformation is stabilized by the Fesik ligand **94a**. The secondary binding cleft is electronegative in character and contains the two acidic residues Glu37 and Asp38 (Figure 86 **B**).

This allows positively charged molecules to bind. Titration experiments with small libraries of low molecular weight molecules should then identify a different binding pocket if accessible.

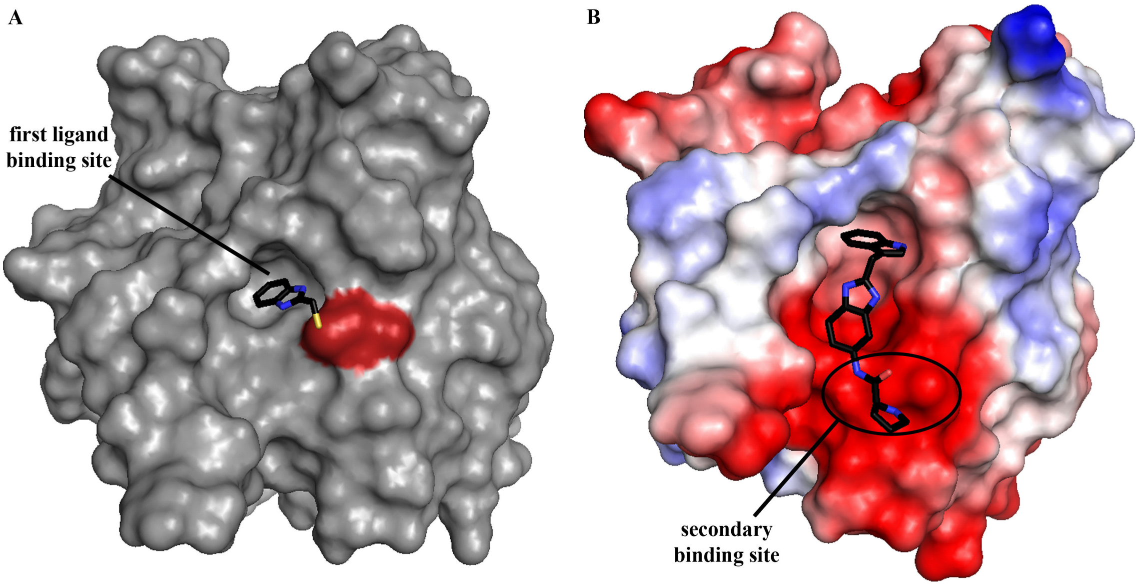

*Figure 86: **A:** Surface of K-Ras4B Ser39Cys mutant with the covalently bound ligand benzimidazolethiomethane shown as a stick model (PDB ID: 4PZZ). The mutated amino acid is highlighted in red. **B:** Electrostatic potential surface of the K-Ras4B protein with the Fesik ligand **94a** shown as a stick model (PDB ID: 4EPY). The secondary binding side is highlighted.*

As a first attempt, a small library of basic molecules was assembled and tested in three sub-libraries (Table 17) of five compounds each. The results of the NMR excess measurements of the mixtures with the wild type *K*-Ras4B protein are shown in Figure 87, Figure 88 and Figure 89, respectively.

Table 17: Basic compounds divided into three sub-libraries submitted for NMR excess measurements with the wild-type K-Ras protein.

Mixture 1	**Mixture 2**	**Mixture 3**
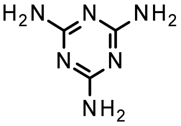 Melamine (**212**)	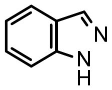 Indazole (**217**)	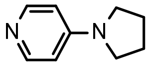 4-Pyrrolidinepyridine (**222**)
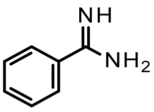 Benzamidine (**213**)	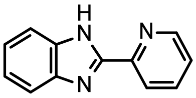 2-(Pyridine-2-yl) benzimidazole (**218**)	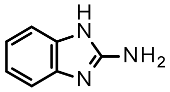 2-Aminobenzimidazole (**223**)
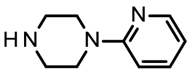 1-(2-Pyridyl)piperazine (**214**)	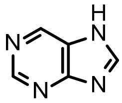 Purine (**219**)	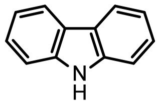 Carbazole (**224**)
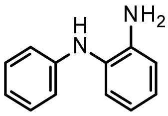 *N*-Phenyl-*o*-phenylene diamine (**215**)	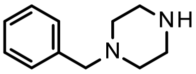 1-Benzylpiperidine-4-amine (**220**)	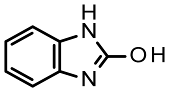 *1H*-Benzimidazole-2-ol (**225**)
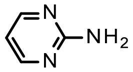 2-Aminopyrimidine (**216**)	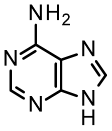 Adenine (**221**)	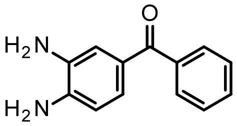 3,4-Diaminobenzophenone (**226**)

The excess measurement in Figure 87 shows no interaction of mixture one with the protein. Although shifts of the labeled peaks such as Thr74 and Gly75, which belong to the ligand binding pocket, can be observed, the range of the shifting signals is insignificant as the His-Tag of the protein is also affected. Usually, this indicates an interaction of the protein with DMSO rather than the added compounds.

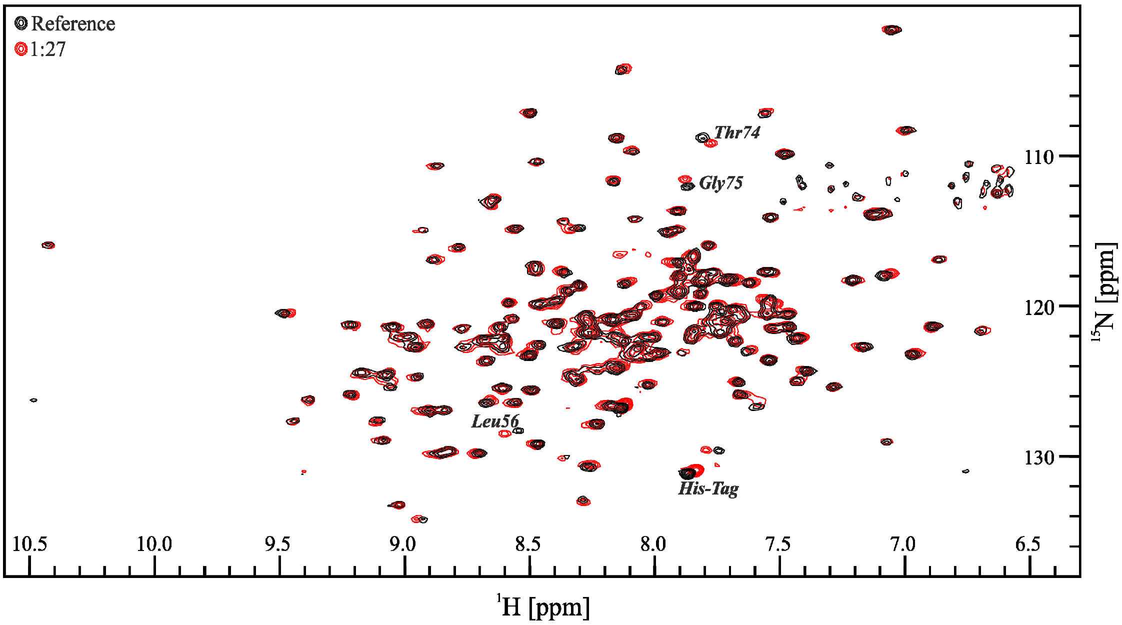

Figure 87: ^{1}H,^{15}N-TROSY NMR overlay of the excess titration step of mixture 1 to the K-Ras protein.[102]

In contrast, the spectra in Figure 88 and Figure 89 clearly indicate an interaction of the compounds of the sub-libraries two and three with the protein. The compounds bind to the known ligand binding pocket, which is indicated by the shift of amino acid peaks such as Thr74 and Gly75. Additionally, allosteric effects (Leu79, Asp57) can be observed as usual for ligands addressing the binding pocket known so far.

In future work, the titration of sublibraries two and three will be repeated in the presence of bisphenol A (**23**) and bisphenol AF (**95**) in order to block the primary binding site. This should force the basic molecules **217-226** to bind to the secondary binding site with lower affinity or not to bind at all. In addition, a *K*-Ras4B Ser39Cys mutant was coupled covalently with thionaphthol by the Stoll group to block the primary binding site as described by Fesik[79]. A screening of the basic mixtures with this modified *K*-Ras4B protein will give additional hints on second site binders.

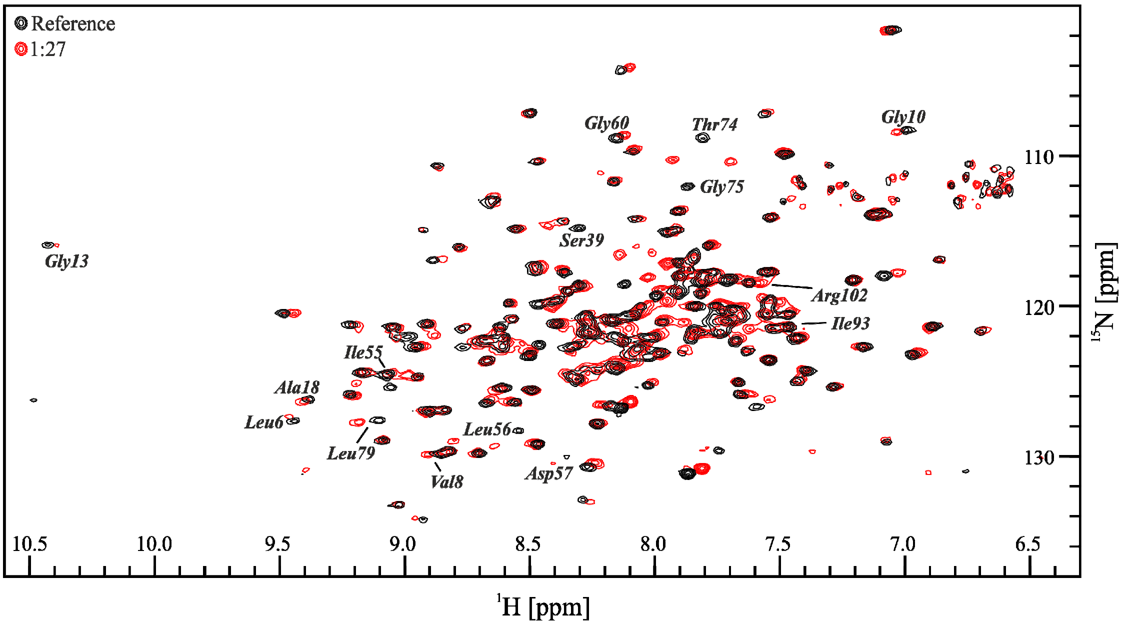

Figure 88: ^{1}H,^{15}N-TROSY NMR overlay of the excess titration step of mixture 2 to the K-Ras protein.[102]

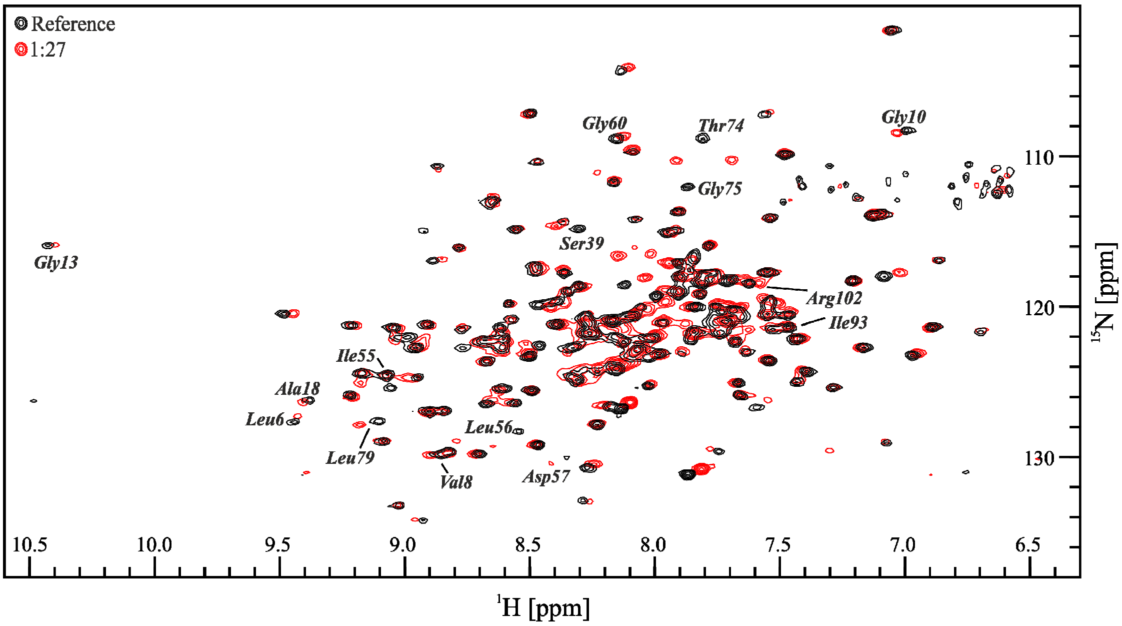

Figure 89: ^{1}H,^{15}N-TROSY NMR overlay of the excess titration step of mixture 3 to the K-Ras protein.[102]

4.5. Investigation of a selection of compounds in whole cell assays

A selection of the commercially available and the synthesized compounds was investigated in whole cell proliferation assays with three different cell types by Lead Discovery GmbH in Dortmund, Germany. These assays are optimized and standardized performed with Cell Titer Glow from Promega. After incubating the cells with the substances for 72 h, the remaining cell mass is weighted to measure the effect of the substances on cell growth. As positive control, both, a Raf and an Akt inhibitor, are used. The results of the tested compounds are summarized in Table 18. Only two compounds, 4,4'-biphenol (**22**) and bisindole A **151**, show a weak activity. Remarkably, bisphenol A (**23**) and bisphenol AF (**95**) did not show any activity in the whole cell assay.

Table 18: Selection of compounds that were tested for their effect in a whole cell assay.[i]

Name	Structure	IC_{50} value [µM]		
		A549	PaTu8902	Panc1
Raf inhibitor		5.435	5.265	8.369
Akt inhibitor		1.272	2.392	2.619
4,4'-Biphenol (22)	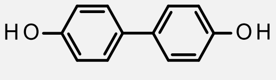 **22**	> 10	5.884	4.932
Benzophenone (227)	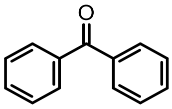 **227**	> 10	> 10	> 10
Bisphenol S (107)	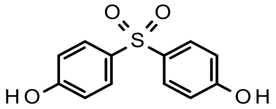 **107**	> 10	> 10	> 10
Bisphenol A (23)	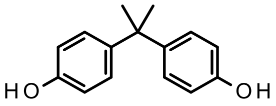 **23**	> 10	> 10	> 10
Bisphenol AF (95)	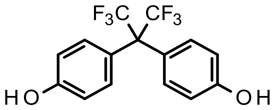 **95**	> 10	> 10	> 10

---

[i] The test assays were conducted by Lead Discovery GmbH.

BPA acetic acid (160)	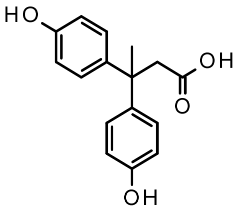 **160**	> 10	> 10	> 10
Bis-3-indole A (151)	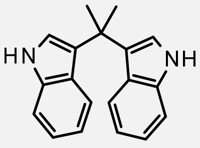 **151**	6.083	5.403	7.038
Fesik inhibitor 94e	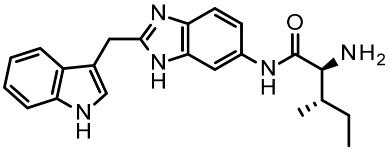 **94e**	> 10	> 10	> 10
Precursor amine 182	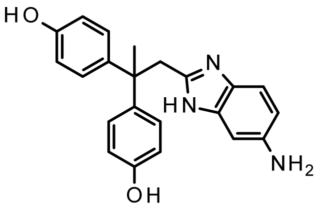 **182**	> 10	> 10	> 10
First generation hybrid molecule 179	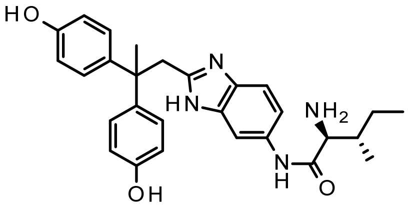 **179**	> 10	> 10	> 10
3-indoleacetic ester derivative of BPA 119a	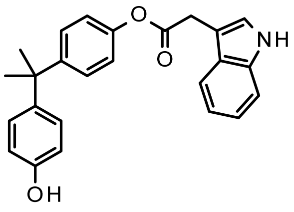 **119a**	> 10	> 10	> 10
3-indoleacetic ester derivative of BPAF 119b	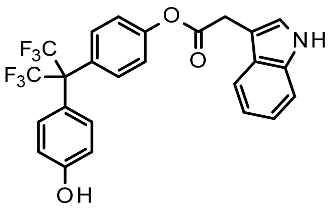 **119b**	> 10	> 10	> 10

Mono-methoxy BPA 136b	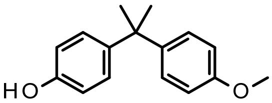 **136b**	> 10	> 10	> 10

In contrast to the NMR titration experiments, where highly polar and therefore water-soluble compounds are preferred, in the whole cell assay the compounds have to penetrate the cell membrane and need to be stable under physiological conditions. In case, the compounds are unable to enter the cell, no effect can be observed. However, this are only preliminary results. More detailed studies are under way currently.

4.6. Screening and synthesis of novel compounds binding to the MIA protein

As described above, the first ligand binding to MIA was the dodecapeptide AR71 with the sequence Ac-Phe-His-Trp-Arg-Tyr-Pro-Leu-Pro-Leu-Pro-Gly-Glu-NH_2. This peptidic molecule interacts with MIA through inhibition of the dimerization of two MIA proteins.[41,43] NMR titration experiments helped to identify the region (Cys17, Ser18, Tyr47, Gly66, Asp67, Leu76, Trp102, Asp103 and Cys106) on the surface of MIA this peptide interacts with. These amino acids form a cleft in the surface of the protein, which can be used as a binding pocket for small molecules.[41] Through studies with the natural binding partner of MIA, fibronectin, and arginine rich synthetic peptides, this amino acid was identified to play a crucial role in the interaction MIA.

From that finding, a search of the ZINC database[94] was conducted, using the guanidine functionality of arginine as a structural characteristic to select compounds. More than 5000 compounds were identified from the database by our cooperation partners in Bochum.[95] The structures were used in modelling experiments with the software Autodock/VINA[81]. The best 20 substances were purchased from commercial vendors and investigated in NMR titration experiments. From these experiments, only ZINC05203919 (**24**) and ZINC01400183 (**25**) were identified as ligands for the MIA protein (Figure 91 **A**). Ligand binding of those two compounds was deduced from the NMR overlays (Figure 91 **B** and **C**) and the amino acids affected by ligand addition. Although both compounds address the same binding pocket, the conformations of the ligands differ (Figure 90). Both compounds interact with Leu76, Gly77 and Tyr78 on the bottom of the binding cleft. ZINC05203919 (**24**) is oriented towards His19, while ZINC01400183 (**25**) addresses Trp102, Asp103 and Tyr105. From the titration experiments, dissociation constants can be calculated. Both compounds exhibit weak k_D values of 328 ± 84 µM in case of ZINC05203919 (**24**) and 320 ± 76 µM for ZINC01400183 (**25**), respectively. The binding modes of both compounds and the protein were predicted from the NMR peak shifts using HADDOCK (High Ambiguity Driven protein-protein DOCKing[44]).

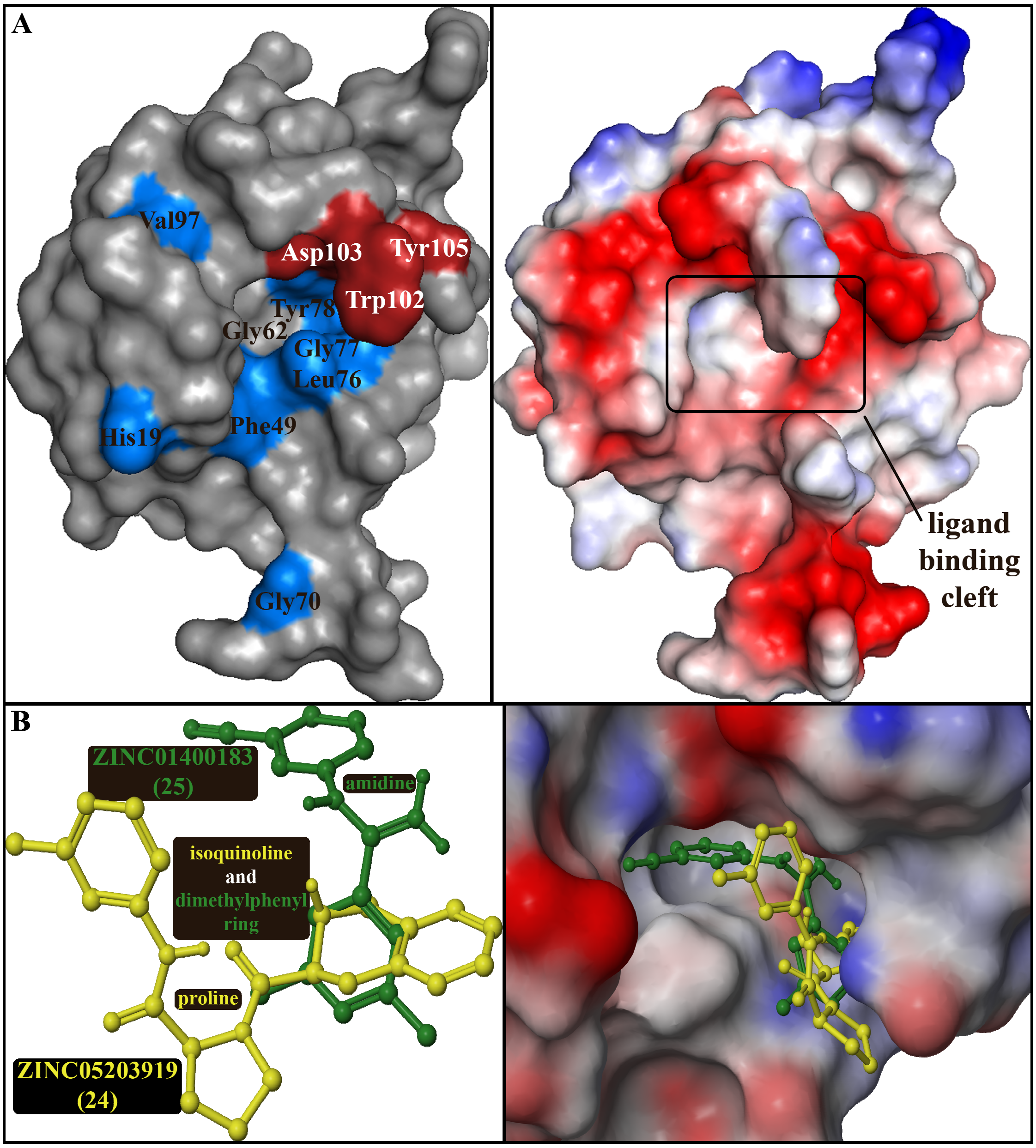

Figure 90: ***A:*** *Surface of the MIA protein with the amino acids affected by ZINC05203919 (****24****) indicated in blue. Additional shifts, which are observed during titration of ZINC01400183 (****25****), are highlighted in red. The ligand binding cleft is highly acidic, which is indicated by the red colour of the electrostatic potential of the MIA surface.* ***B:*** *Partial overlap of the ligands* ***24*** *and* ***25****. The overlay of the molecules was predicted from the HADDOCK calculations, which are based on the NMR titration experiments of the ZINC compounds.*

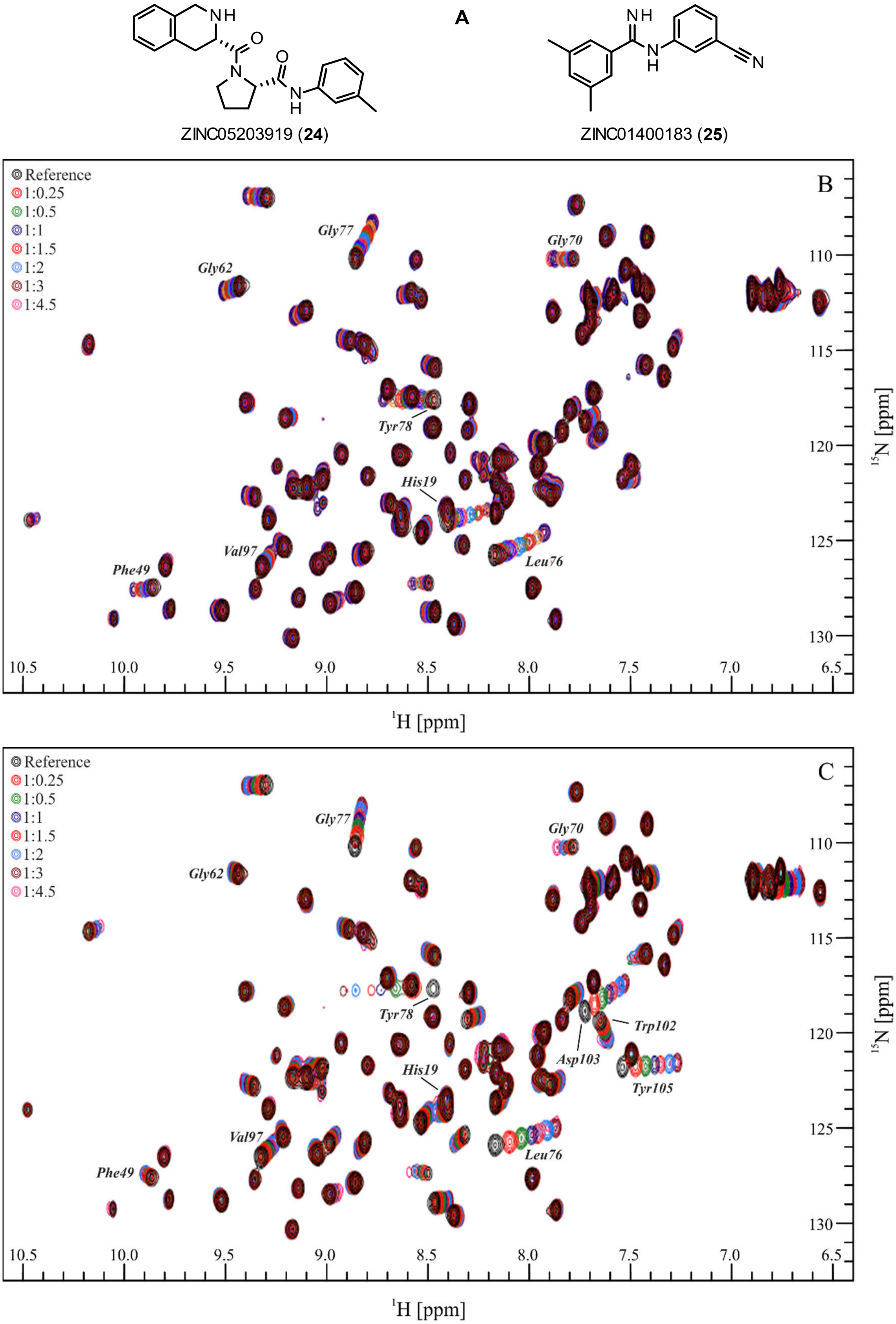

*Figure 91: **A:** Ligands for the MIA protein identified by NMR experiments of commercially available compounds provided by the ZINC database. **B:** NMR titration overlay for ZINC05203919 (**24**). **C:** NMR titration overlay for ZINC01400183 (**25**).*[158]

4.6.1. Structural modifications of ZINC01400183 (25)

To collect structure-activity relationship data, it is most relevant to evaluate the influence of the substituents as well as the amidine functionality of ZINC molecule **25** on the interaction with the MIA protein. Those functional groups were therefore substituted in the following experiments.

4.6.1.1. Relevance of the nitrile and methyl substituents

N-Phenylbenzamidine (**230,** Scheme 33) was synthesized according to Wang and coworkers.[159] Aniline (**228**) and benzonitrile (**229**) were reacted with sodium hydride in DMF.[159] Unfortunately, no product was obtained. Only benzamide was detected in the crude product. A reaction with the more reactive hydrochloride of amine **228** in trifluoroethanol again yielded only benzamide. The reaction of nitrile **229** and aniline (**228**) in the presence of aluminum trichloride at 200 °C for 30 min in a Kugelrohr short-path vacuum distillation apparatus gave amidine **230** in low yield (36%).

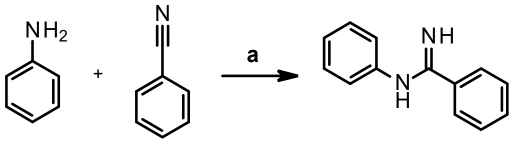

228 **229** **230**

Scheme 33: Test reactions to yield phenyl substituted amidine ***230*** *via the general procedures described in the literature. Reaction conditions: (a) $AlCl_3$, 200 °C, 30 min, 36%.*

The NMR experiment shows only a weak interaction of diphenylamidine **230** with the MIA protein (Figure 93). Shifts can be observed for amino acids Leu76 and Tyr78, which are located at the lower rim of the binding pocket. The HADDOCK model in Figure 92 shows that the diphenylamidine **230** is unable to penetrate the ligand binding pocket of the MIA protein as deeply as its analogue **25**. Instead, the compound can be inserted into the pocket with only one phenyl ring. The amidine group can then interact with Glu16. Other relevant amino acids such as Trp102 or Asp103 are not affected. A comparison with ZINC01400183 (**25**) proves the significance of the nitrile and methyl substituents.

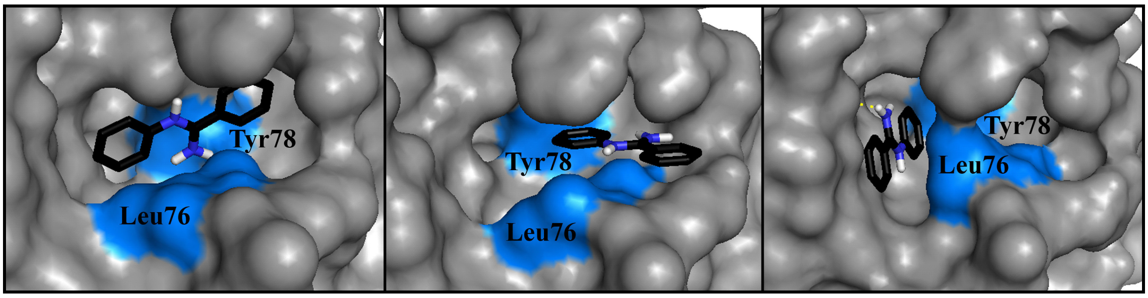

Figure 92: Different conformations of amidine ***230*** *in the binding pocket of MIA (PDB ID: 1I1J) predicted by HADDOCK.*[44] *The amino acids, which were defined as active residues for the HADDOCK calculation, are highlighted in blue.*

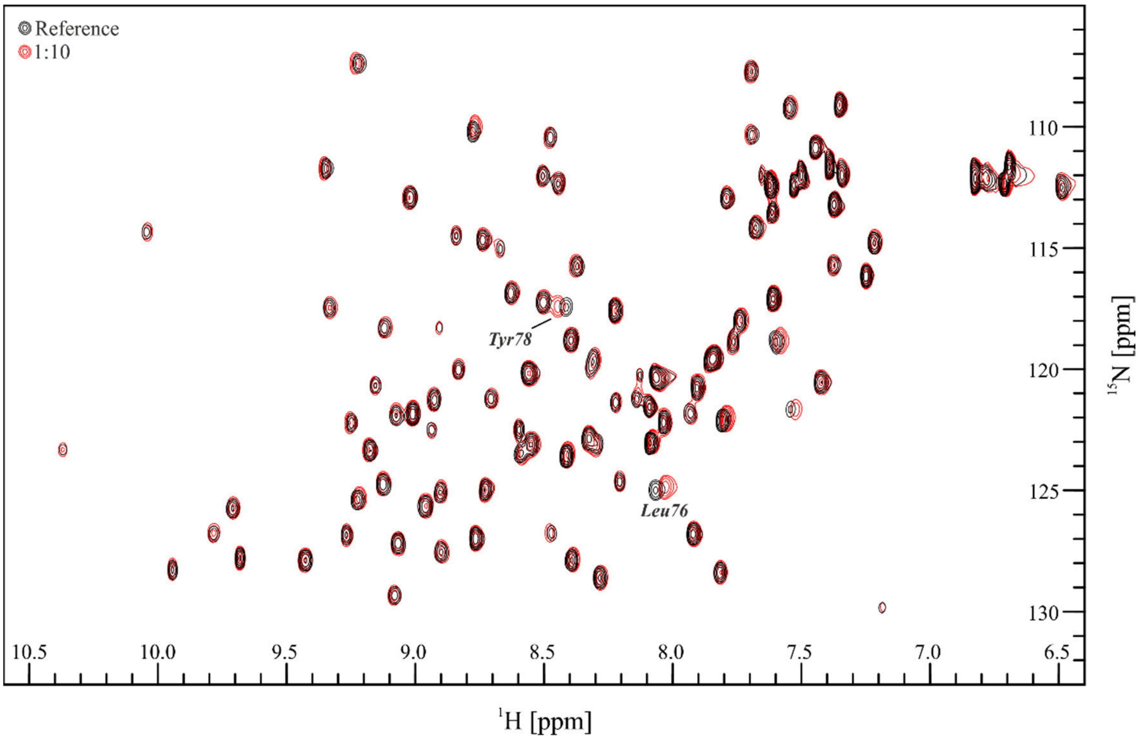

*Figure 93: ^{1}H,^{15}N-TROSY NMR overlay of the excess measurement of diphenylamidine **230** to the MIA protein.*[160]

4.6.1.2. Replacement of the amidine moiety for an amide group

The method used to synthesize phenylamidine **230** can most probably not be applied to more complex and sensitive compounds due to the drastic reaction conditions. Instead, the corresponding amides, which are easily accessible by standard chemistry, were investigated.

In comparison to the corresponding amidine **25**, the Glide score for amide analogue **231** is lower. An overlay of the predicted conformations of amide **231** and amidine **25** shows that amide **231** cannot adopt the same binding mode (Figure 94). In contrast to amidine **25**, amide **231** does not occupy the binding pocket completely. Instead, it either forms a hydrogen bond to Leu76 or the dimethyl substituted phenyl ring is positioned near Glu16 at the left rim of the binding cleft.

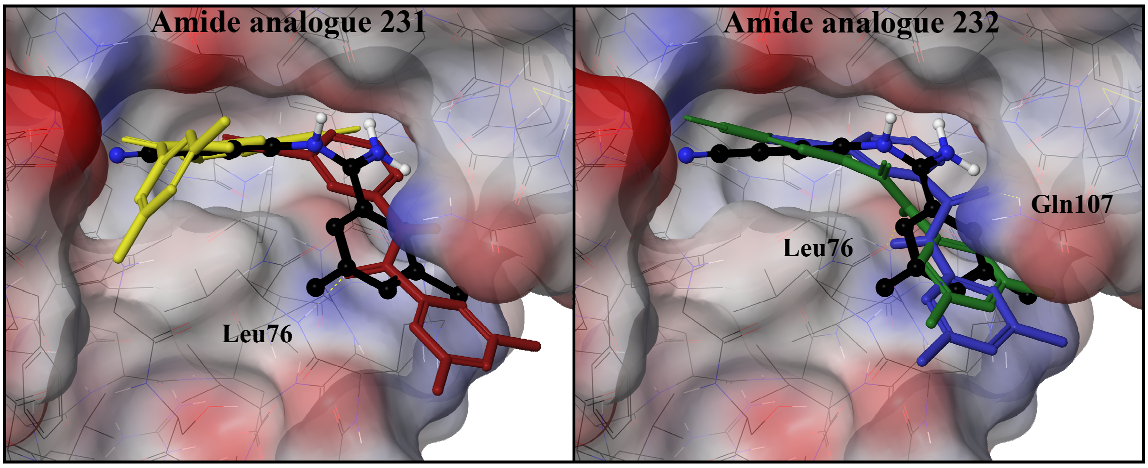

*Figure 94: Comparison of the conformations of the amide analogues **231** (red and yellow) and **232** (green and blue) with amidine **25** as reference (black) predicted by Glide.*

Table 19 shows that the Glide score of the inversely substituted amide **232** is slightly increased in comparison to ZINC01400183 (**25**). This is also supported by the binding mode predicted for this compound (Figure 94). In contrast to amide **231**, analogue **232** can insert itself as deeply into the binding pocket as amidine **25** resulting in a nearly perfect overlay of those two compounds. Amide **232** is also able to form a hydrogen bond with the carboxylic acid functionality of Leu76. Amides **231** and **232** are promising structures, which show negative Glide values for all poses calculated in contrast to ZINC01400183 (**25**). Thus, both molecules were chosen for synthesis.

*Table 19: Glide scores of the amides **231** and **232** in comparison to ZINC01400183 (**25**).*

Substance	Structure	Glide Score	
		max	min
ZINC01400183 (25)		-4.22	1.38
Amide analogue 231	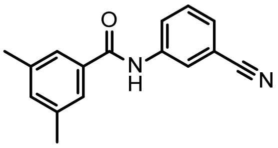 **231**	-3.83	-2.78
Amide analogue 232	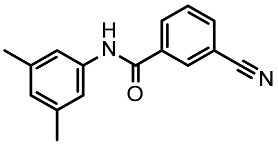 **232**	-4.52	-3.90

3,5-Dimethylaniline (**233**) was coupled with 3-cyanobenzoic acid (**234**) using EDC hydrochloride and HOBt as coupling reagents in DMF (Scheme 34).[161] The desired amide **232** was obtained after chromatographic purification in excellent yield of 95%. Remarkably, the reaction of dimethylbenzoic acid **235** with amine **236** under the same reaction conditions did not give amide

231. Addition of catalytic amounts of DMAP[162] gave amide **231** in moderate yield (51%) after purification.

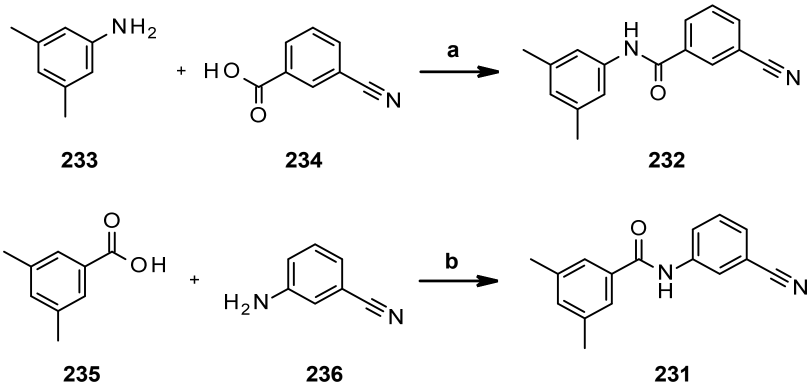

*Scheme 34: Synthesis of amides **231** and **232** Reaction conditions: (a) EDC hydrochloride, HOBt, DIPEA, DMF, r.t., 18 h, 95%, (b) EDC hydrochloride, DMAP, DCM, r.t., 22 h, 51%.*

The NMR overlays in Figure 95 **A** and **B** show no significant interaction of the compounds with the protein. Both substances were added in larger excess than usually (1:25). This led to partial precipitation of the compounds. However, proton-NMR measurements show a significant amount of dissolved material, which was available for binding to the protein.

The shifts in the NMR overlay for amide analogue **231** are more obvious (Figure 95 **A**). It can be seen that all peaks are affected, which indicates a different effect such as DMSO addition rather than ligand binding as this usually evokes shifts of explicit peaks.

In contrast to the prediction by Glide, the compounds do obviously not interact with the protein. This might be a result of the significantly decreased basicity of the amide moiety in comparison to the amidine group. The property seems to be essential as the ligand binding pocket is highly anionic, which favours cationic compounds such as protonated amines or amidines (Figure 90). This result clearly underlines the crucial role of the amidine moiety of ZINC molecule **25** regarding structure-activity relationships.

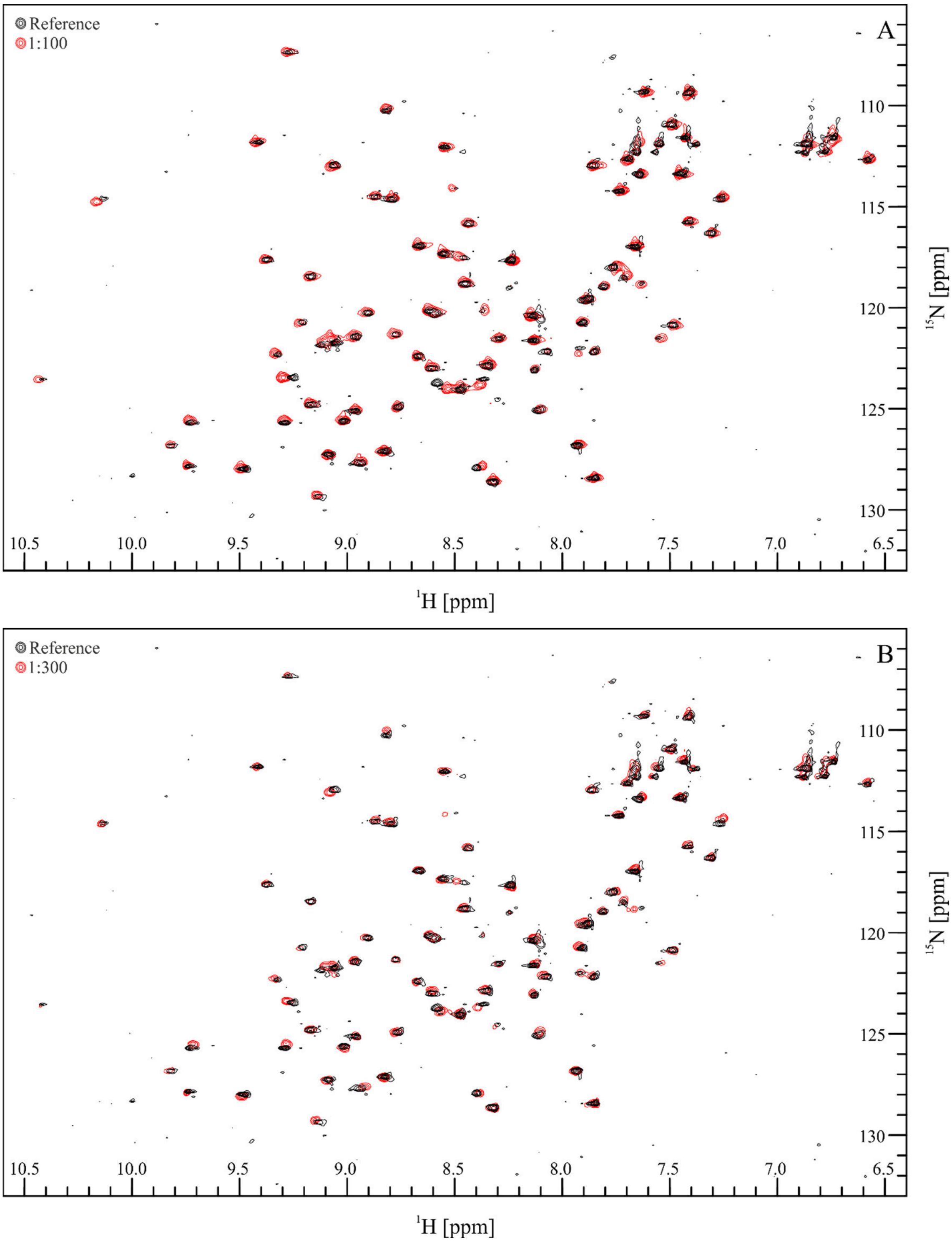

*Figure 95: ^{1}H,^{15}N-SOFAST NMR overlay of the excess titration experiments for the MIA protein with **A:** amide analogue **231**, **B:** amide analogue **232**.*[i]

---

[i] These NMR experiments were measured by Jasmin Müller with the aid of King Yip Tuo, Ruhr Universität Bochum.

4.6.2. Fragment merging of the ZINC molecules 24 and 25

The structures in Figure 90 **B** show a partial overlap of the isoquinoline ring and the dimethyl-substituted phenyl ring. To increase interaction with the protein, the ligands **24** and **25** can be merged accordingly.

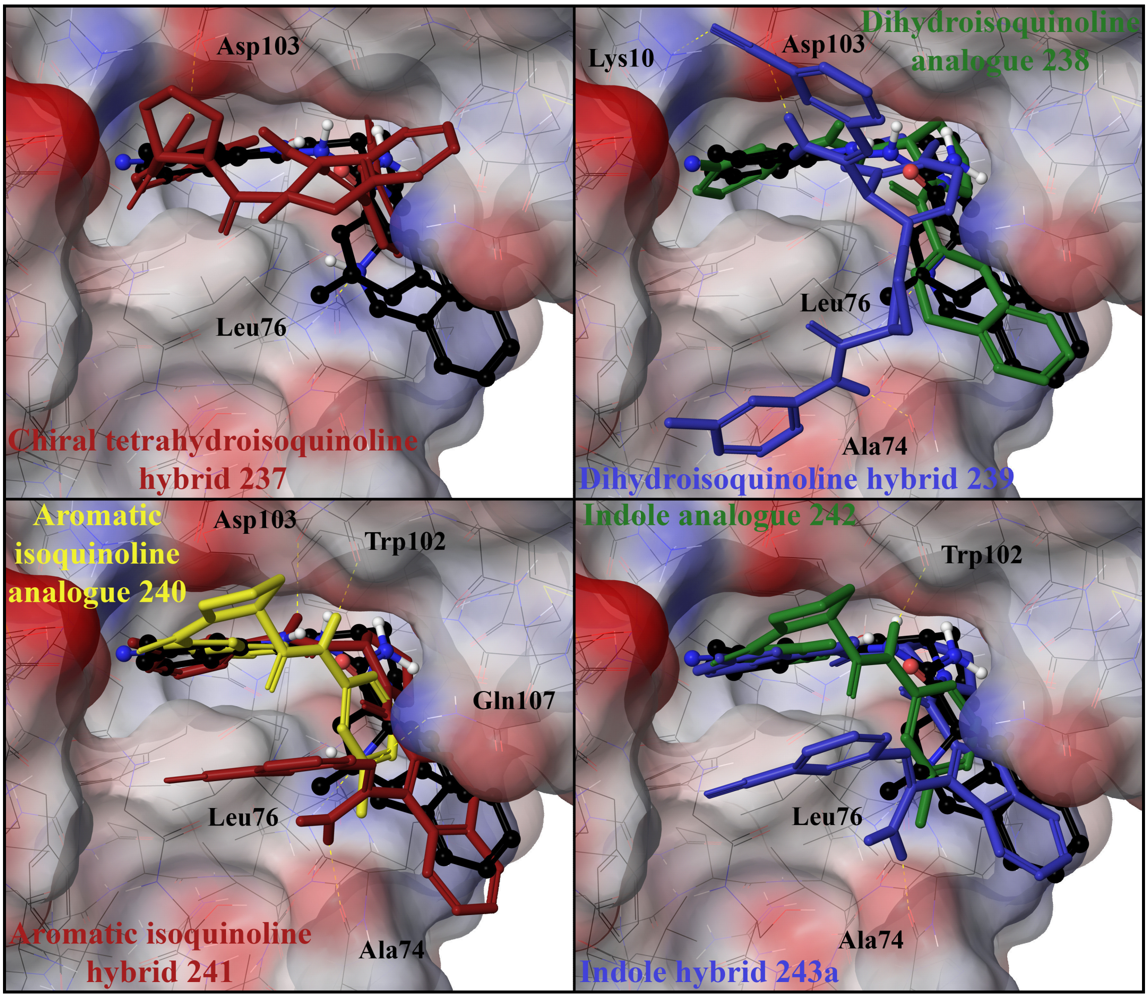

*Figure 96: Comparison of the conformations of the amide analogues **231** (red and yellow) and **232** (green and blue) with amide **24** and amidine **25** as reference (black).*

The resulting molecule **237** is highly complex and shows a Glide score comparable to those of the fragments **24** and **25**. It can therefore be expected to bind to the MIA protein in a similarly strong manner. Remarkably, the hybrid molecule has a highly positive Glide value, which indicates repellent interaction with the protein. In contrast to the overlay of the two ZINC molecules shown in Figure 90, the prediction (Figure 96) orients the hybrid molecule **237** not always as expected. In contrast, the hybrid molecule dos not penetrate the ligand binding pocket as deeply. Instead, the proline ring is oriented toward the top rim of the binding cleft to form a hydrogen bond with Asp103. The isoquinoline ring is also positioned towards Tyr 105 and Gln107 instead of Leu76. The hydrogen bond to this residue can consequently not be formed.

To increase the Glide score, various analogues of hybrid molecule **237** were examined. The effect of additional double bonds in the central tetrahydroisoquinoline ring were studied. Thereto, further double bonds were added stepwise to replace the unsaturated moiety for its aromatic isoquinoline analogue. Additionally, the isoquinoline core structure was replaced for an indole ring. The results of the *in-silico* screening are shown in Table 20 in comparison to the ZINC molecules ZINC05203919 (**24**) and ZINC01400183 (**25**).

*Table 20: Glide scores of the hybrid molecules **237-243a** of the originally found binders in comparison to ZINC05203919 (**24**) and ZINC01400183 (**25**).*

Substance	**Structure**	**Glide Score**	
		max	min
ZINC05203919 (24)	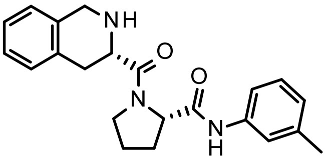 ZINC05203919 (**24**)	-5.60	5.09
ZINC01400183 (25)	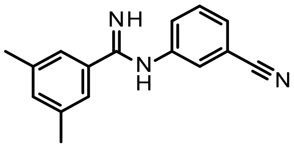 ZINC01400183 (**25**)	-4.22	1.38
Chiral tetrahydro-isoquinoline hybrid 237	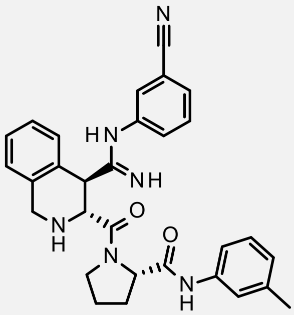 **237**	-5.14	8.95
Dihydro-isoquinoline analogue 238	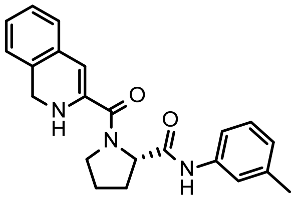 **238**	-4.52	-3.27

Dihydro-isoquinoline hybrid 239	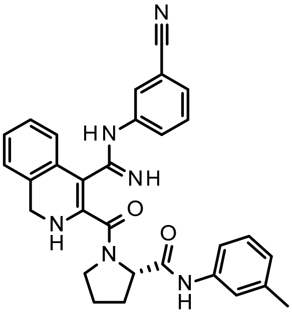 **239**	-6.71	-2.63
Aromatic isoquinoline analogue 240	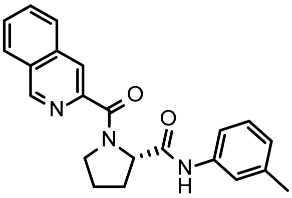 **240**	-6.18	-3.45
Aromatic isoquinoline hybrid 241	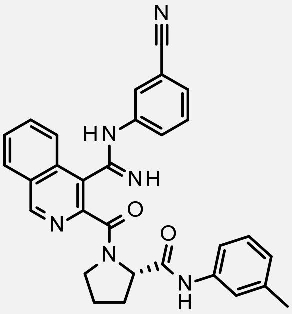 **241**	-4.75	2.92
Indole analogue 242	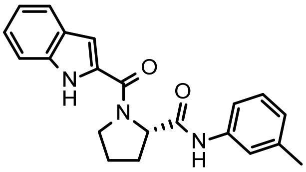 **242**	-6.25	-3.35
Indole hybrid 243a	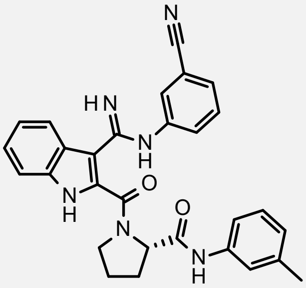 **243a**	-5.46	1.87

As can be seen from Table 20, insertion of a double bond into the isoquinoline core structure to evaluate the influence of the two stereocenters lowers the Glide score of analogue **238** in comparison to ZINC05203919 (**24**). Nevertheless, the prediction (Figure 96) shows that both compounds can adopt the same conformation in the binding pocket of the MIA protein. In contrast, hybrid molecule **239** exhibits an improved binding affinity, but it cannot adopt the same conformation as the fragments **24** and **25**. Instead, the nitrile substituted phenyl ring is located outside the ligand binding pocket to form a hydrogen bond to Lys10. Additionally, the amidine residue interacts with Ala74. Consequently, only the dihydroisoquinoline ring can be inserted into the binding pocket to interact with the protein. As the conformation of the molecule **239** differs significantly, this structure was not chosen for synthesis.

Insertion of another double bond into the isoquinoline core structure affords the corresponding aromatic analogue **240**. This compound can adopt a similar conformation as ZINC05203919 (**24**), which is also reflected in the high Glide scores for this molecule. Consequently, hybridization with ZINC01400183 (**25**) was promising. Although the Glide score for the aromatic hybrid molecule **241** does not exceed the values for the original binders, the binding mode prediction (Figure 96) shows a good positioning of the molecule in the ligand binding pocket. This allows for up to three additional hydrogen bonds to be formed (Ala74, Asp103 and Gln107). As this molecule can adopt the expected conformation, it was chosen to be prepared.

Additionally, the isoquinoline core structure was replaced for an indole moiety. This residue is commercially available carrying various substituents in the different positions. Again, the structural alteration was first applied to ZINC05203919 (**24**) to evaluate the effects on the binding affinity and the conformation. The Glide score shows a positive effect due to the replacement of the isoquinoline core for the indole moiety. The binding mode of the indole derivative **242** is consistent with the conformation of the aromatic analogue **240**, which forms a hydrogen bond with Trp102. This structural alteration was therefore also considered promising. In contrast to the indole derivative **242**, the hybrid molecule **243a** mainly adopts the expected conformation (Figure 96). The hybrid can form three hydrogen bonds with Ala74, Leu76 and Trp105. This qualifies the compound for synthesis as it is expected to bind strongly to the MIA protein. This hypothesis is also underlined by the comparatively high Glide scores of the molecule.

Consequently, three hybrid molecules derived from ZINC05203919 (**24**) and ZINC01400183 (**25**) were chosen for synthesis, two of which simplify the originally found structures to allow for faster synthetic access. The analogues **238**, **240** and **242** of ZINC05203919 (**24**) were used only to evaluate the influence of the chiral centers of the isoquinoline as well as the significance of this residue in general. These compounds were only used for comparison of the Glide values and the predicted conformations with the ZINC molecule **24**. Therefore, the molecules were not considered for synthesis.

For the syntheses of the three hybrid molecules derived from the ZINC molecules ZINC05203919 (**24**) and ZINC01400183 (**25**), the common building block **247** shown in Scheme 35 is required. Coupling of the protected amino acid **244** with the aniline derivative **245** using ethyl chloroformate as coupling reagent[163] afforded the desired amide **246** in a good yield of 77% after refluxing the reaction mixture for several hours. With EDC hydrochloride and HOBt[164] as coupling reagents, the reaction can be performed at room temperature in excellent yield of 87%.

Cleavage of the Boc-group was done under standard conditions using TFA in DCM. This gave the free secondary amine **247** in quantitative yield. Performing the reaction at room temperature as described by Moorthy *et al.*[163] led to a reduced optical rotation value of the product in comparison to a repetition of the reaction at 0 °C according to Lee and coworkers[164].

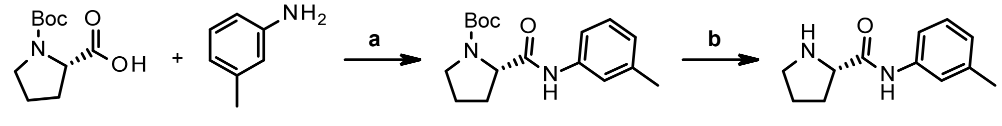

244 **245** **246** **247**

*Scheme 35: Synthesis of the building block **247** derived from proline **244** and 3-methylaniline (**245**). Reaction conditions: (a) EDC hydrochloride, HOBt, DCM, 0 °C → r.t., 18.5 h, (b) TFA, DCM, 0 °C, 3 h, quantitative yield.*

This building block was coupled with tetrahydroisoquinoline derivative **255** or the corresponding aromatic analogue **258**. Ester **250** was synthesized (Scheme 36) as a precursor for both, the aromatic and the saturated isoquinoline derivatives **255** and **258**. The intermediate β-ketoester **249** was obtained from ethyl 4-chloroacetoacetate **248** via a classic nucleophilic substitution reaction with benzyl alcohol in excellent yield of 97%.[165] Compound **249** was then reacted with 2-bromobenzylamine in the presence of copper(I) iodide. The mixture was first refluxed for 24 h then stirred under air at room temperature for 22 h.[166] The isoquinoline building block **250** was obtained in moderate yield (49%). Reduction of the pyridine ring of isoquinoline **250** can be done with platinum oxide in glacial acetic acid to afford a racemic mixture of the two *syn*-products.[167] As the reaction conditions are highly acidic, epimerization of the stereocenter in α-position to the ester functionality leads to the formation of diastereomers. The synthesis of tetrahydroisoquinoline **237** was aborted due to the low yield (32%) and the formation of an inseparable diastereomeric mixture.

The synthesis of the aromatic analogue **241** commences with a direct conversion of isoquinoline **250** to nitrile **256** (Scheme 37) as described by Liguori *et al.*[168] In the first step of nitrile conversion, the corresponding hydroxamic acid is formed, which is then converted to the corresponding nitrile **256**. Unfortunately, no conversion of the starting material was observed when stirring with potassium hydroxide and hydroxyamine hydrochloride in methanol. A similar procedure was tested, which first converts the hydroxyamine salt to the free amine.[169] This method did also not afford the desired hydroxamic acid derivative.

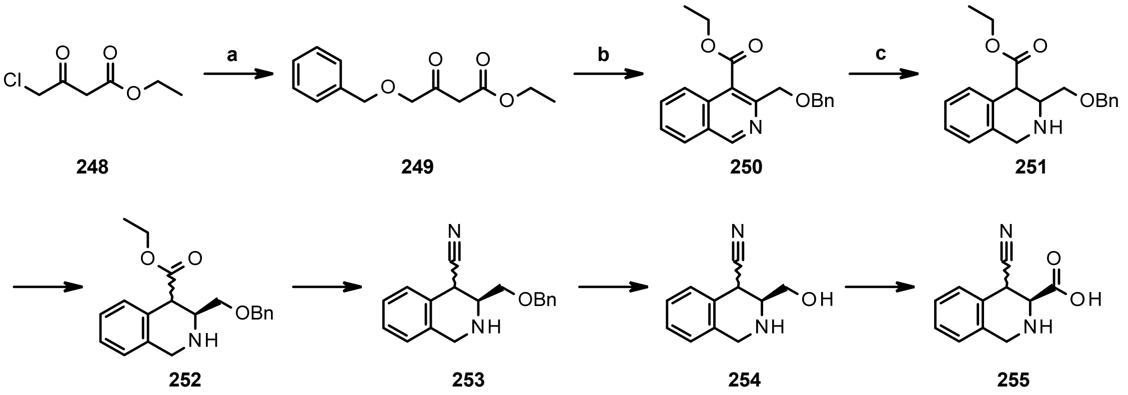

Scheme 36: Synthesis of the tetrahydroisoquinoline derivative **255** required for the synthesis of the unsaturated hybrid analogue **237**. Reaction conditions: (a) NaH, benzyl alcohol, THF, 0 °C → r.t., 18 h, 97%, (b) K_2CO_3, CuI, 2-bromobenzylamine, isopropanol, reflux (24 h) → r.t. (22 h), 49%, (c) PtO_2, AcOH, 18.5 h, 32%.

Another method to convert an ester group into the corresponding nitrile was described by Suzuki and coworkers[170] using DIBAL-H and sodium *tert*-butoxide to form sodium di-*iso*-butyl-*tert*-butoxyaluminium hydride, a sterically highly demanding reductant. After reduction of the ester to the corresponding aldehyde, iodine and aqueous ammonia were added to form the nitrile. Unfortunately, the TLC again did not show any conversion of the starting material.

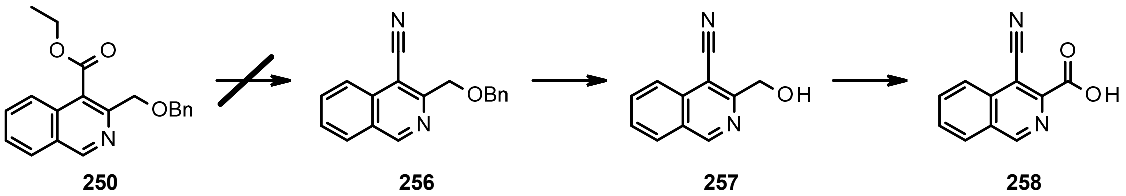

Scheme 37: Attempted reaction sequence for the conversion of ester **250** to the corresponding nitrile **258** necessary for the coupling with the proline derived building block **247**.

Nitrile **258** can alternatively be synthesized from 3-methylisoquinoline (**259**, Scheme 38). Isoquinoline **259** was reacted with *N*-iodosuccinimide in acetic acid for 7 h at 80 °C to afford the halogenated compound **260** in 72% yield.[171,172]

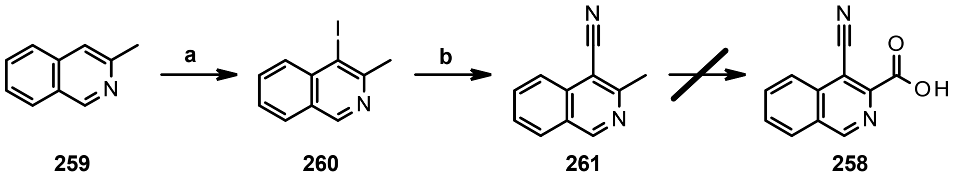

Scheme 38: Alternative route towards nitrile **258**. Reaction conditions: (a) NIS, AcOH, 80 °C, 7 h, 72%, (b) $Zn(CN)_2$, $Pd(PPh_3)_4$, DMF, 120 °C, 21 h, 93%.

Substitution of the halogen atom was conducted by reacting the starting material **260** with zinc cyanide, which is easily accessible from zinc sulfate and potassium cyanide. As catalyst, tetrakis(triphenylphosphine)palladium(0) was added and the mixture was heated to 120 °C over night to yield nitrile **261** in excellent yield (93%).[171,173,174] Unfortunately, oxidation of the methyl group to a carboxylic acid functionality using potassium permanganate in water did not result in the desired product.[175] As described by Singer and McElvain[176], the purple colour of the reaction mixture disappeared over time although it took significantly longer when using isosquinoline **261**. The crude mixture did not contain nitrile **261**, but impure starting material **261**. Isoquinolines are electron-poor aromatics and thus the oxidation of methyl-groups is more difficult. In addition, $KMnO_4$ as one of the strongest oxidants in organic synthesis did not give even traces of the isoquinoline carboxylic acid **258**. Consequently, no further oxidation experiments were attempted.

The indole derivative **268** can be obtained via a similar route from the corresponding ester **263**, which is readily available from ethyl indole-2-carboxylate (**262**) (Scheme 39). Reddy *et al.* use a mixture of copper cyanide, copper bromide and palladium acetate in DMF to accomplish this conversion.[177] Unfortunately, even after several trials, the literature could not be repeated. Instead, a two-step pathway towards nitrile **263** via the halogenated species **264** was chosen. Reaction of ester **262** with *N*-iodosuccinimide[178] afforded the desired iodinated compound in excellent yield (96%). Subsequent conversion to the desired nitrile **263** was achieved using copper cyanide, tetraethylammonium cyanide and a palladium catalyst[178,179] (83%). Ester **263** was cleaved using potassium hydroxide in a mixture of water and ethanol to afford the desired free carboxylic acid **268** in quantitative yield.[180]

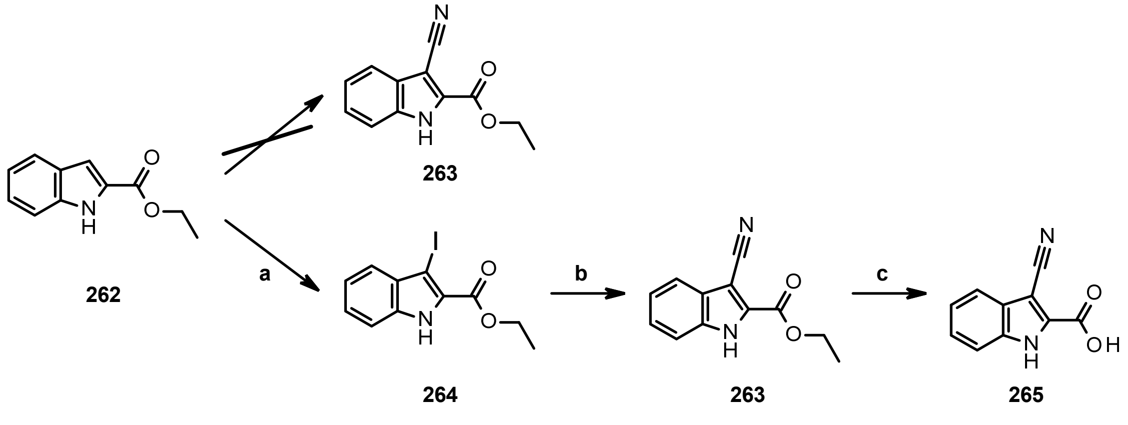

*Scheme 39: Failed synthesis of nitrile **262** and the alternative route leading to the desired acid **265**. Reaction conditions: (a) NIS, DCM, r.t., 2.5 h, 96%, (b) CuCN, $Et_4N^+CN^-$, $Pd_2(dba)_3$, DPPF, DMF/THF (1:1), 120 °C, 27 h, 83%, (c) KOH, H_2O/EtOH (1:2.5), 60 °C, 1.5 h, quantitative yield.*

Coupling of the two building blocks **247** and **265** was carried out using EDC hydrochloride and DMAP as catalyst as described by Hewlett and Tepe[181] to afford the desired amide **266** in good yield of 65%. Preparation of amidine **243a** was first tried via the direct route (Scheme 40) using nitrile **266** as starting material as described by Wang and coworkers.[159] No conversion of the starting material in the presence of sodium hydride[159] was observed. Alternatively, nitrile **266** and aniline were reacted with aluminum trichloride at 120 °C in a microwave reactor. Again no conversion of the starting material to amidine **243b** was observed. Instead of 3-aminobenzonitrile, aniline was used for these reactions, as the bifunctional compound is anticipated to polymerize.

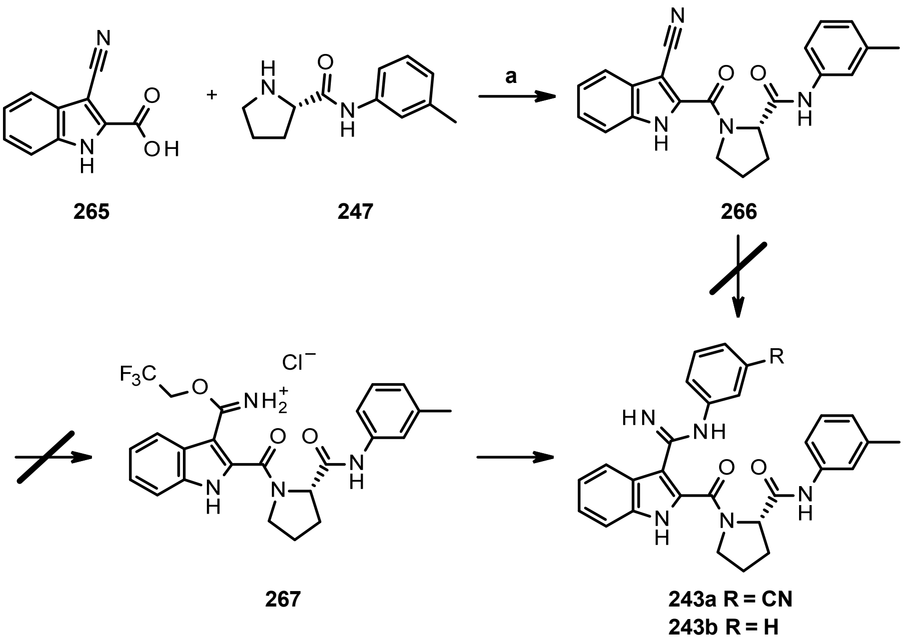

*Scheme 40: Unsuccessful synthesis of amidine **243a**. Reaction conditions: (a) EDC hydrochloride, DMAP, DCM, 0 °C → r.t., 3 h, 65%.*

As both methods were unsuccessful, the precursor nitrile **263** was used instead and reacted with aniline in the presence of sodium hydride to afford the corresponding amidine **268** (Scheme 41). Again, no product was obtained even after 5 days.

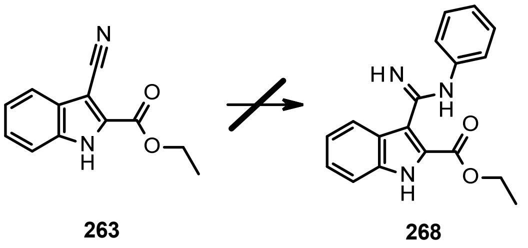

*Scheme 41: Unsuccessful test reaction to convert the precursor nitrile **263** into the corresponding amidine **268**.*

A more indirect method uses the imidate hydrochloride **267** as an intermediate (Scheme 40). This compound can be prepared from the corresponding nitrile **266** via the Pinner reaction. This was conducted with trifluoroethanol in DCM and HCl gas, which was bubbled through the reaction mixture.[182] Again, no product was obtained. The reaction was repeated in neat freshly dried trifluoroethanol. Unfortunately, no product could be detected in the LC-MS measurement.

As the synthesis of amidine **243a** could not be accomplished, the critical amidine functionality was again replaced by an amide group (Scheme 42). To avoid racemisation of proline derivative **266**, milder reaction conditions described by Güven and Jones[183] were applied. Instead of strong bases such as sodium hydroxide, sodium hydrogencarbonate was used to convert indole-3-carbonitriles into the corresponding carboxylic acids. Unfortunately, refluxing nitrile **266** in a concentrated aqueous solution of sodium hydrogencarbonate did not give product **269**. Instead, the starting material was reisolated.

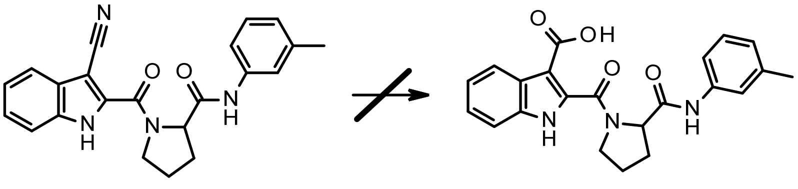

*Scheme 42: Attempted conversion of nitrile **266** to the free acid **269** to be coupled with 3-aminobenzonitrile to afford the triamide derivative of amidine **243a**.*

As the hydrolysis of nitrile **266** turned out to be difficult, an alternative route starting from 2-indolecarboxylic acid was studied. Ethyl 1*H*-indole-2-carboxylate (**262**) was converted into the corresponding indole-3-carbaldehyde (**270**) via Vilsmeier-Haack reaction in quantitative yield (Scheme 43).[184]

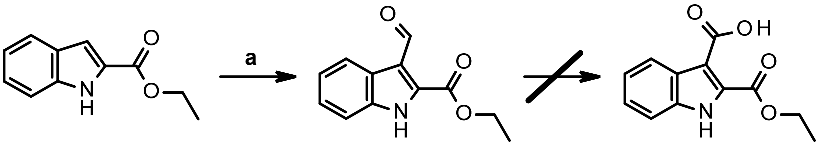

*Scheme 43: Synthesis of indole-3-carboxylic acid **271** via oxidation of the aldehyde **270**, which is easily available through Vilsmeier-Haack reaction. Reaction conditions: (a) $POCl_3$, DMF, r.t. → 70 °C, 21 h, quantitative yield.*

Oxidation of aldehyde **270** to carboxylic acid **271** was first conducted with sulfamic acid and sodium chlorite in a mixture of water/*tert*-butanol (1:1).[185] As no product was obtained, an alternative procedure using potassium permanganate in a mixture of acetone and water was used.[186,187] This gave the desired carboxylic acid **271** in a highly impure form. This route was discontinued as the focus of the project changed due to novel results.

Nonetheless, the intermediate products **247** and **266** were investigated. Unfortunately, neither amine **247** nor nitrile **266** showed any significant shifts in NMR experiments with the MIA protein. These results underline the significance of the tetrahydroisoquinoline moiety of compound **24** regarding structure-activity relationships.

4.6.3. Comprehensive screening of the ZINC database for basic compounds

As described before, the ZINC molecules **24** and **25** were identified from a screening of 5000 molecules, which arose from a restricted search of the ZINC database.[95] All attempts to improve the binding affinity of those two molecules were unsuccessful as described in the previous chapters. Nonetheless, valuable structure-activity relationship data regarding the binding pocket of the protein were collected in the process. Thus, a comprehensive screening of the ZINC database[94], which provides more than 35 million structures, for basic compounds was performed. A structural similarity search with phenylamidine restricting the answer set to molecules with a molecular weight lower than 700 g/mol was conducted. The answer set of about 11 thousand molecules as well as the protein were carefully prepared prior to running a Glide *in silico* screening in standard precision mode. The top one thousand compounds were submitted for a second Glide screening in the extra precision mode. The 50 structures with the highest scores were grouped in three clusters (Figure 97). Compounds, which fill the whole binding pocket were summarized in cluster 1. Typical representatives include ZINC44656532 (**272**), ZINC02526442 (**273**), ZINC50234216 (**274**) and ZINC03129785 (**276**). Compounds belonging to cluster 2 only occupy the right half of the ligand binding pocket and reach either up or down to interact with the surface surrounding the binding pocket. This cluster only contains the four molecules ZINC17861543 (**275**), ZINC70672769 (**279**), ZINC02272707 (**284**) and ZINC66255575 (**287**).
In contrast to cluster 2, cluster 3 contains compounds, which solely occupy the right half of the binding pocket. This cluster contains the majority (25) of compounds. Representative examples include ZINC38532835 (**282**), ZINC67943174 (**283**), ZINC64961003 (**285**) or ZINC64961014 (**286**). Additionally, seven smaller compounds (e.g. ZINC77034386 (**277**), ZINC72261965 (**278**), ZINC14807609 (**280**) and ZINC72261924 (**281**)) showed attractive Glide scores.

The scores of the ZINC molecules shown in Figure 99 significantly exceed the values obtained for any other compounds screened so far. Most remarkably, all compounds with a top score contain an *ortho*-hydroxyphenyl imine. The phenyl ring of the imine structure can also carry a second hydroxy group, a protected hydroxy group or may be annulated with another phenyl ring. ZINC44656532 (**272**) with an impressive Glide score of -8.90 was purchased. According to the prediction shown in Figure 98, the molecule can form four hydrogen bonds (Lys10, Asp100, Asp103 and Tyr105).

ZINC77034386 (**277**) was not chosen for synthesis as it contains an amidine group. As an exemplary compound with a high score but lacking the potentially labile imine moiety, ZINC72261965 (**278**, Figure 98) was selected for synthesis. This compound is predicted to interact with the protein via two hydrogen bonds to Asp103 and Tyr105.

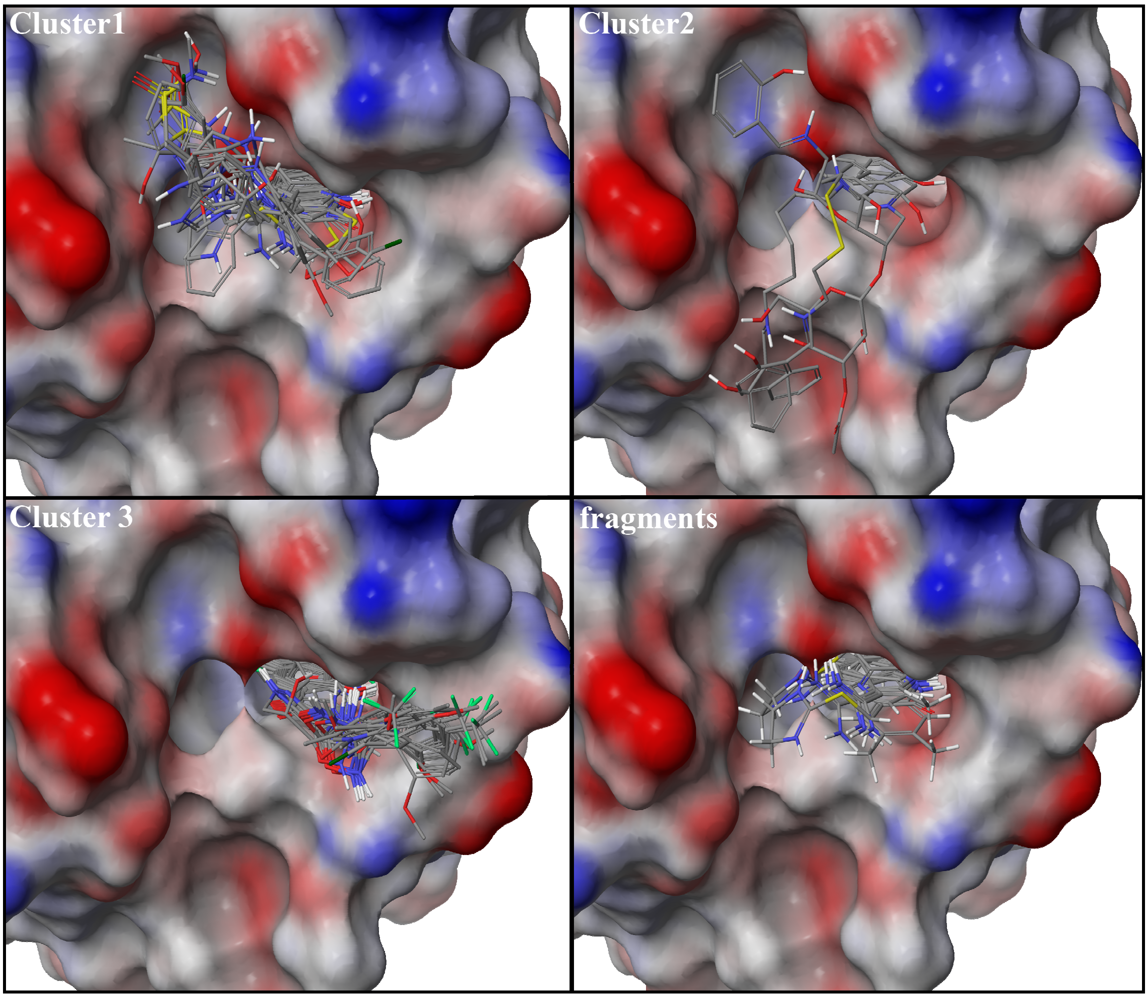

Figure 97: The 50 structures with the highest scores of the second Glide screening were grouped in three clusters. Compounds, which are significantly smaller than the others, were separately grouped as "fragments". The electrostatic potential of the surface of the MIA protein is shown.

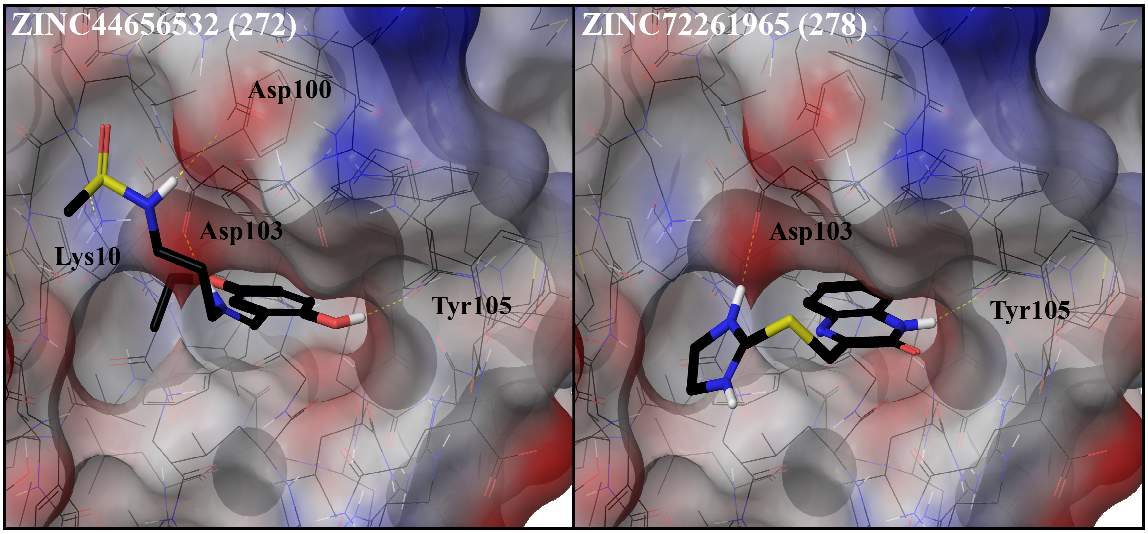

*Figure 98: Preferred conformation of the ZINC molecules **272** and **278** in the binding cleft of the MIA protein.*

Cluster 1

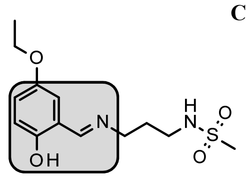
ZINC44656532 (**272**)

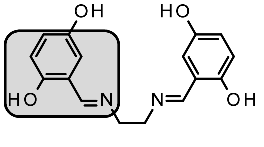
ZINC02526442 (**273**)

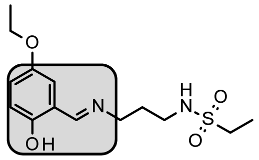
ZINC50234216 (**274**)

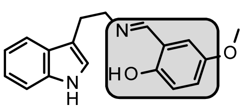
ZINC03129785 (**276**)

Cluster 2

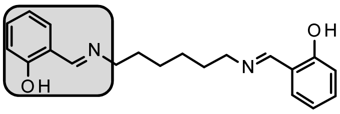
ZINC17861543 (**275**)

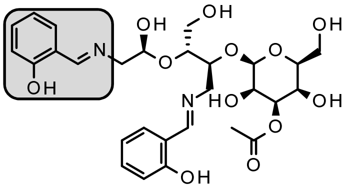
ZINC70672769 (**279**)

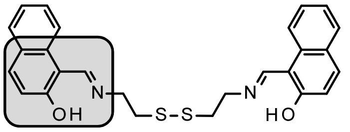
ZINC02272707 (**284**)

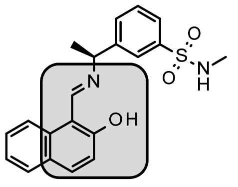
ZINC66255575 (**287**)

Cluster 3

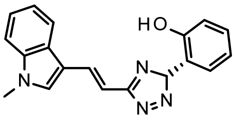
ZINC38532835 (**282**)

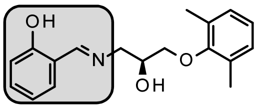
ZINC67943174 (**283**)

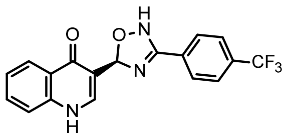
ZINC64961003 (**285**)

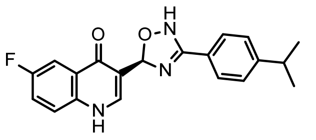
ZINC64961014 (**286**)

Fragments

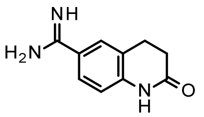
ZINC77034386 (**277**)

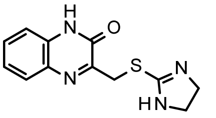
ZINC72261965 (**278**)

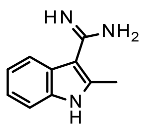
ZINC14807609 (**280**)

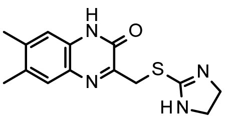
ZINC72261924 (**281**)

#	Molecule	Glide Score
1	ZINC44656532 (**272**)	-8.90
2	ZINC02526442 (**273**)	-8.68
3	ZINC50234216 (**274**)	-8.60
4	ZINC17861543 (**275**)	-8.27
5	ZINC03129785 (**276**)	-8.24
6	ZINC77034386 (**277**)	-7.79
7	ZINC72261965 (**278**)	-7.64
8	ZINC70672769 (**279**)	-7.63
9	ZINC14807609 (**280**)	-7.59
10	ZINC72261924 (**281**)	-7.48
11	ZINC38532835 (**282**)	-7.48
15	ZINC67943174 (**283**)	-7.43
17	ZINC02272707 (**284**)	-7.31
18	ZINC64961003 (**285**)	-7.28
20	ZINC64961014 (**286**)	-7.26
29	ZINC66255575 (**287**)	-7.17

Figure 99. Left: Overview of exemplary structures contained in the clusters 1-3 and some examples of fragments found to bind to the MIA protein. Right: Glide scores of the depicted molecules. Highlighted on both sides are the molecules carrying a phenylimine motif.

Retrosynthetically, ZINC molecule **278** was disassembled to the bromide precursor molecule **289**, which can be coupled with 2-imidazolidinethione (Scheme 44). Building block **289** was synthesized from phenylenediamine **288** and ethyl 3-bromopyruvat following the method described by Blunt *et al.*[188] After chromatographic separation of the crude mixture, no product was found. Alternatively, with 3-bromopyruvic acid as starting material[189], product **289** was obtained in moderate yield of 42% after chromatographic purification followed by recrystallization. Substitution of the bromide with 2-imidazolidinethione under basic conditions[190] failed. Coupling under neutral conditions in ethanol as described by Světlik *et al.* as well as Kawaguchi and coworkers[191,192] gave lactame **278** after silica gel chromatography followed by purification via HPLC on RP18 silica gel in 33%. The desired product **278** was obtained in 14% yield over two steps.

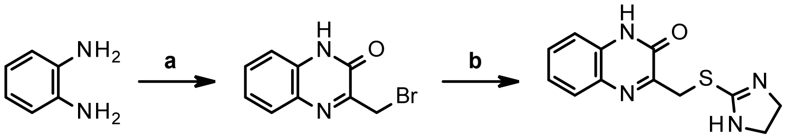

288 **289** **278**

*Scheme 44: Successful synthesis of ZINC72261965 (**278**) via a two-step procedure. Reaction conditions: (a) THF, r.t., 1 h, 42%, (b) 2-imidazolidinethione, ethanol, 85 °C, 22 h, 33%.*

ZINC44656532 (**272**) and ZINC72261965 (**278**) were analysed for their interaction with the MIA protein by NMR. Unfortunately, ZINC72261965 (**278**) precipitated from the aqueous buffer solution. Thus, no interaction with the protein was observed.

In contrast, addition of ZINC44656532 (**272**) to the labeled protein evoked drastic shifts of nearly all peaks of the protein. The original peaks for Met32 and Ala33 disappear with increasing ligand concentration. At the same time, a new set of peaks increase in intensity. Assignment of the peaks is impossible due to the complexity of the resulting spectrum, which will therefore not be depicted here. Nevertheless, the impressive shifts clearly indicate a strong binding of imine **272**. This is underlined by the fact that a 20-fold excess of ligand results in saturation of the protein indicated by only one set of peaks.[103] This result is in accordance with the *in silico* screening, which predicted a strong interaction of the ligand with the MIA protein.

Further experiments to evaluate the strength and binding mode of the ZINC molecule **272** are currently underway.

5. Conclusion

5.1. Improving the binding affinity of 4,4’-biphenol (22) to the Rheb protein

Starting from 4,4’-biphenol (**22**, 1.54 ± 0.23 mM), development of an improved ligand for the Rheb protein was successfully carried out following the “fragment growth” approach. As described before, additional substituents were added to the core structure of 4,4’-biphenol (**22**) to add further possible interaction points with the protein. An overview of the compounds tested during the iterative process is given in Figure 100.

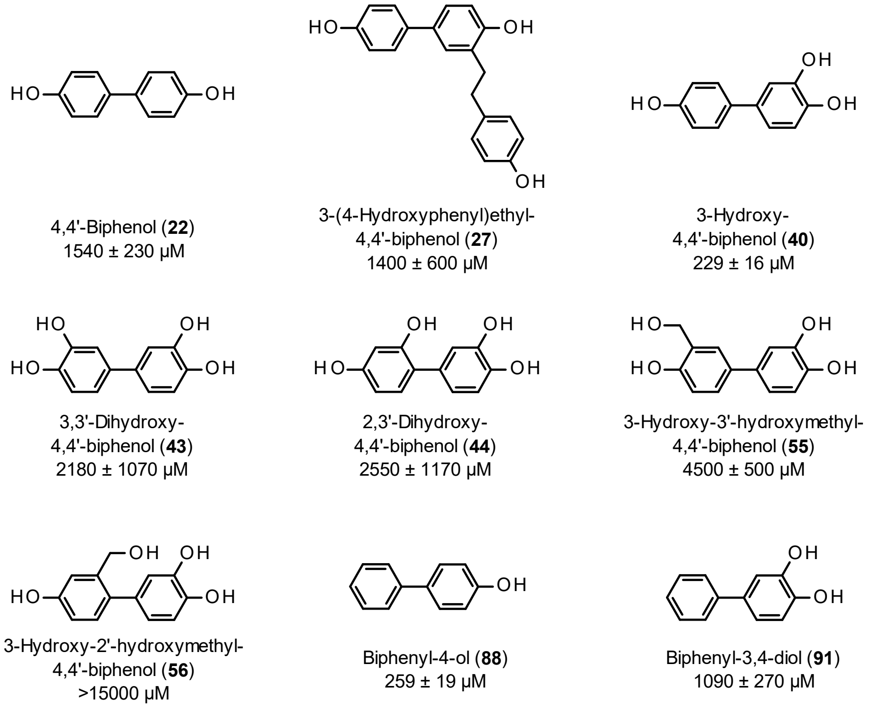

4,4'-Biphenol (**22**)
1540 ± 230 µM

3-(4-Hydroxyphenyl)ethyl-
4,4'-biphenol (**27**)
1400 ± 600 µM

3-Hydroxy-
4,4'-biphenol (**40**)
229 ± 16 µM

3,3'-Dihydroxy-
4,4'-biphenol (**43**)
2180 ± 1070 µM

2,3'-Dihydroxy-
4,4'-biphenol (**44**)
2550 ± 1170 µM

3-Hydroxy-3'-hydroxymethyl-
4,4'-biphenol (**55**)
4500 ± 500 µM

3-Hydroxy-2'-hydroxymethyl-
4,4'-biphenol (**56**)
>15000 µM

Biphenyl-4-ol (**88**)
259 ± 19 µM

Biphenyl-3,4-diol (**91**)
1090 ± 270 µM

*Figure 100: Overview of compounds commercially obtained or synthesized in the iterative process of improving the binding affinity of 4,4-biphenol (**22**) as the lead structure.*

From the weak k_D values of compounds such as phenols **27**, **55** and **56**, it was concluded that more sterically demanding groups attached to the biphenol core are not tolerated by the Rheb protein. Addition of more than one further hydroxy group either in *ortho*- or *meta*-position is also not tolerated as can be seen from compounds **43** and **44**. In contrast, direct attachment of an additional hydroxy groups led to a 6-fold improvement of the binding affinity (phenol **40**). The removal of a hydroxy groups increases the binding affinity while decreasing its sensitivity to oxidation as the result of biphenyl-4-ol (**88**) underlines.

All in all, improvement of the binding affinity of 4,4'-biphenol (**22**) was successfully achieved during the iterative cycles. With regard to the ligand efficiency of the two best molecules, 3-hydroxy-4,4'-biphenol (**40**) and biphenyl-4-ol (**88**), it can be concluded that biphenyl-4-ol (**88**) constitutes the best ligand for Rheb at the moment although it is slightly less affine than 3-hydroxy-4,4'-biphenol (**40**). Summing up all results, the two best ligands for the Rheb protein exhibit a k_D value that is approximately 6 times stronger than that of the originally found hit structure 4,4'-biphenol (**22**).

5.2. Examination of the structure-activity-relationship of Bisphenol A (23) as hit structure for the *K*-Ras protein

During preliminary studies, Bisphenol A (**23**, 600 ± 200 µM) was identified as a weak ligand for the *K*-Ras protein. The structure-activity-relationship of this molecule was examined systematically in the course of this thesis. An overview of the molecules synthesized or purchased and the corresponding k_D values are given in Figure 101.

As a first approach, the hydroxy groups of molecule **23** were derivatised. The esters **119a** and **119b** as well as the ethers **136a** and **136b** did not show any significant interaction with the protein. This result stresses the importance of the hydroxy groups, which form hydrogen bonds to the protein. In addition, the fragments **137** and **138**, which weakly bind to the *K*-Ras protein, validate the significance of the second phenol ring. In a second attempt, both phenol groups were substituted for heteroaromatic rings. The resulting compound **151** is unable to interact with the protein. This result is contradictory to the finding of the indole based inhibitor molecule **94e** by Fesik and coworkers[73], which can penetrate the ligand binding pocket. The third moiety, the methyl groups, were used as an anchor group to attach additional building blocks according to the fragment growth approach. The first derivatives **160**, **170**, **172** and **173** showed no binding to the *K*-Ras protein. These results indicate that elongation of the methyl groups is not tolerated. This hypothesis is also supported by the results of the bisphenol A analogue **97**. A different attempt, fragment merging with the Fesik inhibitor **94e**, was then targeted in the next step. The sterically highly demanding analogue **179** did unfortunately not interact with the protein. Less sterically demanding derivatives **187** and a mixture of **204a** and **204b** exhibit a weak interaction with the protein. These results are promising, but need to be further evaluated by synthesizing the pure amide **204b**.

To sum up the findings, it can be said that the *K*-Ras protein does not tolerate changes to the hydroxy groups as well as the phenol groups of bisphenol A (**23**). Derivatisation of the methyl groups is only tolerated if the sterical demand of the resulting compound is reduced at the central carbon atom. Bisphenol A derivatives, which carry two hydroxy groups, such as **160** and **170** are promising building blocks for polymer synthesis. Other analogues as for example **119a** are particularly interesting as those compounds do not interact with the *K*-Ras protein. Hybrid molecules **187** and **204b** compose promising targets for the development of *K*-Ras4B inhibitors.

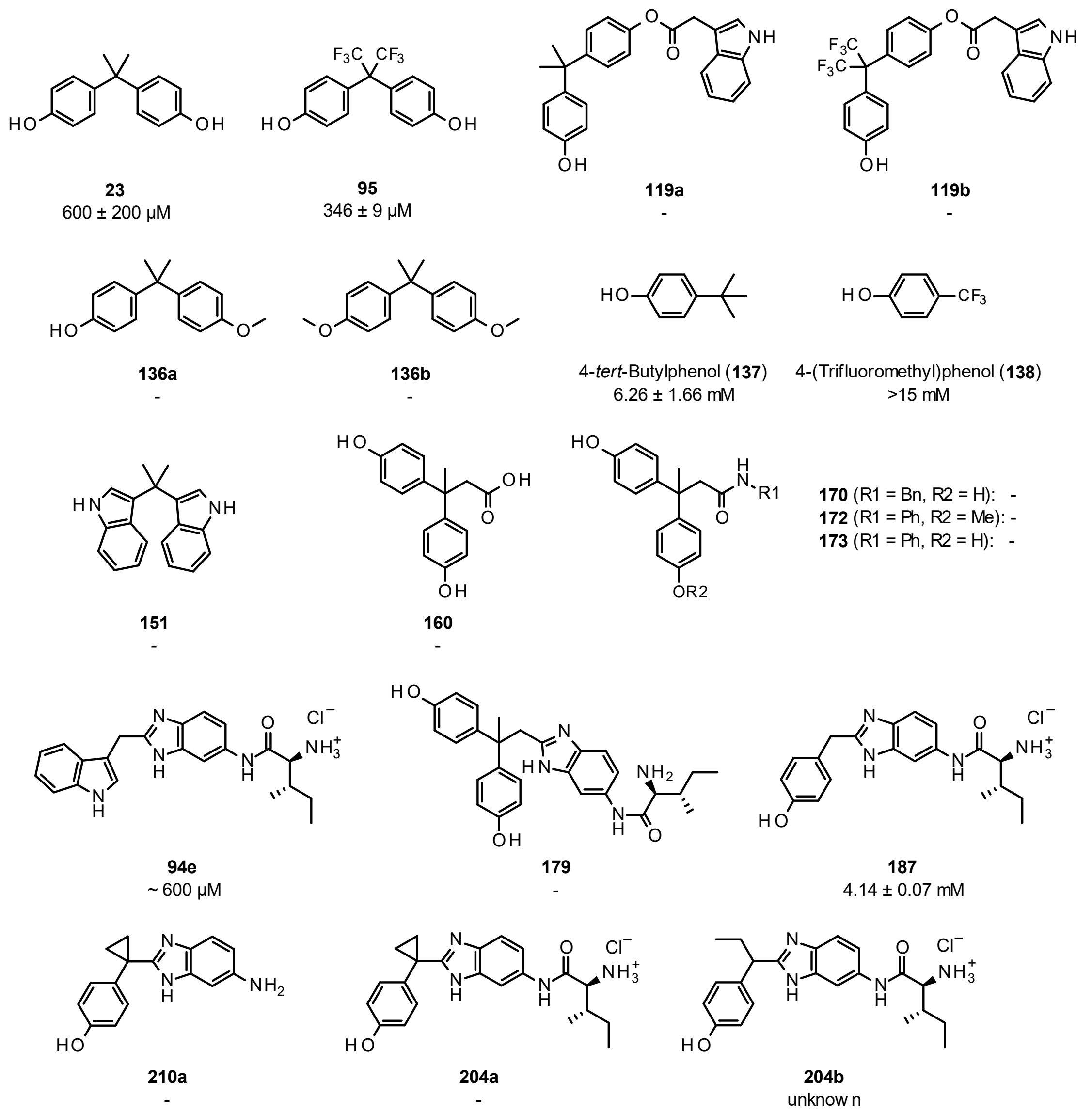

*Figure 101: Bisphenol A (**23**) and its analogues that were prepared and tested for their binding affinity to the K-Ras protein in the course of this thesis.*

5.3. Discovery of a novel small molecule ligand for the MIA protein

For MIA, two molecules (ZINC05203919 (**24**), ZINC01400183 (**25**), Figure 102) were found from a screening of the ZINC database to bind to the protein. It was shown that the methyl and nitrile substituent of amidine **25** are essential for ligand binding as the corresponding unsubstituted derivative **230** did not interact with the protein. Additionally, the amidine group is also necessary as the two amide derivatives **231** and **232** prove. Subsequently, fragment merging of amide **24** and amidine **25** was attempted as both compounds address the same binding pocket. None of the hybrid molecules could be synthesized. Unfortunately, none of the intermediates, which were examined, inflicted any significant shifts in the NMR measurement. As a new approach, a comprehensive search of the ZINC database for compounds incorporating an amidine-like structure was conducted. Subsequent investigation of the structures by molecular docking with Glide yielded ZINC44656532 (**272**) and ZINC72261965 (**278**) as the most promising candidates. In contrast to the thioamide **278**, which did not evoke any significant shifts in the NMR excess measurement, addition of imine **272** caused a new set of peaks for each of the amino acids of the MIA protein indicating a strong interaction. Further studies to evaluate the binding mode and strength of this compound need to be conducted.

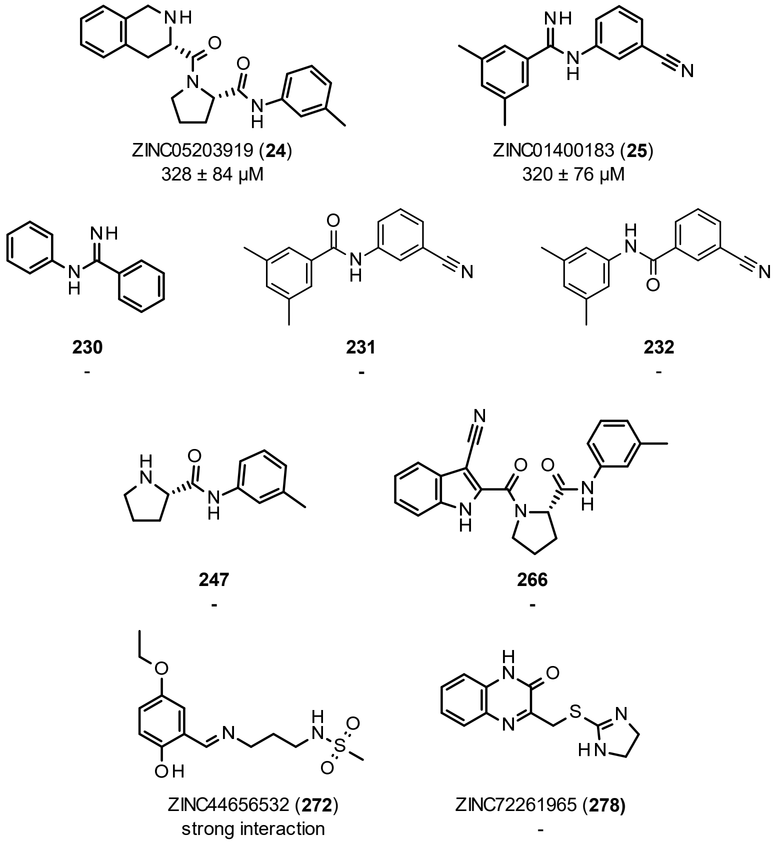
ZINC05203919 (**24**)
328 ± 84 µM

ZINC01400183 (**25**)
320 ± 76 µM

230
-

231
-

232
-

247
-

266
-

ZINC44656532 (**272**)
strong interaction

ZINC72261965 (**278**)
-

Figure 102: Compounds tested for their interaction with the MIA protein in the course of this thesis.

6. Experimental Section

General Part

Unless stated differently, all materials were purchased from commercial sources and used as received. All reactions were carried out under inert atmosphere (nitrogen or argon) using anhydrous solvents. Solvents including diethyl ether, THF and DCM were either dried using a solvent purification system (mBraun MB-SPS-800) or by chemical methods. THF and diethyl ether were freshly distilled from $LiAlH_4$. DCM, DMF, TEA, DIPEA, piperidine and pyridine were either distilled from CaH_2 or filtered through a short column of basic aluminum oxide. Methanol was distilled from magnesium after refluxing for several hours.

Microwave reactions were carried out on a CEM Discover Microwave.

Thin layer chromatography was performed on E. Merck silica gel 60 F_{254} aluminum backed plates and visualized under UV light or by staining with potassium permanganate solution or cerium molybdenum solution followed by heating. Column chromatography was performed using silica gel (Macherey Nagel silica gel 60, 0.04 - 0.063 nm).

HPLC-MS measurements were carried out on a Varian 500IonTrap (LC-ESI-MS, RP18, 5 µm) or Bruker MicrOTOF (LC-ESI-MS) on a C_{18}-column by MZ Analysentechnik (PerfectSil Target ODS-3 HD 5 µm, 100 · 4.6 mm). High resolution mass spectra were recorded using a Bruker MicrOTOF.

^1H and ^{13}C NMR spectra were measured using Bruker Avance 400 (^1H at 400.13 MHz, ^{13}C at 100.62 MHz) or Bruker Avance III 600 (^1H at 600.13 MHz, ^{13}C at 150.90 MHz) spectrometers. Chemical shifts are reported in ppm referenced to residual solvent signals. Spin multiplicity is quoted as follows: s (singlet), d (doublet), t (triplet), q (quartet), qui (quintet), dd (doublet from doublet), dt (doublett from triplet) and m (multiplet). Coupling constants are reported in Hz.

Protein preparation: 50 mL of LB medium containing 100 µg/mL ampicillin was inoculated with an aliquot of *E. coli* bacteria and grown overnight at 37 °C with vigorous shaking. The culture was then grown in 2 L of LB broth at 37 °C with vigorous shaking until an OD_{600} of 1.0 was reached. The cells were then harvested by centrifugation and the supernatant was removed. The cells were resuspended in M9 minimal medium containing ^{15}N-ammonium chloride. The cell culture was incubated at 30 °C for 1 h before inducing expression by addition of IPTG (isopropyl β-D-1-thiogalactopyranoside) to a final concentration of 1 mM. The culture was then vigorously shaken overnight. The cells were harvested by centrifugation and resuspended in a HEPES (2-[4-(2-hydroxyethyl)piperazin-1-yl]ethanesulfonic acid)/imidazole buffer. The mixture was repeatedly frozen and defrozen for lysis of the cells. Additionally, the cell/buffer suspension was applied to a Manton-Gaulin homogenizer for better cell lysis. The cells were harvested by centrifugation and the supernatant was collected. The lysate was applied to chromatography on Ni-NTA resin. The column was washed with a HEPES buffer containing 20 mM imidazole before eluting the protein with 220 mM imidazole. The collected fractions were applied to gel permeation chromatography to identify fractions containing the desired protein. The identified fractions were then collected and concentrated by centrifugation until a volume of 2.5 mL was reached. The purified protein was then rebuffered for NMR spectroscopy by a short column in 3.5 mL. By UV-measurement, a yield of 24 mg of the desired protein was determined. Finally, the solution was diluted, aliquoted and stored at -20 °C until use.

Molecular docking experiments with Autodock/VINA: To start a calculation with Autodock/VINA, the desired protein needs to be loaded either from the computer itself or from the protein data bank using the corresponding PDB ID. Then, starting the Autodock/VINA plugin, a grid needs to be defined comprising the designated ligand binding pocket of the protein. For higher comparability, the grid can be saved and used again for further dockings. In the next step, the receptor molecule, the protein, will be generated, followed by the ligands, which should not exceed a maximum number of 30 molecules for each docking run. Then, VINA can be launched docking all ligands prepared. In contrast, for Autodock runs, only a single ligand can be calculated in each docking run. Consequently, each ligand needs to be selected individually, followed by running “AutoGrid”, a program that pre-calculates grid maps of interaction energies of the atoms of the ligand with the protein. If Autogrid was successfully finished, the Autodock run itself can be started. When finishing either Autodock or VINA, the calculated poses need to be loaded and visualized in the “View Poses” tab. In the “Score/Rank” tab, the calculated scores for each of the 10 poses predicted for each ligand can be examined.

Molecular docking experiments with Glide: Similar to calculations with Autodock/VINA, the protein needs to be loaded and subsequently prepared using the “Protein Preparation Wizard”. In the tab “Import and Process”, no changes regarding the default settings need to be made before pressing “Preprocess”. After finishing, the next tab can be skipped proceeding directly to the “Refine” tab to “Optimize” and subsequently “Minimize” the protein with the corresponding force field, usually OPLS2005. In case that water atoms remain in the ligand binding pocket, those can be removed either manually or by using the “Remove Waters” function before minimizing the protein structure. After successfully preparing the protein, the ligands need to be initialized, too. Therefore, the ligands are imported into the Project Table and for reasons of clarity, should be moved to a new group. Then, the ligands are selected and the “LigPrep” tool can be started. The structures to be included can be taken from the Project Table. For the ionization step, physiological properties (pH 7 ± 1) should be chosen. Also, regarding the computation of stereoisomers of the ligand, if dedicated enantiomers were defined before, the “Determine chiralities from 3D structure” option should be selected. Otherwise, the default option can be kept. For ligands incorporating numerous aromatic rings, the number of “low energy ring conformations” generated should be increased to 10 per ligand. After selecting “Append new entries as a new group” for the output, the calculation can be started. After the job has finished, a grid has to be defined. In contrast to Autodock/VINA, the grid can be automatically calculated if a protein structure incorporating a ligand is given. Therefore, the Glide “Receptor Grid Generation” tools needs a ligand to be selected from the protein structure. Otherwise, the grid has to be defined manually. Usually, no changes to the default settings are made to the following tabs of this subprogram, thus, the calculation can be launched. When finishing, all precalculated files will be used by the application “Glide Ligand Docking”. In the tab “Settings”, the grid previously computed needs to be loaded followed by designating the desired effort and accuracy of the calculation by choosing between HTVS (high-throughput virtual screening), an option used for ligand amounts greater than 1000, SP (standard precision), usually used for first time dockings of moderate amounts (50-100) of ligands, and XP (extra precision), the highest precision available, which is typically used when calculating a small number of ligands to choose from for synthesis. In the ligands tab, the previously primed ligands need to be defined. By default, ligands will be used from a file, but instead, “Project Table” should be selected. The following tabs can be usually skipped proceeding directly to the “Output” tab, increasing the maximum number of poses written to 10 and the “Number of poses per ligand to include” to 50. Additionally, the accuracy of the minimization can be increased by raising the threshold to 0.05 kcal/mol, an option that is only available in the extra precision mode. Afterwards, the calculation can be started. The predicted structures of each protein-ligand complex will be incorporated into the Project Table including the calculated docking scores. There, the ligands can be sorted either according to their names to find all poses for each ligand or by the computed Glide score as by default to find the best ligand.

NMR titration/excess measurements: To perform protein binding studies, uniformly ^{15}N-enriched protein samples with a usual concentration of 0.1 M to 0.3 M were used. The standard procedure comprises measurement of a reference ^{1}H,^{15}N-HSQC spectrum of the protein itself to ensure correct folding of the protein. Then, typically, an excess of the desired ligand (usually up to 25-fold) is added to the protein. As compounds can influence the pH value of the aqueous buffer solution, which can affect the protein peaks, the pH needs to be readjusted before observing the changes in chemical shifts and line widths of the backbone amide resonances in a ^{1}H,^{15}N-HSQC spectrum. In case that the ligands evoke significant shifts to the peaks of the protein, whereafter a titration experiment is usually performed. The assignments of peaks for the three proteins examined here were obtained from the literature. Quantitative analysis of ligand-induced chemical shift perturbation was performed by applying Pythagoras' equation to the weighted chemical shifts. From the resulting data, k_D values can be calculated using the appropriate amino acid peaks.[193–195]

6.1. Synthesis of ligands to bind to the Rheb protein

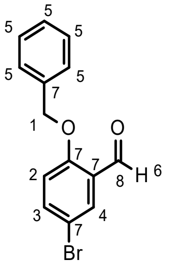

2-Benzyloxy-5-bromobenzyldehyde (AUJ-066, 31): 5-Bromosalicylaldehyde (**30,** 1.01 g, 5.00 mmol, 1.0 equiv.) and potassium carbonate (2.63 g, 18.99 mmol, 3.8 equiv.) were dissolved in dry DMF (7 mL). To this solution, benzyl bromide (720 µL, 6.06 mmol, 1.2 equiv.) was added and the resulting mixture was stirred at room temperature for 21 h. After that time, the reaction mixture was poured into distilled water upon which a colorless precipitate was formed. The solids were collected, washed with water and dried *in vacuo* to yield 2-benzyloxy-5-bromobenzyldehyde (1.42 g, 4.87 mmol, 97%) as a colorless solid: ^{1}H NMR (600 MHz, $CDCl_3$): **δ** 5.21 (s, 2H, H-1), 6.98 (d, *J* = 9.04 Hz, 1H, H-2), 7.39-7.45 (m, 5H, H-5), 7.63 (dd, *J* = 8.91 Hz, *J* = 2.61 Hz, 1H, H-3), 7.97 (d, *J* = 2.60 Hz, 1H, H-4), 10.49 (s, 1H, H-6). ^{13}C NMR (150 MHz, $CDCl_3$): **δ** 70.9 (C-1), 113.8 (C-7), 115.2 (C-2), 126.5 (C-7), 127.3 (C-5), 128.5 (C-5), 128.8 (C-5), 131.0 (C-4), 135.5 (C-7), 138.2 (C-3), 159.9 (C-7), 188.2 (C-8). LC-MS *m/z* (% relative intensity): 313.0 $[M(Br^{79})+Na]^+$ (100), 315.0 $[M(Br^{81})+Na]^+$ (100). HR-ESI-MS (*m/z*): calcd for $C_{14}H_{11}BrNaO_2$, 312.9835 and 314.9821 found, 312.9835 and 314.9815. IR (neat) $\tilde{v}_{max}$ (cm^{-1}): 1677 (C=O). r_f 0.08 (CH).

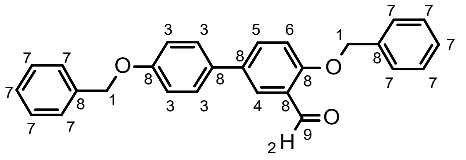

2-Benzyloxy-5-(4-benzyloxyphenyl)benzaldehyde (AUJ-070, 32): Sodium carbonate (1.53 g, 14.46 mmol, 4.0 equiv.) in degassed water (7 mL) was added to a solution of 2-benzyloxy-5-bromobenzyldehyde (**AUJ-066, 31**, 1.04 g, 3.57 mmol, 1.0 equiv.), 4-benzyloxyphenylboronic acid (1.00 g, 5.04 mmol, 1.4 equiv.), tetrakis(triphenylphosphine)palladium(0) (199.8 mg, 0.17 mmol, 0.05 equiv.) and lithium chloride (462.0 mg, 10.90 mmol, 3.0 equiv.) in degassed dimethoxyethane (30 mL). The resulting mixture was stirred at 80 °C for 23 h. The suspension was then filtered and the filtrate was diluted with water (10 mL) and diethyl ether (10 mL). The aqueous layer was extracted with diethyl ether (2 x 10 mL). The combined organic layers were washed with brine, dried over Na_2SO_4 and concentrated *in vacuo*. The crude product (1.83 g) was purified by column chromatography (CH:EtOAc 19:1) to afford pure 2-benzyloxy-5-(4-benzyloxyphenyl)benzaldehyde (933.4 mg, 2.37 mmol, 66%) as a colorless solid: ^{1}H NMR

(600 MHz, CDCl$_3$): **δ** 5.14 (S, 2H, H-1), 5.26 (s, 2H, H-1), 7.08 (m, 2H, H-3), 7.13 (d, *J* = 8.70 Hz, 1H, H-6), 7.37-7.47 (m, 6H, H-7), 7.50 (m, 4H, H-7), 7.54 (m, 2H, H-3), 7.75 (dd, *J* = 8.70 Hz, *J* = 2.52 Hz, 1H, H-5), 8.10 (d, *J* = 2.52 Hz, 1H, H-4), 10.65 (s, 1H, H-2). ^{13}C NMR (150 MHz, CDCl$_3$): **δ** 70.1 (C-1), 70.7 (C-1), 113.5 (C-6), 115.3 (C-3), 125.3 (C-8), 126.1 (C-4), 127.3 (C-7), 127.4 (C-7), 127.7 (C-3), 128.0 (C-7), 128.3 (C-7), 128.6 (C-7), 128.7 (C-7), 132.2 (C-8), 133.8 (C-5), 136.1 (C-8), 136.9 (C-8), 158.4 (C-8), 160.0 (C-8), 189.6 (C-2). LC-MS *m/z* (% relative intensity): 395.2 [M+H]$^+$ (100). HR-ESI-MS (*m/z*): calcd for $C_{27}H_{22}NaO_3$, 417.1461 found, 417.1461. IR (neat) $\tilde{\nu}_{max}$ (cm^{-1}): 1676 (C=O). r$_f$ 0.30 (CH:EtOAc 9:1).

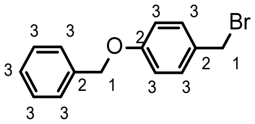

1-Benzyloxy-4-(bromomethyl)benzene (AUJ-076, 34): To a solution of 4-benzyloxybenzylalcohol (**33**, 306.0 mg, 1.43 mmol, 1.0 equiv.) in DCM (10 mL) at 0 °C was added phosphorus tribromide (140.0 µL, 1.49 mmol, 1.04 equiv.). The mixture was kept in the dark with aluminum foil around the flask. The mixture was stirred for 60 min at 0 °C and then further 60 min at room temperature. The solution was then poured on ice, extracted with diethyl ether (3 x 20 mL) and the combined organic layers were dried over Na_2SO_4. After evaporation of the solvent 1-benzyloxy-4-(bromomethyl)benzene (388.0 mg, 1.40 mmol, 98%) was obtained as a colorless solid. The compound is very unstable (decomposition within several hours) and was used for the next reaction immediately without further purification: ^{1}H NMR (400 MHz, CDCl$_3$): **δ** 4.54 (s, 2H, H-1), 5.11 (s, 2H, H-1), 6.99 (m, 2H, H-3), 7.42 (m, 7H, H-3). ^{13}C NMR (100 MHz, CDCl$_3$): **δ** 33.8 (C-1), 70.0 (C-1), 115.1 (C-3), 127.4 (C-3), 128.0 (C-3), 128.6 (C-3), 130.2 (C-2), 130.4 (C-3), 136.7 (C-2), 158.8 (C-2). LC-MS *m/z* (% relative intensity): 197.0833 [M-Br]$^+$ (35). r$_f$ 0.63 (CH:EtOAc 7:3).

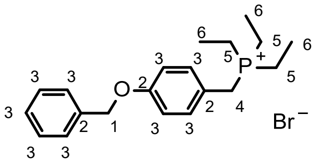

(4-Benzyloxyphenyl)methyl(triethyl)phosphonium bromide (AUJ-078, 35): A solution of 1-benzyloxy-4-(bromomethyl)benzene (**AUJ-076**, **34**, 375.6 mg, 1.36 mmol, 1.0 equiv.) in DCM (3.0 mL) was cooled to 0 °C. To this 10% triethylphosphine in hexane (1.65 g, 1.39 mmol. 1.03 equiv.) were added and the mixture was stirred for 17.5h at room temperature. The solvent was then evaporated and the residue was dried under high vacuum yielding (4-benzyloxyphenyl)methyl(triethyl)phosphonium bromide (534.0 mg, 1.35 mmol, 100%) as a colorless solid: ^{1}H NMR (600 MHz, CDCl$_3$): **δ** 1.17 (dt, *J* = 7.85 Hz, *J* = 17.54 Hz, 9H, H-6), 2.42 (m, 6H, H-5), 4.13 (d, *J* = 14.63 Hz, 2H, H-4), 4.97 (s, 2H, H-1), 6.89 (m, 2H, H-3), 7.32 (m, 7H, H-3). ^{13}C NMR (150 MHz, $CDCl_3$): **δ** 5.8 (d, C-6), 11.8 (d, C-5), 25.0 (d, C-4), 69.9 (C-1), 115.6 (C-3), 119.9 (C-2), 127.3 (C-3), 127.9 (C-3), 128.4 (C-3), 131.2 (d, C-3), 136.3 (C-2), 158.6 (d, C-2). LC-MS *m/z* (% relative intensity): 315.1714 $[M-Br^-]^+$ (100). HR-ESI-MS (*m/z*): calcd for $C_{20}H_{28}OP$, 315.1872 found, 315.1870. IR (neat) $\tilde{\nu}_{max}$ (cm^{-1}): 2920, 2893 (P-CH2).

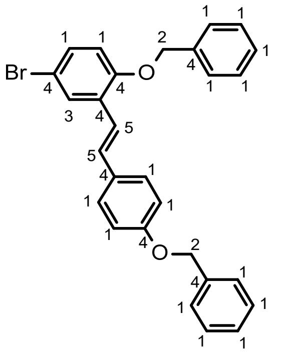

1-Benzyloxy-2-[(E/Z)-2-(4-benzyloxyphenyl)vinyl]-4-bromo-benzene (AUJ-096, 39): A solution of (4-benzyloxyphenyl)methyl (triethyl)phosphonium bromide (**AUJ-078**, **35**, 541 mg, 1.37 mmol, 1.1 equiv.) in degassed water (5 mL) was stirred for 15 min at room temperature. Then, sodium hydroxide (224 mg, 5.60 mmol, 4.5 equiv.) was added slowly and after stirring for 5 min 2-benzyloxy-5-bromobenzyldehyde (**AUJ-066**, **31**, 366 mg, 1.26 mmol, 1.0 equiv.) was added. The reaction mixture was then heated to 70 °C under vigorous stirring for 6 h. The resulting suspension was cooled in an ice bath and the residue was collected by vacuum filtration and then dried under high vacuum to yield 1-benzyloxy-2-[(E/Z)-2-(4-benzyloxyphenyl)vinyl]-4-bromo-benzene (576 mg, 1.22 mmol, 97%) as an off-white solid: ^{1}H NMR (400 MHz, $CDCl_3$): **δ** 5.12 (s, 2H, H-2), 5.15 (s, 2H, H-2), 6.83 (d, *J* = 8.76 Hz, 1H, H-1), 7.00 (m, 2H, H-1), 7.11 (d, *J* = 16.44 Hz, 1H, H-5), 7.28 (m, 1H, H-1), 7.33 (d, *J* = 16.37 Hz, 1H, H-5), 7.37-7.50 (m, 12H, H-1), 7.73 (d, *J* = 2.4 Hz, 1H, H-3). ^{13}C NMR (100 MHz, $CDCl_3$): **δ** 70.0 (C-2), 70.1 (C-2), 113.7 (C-4), 114.4 (C-1), 115.1 (C-1), 120.1 (C-5), 127.2 (C-1), 127.4 (C-1), 127.9 (C-1), 128.0 (C-1), 128.0 (C-1), 128.6 (C-1), 128.6 (C-1), 128.9 (C-3), 130.0 (C-5), 130.4 (C-1), 130.5 (C-1), 136.7 (C-4), 136.9 (C-4), 154.9 (C-4), 158.6 (C-4). LC-MS *m/z* (% relative intensity): 471.1 $[M(^{79}Br)+H]^+$ (74), 473.1 $[M(^{81}Br)+H]^+$ (80), 488.1 $[M(^{79}Br)+NH_4]^+$ (99), 490.1 $[M(^{81}Br)+NH_4]^+$ (100). HR-ESI-MS (*m/z*): calcd for $C_{28}H_{23}BrNaO_2$, 493.0774 and 495.0757 found, 493.0758 and 495.0757. IR (neat) $\tilde{\nu}_{max}$ (cm^{-1}): 2920, 2865 (C-H$_{arom.}$). r_f 0.45 (CH:EtOAc 9:1).

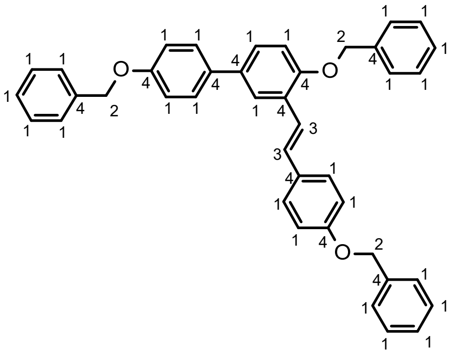

1-Benzyloxy-4-(4-benzyloxyphenyl)-2-[(E)-2-(4-benzyloxyphenyl)vinyl]benzene (AUJ-079, 36): To a solution of sodium carbonate (195.0 mg, 1.84 mmol, 4.1 equiv.) in degassed water (0.7 mL) was added a solution of 1-benzyloxy-2-[(E/Z)-2-(4-benzyloxyphenyl)vinyl]-4-bromo-benzene (**AUJ-096**, **39**, 210.0 mg, 0.45 mmol, 1.0 equiv.) 4-benzyloxyphenylboronic acid (142.5 mg, 0.62 mmol, 1.4 equiv.), tetrakis(triphenylphosphine)palladium(0) (33.6 mg, 0.03 mmol, 0.07 equiv.) and lithium chloride (72.7 mg, 1.71 mmol, 3.8 equiv.) in dimethoxyethane (3 mL). The mixture was stirred at 80 °C for 19 h. After cooling to room temperature, the suspension was filtered and the filtrate was diluted with water (10 mL) and EtOAc (20 mL). The phases were separated and the aqueous layer was extracted with EtOAc (3 x 20 mL). The combined organic layers were washed with brine, dried over Na_2SO_4 and evaporated to dryness. The crude product (236 mg) was purified by column chromatography (CH:DCM 9:1 → 1:1 → 100% DCM) to afford 1-benzyloxy-4-(4-benzyloxyphenyl)-2-[(E)-2-(4-benzyloxyphenyl)vinyl]benzene (113.2 mg, 0.20 mmol, 44%) as an off-white solid: ^{1}H NMR (400 MHz, $CDCl_3$): **δ** 5.21 (s, 2H, H-2), 5.14 (s, 2H, H-2), 5.21 (s, 2H, H-2), 7.00 (m, 3H, H-1), 7.08 (m, 2H, H-1), 7.19 (d, *J* = 16.48 Hz, 1H, H-3), 7.33-7.59 (m, 22H, H-1, H-3), 7.78 (m, 1H, H-1). ^{13}C NMR (150 MHz, $CDCl_3$): **δ** 70.0 (C-2), 70.1 (C-2), 70.7 (C-2), 113.1 (C-) 115.1 (C-1), 115.2 (C-1), 121.6 (C-4), 124.8 (C-4), 127.3 (C-1), 127.5 (C-1), 127.8 (C-1), 127.9 (C-1), 128.0 (C-1), 128.6 (C-1), 129.0 (C-3), 131.0 (C-4). LC-MS *m/z* (% relative intensity): 592.3 $[M+NH_4]^+$ (100). HR-ESI-MS (*m/z*): calcd for $C_{41}H_{34}NaO_3$, 597.2400 found, 597.2401. IR (neat) $\tilde{v}_{max}$ (cm^{-1}): 2922, 2865 (C-H$_{arom.}$). r_f 0.46 (CH:EtOAc 9:1).

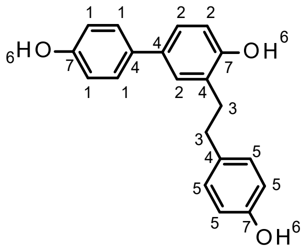

4-(4-Hydroxyphenyl)-2-[2-(4-hydroxyphenyl)ethyl]phenol (AUJ-090, 27): A solution of 1-benzyloxy-4-(4-benzyloxyphenyl)-2-[(E)-2-(4-benzyloxyphenyl)vinyl]benzene (**AUJ-079**, **36**, 73.4 mg, 128 µmol, 1.0 equiv.) and 10% palladium on charcoal (14.0 mg, 13 µmol, 0.1 equiv.) in acetic acid (3 mL) was purged with hydrogen (3 x) and then stirred under 5.5 bar of hydrogen for 20 h at room temperature. The solvent was then removed under reduced pressure. The residue was suspended in methanol and filtered through a pad of silica gel which was washed extensively with EtOAc. The solvent was then removed and the crude product (87.1 mg) was subjected to column chromatography. 4-(4-Hydroxyphenyl)-2-[2-(4-hydroxyphenyl)ethyl]phenol (33.8 mg, 110 µmol, 86%) was obtained as a colorless solid: ^{1}H NMR (400 MHz, MeOD-D$_4$): **δ** 2.86 (m, 4H, H-3), 6.71 (m, 2H, H-5), 6.81 (m, 3H, H-1, H-2), 7.03 (m, 2H, H-5), 7.12 (m, 1H, H-2), 7.18 (m, 1H, H-2), 7.30 (m, 2H, H-1). ^{13}C NMR (100 MHz, MeOD-D$_4$): **δ** 33.8 (C-3), 36.2 (C-3), 115.7 (C-5), 116.0 (C-2), 116.2 (C-1), 125.7 (C-2), 128.3 (C-1), 129.3 (C-2), 129.4 (C-4), 130.3 (C-5), 133.5 (C-4), 134.0 (C-4), 134.5 (C-4), 154.8 (C-7), 155.8 (C-7), 156.7 (C-7). LC-MS *m/z* (% relative intensity): 305.2 [M-H]$^-$ (100). HR-ESI-MS (*m/z*): calcd for $C_{20}H_{17}O_3$, 305.1183 found, 305.1176. IR (neat) $\tilde{v}_{max}$ (cm^{-1}): 3497, 3424, 3359 (O-H). r$_f$ 0.31 (CH:EtOAc 2:1).

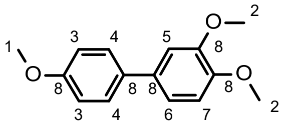

1,2-Dimethoxy-4-(4-methoxyphenyl)benzene (AUJ-068, 50): 4-Bromoanisole (**48**, 522.9 mg, 2.80 mmol. 1.0 equiv.), 3,4-dimethoxybenzeneboronic acid (**49**, 610.6 mg, 3.36 mmol, 1.2 equiv.), potassium carbonate (778.3 mg, 5.63 mmol, 2.0 equiv.), 10% palladium on charcoal (153.0 mg, 0.14 mmol, 0.05 equiv.) and 18-crown-6 (754.5 mg, 2.85 mmol, 1.0 equiv.) were suspended in 1:1 methanol/water (10 mL each) and heated to 45 °C for 1.5 h. The reaction mixture was then diluted with water (50 mL) and ethyl acetate (50 mL) and filtered. The filtrate was separated into two layers and the aqueous layer was extracted with ethyl acetate (2 x 50 mL). The combined organic layers were washed with brine, dried over Na_2SO_4 and concentrated *in vacuo*. The crude product (833.6 mg) was purified by column chromatography (CH) to afford 1,2-dimethoxy-4-(4-methoxyphenyl)benzene (498.6 mg, 2.04 mmol, 73%) as a colorless solid: ^{1}H NMR (600 MHz, CDCl$_3$): **δ** 3.88 (s, 3H, H-1), 3.95 (s, 3H, H-2), 3.98 (s, 3H, H-2) 6.96 (d, *J* = 8.28 Hz, 2H, H-7), 7.00 (m, 2H, H-4), 7.10 (d, *J* = 2.13 Hz, 1H, H-5), 7.12 (dd, *J* = 8.17, *J* = 2.16, 1H, H-6), 7.51 (m, 2H, H-3). ^{13}C NMR (150 MHz, CDCl$_3$): **δ** 55.3 (C-1), 55.9 (C-2), 56.0 (C-2), 110.3 (C-5), 111.6 (C-7), 114.2 (C-4), 118.9 (C-6), 127.8 (C-3), 133.7 (C-8), 134.0 (C-8), 148.2 (C-8), 149.2 (C-8), 158.8 (C-8). LC-MS *m/z* (% relative intensity): 245.1096 [M+H]$^+$ (100). HR-ESI-MS (*m/z*): calcd for $C_{15}H_{16}NaO_3$, 267.0992 found, 267.0984. IR (neat) $\tilde{v}_{max}$ (cm^{-1}): 2835 (O-CH$_3$). r$_f$ 0.23 (CH:EtOAc 9:1).

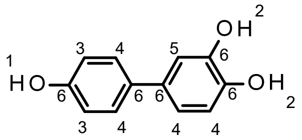

4-(4-Hydroxyphenyl)benzene-1,2-diol (AUJ-069, 40): 1,2-Dimethoxy-4-(4-methoxyphenyl)benzene (**AUJ-068**, **50**, 258.0 mg, 1.06 mmol, 1.0 equiv.) was dissolved in DCM (10 mL) and the solution was then cooled to -78 °C. To this 1M boron tribromide solution in DCM (4.5 mL, 4.50 mmol, 4.3 equiv.) was added and the resulting mixture was stirred at room temperature for 19 h. The reaction mixture was cooled in an ice bath and ice was added carefully. The aqueous layer was extracted with ethyl acetate (3 x 20 mL). The combined organic layers were washed with brine and dried over Na_2SO_4. The solvent was removed under reduced pressure to give the crude product which was purified by column chromatography (CH:EtOAc 2:1) to obtain 4-(4-hydroxyphenyl)benzene-1,2-diol (174.0 mg, 0.86 mmol, 81%) as a light pink solid: ^{1}H NMR (400 MHz, DMSO-D$_6$): **δ** 6.78 (m, 4H, H-4), 6.94 (m, 1H, H-5), 7.30 (m, 2H, H-3), 8.78 (s, 1H, H-2), 8.82 (s, 1H, H-2), 9.28 (s, 1H, H-1). ^{13}C NMR (100 MHz, DMSO-D6): **δ** 113.4 (C-5), 115.5 (C-4), 115.9 (C-4), 116.9 (C-4), 126.9 (C-3), 131.5 (C-6), 132.0 (C-6), 144.1 (C-6), 145.3 (C-6), 156.1 (C-6). LC-MS *m/z* (% relative intensity): 201.1 [M-H]$^-$ (100). HR-ESI-MS (*m/z*): calcd for $C_{12}H_9O_3$, 201.0557 found, 201.0557. IR (neat) $\tilde{v}_{max}$ (cm^{-1}): 3299 (O-H). r$_f$ 0.43 (CH:EtOAc 2:1).

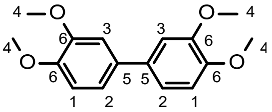

4-(3,4-Dimethoxyphenyl)-1,2-dimethoxybenzene (AUJ-202, 52): 4-Bromoveratrole (**51**, 0.10 mL, 0.70 mmol, 1.0 equiv.), 3,4-dimethoxybenzeneboronic acid (**49**, 152 mg, 0.84 mmol, 1.2 equiv.), potassium carbonate (193 mg, 1.40 mmol, 2.0 equiv.), 10% palladium on charcoal (36 mg, 0.03 mmol, 0.05 equiv.) and 18-crown-6 (181 mg, 0.69 mmol, 1.0 equiv.) were dissolved in 1:1 methanol/water (4 mL). Then, the reaction mixture was heated to 45 °C for 27 h. After cooling to room temperature, water and EtOAc were added and the mixture was filtered. The layers were separated and the aqueous layer was extracted with EtOAc (3 x 10 mL). The combined organic layers were washed with brine, dried over Na_2SO_4 and evaporated to dryness. The crude product was purified by column chromatography (CH:EtOAc 8:2) to afford 4-(3,4-dimethoxyphenyl)-1,2-dimethoxybenzene (124 mg, 0.45 mmol, 65%) as a colorless solid: ^{1}H NMR (600 MHz, $CDCl_3$): **δ** 3.91 (s, 6H, H-4), 3.94 (s, 6H, H-4), 6.93 (d, *J* = 8.3 Hz, 2H, H-1), 7.06 (d, *J* = 2.2 Hz, 2H, H-3), 7.09 (dd, *J* = 8.3 Hz, *J* = 2.1 Hz, 2H, H-2). ^{13}C NMR (150 MHz, $CDCl_3$): **δ** 56.1 (C-4), 110.6 (C-3), 111.7 (C-1), 119.2 (C-2), 134.4 (C-5), 148.5 (C-3), 149.3 (C-3). LC-MS *m/z* (% relative intensity): 275.1 [M+H]+ (100). HR-ESI-MS (*m/z*): calcd for

$C_{16}H_{18}NaO_4$, 297.1097 found, 297.1100. IR (neat) ṽ$_{max}$ (cm^{-1}): 2948 (w), 2930, 2906, 2833 (O-CH_3). r$_f$ 0.37 (CH:EtOAc 7:3).

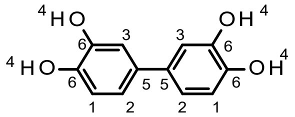

4-(3,4-Dihydroxyphenyl)benzene-1,2-diol (AUJ-204, 43): To a solution of 4-(3,4-dimethoxyphenyl)-1,2-dimethoxybenzene (**AUJ-202**, **52**, 76 mg, 0.28 mmol, 1.0 equiv.) in DCM (5 mL) cooled to -78 °C was added 1 M boron tribromide in DCM (1.40 mL, 1.40 mmol, 5.5 equiv.) dropwise. The reaction mixture was then stirred at room temperature for 20 h. After adding ice and 1 M HCl subsequently, the aqueous layer was extracted with EtOAc (3 x 20 mL). The combined organic layers were washed with brine, dried over Na_2SO_4 and evaporated *in vacuo*. The crude product was purified chromatographically (DCM + 7.5% methanol) to afford 4-(3,4-dihydroxyphenyl)benzene-1,2-diol (55 mg, 0.25 mmol, 89%) as a greyish solid: ^{1}H NMR (400 MHz, Acetone-d$_6$): **δ** 6.84 (d, *J* = 8.2 Hz, 2H, H-1) 6.88 (dd, *J* = 8.2 Hz, *J* = 2.1 Hz, 2H, H-2), 7.03 (d, *J* = 2.1 Hz, 2H, H-3), 7.81 (s, 2H, H-4), 7.78 (s, 2H, H-4). ^{13}C NMR (100 MHz, Acetone-d$_6$): **δ** 114.5 (C-3) 116.5 (C-1), 118.8 (C-2), 134.4 (C-5), 145.1 (C-6), 146.2 (C-6). LC-MS *m/z* (% relative intensity): 217.1 [M-H]$^-$ (76). HR-ESI-MS (*m/z*): calcd for $C_{12}H_9O_4$, 217.0506 found, 217.0504. IR (neat) ṽ$_{max}$ (cm^{-1}): 3397, 3178 (OH). r$_f$ 0.42 (DCM + 20% MeOH).

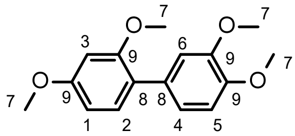

1-(3,4-Dimethoxyphenyl)-2,4-dimethoxybenzene (AUJ-203, 54): Bromo-2,4-dimethoxybenzene (**53**, 0.20 mL, 1.39 mmol, 1.0 equiv.), 3,4-dimethoxybenzeneboronic acid (**49**, 303 mg, 1.67 mmol, 1.2 equiv.), potassium carbonate (390 mg, 2.82 mmol, 2.0 equiv.), 10% palladium on charcoal (71 mg, 0.07 mmol, 0.05 equiv.) and 18-crown-6 (370 mg, 1.40 mmol, 1.0 equiv.) were dissolved in 1:1 methanol/water (8 mL). Then, the reaction mixture was heated to 45 °C for 29 h. After cooling to room temperature, water and EtOAc were added and the mixture was filtered. The layers were separated and the aqueous layer was extracted with EtOAc (3 x 10 mL). The combined organic layers were washed with brine, dried over Na_2SO_4 and evaporated to dryness. The crude product was purified by column chromatography (CH:EtOAc 9:1) to afford 1-(3,4-dimethoxyphenyl)-2,4-dimethoxybenzene (262 mg, 0.96 mmol, 68%) as a colorless solid: ^{1}H NMR (400 MHz, $CDCl_3$): **δ** 3.81 (s, 3H, H-7), 3.85 (s, 3H, H-7), 3.91 (s, 3H, H-7), 3.91 (s, 3H, H-7), 6.57 (m, 2H, H-1, H-3), 6.92 (d, *J* = 8.1 Hz, 1H, H-5), 7.05 (dd, *J* = 8.1 Hz, *J* = 2.0 Hz, 1H, H-4), 7.07 (d, *J* = 2.0 Hz, 1H, H-6), 7.24 (d, *J* = 8.3 Hz, 1H, H-2). ^{13}C NMR (100 MHz, $CDCl_3$): **δ** 55.5 (C-7), 55.7 (C-7), 56.0 (C-7), 56.0 (C-7), 99.2 (C-3), 104.7

(C-1), 111.1 (H-5), 113.2 (C-6), 121.8 (C-4), 123.5 (C-8), 131.1 (C-2), 131.3 (C-8), 148.0 (C-9), 148.5 (C-9), 157.5 (C-9), 160.2 (C-9). LC-MS *m/z* (% relative intensity): 275.1 [M+H]+ (100). HR-ESI-MS (*m/z*): calcd for $C_{16}H_{18}NaO_4$, 297.1097 found, 297.1100. IR (neat) $\tilde{v}_{max}$ (cm^{-1}): 2998, 2965, 2933, 2902, 2830 (O-CH_3). r_f 0.25 (CH:EtOAc 8:2).

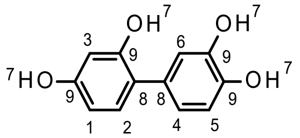

4-(2,4-Dihydroxyphenyl)benzene-1,2-diol (AUJ-205, 44): To a solution of 1-(3,4-dimethoxyphenyl)-2,4-dimethoxybenzene (**AUJ-203**, **54**, 100 mg, 0.37 mmol, 1.0 equiv.) in DCM (5 mL) cooled to -78 °C was added 1 M boron tribromide in DCM (2.00 mL, 2.00 mmol, 5.5 equiv.) dropwise. The reaction mixture was then stirred at room temperature for 20 h. After adding ice and 1 M HCl subsequently, the aqueous layer was extracted with EtOAc (3 x 20 mL). The combined organic layers were washed with brine, dried over Na_2SO_4 and evaporated *in vacuo*. The crude product was purified chromatographically (DCM + 10% methanol, then DCM + 5% methanol) to afford 4-(2,4-dihydroxyphenyl)benzene-1,2-diol (35 mg, .16 mmol, 44%) as a grey solid: ^{1}H NMR (400 MHz, Acetone-d_6): **δ** 6.39 (dd, *J* = 8.3 Hz, *J* = 2,4 Hz, 1H, H-1), 6.46 (d, *J* = 2.4 Hz, 1H, H-3), 6.82 (dd, *J* = 8.2 Hz, *J* = 0.4 Hz, 1H, H-5), 6.84 (dd, *J* = 8.2 Hz, *J* = 1.8 Hz, 1H, H-4), 7.04 (m, 2H, H-5, H-6), 7.72 (s, 1H, H-7), 7.77 (s, 1H, H-7), 7.84 (s, 1H, H-7), 8.17 (s, 1H, H-7). ^{13}C NMR (100 MHz, Acetone-d_6): **δ** 103.8 (C-3), 107.9 (C-1), 115.7 (C-5), 117.2 (C-6), 121.1 (C-8), 121.4 (C-4), 131.6 (C-2, C-8), 144.4 (C-9), 145.2 (C-9), 155.6 (C-9), 158.1 (C-9). LC-MS *m/z* (% relative intensity): 217.1 $[M-H]^-$ (100). HR-ESI-MS (*m/z*): calcd for $C_{12}H_9O_4$, 217.0506 found, 217.0504. IR (neat) $\tilde{v}_{max}$ (cm^{-1}): 3356 (OH). r_f 0.47 (DCM + 20% MeOH).

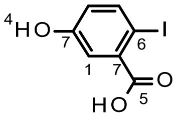

5-Hydroxy-2-iodobenzoic acid (AUJ-100, 61): A solution of 5-hydroxyanthranilic acid (**60**, 1.55 g, 10.15 mmol, 1.0 equiv.) and concentrated hydrochloric acid (8 mL) in water (20 mL) was cooled to 0 °C. To this, a solution of sodium nitrite (746 mg, 10.81 mmol, 1.1 equiv.) in water (4 mL) was added and the mixture was stirred for 30 min at 0 °C. Then, a solution of potassium iodide (2.58 g, 15.54 mmol, 1.5 equiv.) in water (4 mL) was added slowly and the reaction mixture was stirred for an additional 20 min at 0 °C and then heated to 90 °C for 30 min. After cooling to room temperature, the mixture was extracted with EtOAc (3 x 50 mL). The combined organic layers were washed with saturated $NaHSO_3$ and water, dried over Na_2SO_4 and evaporated under reduced pressure to afford 5-hydroxy-2-iodobenzoic acid (2.13 g, 8.07 mmol, 80%) as a brown solid: ^{1}H NMR (600 MHz, DMSO-d$_6$): **δ** 6.69 (dd, *J* = 8.55 Hz, *J* = 2.97 Hz, 1H, H-2), 7.14 (d, *J* = 3.00 Hz, 1H, H-1), 7.70 (d, *J* = 8.58 Hz, 1H, H-3), 9.98 (s, 1H, H-4). ^{13}C NMR (150 MHz, DMSO-d$_6$): **δ** 79.9 (C-6), 117.3 (C-1), 120.1 (C-2), 137.5 (C-7), 141.2 (C-3), 157.4 (C-7), 167.8 (C-5). LC-MS *m/z* (% relative intensity): 262.9 [M-H]$^-$ (36). HR-ESI-MS (*m/z*): calcd for C$_7$H$_4$IO$_3$, 262.9211 found, 262.9213. IR (neat) ṽ$_{max}$ (cm^{-1}): 3059 (O-H), 1705 (C=O). r$_f$ 0.12 (CH:EtOAc 1:1).

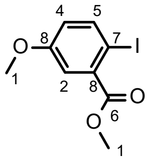

Methyl 2-iodo-5-methoxybenzoate (AUJ-102, 62): To a solution of 5-hydroxy-2-iodobenzoic acid (**AUJ-100**, **61**, 2.10 g, 7.95 mmol, 1.0 equiv.), and potassium carbonate (2.30 g, 16.66 mmol, 2.1 equiv.) in anhydrous acetone (40 mL) dimethyl sulfate (1.6 mL, 16.87 mmol, 2.1 equiv.) was added. The reaction mixture was heated to reflux for 6 h, cooled to room temperature and filtered. The crude product (2.36 g) was purified by column chromatography (CH:EtOAc 8:2) to give methyl 2-iodo-5-methoxybenzoate (2.28 g, 7.79 mmol, 98%) as a yellow oil: ^{1}H NMR (600 MHz, CDCl$_3$): **δ** 3.83 (s, 3H, H-1), 3.94 (s, 3H, H-1), 6.76 (dd, *J* = 8.70 Hz, *J* = 3.06 Hz, 1H, H-4), 7.36 (d, *J* = 3.12 Hz, 1H, H-2), 7.84 (d, *J* 8.70 Hz, 1H, H-5). ^{13}C NMR (150 MHz, CDCl$_3$): **δ** 52.4 (C-1), 55.5 (C-1), 82.3 (C-7), 116.4 (C-2), 119.3 (C-4), 135.9 (C-5), 141.8 (C-8), 159.5 (C-8), 166.7 (C-6). LC-MS *m/z* (% relative intensity): 292.9 [M+H]$^+$ (100), 166.1 [M-I+H]$^+$ (61). HR-ESI-MS (*m/z*): calcd for C$_9$H$_9$INaO$_3$, 314.9489 found, 314.9489. IR (neat) ṽ$_{max}$ (cm^{-1}): 1726 (C=O). r$_f$ 0.50 (CH:EtOAc 1:1).

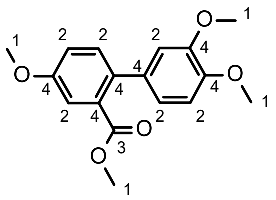

Methyl 2-(3,4-dimethoxyphenyl)-5-methoxybenzoate (AUJ-103, 63): A solution of sodium carbonate (545 mg, 5.14 mmol, 4.1 equiv.) in degassed water (4 mL) was added to a suspension of methyl 2-iodo-5-methoxybenzoate (**AUJ-102**, **62**, 369 mg, 1.26 mmol, 1.0 equiv.), 3,4-dimethoxybenzeneboronic acid (**49**, 352 mg, 1.94 mmol, 1.5 equiv.), tetrakis(triphenylphosphine)palladium(0) (76 mg, 0.07 mmol, 0.05 equiv.) and lithium chloride (165 mg, 3.90 mmol, 3.1 equiv.) in dimethoxyethane. The resulting mixture was stirred at 80 °C for 15 h. After cooling to room temperature, the suspension was filtered, diluted with water and extracted with EtOAc (3 x 30 mL). The combined organic layers were washed with brine, dried over Na_2SO_4 and concentrated *in vacuo*. The crude product was purified chromatographically (CH:EtOAc 8:2) to afford methyl 2-(3,4-dimethoxyphenyl)-5-methoxybenzoate (341 mg, 1.13 mmol, 89%) as a brown solid: ^{1}H NMR (400 MHz, $CDCl_3$): **δ** 3.67 (s, 3H, H-1), 3.88 (s, 3H, H-1), 3.89 (s, 3H, H-1), 3.92 (s, 3H, H-1), 6.83-6.91 (m, 3H, H-2), 7.07 (dd, *J* = 8.50 Hz, *J* = 2.82 Hz, 1H, H-2), 7.30 (m, 2H, H-2). ^{13}C NMR (100 MHz, $CDCl_3$): **δ** 52.0 (C-1), 55.5 (C-1), 55.8 (C-1), 110.8 (C-2), 111.9 (C-2), 114.1 (C-2), 117.3 (C-2), 120.6 (C-2), 131.7 (C-2), 131.9 (C-4), 133.7 (C-4), 134.4 (C-4), 148.1 (C-4), 148.5 (C-4), 158.4 (C-4), 169.3 (C-3). LC-MS *m/z* (% relative intensity): 303.1 $[M+H]^+$ (10), 271.1 $[M-OMe]^+$ (100). HR-ESI-MS (*m/z*): calcd for $C_{17}H_{18}NaO_5$, 325.1046 found, 325.1047. IR (neat) $\tilde{\nu}_{max}$ (cm^{-1}): 1717 (C=O). r_f 0.21 (CH:EtOAc 8:2).

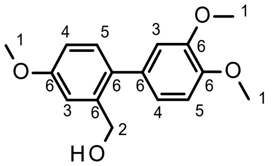

[2-(3,4-Dimethoxyphenyl)-5-methoxy-phenyl]methanol (AUJ-105, 64): To a suspension of lithium aluminium hydride (30 mg, 0.80 mmol, 1.9 equiv.) in THF (1 mL) cooled to 0 °C was added methyl 2-(3,4-dimethoxyphenyl)-5-methoxybenzoate (**AUJ-103**, **63**, 129 mg, 0.43 mmol, 1.0 equiv.) in THF (1 mL). The reaction mixture was stirred at room temperature for 21 h. At 0 °C, EtOAc and 1M HCl were added subsequently followed by extraction of the aqueous layer with EtOAc (3 x 10 mL). The combined organic layers were washed with brine, dried over Na_2SO_4 and concentrated under reduced pressure. The crude product was purified by column chromatography (CH:EtOAc 7:3) to afford [2-(3,4-dimethoxyphenyl)-5-methoxy-phenyl]methanol (112 mg, 0.41 mmol, 96%) as a brown oil: ^{1}H NMR (600 MHz, MeOH-d_4): **δ** 3.85 (m, 6H, H-1), 3.88 (s, 3H, H-1), 4.52 (s, 2H, H-2), 6.88 (m, 2H, H-4), 6.97 (d, *J* = 1.98 Hz, 1H, H-3), 6.99 (d, *J* = 8.22 Hz, 1H, H-5), 7.15 (d, *J* = 2.70 Hz, 1H, H-3), 7.17 (d, *J* = 8.40 Hz, 1H, H-5). ^{13}C NMR (150 MHz, MeOH-d_4): **δ** 55.7 (C-1), 56.5 (C-1), 55.6 (C-1), 63.1 (C-2), 112.9 (C-5), 113.8 (C-4), 114.6 (C-3), 114.8 (C-3), 123.0 (C-4), 131.9 (C-5), 134.8 (C-6), 135.1 (C-6), 141.0 (C-6), 149.6 (C-6), 150.1 (C-6), 160.5 (C-6). LC-MS *m/z* (% relative intensity): 292.2 $[M+NH_4]^+$ (4), 297.1 $[M+Na]^+$ (8), 257.1 $[M-OH]^+$ (100). HR-ESI-MS (*m/z*): calcd for $C_{16}H_{18}NaO_4$, 297.1097 found, 297.1096. IR (neat) $\tilde{\nu}_{max}$ (cm^{-1}): 3475 (O-H). r_f 0.28 (CH:EtOAc 1:1).

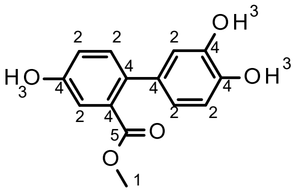

Methyl 2-(3,4-dihydroxyphenyl)-5-hydroxybenzoate (AUJ-124, 65): A mixture of methyl 2-(3,4-dimethoxyphenyl)-5-methoxy-benzoate (**AUJ-103**, **63**, 229 mg, 0.76 mmol, 1.0 equiv.) and aluminium tribromide (1.61 g, 6.05 mmol, 8.0 equiv.) in toluene (10 mL) was heated to reflux for 3 d. Then, 1M HCl was added and the aqueous layer was extracted with diethyl ether (3 x 20 mL). The combined organic layers were washed with brine, dried over Na_2SO_4 and evaporated *in vacuo*. The crude product (279 mg) was purified by column chromatography (CH:EtOAc 1:1) to afford methyl 2-(3,4-dihydroxyphenyl)-5-hydroxybenzoate (124 mg, 0.47 mmol, 63%) as a light brown solid: ^{1}H NMR (600 MHz, Acetone-d_6): **δ** 3.62 (s, 3H, H-1), 6.64 (m, 1H, H-2), 6.81 (m, 1H, H-2), 6.82 (m, 1H, H-2), 7.03 (m, 1H, H-2), 7.16 (m, 1H, H-2), 7.24 (m, 1H, H-2), 7.83 (s, 1H, H-3), 7.82 (s, 1H, H-3), 8.64 (s, 1H, H-3). ^{13}C NMR (150 MHz, Acetone-d_6): **δ** 52.7 (C-1), 116.5 (C-2), 117.0 (C-2), 117.1 (C-2), 119.4 (C-2), 121.5 (C-2), 133.0 (C-2), 134.1 (C-4), 134.6 (C-4), 145.7 (C-4), 146.1 (C-4), 157.5 (C-4), 170.7 (C-5). LC-MS *m/z* (% relative intensity): 259.1 $[M-H]^-$ (100). HR-ESI-MS (*m/z*): calcd for $C_{14}H_{11}O_5$, 259.0612 found, 259.0611. IR (neat) $\tilde{\nu}_{max}$ (cm^{-1}): 3308 (O-H), 1696 (C=O). r_f 0.48 (CH:EtOAc 1:1).

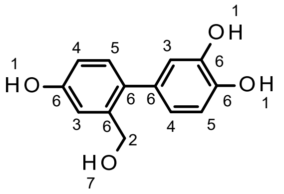

4-[4-Hydroxy-2-(hydroxymethyl)phenyl]benzene-1,2-diol (AUJ-119, 56): To a suspension of lithium aluminium hydride (105 mg, 2.77 mmol, 6.3 equiv.) in THF (3 mL) was added dropwise a solution of methyl 2-(3,4-dihydroxyphenyl)-5-hydroxybenzoate (**AUJ-124**, **65**, 115 mg, 0.44 mmol, 1.0 equiv.) in THF (3 mL). The reaction mixture was heated to reflux for 18 h. After cooling to room temperature, EtOAc and 1M HCl were added subsequently and the aqueous layers was then extracted with EtOAc (3 x 20 mL). The combined organic layers were washed with brine, dried over Na_2SO_4 and concentrated under reduced pressure. The crude product (104 mg) was purified chromatographically (CH:EtOAc 2:1 → 1:1) to afford 4-[4-hydroxy-2-(hydroxymethyl)phenyl]benzene-1,2-diol (64 mg, 0.28 mmol, 62%) as an off-white solid: ^{1}H NMR (400 MHz, Aceton-d_6): **δ** 3.15 (s, 1H, H-7), 4.54 (d, J = 5.16 Hz, 2H, H-2), 6.67 (dd, J = 8.02 Hz, J = 2.18 Hz, 1H, H-4), 6.76 (dd, J = 8.22 Hz, J = 2.66 Hz, 1H, H-4), 6.85 (m, 2H, H-3, H-5), 7.04 (d, J = 8.24 Hz, 1H, H-5), 7.12 (d, J = 2.60 Hz, 1H, H-3), 7.83 (s, 1H, H-1), 7.91 (s, 1H, H-1), 8.24 (s, 1H, H-1). ^{13}C NMR (100 MHz, Aceton-d_6): **δ** 63.4 (C-2), 115.2 (C-4), 116.0

(C-3), 116.4 (C-5), 118.0 (C-3), 122.4 (C-4), 132.1 (C-5), 133.7 (C-6), 134.5 (C-6), 142.2 (C-6), 145.5 (C-6), 146.1 (C-6), 157.9 (C-6). LC-MS *m/z* (% relative intensity): 231.1 [M-H]$^-$ (100). HR-ESI-MS (*m/z*): calcd for $C_{13}H_{11}O_4$, 231.0663 found, 231.0662. IR (neat) $\tilde{\nu}_{max}$ (cm^{-1}): 3315 (O-H). r_f 0.33 (CH:EtOAc 1:2).

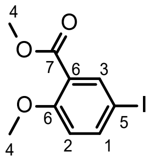

Methyl 5-iodo-2-methoxy-benzoate (AUJ-097, 67): To a solution of 5-iodosalicylic acid (**66**, 1.01 g, 3.83 mmol, 1.0 equiv.) and potassium carbonate (1.18 g, 8.09 mmol, 2.1 equiv.) in anhydrous acetone (20 mL) was added dimethyl sulfate (750 µL, 7.91 mmol, 2.1 equiv.). The reaction mixture was heated to reflux for 4.5 h. After cooling to room temperature, the solid was filtered off and the filtrate was evaporated *in vacuo* to give a yellow oil. The crude product (1.13 g) was purified by column chromatography (CH:EtOAc 3:1) to give methyl 5-iodo-2-methoxy-benzoate (1.07 g, 3.66 mmol, 96%) as a colorless solid: ^{1}H NMR (600 MHz, CDCl$_3$): **δ** 3.89 (m, 6H, H-4), 6.76 (d, *J* = 8.82 Hz, 1H, H-2), 7.73 (dd, *J* = 8.76 Hz, *J* = 2.34 Hz, 1H, H-1), 8.07 (d, *J* = 2.34 Hz, 1H, H-3). ^{13}C NMR (150 MHz, CDCl$_3$): **δ** 52.2 (C-4), 56.1 (C-4), 81.7 (C-5), 114.3 (C-2), 122.2 (C-6), 139.9 (C-3), 141.9 (C-1), 158.9 (C-6), 165.1 (C-7). LC-MS *m/z* (% relative intensity): 260.9 [M-OMe]$^+$ (100), 293.0 [M+H]$^+$ (6). HR-ESI-MS (*m/z*): calcd for $C_9H_9INaO_3$, 314.9489 found, 314.9486. IR (neat) $\tilde{\nu}_{max}$ (cm^{-1}): 1698 (C=O). r_f 0.51 (CH:EtOAc 1:1).

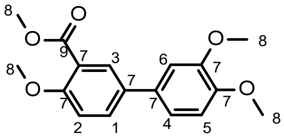

Methyl 5-(3,4-dimethoxyphenyl)-2-methoxy-benzoate (AUJ-098, 68): A solution of sodium carbonate (234 mg, 2.21 mmol, 4.4 equiv.) in degassed water was added to a solution of methyl 5-iodo-2-methoxy-benzoate (**AUJ-097**, **67**, 148 mg, 0.51 mmol, 1.0 equiv.), 3,4-dimethoxybenzeneboronic acid (**49**, 146 mg, 0.80 mmol, 1.6 equiv.), tetrakis(triphenylphosphine)palladium(0) (39 mg, 0.03 mmol, 0.07 equiv.) and lithium chloride (79 mg, 1.86 mmol, 3.7 equiv.) in dimethoxyethane (5 mL). The mixture was stirred at 80 °C for 19 h. After cooling to room temperature, the mixture was filtered, diluted with water and extracted with diethyl ether (3 x 20 mL). The combined organic layers were washed with brine, dried over Na_2SO_4 and concentrated under reduced pressure. The crude product was purified chromatographically (CH:EtOAc 8:2) to yield methyl 5-(3,4-dimethoxyphenyl)-2-methoxy-benzoate (138 mg, 0.46 mmol, 90%) as a light brown solid: ^{1}H NMR (600 MHz, CDCl$_3$): **δ** 3.93 (s, 3H, H-8), 3.94 (s, 3H, H-8), 3.95 (s, 3H, H-8), 3.96 (s, 3H, H-8), 6.94 (d, *J* = 8.28 Hz, 1H, H-

5), 7.05 (d, *J* = 8.64, 1H, H-2), 7.08 (d, *J* = 2.10 Hz, 1H, H-6), 7.11 (dd, *J* = 8.22 Hz, *J* = 2.16 Hz, 1H, H-4), 7.66 (dd, *J* = 8.65 Hz, *J* = 2.52 Hz, 1H, H-1), 8.00 (d, *J* = 2.52 Hz, 1H, H-3). ^{13}C NMR (150 MHz, $CDCl_3$): **δ** 52.0 (C-8), 55.9 (C-4), 56.0 (C-8), 56.1 (C-8), 110.2 (C-6), 111.7 (C-5), 112.5 (C-2), 119.1 (C-4), 120.0 (C-7), 129.8 (C-3), 131.5 (C-1), 132.8 (C-7), 133.2 (C-7), 148.6 (C-7), 149.3 (C-7), 158.2 (C-7), 166.7 (C-9). LC-MS *m/z* (% relative intensity): 303.1 $[M+H]^+$ (100), 271.1 $[M-OMe]^+$ (95). HR-ESI-MS (*m/z*): calcd for $C_{17}H_{18}NaO_5$, 325.1046 found, 325.1034. IR (neat) $\tilde{\nu}_{max}$ (cm^{-1}): 1699 (C=O). r_f 0.43 (CH:EtOAc 1:1).

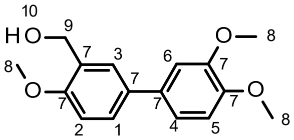

[5-(3,4-Dimethoxyphenyl)-2-methoxy-phenyl]methanol (AUJ-101, 69): To a suspension of lithium aluminium hydride (17 mg, 0.45 mmol, 1.4 equiv.) in THF (1 mL) cooled to 0 °C was added methyl 5-(3,4-dimethoxyphenyl)-2-methoxybenzoate (**AUJ-098**, **68**, 97 mg, 0.32 mmol, 1.0 equiv.) in THF (1 mL). The reaction mixture was stirred for 16.5 h at room temperature. The suspension was then cooled to 0 °C and EtOAc and 1M HCl were added subsequently. The aqueous layer was extracted with EtOAc (3 x 10 mL). The combined organic layers were washed with brine, dried over Na_2SO_4 and evaporated to dryness. The crude product (151 mg) was purified by column chromatography (CH:EtOAc 7:3) to give [5-(3,4-dimethoxyphenyl)-2-methoxy-phenyl]methanol (79 mg, 0.29 mmol, 90%) as a brown solid: ^{1}H NMR (600 MHz, $CDCl_3$): **δ** 3.92 (s, 3H, H-8), 3.93 (s, 3H, H-8), 3.96 (s, 3H, H-8), 4.77 (s, 2H, H-9), 6.95 (m, 2H, H-2, H-5, H-2), 7.09 (d, *J* = 2.10 Hz, 1H, H-6), 7.12 (dd, *J* = 8.22 Hz, *J* = 2.16 Hz, 1H, H-4), 7.48 (dd, *J* = 8.41 Hz, *J* = 2.41 Hz, 1H, H-1), 7.51 (d, *J* = 2.34 Hz, 1H, H-3). ^{13}C NMR (150 MHz, $CDCl_3$): **δ** 55.4 (C-8), 55.9 (C-8), 56.0 (C-8), 62.0 (C-9), 110.4 (C-6), 110.5 (C-2/C-5), 111.7 (C-2/C-5), 119.0 (C-4), 127.0 (C-1), 127.2 (C-3), 129.4 (C-7), 133.7 (C-7), 133.9 (C-7), 148.3 (C-7), 149.2 (C-7), 156.6 (C-7). LC-MS *m/z* (% relative intensity): 275.1 $[M+H]^+$ (16), 297.1 $[M+Na]^+$ (11), 257.1 $[M-OH]^+$ (100). HR-ESI-MS (*m/z*): calcd for $C_{16}H_{18}NaO_4$, 297.1097 found, 297.1097. IR (neat) $\tilde{\nu}_{max}$ (cm^{-1}): 3518 (O-H). r_f 0.30 (CH:EtOAc 1:1).

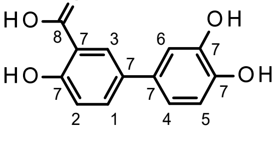

5-(3,4-Dihydroxyphenyl)-2-hydroxy-benzoic acid (AUJ-123, 70): A solution of methyl 5-(3,4-dimethoxyphenyl)-2-methoxybenzoate (**AUJ-098**, **68**, 257 mg, 0.85 mmol, 1.0 equiv.) in DCM (5 mL) was cooled to -78 °C. To this, boron tribromide (1M in DCM, 4.0 mL, 4.00 mmol, 4.7 equiv.) was added dropwise and the reaction mixture was then stirred at room temperature for

23 h. Upon completion, the mixture was cooled to 0 °C and ice was added. The aqueous layer was extracted with EtOAc (3 x 20 mL). The combined organic layers were washed with brine, dried over Na_2SO_4 and the solvent was removed under reduced pressure. The crude 5-(3,4-dihydroxyphenyl)-2-hydroxy-benzoic acid (203 mg, 0.85 mmol, quant.) was obtained as a black solid: ^{1}H NMR (600 MHz, MeOH-d_4): **δ** 6.84 (d, *J* = 8.16 Hz, 1H, H-5), 6.91 (dd, *J* = 8.19 Hz, *J* = 2.19 Hz, 1H, H-4), 6.97 (d, *J* = 8.64 Hz, 1H, H-2), 7.02 (d, *J* = 2.22 Hz, 1H, H-6), 7.66 (dd, *J* = 8.58 Hz, *J* = 2.40 Hz, 1H, H-1), 8.01 (d, *J* = 2.40 Hz, 1H, H-3). ^{13}C NMR (150 MHz, MeOH-d_4): **δ** 113.9 (C-7), 114.6 (C-6), 116.8 (C-5), 118.5 (C-2), 119.0 (C-4), 128.8 (C-3), 133.4 (C-7), 133.8 (C-7), 134.8 (C-1), 145.9 (C-7), 146.6 (C-7), 161.9 (C-7), 173.5 (C-8). LC-MS *m/z* (% relative intensity): 245.1 (M-H]$^-$ (100), 201.1 [M-CO_2H]$^-$ (21). HR-ESI-MS (*m/z*): calcd for $C_{13}H_9O_5$, 245.0455 found, 245.0455. IR (neat) $\tilde{v}_{max}$ (cm^{-1}): 3178 (O-H), 1661 (C=O). r_f 0.20 (CH:EtOAc 1:1).

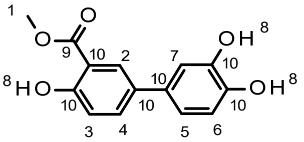

Methyl 5-(3,4-dihydroxyphenyl)-2-hydroxy-benzoate (AUJ-145, 71): A solution of methyl 5-(3,4-dimethoxyphenyl)-2-methoxybenzoate (**AUJ-098**, **68**, 307 mg, 1.02 mmol, 1.0 equiv.) and aluminium tribromide (2.12 g, 7.93 mmol, 7.8 equiv.) in toluene (10 mL) was heated to 80 °C for 3 h. After cooling to room temperature, 1M HCl was added and the aqueous layer was extracted with EtOAc (3 x 10 mL). The combined organic layers were washed with brine, dried over Na_2SO_4 and evaporated to dryness. The crude product was purified by column chromatography (CH:EtOAc 9:1 → 8:2) to afford methyl 5-(3,4-dihydroxyphenyl)-2-hydroxy-benzoate (201 mg, 0.77 mmol, 76%) as a brown solid: ^{1}H NMR (400 MHz, Aceton-d_6): **δ** 3.99 (s, 3H, H-1), 6.92 (d, *J* = 8.20 Hz, 1H, H-6), 6.96 (dd, *J* = 8.18 Hz, *J* = 2.06 Hz, 1H, H-5), 7.00 (d, *J* = 8.60 Hz, 1H, H-3), 7.11 (d, *J* = 2.04 Hz, 1H, H-7), 7.72 (dd, *J* = 8.64 Hz, *J* = 2.48 Hz, 1H, H-4), 7.99 (m, 3H, H-2, H-8), 10.68 (s, 1H, H-8). ^{13}C NMR (100 MHz, Aceton-d_6): **δ** 53.6 (C-1), 113.9 (C-10), 115.0 (C-7), 117.3 (C-6), 119.2 (C-3), 119.5 (C-5), 128.6 (C-2), 133.3 (C-10), 134.0 (C-10), 135.4 (C-4), 146.2 (C-10), 147.0 (C-10), 161.8 (C-10), 172.0 (C-9). LC-MS *m/z* (% relative intensity): 259.1 [M-H]$^-$ (100). HR-ESI-MS (*m/z*): calcd for $C_{14}H_{11}O_5$, 259.0612 found, 259.0611. IR (neat) $\tilde{v}_{max}$ (cm^{-1}): 3449, 3352, 3228 (O-H), 1653 (C=O). r_f 0.16 (CH:EtOAc 7:3).

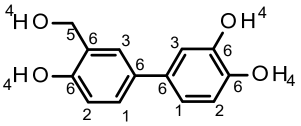

4-[4-Hydroxy-3-(hydroxymethyl)phenyl]benzene-1,2-diol (AUJ-104, 55): To a suspension of lithium aluminium hydride (91.3 mg, 2.41 mmol, 5.1 equiv.) in THF (5 mL) cooled to 0 °C a solution of methyl 5-(3,4-dihydroxyphenyl)-2-hydroxy-benzoate (**AUJ-145**, **71**, 122.6 mg, 0.47 mmol, 1.0 equiv.) in THF (5 mL) was added dropwise. The mixture was then heated to reflux for 17 h. The reaction mixture was then diluted with EtOAc and 1M HCl was added slowly until all aluminium salts were dissolved. The aqueous layer was extracted with EtOAc (3 x 15 mL) and the combined organic layers were washed with brine and dried over Na_2SO_4. The crude product (123 mg) was purified by column chromatography (n-hexanes:acetone 2:1) to afford 4-[4-hydroxy-3-(hydroxymethyl)phenyl]benzene-1,2-diol (39.1 mg, 0.17 mmol, 36%) as a brownish solid: ^{1}H NMR (400 MHz, acetone-d$_6$): **δ** 4.81 (s, 2H, H-5), 6.87 (m, 2H, H-2), 6.94 (m, 1H, H-1), 7.09 (m, 1H, H-3), 7.31 (m, 1H, H-1), 7.48 (m, 1H, H-3), 8.01 (s, 2H, H-4). ^{13}C NMR (100 MHz, acetone-d$_6$): **δ** 62.6 (C-5), 115.0 (C-3), 117.0 (C-2), 117.1 (C-2), 119.4 (C-1), 127.2 (C-3), 127.4 (C-1), 129.1 (C-6), 134.1 (C-6), 135.0 (C-6), 145.6 (C-6), 146.8 (C-6), 155.8 (C-6). LC-MS *m/z* (% relative intensity): 231.1 $[M-H]^-$ (100). HR-ESI-MS (*m/z*): calcd for $C_{13}H_{11}O_4$, 231.0663 found, 231.0663. IR (neat) $\tilde{\nu}_{max}$ (cm^{-1}): 3452, 3346, 3222 (O-H). r_f 0.68 (CH:EtOAc 1:1).

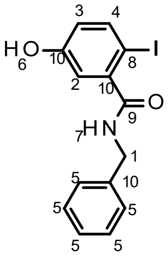

***N*-Benzyl-5-hydroxy-2-iodobenzamide (AUJ-127, 81):** To a solution of 5-hydroxy-2-iodo-benzoic acid (**AUJ-100**, **66**, 800 mg, 3.03 mmol, 1.0 equiv.), 1-hydroxybenzotriazole hydrate (248 mg, 1.83 mmol, 0.6 equiv.) and benzylamine (360 µL, 3.30 mmol, 1.1 equiv.) in DCM was added 1-ethyl-3-(3-dimethylaminopropyl)carbodiimide hydrochloride (EDC, 696 mg, 3.63 mmol, 1.2 equiv.) and the resulting mixture was stirred at room temperature for 19 h. Upon completion, 1M HCl was added and the aqueous layer was extracted with EtOAc (3 x 30 mL). The combined organic layers were washed with saturated $NaHCO_3$ and brine, dried over Na_2SO_4 and evaporated to dryness. The crude product (852 mg) was purified by column chromatography (CH:EtOAc 7:3) to afford *N*-benzyl-5-hydroxy-2-iodobenzamide (715 mg, 2.03 mmol, 67%) as a light yellow solid: ^{1}H NMR (600 MHz, DMSO-d$_6$): **δ** 4.44 (m, 2H, H-1), 6.63 (m, 1H, H-3), 6.80 (m, 1H, H-2), 7.25 (m, 1H, H-5), 7.33 (m, 2H, H-5), 7.39 (m, 2H, H-5), 7.59 (m, 1H, H-4)

8.81 (s, 1H, H-7), 9.89 (s, 1H, H-6). ^{13}C NMR (150 MHz, DMSO-d$_6$): **δ** 42.5 (C-1), 79.0 (C-8), 115.6 (C-2), 118.4 (C-3), 126.7 (C-5), 127.3 (C-5), 128.1 (C-5), 139.1 (C-10), 139.8 (C-4), 143.5 (C-10), 157.4 (C-10), 168.8 (C-9). LC-MS *m/z* (% relative intensity): 354.0 $[M+H]^+$ (100). HR-ESI-MS (*m/z*): calcd for $C_{14}H_{13}INO_2$, 353.9985 found, 353.9978. IR (neat) $\tilde{\nu}_{max}$ (cm^{-1}): 3296 (O-H), 1542 (C=O). r_f 0.36 (CH:EtOAc 6:4).

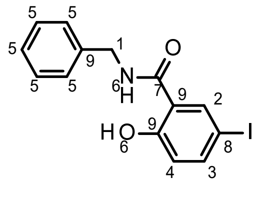

N-Benzyl-2-hydroxy-5-iodobenzamide (AUJ-128, 83): To a solution of 5-iodosalicylic acid (**61**, 802 mg, 3.04 mmol, 1.0 equiv.), 1-hydroxybenzotriazole hydrate (250 mg, 1.85 mmol, 0.6 equiv.) and benzylamine (360 µL, 3.30 mmol, 1.1 equiv.) in DCM was added 1-ethyl-3-(3-dimethylaminopropyl)carbodiimide hydrochloride (EDC, 697 mg, 3.64 mmol, 1.2 equiv.) and the resulting mixture was stirred at room temperature for 19 h. Upon completion, 1M HCl was added and the aqueous layer was extracted with EtOAc (3 x 30 mL). The combined organic layers were washed with saturated $NaHCO_3$ and brine, dried over Na_2SO_4 and evaporated to dryness. The crude product (960 mg) was purified by column chromatography (CH:EtOAc 8:2) to afford *N*-benzyl-2-hydroxy-5-iodobenzamide (877 mg, 2.48 mmol, 82%) as a light yellow crystals: ^{1}H NMR (600 MHz, DMSO-d$_6$): **δ** 4.51 (m, 2H, H-1), 6.78 (d, *J* = 8.70 Hz, 1H, H-4), 7.27 (m, 1H, H-5), 7.34 (m, 4H, H-5), 7.69 (dd, *J* = 8.67 Hz, *J* = 2.19 Hz, 1H, H-3), 8.24 (d, *J* = 2.16 Hz, 1H, H-2), 9.38 (m, 1H, H-6), 12.57 (s, 1H, H-6). ^{13}C NMR (150 MHz, DMSO-d$_6$): **δ** 42.5 (C-1), 80.5 (C-8), 117.8 (C-9), 120.1 (C-4), 127.0 (C-5), 127.4 (C-5), 128.4 (C-5), 136.0 (C-2), 138.7 (C-9), 141.8 (C-3), 159.6 (C-9), 167.4 (C-7). LC-MS *m/z* (% relative intensity): 354.0 $[M+H]^+$ (100). HR-ESI-MS (*m/z*): calcd for $C_{14}H_{13}INO_2$, 353.9985 found, 353.9975. IR (neat) $\tilde{\nu}_{max}$ (cm^{-1}): 3348 (N-H, O-H), 1629, 1579 (C=O). r_f 0.48 (CH:EtOAc 8:2).

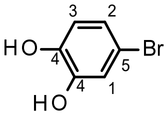

4-Bromobenzene-1,2-diol (AUJ-129, 85): To a suspension of 5-bromo-2-hydroxybenzaldehyde (**30**, 1.07 g, 5.30 mmol, 1.0 equiv.) in 3M NaOH (374 mg, 9.35 mmol, 1.8 equiv.) was added hydrogen peroxide (35%, 680 µL, 7.91 mmol, 1.5 equiv.). The mixture was stirred for 4 h, acidified to pH 4 by addition of concentrated sulfuric acid, neutralized with saturated $NaHCO_3$ and extracted with diethyl ether (3 x 50 mL). The combined organic layers were washed with brine, dried over Na_2SO_4 and evaporated under reduced pressure to yield 4-bromobenzene-1,2-diol (935 mg, 4.95 mmol, 93%) as colorless crystals: ^{1}H NMR (600 MHz, $CDCl_3$): **δ** 6.76 (d,

J = 8.46 Hz, 1H, H-3), 6.94 (dd, J = 8.46 Hz, J = 2.28 Hz, 1H, H-2), 7.04 (d, J = 2.28 Hz, 1H, H-1). ^{13}C NMR (150 MHz, CDCl$_3$): **δ** 112.4 (C-5), 116.6 (C-1/2/3), 118.6 (C-1/2/3), 123.8 (C-1/2/3), 142.9 (C-4), 144.6 (C-4). IR (neat) $\tilde{\nu}_{max}$ (cm^{-1}): 3344 (O-H). r$_f$ 0.39 (CH:EtOAc 1:1).

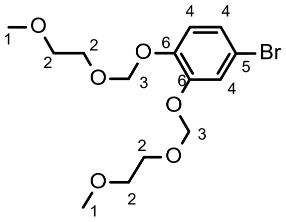

4-Bromo-1,2-bis(2-methoxyethoxymethoxy)benzene (AUJ-130, 86): To a solution of 4-bromobenzene-1,2-diol (**AUJ-129**, **85**, 862 mg, 4.56 mmol, 1.0 equiv.) in DCM (20 mL) cooled to 0 °C were added DIPEA (2.70 mL, 15.88 mmol, 3.5 equiv.) and 2-methoxyethoxymethyl chloride (MEM Cl, 1.50 mL, 131.13 mmol, 2.9 equiv.) dropwise. The reaction mixture was stirred at 0 °C for 60 min and then at room temperature for further 5.5 d. The reaction mixture was then diluted with DCM (50 mL), washed with 1M HCl, saturated NaHCO$_3$, water and brine, dried over Na$_2$SO$_4$ and concentrated *in vacuo*. The crude product (2.16 g) was purified by column chromatography (CH:EtOAc 9:1→ 7:3) to afford 4-bromo-1,2-bis(2-methoxyethoxymethoxy)benzene (1.49 g, 4.08 mmol, 90%) as a yellow oil: ^{1}H NMR (600 MHz, CDCl$_3$): **δ** 3.40 (m, 6H, H-1), 3.58 (m, 4H, H-2), 3.87 (m, 4H, H-2), 5.30 (m, 4H, H-3), 7.09 (m, 2H, H-4), 7.37 (m, 1H, H-4). ^{13}C NMR (150 MHz, CDCl$_3$): **δ** 59.0 (C-1), 67.9 (C-2), 68.0 (C-2), 71.5 (C-2), 94.6 (C-3), 114.5 (C-5), 118.2 (C-4), 120.2 (C-4), 125.4 (C-4), 146.6 (C-6), 148.1 (C-6). LC-MS *m/z* (% relative intensity): 382.1 [M(^{79}Br)+NH$_4$]$^+$ (100), 384.1 [M(^{81}Br)+NH$_4$]$^+$ (98). HR-ESI-MS (*m/z*): calcd for $C_{14}H_{21}BrNaO_6$, 387.0414 and 389.0395 found, 387.0415 and 389.0407. IR (neat) $\tilde{\nu}_{max}$ (cm^{-1}): 2818 (O-CH$_3$). r$_f$ 0.18 (CH:EtOAc 7:3).

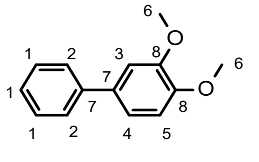

1,2-Dimethoxy-4-phenylbenzene (AUJ-200, 90): Bromobenzene (**89**, 500 mg, 3.18 mmol. 1.0 equiv.), 3,4-dimethoxybenzeneboronic acid (**49**, 696 mg, 3.82 mmol, 1.2 equiv.), potassium carbonate (887 mg, 6.41 mmol, 2.0 equiv.), 10% palladium on charcoal (174 mg, 0.16 mmol, 0.05 equiv.) and 18-crown-6 (859 mg, 3.25 mmol, 1.0 equiv.) were suspended in 1:1 methanol/water (20 mL) and heated to 45 °C for 2 h. The reaction mixture was then diluted with water (50 mL) and EtOAc (50 mL) and filtered. The two layers of the filtrate were separated and the aqueous layer was extracted with EtOAc (2 x 50 mL). The combined organic layers were washed with brine, dried over Na$_2$SO$_4$ and concentrated *in vacuo*. The crude product (589 mg) was purified by column chromatography (CH:EtOAC 9:1) to afford 1,2-dimethoxy-4-phenylbenzene (530 mg, 2.47 mmol, 78%) as a light yellow solid: ^{1}H NMR (400 MHz, $CDCl_3$): **δ** 3.95 (s, 3H, H-3), 3.98 (s, 3H, H-3), 6.98 (d, *J* = 8.24 Hz, 1H, H-5), 7.15 (d, *J* = 2.09 Hz, 1H, H-3), 7.18 (dd, *J* = 8.26 Hz, *J* = 2.14 Hz, 1H, H-4), 7.34 (m, 1H, H-1), 7.45 (m, 1H, H-1), 7.59 (m, 1H, H-2). ^{13}C NMR (100 MHz, $CDCl_3$): **δ** 66.0 (C-6), 110.5 (C-3/C-4/C-5), 111.5 (C-3/C-4/C-5), 119.4 (C-3/C-4/C-5), 126.8 (C-1/C-2), 128.7 (C-1/C-2) 134.3 (C-7), 141.0 (C-7), 148.6 (C-8), 149.2 (C-8). LC-MS *m/z* (% relative intensity): 215.1 $[M+H]^+$ (100). HR-ESI-MS (*m/z*): calcd for $C_{14}H_{14}NaO_2$, 237.0886 found, 237.0887. IR (neat) $\tilde{\nu}_{max}$ (cm^{-1}): 2960, 2936, 2913 ($O-CH_3$). r_f 0.29 (CH:EtOAc 9:1).

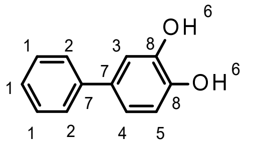

4-Phenylbenzene-1,2-diol (AUJ-201, 91): 1,2-Dimethoxy-4-phenylbenzene (**AUJ-200**, **90** 207.0 mg, 0.97 mmol, 1.0 equiv.) was dissolved in DCM (10 mL) and the solution was then cooled to -78 °C. To this, 1M boron tribromide solution in DCM (4.0 mL, 4.00 mmol, 4.2 equiv.) was added and the resulting mixture was stirred at room temperature for 19 h. The reaction mixture was cooled in an ice bath and ice was added carefully. The aqueous layer was extracted with EtOAc (3 x 20 mL). The combined organic layers were washed with brine and dried over Na_2SO_4. The solvent was removed under reduced pressure to give the crude product (260 mg) which was purified by column chromatography (CH:EtOAc 2:1) to obtain 4-phenylbenzene-1,2-diol (172.0 mg, 0.92 mmol, 95%) as a green solid: ^{1}H NMR (600 MHz, $CDCl_3$): **δ** 5.21 (s, 1H, H-6), 5.25 (s, 1H, H-6), 6.97 (d, *J* = 8.22 Hz, 1H, H-5), 7.09 (dd, *J* = 8.19 Hz, *J* = 2.01 Hz, 1H, H-4), 7.16 (d, *J* = 1.92 Hz, 1H, H-3), 7.33 (t, *J* = 7.38 Hz, 1H, H-1), 7.43 (t, *J* = 7.68 Hz, 2H, H-1), 7.55 (d, *J* = 7.32 Hz, 2H, H-2). ^{13}C NMR (150 MHz, $CDCl_3$): **δ** 114.3 (C-3/C-4/C-5), 115.8 (C-3/C-4/C-5), 120.0 (C-3/C-4/C-5), 126.7 (C-1/C-2), 126.9 (C-1), 128.7 (C-1/C-2), 134.9 (C-7), 140.6 (C-7), 143.0 (C-8), 143.7 (C-8). LC-MS *m/z* (% relative intensity): 185.1 [M-H]+ (100). HR-ESI-MS (*m/z*): calcd for $C_{12}H_{10}O_2$, 185.0617 found, 185.0610. IR (neat) $\tilde{\nu}_{max}$ (cm^{-1}): 3363 (O-H). r_f 0.28 (CH:EtOAc 2:1).

6.2. Synthesis of ligands to bind to the *K*-Ras protein

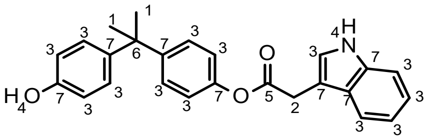

[4-[1-(4-Hydroxyphenyl)-1-methylethyl]phenyl]-2-(1*H*-indole-3-yl)acetate (AUJ-139, 119a): Bisphenol A (**23**, 132 mg, 0.58 mmol, 2.0 equiv.), *N',N'*-dicyclohexylcarbodiimid (DCC, 65 µL, 0.30 mmol, 1.1 equiv.) and *N,N*-dimethylpyridin-4-amin (DMAP, 3.5 mg, 0.03 mmol, 0.1 equiv.) were dissolved in DCM (1 mL). To this, a solution of indole-3-acetic acid (**135**, 50 mg, 0.29 mmol, 1.0 equiv.) in DCM (10 mL) and DMF (100 µL) was added dropwise via a syringe pump over 24 h. When the addition was complete, the mixture was stirred for further 2 d. Upon completion of the reaction, the mixture was filtered and evaporated to dryness. The crude product was purified by column chromatography (CH:EtOAc 9:1) and then suspended in EtOAc and filtered to remove excess of BPA. The product [4-[1-(4-hydroxyphenyl)-1-methyl-ethyl]phenyl]-2-(1*H*-indole-3-yl)acetate (23 mg, 0.06 mmol, 21%) was obtained as a colorless oil: ^{1}H NMR (400 MHz, CDCl$_3$): **δ** 1.64 (s, 6H, H-1), 4.03 (s, 2H, H-2), 6.72 (m, 2H, H-3), 6.98 (m, 2H, H-3), 7.06 (m, 2H, H-3), 7.16-7.25 (m, 5H, H-3), 7.37 (m, 1H, H-3), 7.73 (m, 1H, H-3), 8.22 (m, 1H, H-4). ^{13}C NMR (100 MHz, CDCl$_3$): **δ** 30.9 (C-1), 31.6 (C-2), 42.0 (C-6), 107.8 (C-7), 111.2 (C-3), 114.8 (C-3), 118.8 (C-3), 119.8 (C-3), 120.7 (C-3), 122.2 (C-3), 123.3 (C-3), 127.2 (C-7), 127.7 (C-3), 127.9 (C-3), 136.1 (C-7), 142.4 (C-7), 148.5 (C-7), 148.6 (C-7), 153.6 (C-7), 170.8 (C-5). LC-MS *m/z* (% relative intensity): 384.2 [M-H]$^-$ (100). HR-ESI-MS (*m/z*): calcd for $C_{25}H_{22}NO_3$, 384.1605 found, 384.1605. IR (neat) $\tilde{v}_{max}$ (cm^{-1}): 3339 (O-H, N-H), 1733, 1702 (C=O). r$_f$ 0.14 (CH:EtOAc 7:3).

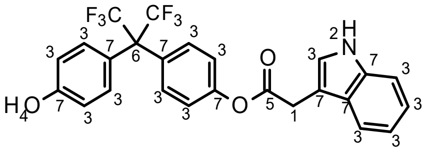

[4-[2,2,2-Trifluoro-1-(4-hydroxyphenyl)-1-(trifluoromethyl)ethyl]phenyl]-2-(1*H*-indole-3-yl) acetate (AUJ-140, 119b): Bisphenol AF (**95**, 203 mg, 0.60 mmol, 2.0 equiv.), *N',N'*-dicyclohexylcarbodiimid (DCC, 69 µL, 0.32 mmol, 1.1 equiv.) and *N,N*-dimethylpyridin-4-amin (DMAP, 3.7 mg, 0.03 mmol, 0.1 equiv.) were dissolved in DCM (1 mL). To this, a solution of indole-3-acetic acid (**135**, 53 mg, 0.30 mmol, 1.0 equiv.) in DCM (10 mL) and DMF (100 µL) was added dropwise via a syringe pump over 24 h. When the addition was complete, the mixture was stirred for further 24 h. Upon completion of the reaction, the mixture was filtered and evaporated to dryness. The crude product was purified by column chromatography (CH:EtOAc 9:1) and then suspended in EtOAc and filtered to remove excess of BPAF. The product [4-[2,2,2-trifluoro-1-(4-hydroxyphenyl)-1-(trifluoromethyl)ethyl]phenyl]-2-(1*H*-indole-3-yl)acetate (21 mg, 0.04 mmol, 14%) was obtained as a colorless oil: ^{1}H NMR (600 MHz, Acetone-d$_6$): **δ** 4.10 (s, 2H, H-1), 6.94 (m, 2H, H-3), 7.09 (m, 1H, H-3), 7.16 (m, 1H, H-3), 7.22-7.26 (m, 4H, H-3), 7.42-7.47 (m, 4H, H-3), 7.71 (m, 1H, H-3), 8.86 (s, 1H, H-4), 10.22 (s, 1H, H-2). ^{13}C NMR (150 MHz, Acetone-d$_6$): **δ** 32.6 (C-1), 108.7 (C-7), 113.0 (C-3), 116.4 (C-3), 120.1 (C-3), 120.6 (C-3), 123.1 (C-3), 123.2 (C-3), 124.9 (C-7), 125.6 (C-3), 129.1 (C-7), 132.2 (C-7), 132.8 (C-3), 132.9 (C-3), 138.3 (C-7), 153.3 (C-7), 159.8 (C-7), 171.4 (C-5). LC-MS *m/z* (% relative intensity): 492.2 [M-H]$^-$ (100). HR-ESI-MS (*m/z*): calcd for $C_{25}H_{16}F_6NO_3$, 492.1040 found, 492.1034. IR (neat) ṽ$_{max}$ (cm^{-1}): 3394 (O-H, N-H), 1742 (C=O), 1168 (CF$_3$). r$_f$ 0.13 (CH:EtOAc 7:3).

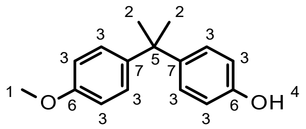

and

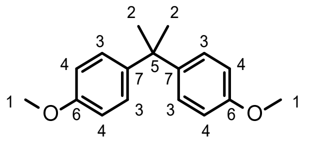

4-[1-(4-Methoxyphenyl)-1-methyl-ethyl]phenol and 1-methoxy-4-[1-(4-methoxyphenyl)-1-methyl-ethyl]benzene (AUJ-156, 136a, 136b): To a solution of Bisphenol A (**23**, 509 mg, 2.23 mmol, 1.0 equiv.) and potassium carbonate (311 mg, 2.25 mmol, 1.0 equiv.) in acetone (10 mL) was added dimethyl sulfate (250 µL, 2.64 mmol, 1.2 equiv.). The resulting mixture was heated to reflux for 7 h. Then, the solvent was removed under reduced pressure and the residue was diluted with EtOAc. The precipitate (unreacted starting material) was filtered off and the filtrate was concentrated *in vacuo* and subjected to column chromatography to yield 4-[1-(4-methoxyphenyl)-1-methylethyl]phenol (**136a**, 207 mg, 0.85 mmol, 38%) and 1-methoxy-4-[1-(4-methoxyphenyl)-1-methylethyl]benzene (**136b**, 260 mg, 1.01 mmol, 45%) as colorless oils: 4-[1-(4-methoxyphenyl)-1-methylethyl]phenol (**136a**): ^{1}H NMR (600 MHz, CDCl$_3$): **δ** 1.67 (s, 6H, H-2), 3.83 (s, 3H, H-1), 5.06 (s, 1H, H-10), 6.76 (m, 2H, H-3), 6.85 (m, 2H, H-3), 7.13 (m, 2H, H-3), 7.19 (m, 2H, H-3). ^{13}C NMR (150 MHz, CDCl$_3$): **δ** 31.0 (C-2), 41.7 (C-1), 55.2 (C-5), 113.3 (C-3), 114.7 (C-3), 127.7 (C-3), 127.9 (C-3), 143.2 (C-7), 143.3 (C-7), 153.3 (C-6), 157.3 (C-6). LC-MS *m/z* (% relative intensity): 241.2 [M-H]$^-$ (100), 483.3 [2M-H]$^-$ (0.5). HR-ESI-MS (*m/z*): calcd for $C_{16}H_{17}O_2$, 241.1234 found, 241.1233. IR (neat) ṽ$_{max}$ (cm^{-1}): 3380 (O-H). r$_f$ 0.31 (CH:EtOAc 9:1). 1-methoxy-4-[1-(4-methoxyphenyl)-1-methylethyl]benzene (**136b**): ^{1}H NMR (600 MHz, CDCl$_3$): **δ** 1.70 (s, 6H, H-2), 3.83 (s, 6H, H-1), 6.86 (m, 4H, H-4), 7.20 (m, 4H, H-3). ^{13}C NMR (150 MHz, CDCl$_3$): **δ** 31.0 (C-2), 41.6 (C-5), 55.2 (C-1), 113.25 (C-4), 127.7 (C-3), 143.1 (C-7), 157.4 (C-6). LC-MS *m/z* (% relative intensity): 279.1 [M+Na]$^+$ (14), 149.1 [M-Ph-OMe]$^+$ (23), 135.1 [M-Ph-OMe-CH$_2$]$^+$ (100). HR-ESI-MS (*m/z*): calcd for $C_{17}H_{20}NaO_2$, 279.1356 found, 279.1373. IR (neat) ṽ$_{max}$ (cm^{-1}): 2963 (C-H$_{arom.}$), 2834 (O-CH$_3$). r$_f$ 0.26 (CH:EtOAc 19:1).

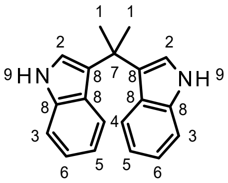

3-[1-(1*H*-Indole-3-yl)-1-methyl-ethyl]-1*H*-indole (AUJ-159, 151): To a solution of indole (**156**, 1.25 g, 10.67 mmol, 3.9 equiv.) and acetone (200 µL, 2.72 mmol, 1.0 equiv.) in ACN (10 mL), aluminium trichloride (60 mg, 0.45 mmol, 0.2 equiv.) was added. The mixture was stirred at room temperature for 20 min. Then, water was added and the aqueous layer was extracted with EtOAc (3 x 20 mL). The combined organic layers were washed with brine, dried over Na_2SO_4 and evaporated to dryness. The crude product was purified twice by column chromatography (CH:EtOAc 19:1 → 9:1, CH:EtOAc 19:1 → 8:2) to remove traces of indole completely. 3-[1-(1*H*-Indole-3-yl)-1-methyl-ethyl]-1*H*-indole (84 mg, 0.31 mmol, 11%) was afforded as a brown solid: ^{1}H NMR (400 MHz, $CDCl_3$): **δ** 2.00 (s, 6H, H-1), 6.99 (m, 2H, H-5/H-6), 7.04 (d, *J* = 2.44 Hz, 2H, H-2), 7.17 (m, 2H, H-5/H-6), 7.35 (m, 2H, H-3/H-4), 7.52 (m, 2H, H-3/H-4), 7.78 (bs, 2H, H-9). ^{13}C NMR (100 MHz, $CDCl_3$): **δ** 29.9 (C-1), 34.9 (C-7), 111.0 ((C-3/C-4), 118.6 (C-5/C-6), 120.5 (C-2), 121.2 (C-3/C-4), 121.3 (C-5/C-6), 125.4 (C-8), 126.3 (C-8), 137.0 (C-8). LC-MS *m/z* (% relative intensity): 275.2 $[M+H]^+$ (4), 158.1 $[M\text{-indole}]^+$ (100). HR-ESI-MS (*m/z*): calcd for $C_{19}H_{18}N_2Na$, 297.1362 found, 297.1354. IR (neat) $\tilde{\nu}_{max}$ (cm^{-1}): 3403, 3390 (N-H). r_f 0.46 (CH:EtOAc 8:2).

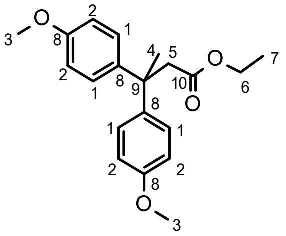

Ethyl 3,3-bis(4-methoxyphenyl)butanoate (AUJ-080, 165a): To a mixture of anisole (**164**, 1.8 mL, 16.48 mmol, 8.3 equiv.) and ethyl acetoacetate (**162b**, 250 µL, 1.98 mmol, 1.0 equiv.) cooled to 0 °C was added concentrated sulfuric acid (1.0 mL, 18.76 mmol, 9.5 equiv.) dropwise. The solution was stirred at room temperature for further 22h and was then poured on ice. The aqueous layer was extracted with diethyl ether (3 x 10 mL) and the combined organic layers were dried over Na_2SO_4 and concentrated under reduced pressure. The crude product (835.2 mg) were purified by column chromatography (CH:EtOAc 9:1) to yield ethyl 3,3-bis(4-methoxyphenyl) butanoate (354.1 mg, 1.08 mmol, 55%) as a colorless oil: ^{1}H NMR (600 MHz, $CDCl_3$): **δ** 1.04 (t, *J* = 7.14 Hz, 3H, H-7), 1.86 (s, 3H, H-4), 3.10 (s, 2H, H-5), 3.81 (s, 6H, H-3), 3.93 (q, *J* = 7.12 Hz, 2H, H-6), 6.84 (m, 4H, H-2), 7.14 (m, 4H, H-1). ^{13}C NMR (150 MHz, $CDCl_3$): **δ** 14.0 (C-7), 28.6 (C-4), 44.3 (C-9), 46.9 (C-5), 55.2 (C-3), 60.0 (C-6), 113.3 (C-2), 128.1 (C-1), 140.8 (C-8), 157.7 (C-8), 171.4 (C-10). LC-MS *m/z* (% relative intensity): 221.1222 [M-PhOMe]$^+$ (100), 346.2099 [M+NH$_4$]$^+$ (5), 351.1657 [M+Na]$^+$ (5). HR-ESI-MS (*m/z*): calcd for $C_{20}H_{24}NaO_4$, 351.1567 found, 351.1564. IR (neat) $\tilde{\nu}_{max}$ (cm^{-1}): 2835 (O-CH$_3$), 1726 (C=O). r_f 0.32 (CH:EtOAc 9:1).

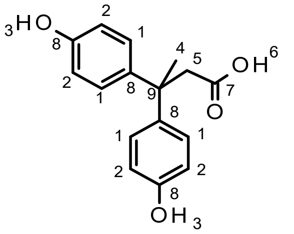

3,3-Bis(4-methoxyphenyl)butanoic acid (AUJ-081, 160): A solution of ethyl 3,3-bis(4-methoxyphenyl) butanoate (**AUJ-080**, **165a**, 314.0 mg, 0.96 mmol, 1.0 equiv.) in DCM (8 mL) was cooled to -78 °C. To this boron tribromide (2.90 mL, 2.90 mmol, 3.0 equiv.) was added dropwise and the reaction mixture was stirred at room temperature for 19h. The mixture was then cooled and ice was slowly added. The aqueous layer was extracted with EtOAc (3 x 20 mL) and the combined organic layers were washed with brine, dried over Na_2SO_4 and the solvent was evaporated under reduced pressure. The crude product was purified chromatographically (CH:EtOAc 3:1) to obtain 3,3-bis(4-methoxyphenyl)butanoic acid (198.5 mg, 0.73 mmol, 76%) as a light yellow oil: ^{1}H NMR (400 MHz, MeOD-D$_4$): **δ** 1.81 (s, 3H, H-4), 3.06 (s, 2H, H-5), 4.94 (s, 2H, H-3), 6.71 (m, 4H, H-2), 7.04 (m, 4H, H-1), 9.05 (s, 1H, H-6). ^{13}C NMR (100 MHz, MeOD-D$_4$): **δ** 29.0 (C-4), 44.9 (C-5), 47.6 (C-9), 115.5 (C-2), 129.0 (C-1), 141.1 (C-8), 155.9 (C-8), 175.4 (C-7). LC-MS *m/z* (% relative intensity): 271.1 [M-H]$^-$ (100), 543.3 [2M-H]$^-$ (24). HR-ESI-MS (*m/z*): calcd for $C_{16}H_{15}O_4$, 271.0976 found, 271.0976. IR (neat) $\tilde{\nu}_{max}$ (cm^{-1}): 3277 (O-H), 1701 (C=O). r_f 0.31 (CH:EtOAc 3:1).

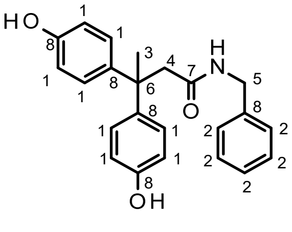

***N*-Benzyl-3,3-bis(4-hydroxyphenyl)butanamide (AUJ-135, 170):** To a solution of 3,3-bis(4-hydroxyphenyl)butanoic acid (**AUJ-081**, **160**, 79 mg, 0.29 mmol, 1.0 equiv.) and benzylamine (31.5 µL, 0.29 mmol, 1.0 equiv.) in DMF (5 mL) was added 1-[bis(dimethylamino)methylene]-1*H*-1,2,3-triazolo[4,5-*b*]pyridinium-3-oxide hexafluorophosphate (HATU, 121 mg, 0.32 mmol, 1.1 equiv.) and DIPEA (150 µL, 0.88 mmol, 3.1 equiv.) and the reaction mixture was stirred at room temperature for 15 h. Then, EtOAc was added and the organic layer was washed with 1M HCl. The aqueous layer was extracted with EtOAc (3 x 10 mL). The combined organic layers were washed with brine, dried over Na_2SO_4 and evaporated to dryness. The crude product was purified chromatographically (CH:EtOAc 1:1) to yield *N*-benzyl-3,3-bis(4-hydroxyphenyl)butanamide (80 mg, 0.22 mmol, 77%) as a light yellow solid: ^{1}H NMR (400 MHz, MeOH-d_4): **δ** 1.80 (s, 3H, H-3), 3.01 (s, 2H, H-4), 4.13 (s, 2H, H-5), 6.71 (m ,4H, H-1), 6.82 (m, 2H, H-2), 7.03 (m, 4H, H-1), 7.17 (m, 1H, H-2), 7.23 (m, 2H, H-2). ^{13}C NMR (100 MHz, MeOH-d_4): **δ** 29.6 (C-3), 43.9 (C-5), 45.8 (C-6), 49.2 (C-4), 115.7 (C-1), 127.8 (C-2), 128.2 (C-2), 129.2 (C-2), 129.3 (C-1), 139.3 (C-8), 141.4 (C-8), 156.3 (C-8), 173.9 (C-7). LC-MS *m/z* (% relative intensity): 362.2 $[M+H]^+$ (100). HR-ESI-MS (*m/z*): calcd for $C_{23}H_{23}NNaO_3$, 384.1568 found, 384.1570. IR (neat) $\tilde{\nu}_{max}$ (cm^{-1}): 3368 (O-H, N-H), 1611 (C=O). r_f 0.24 (CH:EtOAc 1:1).

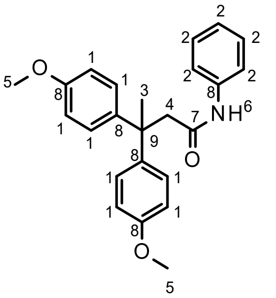

3,3-Bis(4-methoxyphenyl)-*N*-phenyl-butanamide (AUJ-132, 171): To a solution of 3,3-bis(4-methoxyphenyl)butanoic acid (side product of **AUJ-080**, **165b**, 200 mg, 0.67 mmol, 1.0 equiv.) and aniline (61 µL, 0.67 mmol, 1.0 equiv.) in DMF (6 mL) was added 1-[bis(dimethylamino)methylene]-1*H*-1,2,3-triazolo[4,5-*b*]pyridinium-3-oxide hexafluorophosphate (HATU, 285 mg, 0.75 mmol, 1.1 equiv.) and DIPEA (340 µL, 2.00 mmol, 3.0 equiv.) and the reaction mixture was stirred at room temperature for 16 h. Then, EtOAc was added and the organic layer was washed with 1M HCl. The aqueous layer was extracted with EtOAc (3 x 20 mL). The combined organic layers were washed with brine, dried over Na_2SO_4 and evaporated to dryness. The crude product was purified chromatographically (CH:EtOAc 8:2) to give 3,3-bis(4-methoxyphenyl)-*N*-phenyl-butanamide (205 mg, 0.55 mmol, 82%) as a colorless solid: ^{1}H NMR (600 MHz, $CDCl_3$): **δ** 1.82 (s, 3H, H-3), 3.17 (s, 2H, H-4), 3.83 (s, 6H, H-5), 6.33 (m, 1H, H-6), 6.90 (m, 2H, H-1), 7.04 (m, 1H, H-2), 7.08 (m, 2H, H-2), 7.22 (m, 6H, H-1, H-2). ^{13}C NMR (150 MHz, $CDCl_3$): **δ** 27.9 (C-3), 44.7 (C-9), 50.9 (C-4), 55.2 (C-5), 113.8 (C-1), 119.7 (C-2), 123.9 (C-2), 128.1 (C-1), 128.7 (C-2), 137.6 (C-8), 140.5 (C-8), 157.9 (C-8), 169.3 (C-7). LC-MS *m/z* (% relative intensity): 376.2 $[M+H]^+$ (100), 268.1 $[M\text{-}PhOMe]^+$ (32), 751.4 $[2M+H]^+$ (28). HR-ESI-MS (*m/z*): calcd for $C_{24}H_{25}NNaO_3$, 398.1727 found, 398.1726. IR (neat) $\tilde{\nu}_{max}$ (cm^{-1}): 3339 (N-H), 1658 (C=O). r_f 0.37 (CH:EtOAc 7:3).

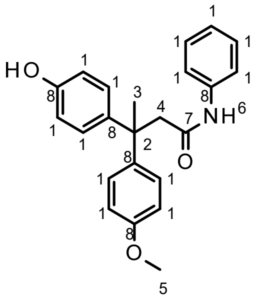

3-(4-Hydroxyphenyl)-3-(4-methoxyphenyl)-*N*-phenyl-butanamide (AUJ-133, 172): A solution of 3,3-bis(4-methoxyphenyl)-*N*-phenyl-butanamide (**AUJ-132**, **171**, 153 mg, 0.41 mmol, 1.0 equiv.) in DCM (10 mL) was cooled to -78 °C. Then, boron tribromide (1M in DCM, 1.2 mL, 1.2 mmol, 2.9 equiv.) was added dropwise and the mixture was stirred at room temperature for 40 h. Due to incomplete reaction another portion of boron tribromide (1M in DCM, 1.2 mL, 1.2 mmol, 2.9 equiv.) was added and the mixture was stirred for further 74 h. The mixture was then cooled in an ice bath and ice was slowly added. The aqueous layer was extracted with EtOAc (3 x 20 mL). The combined organic layers were washed with brine, dried over Na_2SO_4 and evaporated under reduced pressure. The crude product was purified by chromatography (CH:EtOAc 7:3) to afford 3-(4-hydroxyphenyl)-3-(4-methoxyphenyl)-*N*-phenyl-butanamide (20 mg, 0.05 mmol, 13%) as a light brown solid: ^{1}H NMR (400 MHz, $CDCl_3$): **δ** 1.78 (s, 3H, H-3), 3.16 (s, 2H, H-4), 3.82 (s, 3H, H-5), 6.28 (s, 1H, H-6), 6.83 (m, 2H, H-1), 6.88 (m, 2H, H-1), 7.04 (m, 3H, H-1), 7.13 (m, 2H, H-1), 7.21 (m, 4H, H-1). ^{13}C NMR (100 MHz, $CDCl_3$): **δ** 27.9 (C-3), 44.6 (C-2), 51.0 (C-4), 55.3 (C-5), 113.9 (C-1), 115.4 (C-1), 119.9 (C-1), 124.2 (C-1), 128.1 (C-1), 128.3 (C-1), 128.8 (C-1), 137.3 (C-8), 140.0 (C-8), 140.5 (C-8), 154.5 (C-8), 158.0 (C-8), 169.7 (C-7). LC-MS *m/z* (% relative intensity): 362.2 $[M+H]^+$ (100). HR-ESI-MS (*m/z*): calcd for $C_{23}H_{23}NNaO_3$, 384.1570 found, 384.1570. IR (neat) $\tilde{\nu}_{max}$ (cm^{-1}): 3345 (N-H), 3194 (O-H), 1647 (C=O). r_f 0.17 (CH:EtOAc 7:3).

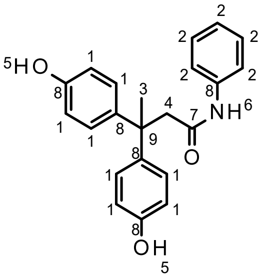

3,3-Bis(4-hydroxyphenyl)-*N*-phenyl-butanamide (AUJ-134, 173): To a solution of 3,3-bis(4-hydroxyphenyl)butanoic acid (**AUJ-080**, **160**, 79 mg, 0.29 mmol, 1.0 equiv.) and aniline (26.5 µL, 0.29 mmol, 1.0 equiv.) in DMF (5 mL) was added 1-[bis(dimethylamino)methylene]-1*H*-1,2,3-triazolo[4,5-*b*]pyridinium-3-oxide hexafluorophosphate (HATU, 122 mg, 0.32 mmol, 1.1 equiv.) and DIPEA (150 µL, 0.88 mmol, 3.1 equiv.) and the reaction mixture was stirred at room temperature for 15 h. Then, EtOAc was added and the organic layer was washed with 1M HCl. The aqueous layer was extracted with EtOAc (3 x 10 mL). The combined organic layers were washed with brine, dried over Na_2SO_4 and evaporated to dryness. The crude product was purified chromatographically (CH:EtOAc 1:1) to afford 3,3-bis(4-hydroxyphenyl)-*N*-phenyl-butanamide (56.1 mg, 0.16 mmol, 56%) as a light brown solid: ^{1}H NMR (400 MHz, Acetone-d$_6$): **δ** 1.85 (s, 3H, H-3), 3.15 (s, 2H, H-4), 6.75 (m, 4H, H-1), 6.98 (m, 1H, H-2), 7.10 (m, 4H, H-1), 7.19 (m, 2H, H-2), 7.38 (m, 2H, H-2), 8.34 (m, 2H, H-5). ^{13}C NMR (100 MHz, Acetone-d$_6$): **δ** 29.6 (C-3), 46.0 (C-9), 50.6 (C-4), 116.2 (C-1), 121.0 (C-2), 124.7 (C-2), 129.6 (C-1), 129.9 (C-2), 140.6 (C-8), 141.6 (C-8), 156.8 (C-8), 170.9 (C-7). LC-MS *m/z* (% relative intensity): 348.2 $[M+H]^+$ (100). HR-ESI-MS (*m/z*): calcd for $C_{22}H_{21}NNaO_3$, 370.1415 found, 370.1414. IR (neat) $\tilde{v}_{max}$ (cm^{-1}): 3324 (N-H), 1668 (C=O). r_f 0.18 (CH:EtOAc 1:1).

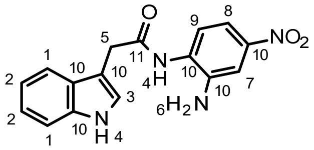

N-(2-Amino-4-nitrophenyl)-2-(1*H*-indole-3-yl)acetamide (DWE-005, 175a): Indole-3-acetic acid (**135**, 1.12 g, 6.41 mmol, 1.0 equiv.) and 4-nitrophenylenediamine (**174**, 1.00 g, 6.58 mmol, 1.0 equiv.) were dissolved in DMF (15 mL) and then 1-[bis(dimethylamino)methylene]-1*H*-1,2,3-triazolo[4,5-*b*]pyridinium-3-oxide hexafluorophosphate (HATU, 2.47 g, 6.50 mmol, 1.0 equiv.) and DIPEA (3.2 mL, 18.82 mmol, 2.9 equiv.) were added. The reaction mixture was stirred for 16 h at room temperature. Then, water was added and the aqueous layer was extracted with EtOAc (3 x 20 mL). The combined organic layers were washed with brine, dried over Na_2SO_4 and evaporated to dryness. The crude product was purified by column chromatography (DCM + 1% MeOH) to afford *N*-(2-amino-4-nitrophenyl)-2-(1*H*-indole-3-yl)acetamide (1.83 g, 5.90 mmol, 92%) as an orange solid: ^{1}H NMR (400 MHz, DMSO-d$_6$): **δ** 3.83 (s, 2H, H-5), 6.55 (s, 2H, H-6), 6.78 (d, *J* = 8.9 Hz, 1H, H-9), 7.01 (t, *J* = 7.3 Hz, 1H, H-2), 7.09 (t, *J* = 7.3 Hz, 1H, H-2), 7.31 (s, 1H, H-3), 7.37 (d, *J* = 8.0 Hz, 1H, H-1), 7.65 (d, *J* = 7.7 Hz, 1H, H-1), 7.84 (d, *J* = 8.9 Hz, 1H, H-8), 8.28 (s, 1H, H-7), 9.48 (s, 1H, H-4), 10.92 (s, 1H, H-4). ^{13}C NMR (400 MHz, DMSO-d$_6$): **δ** 33.1 (C-5), 108.4 (C-10), 111.3 (C-1), 113.6 (C-9), 118.4 (C-2), 118.6 (C-1), 120.8 (C-10), 121.0 (C-2), 121.8 (C-7), 122.5 (C-8), 124.0 (C-3), 127.2 (C-10), 135.5 (C-10), 136.1 (C-10), 148.7 (C-10), 170.4 (C-11). LC-MS *m/z* (% relative intensity): 311.1 $[M+H]^+$ (100), 621.2 $[2M+H]^+$ (12), 130.1 $[\text{indole-CH}_2]^+$ (81). HR-ESI-MS (*m/z*): calcd for $C_{16}H_{15}N_4O_3$, 311.1139 found, 311.1137. IR (neat) $\tilde{v}_{max}$ (cm^{-1}): 3384, 3336, 3262 (N-H), 1652 (C=O). r_f 0.21 (DCM + 1% MeOH).

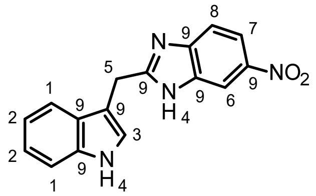

2-(1*H*-Indole-3-ylmethyl)-6-nitro-1*H*-benzimidazole (DWE-006, 176): *N*-(2-Amino-4-nitrophenyl)-2-(1*H*-indole-3-yl)acetamide (**DWE-005**, **175a**, 1.03 g, 3.33 mmol, 1.0 equiv.) was dissolved in glacial acetic acid (25 mL). In fractions of 5 mL volume, the mixture was heated to 120 °C in a microwave reactor for 30 min. The combined reaction mixtures were added to sat. $NaHCO_3$ solution. The aqueous layer was extracted with EtOAc (3 x 25 mL). The combined organic layers were washed with brine, dried over Na_2SO_4 and concentrated *in vacuo*. The crude product was purified by column chromatography (CH:EE 1:1) to yield 2-(1*H*-indole-3-ylmethyl)-6-nitro-1*H*-benzimidazole (704 mg, 2.41 mmol, 72%) as an orange solid: ^{1}H NMR (600 MHz, MeOD-d_4): **δ** 4.44 (s, 2H, H-5), 6.97 (t, *J* = 7.8 Hz, 1H, H-2), 7.10 (t, *J* = 7.6 Hz, 1H, H-2), 7.26 (s, 1H, H-3), 7.37 (d, *J* = 8.3 Hz, 1H, H-1), 7.41 (d, *J* = 7.9 Hz, 1H, H-1), 7.55 (d, *J* = 8.9 Hz, 1H, H-8), 8.11 (dd, *J* = 2.2 Hz, 8.9 Hz, 1H, H-7), 8.39 (d, *J* = 1.5 Hz, 1H, H-6). ^{13}C NMR (150 MHz, MeOD-d_4): **δ** 26.6 (C-5), 109.9 (C-9), 112.4 (C-1), 118.9 (C-6), 119.0 (C-1), 120.1 (C-2), 122.7 (C-2), 124.8 (C-3), 128.3 (C-9), 138.3 (C-9), 144.7 (C-9), 161.3 (C-9). LC-MS *m/z* (% relative intensity): 293.1 $[M+H]^+$ (100). HR-ESI-MS (*m/z*): calcd for $C_{16}H_{13}N_4O_2$, 293.1033 found, 293.1020. IR $\tilde{v}_{max}$ (cm^{-1}): 3384 (N-H), 2913(CH). r_f 0.09 (Chloroform + 2% MeOH).

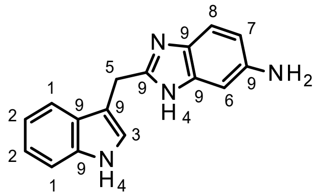

2-(1*H*-indole-3-ylmethyl)-3*H*-benzimidazole-5-amine (DWE-004, 177): 2-(1*H*-Indole-3-ylmethyl)-6-nitro-1*H*-benzimidazole (**DWE-006**, **176**, 683 mg, 2.34 mmol, 1.0 equiv.) was dissolved in EtOAc (50 mL) and 10% palladium on charcoal (193 mg, 0.18 mmol, 0.1 equiv.) was added. The flask was then purged with hydrogen (3 x). The reaction mixture was hydrogenated at 1 bar at room temperature for 4 days and was then directly applied to column chromatography (DCM:MeOH 9:1) to give 2-(1*H*-indole-3-ylmethyl)-3*H*-benzimidazole-5-amine (598 mg, 2.28 mmol, 98%) as a red solid: ^{1}H NMR (400 MHz, MeOD-d_4): **δ** 4.31 (s, 2H, H-5), 6.70 (dd, *J* = 2.2 Hz, 8.5 Hz, 1H, H-7), 6.84 (d, *J* = 2.2 Hz, 1H, H-6), 6.97 (t, *J* = 7.5 Hz, 1H, H-2), 7.09 (t, *J* = 7.6 Hz, 1H, H-2), 7.18 (s, 1H, H-3), 7.27 (d, *J* = 8.6 Hz, 1H, H-8), 7.36 (d, *J* = 8.2 Hz, 1H, H-1), 7.44 (d, *J* = 8.1 Hz, 1H, H-1). ^{13}C NMR (100 MHz, MeOD-d_4): **δ** 26.3 (C-3), 100.7 (C-6), 111.0 (C-9), 112.3 (C-1), 113.8 (C-7), 116.3 (C-8), 119.3 (C-1), 119.9 (C-2), 122.6 (C-2), 124.4 (C-3), 128.4 (C-9), 138.3 (C-9), 143.9 (C-9), 154.9 (C-9). LC-MS *m/z*

(% relative intensity): 263.1 $[M+H]^+$ (100), 146.1 [benzimidazole-CH_2]$^+$ (6). HR-ESI-MS (*m/z*): calcd for $C_{16}H_{15}N_4$, 263.1291 found, 263.1284. IR $\tilde{\nu}_{max}$ (cm^{-1}): 3096 (N-H). r_f 0.25 (DCM:MeOH 9:1).

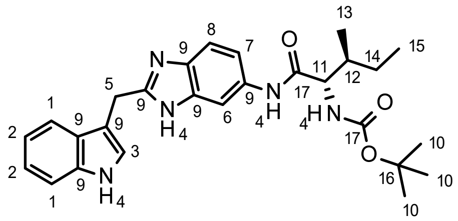

***tert*-Butyl *N*-[(1S,2S)-1-[[2-(1*H*-indole-3-ylmethyl)-3*H*-benzimidazole-5-yl]carbamoyl]-2-methyl-butyl]carbamate (GEI-001, 178):** To a solution of 2-(1*H*-indole-3-ylmethyl)-3*H*-benzimidazole-5-amine (**DWE-004**, **177**, 595 mg, 2.27 mmol, 1.0 equiv.) in DMF (16 mL) was added Boc-Ile-OH (571 mg, 2.42 mmol, 1.1 equiv.), 1-[bis(dimethylamino)methylene]-1*H*-1,2,3-triazolo[4,5-*b*]pyridinium-3-oxide hexafluorophosphate (HATU, 596 mg, 2.51 mmol, 1.1 equiv.) and DIPEA (1.2 mL, 6.82 mmol, 3.0 equiv.) subsequently. The reaction mixture was stirred for 20 h at room temperature. Then, sat. $NaHCO_3$ was added and the aqueous layer was extracted with EtOAc (3 x 20 mL). The combined organic layers were washed with brine, dried over Na_2SO_4 and evaporated under reduced pressure. The crude product was purified chromatographically (DCM + 1% MeOH → DCM + 1.5% MeOH) to afford *tert*-butyl *N*-[(1S,2S)-1-[[2-(1*H*-indole-3-ylmethyl)-3*H*-benzimidazole-5-yl]carbamoyl]-2-methyl-butyl]carbamate (1.00 g, 2.11 mmol, 93%) as a reddish solid: ^{1}H NMR (400 MHz, DMSO-d_6): **δ** 0.78-0.92 (m, 6H, H-13, H-15), 1.09-1.21 (m, 1H, H-14), 1.39 (s, 9H, H-10), 1.44-1.59 (m, 1H, H-14), 1.69-1.83 (m, 1H, H-12), 3.91-4.05 (m, 1H, H-11), 4.32 (s, 2H, H-5), 6.87 (s, 1H, H-4), 6.95 (t, *J* = 7.5 Hz, 1H, H-2), 7.07 (t, *J* = 7.5 Hz, 1H, H-2), 7.27 (d, *J* = 8.6 Hz, 1H, H-7), 7.31 (s, 1H, H-3), 7.37 (d, *J* = 8.2 Hz, 1H, H-1), 7.43 (d, *J* = 8.9 Hz, 1H, H-8), 7.46 (d, *J* = 8.4 Hz, 1H, H-1), 7.97 (s, 1H, H-6), 9.96 (s, 1H, H-4), 10.99 (s, 1H, H-4), 12.76 (s, 1H, H-4). ^{13}C NMR (100 MHz, DMSO-d_6): **δ** 10.8 (C-13/C-15), 15.3 (C-13/C-15), 24.6 (C-14), 24.9 (C-5), 28.1 (C-10), 36.4 (C-12), 59.4 (C-11), 78.0 (C-16), 109.1 (C-6), 111.4 (H-1), 114.8 (C-7/C-8), 118.3 (C-1), 118.5 (C-2), 121.1 (C-2), 123.8 (C-3), 123.9 (C-9), 126.8 (C-9), 133.7 (C-9), 136.2 (C-9), 154.2 (C-17), 155.4 (C-9), 170.5 (C-17). LC-MS *m/z* (% relative intensity): 476.3 $[M+H]^+$ (100), 951.5 $[2M+H]^+$ (14). HR-ESI-MS (*m/z*): calcd for $C_{27}H_{34}N_5O_3$, 476.2656 found, 476.2655. IR $\tilde{\nu}_{max}$ (cm^{-1}): 3398, 3269 (N-H), 1673 (C=O). r_f 0.09 (DCM + 1% MeOH).

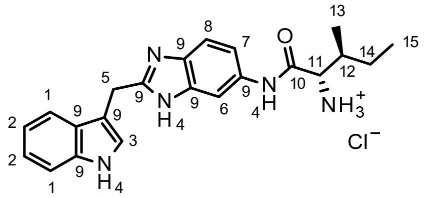

(2S,3S)-2-Amino-*N*-[2-(1*H*-indole-3-ylmethyl)-3*H*-benzimidazole-5-yl]-3-methylpentanamide hydrochloride (GEI-003, 94e): A solution of *tert*-butyl *N*-[(1S,2S)-1-[[2-(1*H*-indole-3-ylmethyl)-3*H*-benzimidazole-5-yl]carbamoyl]-2-methyl-butyl]carbamate (**GEI-001**, **178**, 99 mg, 0.21 mmol, 1.0 equiv.) in DCM (3.3 mL) was cooled to 0 °C. Then, trifluoroacetic acid (3.3 mL) and TIPS (0.17 mL, 0.83 mmol, 4.0 equiv.) were added slowly. After 1.5 h, sat. $NaHCO_3$ was added and the aqueous layer was extracted with EtOAc (3 x 10 mL). The combined organic layers were washed with brine, dried over Na_2SO_4 and evaporated to dryness. The crude product was purified by column chromatography to yield (2S,3S)-2-amino-*N*-[2-(1*H*-indole-3-ylmethyl)-3*H*-benzimidazole-5-yl]-3-methylpentanamide (**GEI-002**, 76 mg, 0.20 mg, 97%) as a brown solid: ^{1}H NMR (600 MHz, DMSO-d$_6$): **δ** 0.87 (t, *J* = 7.4 Hz, 3H, H-15), 0.93 (d, *J* = 6.8 Hz, 3H, H-13), 1.11-1.21 (m, 1H, H-14), 1.51-1.60 (m, 1H, H-14), 1.70-1.80 (m, 1H, H-12), 3.29 (d, *J* = 5.9 Hz, 1H, H-11), 4.26 (s, 2H, H-5), 6.94 (t, *J* = 7.5 Hz, 1H, H-2), 7.07 (t, *J* = 7.5 Hz, 1H, H-2), 7.22 (m, 1H, H-7), 7.29 (s, 1H, H-3), 7.37 (m, 2H, H-1, H-8), 7.48 (d, *J* = 7.9 Hz, 1H, H-1), 7.93 (s, 1H, H-6), 9.90 (s, 1H, H-4), 10.96 (s, 1H, H-4), 12.00 (s, 1H, H-4). ^{13}C NMR (150 MHz, DMSO-d$_6$): **δ** 11.3 (C-15), 15.6 (C-13), 23.9 (C-14), 25.4 (C-5), 38.1 (C-12), 59.4 (C-11), 109.9 (C-9), 111.3 (C-1, C-8), 118.4 (C-1, C-2), 121.0 (C-2), 123.6 (C-3), 126.9 (C-9), 136.2 (C-9). LCMS *m/z* (% relative intensity): 376.2 [M+H]$^+$ (100), 751.4 [2M+H]$^+$ (16). HR-ESI-MS (*m/z*): calcd for $C_{22}H_{26}N_5O$, 376.2132 found, 376.2123. IR $\tilde{v}_{max}$ (cm^{-1}): 3245 (N-H), 2962, 2917 (CH), 1672 (C=O). r$_f$ 0.03 (DCM + 4% MeOH). (2S,3S)-2-Amino-*N*-[2-(1*H*-indole-3-ylmethyl)-3*H*-benzimidazole-5-yl]-3-methylpentanamide (**GEI-002**, 684 mg, 1.82 mmol, 1.0 equiv.) was dissolved in methanol (5 mL) and 0.1M HCl (20 mL, 2.00 mmol, 1.1 equiv.) was added. The mixture was lyophilized and the procedure was repeated once. (2S,3S)-2-Amino-*N*-[2-(1*H*-indole-3-ylmethyl)-3*H*-benzimidazole-5-yl]-3-methyl-pentanamide hydrochloride (678 mg, 1.81 mmol, 99%) was obtained as a light brown solid: ^{1}H NMR (600 MHz, MeOD-d4): **δ** 1.02 (t, *J* = 7.4 Hz, 3H, H-15), 1.14 (d, *J* = 6.9 Hz, 3H, H-13), 1.27-1.38 (m, 1H, H-14), 1.57-1.60 (m, 1H, H-14), 2.07-2.15 (m, 1H, H-12), 4.02 (d, *J* = 6.0 Hz, 1H, H-11), 4.72 (s, 2H, H-5), 7.05 (t, *J* = 7.6 Hz, 1H, H-2), 7.17 (t, *J* = 7.5 Hz, 1H, H-2), 7.43 (d, *J* = 7.9 Hz, 1H, H-1), 7.44-7.48 (m, 2H, H-1, H-7), 7.66-7.71 (m, 2H, H-3, H-8), 8.32 (s, 1H, H-6). ^{13}C NMR (150 MHz, MeOD-d4): **δ** 11.6 (C-15), 15.3 (C-13), 24.1 (C-5), 25.4 (C-14), 38.2 (C-12), 59.7 (C-11), 105.7 (C-6), 106.1 (C-9), 112.9 (C-1/C-7), 115.2 (C-3/C-8), 118.5 (C-1), 120.3 (C-3/C-8), 120.7 (C-2), 123.2 (C-2), 126.1 (C-1/C-7), 127.8 (C-9), 129.1 (C-9), 132.7 (C-9), 137.6 (C-9), 138.4 (C-9), 155.9 (C-9), 168.5 (C-10). LCMS *m/z* (% relative intensity): 376.2 [M+H]$^+$ (100), 751.4 [2M+H]$^+$ (9). HR-ESI-MS (*m/z*): calcd for $C_{22}H_{26}N_5O$, 376.2132 found, 376.2132. IR ṽ$_{max}$ (cm^{-1}): 2920, 2852 (CH), 1680 (C=O).

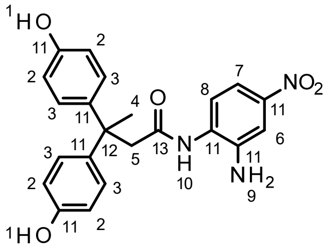

***N*-(2-Amino-4-nitrophenyl)-3,3-bis(4-hydroxyphenyl)butanamide (DWE-002, 180a):** To a solution of 3,3-bis(4-methoxyphenyl)butanoic acid (**AUJ-081**, **160**, 409 mg, 1.56 mmol, 1.0 equiv.), 4-nitrophenylenediamine (**174**, 240 mg, 1.56 mmol 1.0 equiv.) and 1-[bis(dimethylamino)methylene]-1*H*-1,2,3-triazolo[4,5-*b*]pyridinium-3-oxide hexafluorophosphate (HATU, 654 mg, 1.72 mmol, 1.1 equiv.) in DMF (12 mL) was added DIPEA (0.8 mL, 4.70 mmol, 3.1 equiv.). The reaction mixture was stirred at room temperature for 29 h. Then, sat. $NaHCO_3$ was added and the aqueous layer was extracted with DCM (3 x 50 mL). The combined organic layers were washed with brine, dried over Na_2SO_4 and evaporated under reduced pressure. The crude product was purified by column chromatography (DCM + 1% MeOH, then DCM + 4% MeOH) to afford *N*-(2-amino-4-nitrophenyl)-3,3-bis(4-hydroxyphenyl)butanamide (82 mg, 0.20 mmol, 13%) as a yellow solid: ^{1}H NMR (600 MHz, DMSO-d$_6$): **δ** 1.79 (s, 3H, H-4), 3.11 (s, 2H, H-5), 6.08 (s, 2H, H-1), 6.62-6.73 (m, 5H, H-3, H-8), 7.01 (m, 4H, H-2), 7.80 (d, *J* = 9.2 Hz, 1H, H-7), 7.92 (s, 1H, H-6), 8.88 (s, 1H, H-10), 9.17 (s, 2H, H-9). ^{13}C NMR (150 MHz, DMSO-d$_6$): **δ** 28.4 (C-4), 44.1 (C-12), 47.3 (C-5), 113.4 (C-8), 114.4 (C-3), 121.3 (C-6), 122.6 (C-7), 127.8 (C-2), 135.4 (C-11), 139.4 (C-11), 148.8 (C-11), 155.0 (C-11), 169.9 (C-13). LC-MS *m/z* (% relative intensity): 408.2 [M+H]$^+$ (100), 815.3 [2M+H] (18). HR-ESI-MS (*m/z*): calcd for $C_{22}H_{21}N_3NaO_5$, 430.1373 found, 430.1373. IR (neat) ṽ$_{max}$ (cm^{-1}): 3366 (O-H, N-H), 1637 (C=O). r$_f$ 0.10 (DCM +1% MeOH).

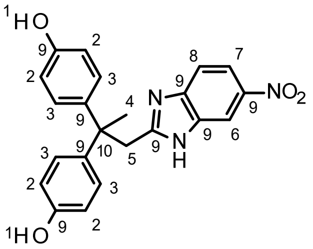

4-[1-(4-Hydroxyphenyl)-1-methyl-2-(6-nitro-1*H*-benzimidazole-2-yl)ethyl]phenol (DWE-009, 181): *N*-(2-Amino-4-nitrophenyl)-3,3-bis(4-hydroxyphenyl)butanamide (**DWE-002**, **180a**, 153 mg, 0.38 mmol, 1.0 equiv.) was dissolved in acetic acid (10 mL) and then reacted in a microwave for 30 min at 120 °C. The mixture was then added to sat. $NaHCO_3$ and the aqueous layer was extracted with EtOAc (3 x 20 mL). The combined organic layers were washed with brine, dried over Na_2SO_4 and evaporated *in vacuo*. The crude 4-[1-(4-hydroxyphenyl)-1-methyl-2-(6-nitro-1*H*-benzimidazole-2-yl)ethyl]phenol (131 mg, 0.34 mmol, 89%) was afforded as a colorless solid and used without further purification: ^{1}H NMR (600 MHz, MeOD-d_4): **δ** 1.80 (s, 3H, s, H-4), 3.68 (s, 2H, H-5), 6.69 (m, 4H, H-3), 7.01 (m, 4H, H-2), 7.51 (m, 1H, H-8), 8.12 (d, *J* = 8.8 Hz, 1H, H-7), 8.37 (s, 1H, H-6). ^{13}C NMR (150 MHz, MeOD-d_4): **δ** 29.3 (C-4), 42.9 (C-10), 47.0 (C-5), 115.9 (C-3), 129.3 (C-2), 140.7 (C-9), 144.6 (C-9), 156.6 (C-9). LC-MS *m/z* (% relative intensity): 390.1 $[M+H]^+$ (100). HR-ESI-MS (*m/z*): calcd for $C_{22}H_{20}N_3O_4$, 390.1448 found, 390.1449. IR (neat) $\tilde{v}_{max}$ (cm^{-1}): 3210 (O-H, N-H). r_f 0.17 (DCM + 4% MeOH).

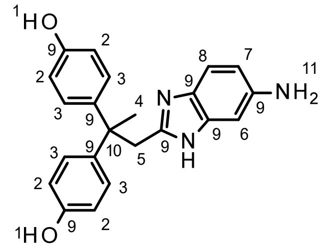

4-[2-(6-Amino-1*H*-benzimidazole-2-yl)-1-(4-hydroxyphenyl)-1-methylethyl]phenol (DWE-011, 182): 4-[1-(4-Hydroxyphenyl)-1-methyl-2-(6-nitro-1*H*-benzimidazole-2-yl)ethyl]phenol (**DWE-009**, **181**, 73 mg, 0.19 mmol, 1.0 equiv.) and 10% palladium on charcoal (21 mg, 0.02 mmol, 0.1 equiv.) were suspended in EtOAc (5 mL) and methanol (2 mL). The mixture was purged with hydrogen (3 x) and then hydrogenated at 1 bar for 26 h at room temperature. The crude product was purified chromatographically (DCM:MeOH 9:1) to yield 4-[2-(6-amino-1*H*-benzimidazole-2-yl)-1-(4-hydroxyphenyl)-1-methylethyl]phenol (37 mg, 0.10 mmol, 56%) as a colorless solid: ^{1}H NMR (400 MHz, DMSO-d_6): **δ** 1.79 (s, 3H, H-4), 3.42 (s, 2H, H-5), 6.41 (d, *J* = 8.5 Hz, 1H, H-7), 6.51 (s, 1H, H-6), 6.62 (m, 4H, H-3), 7.00 (m, 4H, H-2), 7.08 (d, *J* = 8.4 Hz, H-8), 9.17 (s, 2H, H-11). ^{13}C NMR (100 MHz, DMSO-d_6): **δ** 28.2 (C-4), 40.9 (C-5), 44.9 (C-10), 110.4 (H-7), 114.5 (C-3), 127.8 (C-2), 139.5 (C-9), 143.6 (C-9), 154.9 (C-9). LC-MS *m/z* (% relative intensity): 360.2 $[M+H]^+$ (100). HR-ESI-MS (*m/z*): calcd for $C_{22}H_{22}N_3O_2$, 360.1707 found, 360.1711. IR (neat) $\tilde{v}_{max}$ (cm^{-1}): 3257 (O-H, N-H), 2919 (CH). r_f 0.16 (DCM + 7% MeOH).

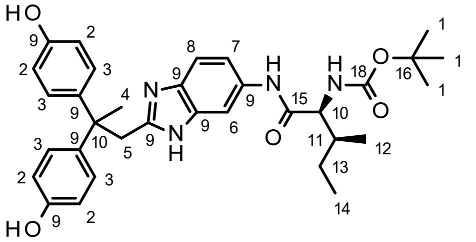

***tert*-Butyl N-[(1S,2S)-1-[[2-[2,2-bis(4-hydroxyphenyl)propyl]-3*H*-benzimidazole-5-yl]carbamoyl]-2-methylbutyl]carbamate (GEI-004, 183):** To a solution of 4-[2-(6-amino-1*H*-benzimidazole-2-yl)-1-(4-hydroxyphenyl)-1-methylethyl]phenol (**DWE-011**, **182**, 33 mg, 0.09 mmol, 1.0 equiv.), Boc-Ile-OH (24 mg, 0.10 mmol, 1.1 equiv.) and 1-[bis(dimethylamino)methylene]-1*H*-1,2,3-triazolo[4,5-*b*]pyridinium-3-oxide hexafluorophosphate (HATU, 38 mg, 0.10 mmol, 1.1 equiv.) in DMF (2.4 mL) was added DIPEA (50 µL, 0.29 mmol, 3.2 equiv.). The resulting mixture was stirred at room temperature for 19 h. Then, sat. $NaHCO_3$ was added and the aqueous layer was extracted with EtOAc (3 x 20 mL). The combined organic layers were washed with brine, dried over Na_2SO_4 and evaporated under reduced pressure. The crude product was purified chromatographically (DCM + 3% MeOH) to afford *tert*-butyl N-[(1S,2S)-1-[[2-[2,2-bis(4-hydroxyphenyl)propyl]-3*H*-benzimidazole-5-yl]carbamoyl]-2-methylbutyl]carbamate (38 mg, 0.07 mmol, 74%) as a brown solid: ^{1}H NMR (400 MHz, MeOD-d$_4$): **δ** 0.95 (t, J = 7.5 Hz, 3H, H-14), 1.01 (d, J = 6.5 Hz, 3H, H-12), 1.21-1.29 (m, 1H, H-13), 1.46 (s, 9H, H-1), 1.58-1.68 (m, 1H, H-13), 1.75 (s, 3H, H-4), 1.81-1.93 (m, 1H, H-11), 3.60 (s, 2H, H-5), 4.06 (d, J = 7.3 Hz, 1H, H-10), 6.69 (m, 4H, H-3), 7.02 (m, 4H, H-2), 7.21 (d, J = 8.9 Hz, 1H, H-7), 7.36 (d, J = 8.9 Hz, 1H, H-8), 7.81 (s, 1H, H-6). ^{13}C NMR (100 MHz, MeOD-d$_4$): **δ** 11.4 (C-14), 16.0 (C-12), 26.0 (C-13), 29.2 (C-1), 30.7 (C-4), 38.7 (C-11), 42.7 (C-5), 46.8 (C-17), 61.3 (C-10), 80.6 (C-16), 107.4 (C-6), 115.6 (C-8), 115.8 (C-3), 117.2 (C-7), 129.3 (C-2), 134.1 (C-9), 141.0 (C-9), 154.6 (C-18), 156.5 (C-9), 173.1 (C-15). LC-MS *m/z* (% relative intensity): 573.3 [M+H]$^+$ (100). HR-ESI-MS (*m/z*): calcd for $C_{33}H_{41}N_4O_5$, 573.3071 found, 573.3077. IR (neat) $\tilde{\nu}_{max}$ (cm^{-1}): 3293 (O-H, N-H), 2922 (CH), 1666 (C=O). r_f 0.19 (DCM + 7% MeOH).

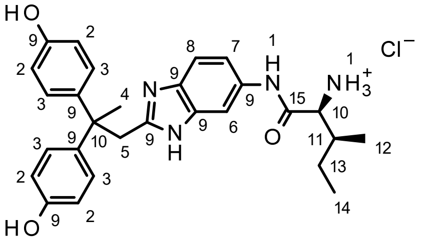

(2S,3S)-2-Amino-*N*-[2-[2,2-bis(4-hydroxyphenyl)propyl]-3*H*-benzimidazole-5-yl]-3-methyl-pentanamide hydrochloride (GEI-005, 179): To a solution of *tert*-butyl *N*-[(1S,2S)-1-[[2-[2,2-bis(4-hydroxyphenyl)propyl]-3*H*-benzimidazole-5-yl]carbamoyl]-2-methylbutyl]carbamate (**GEI-004**, **183**, 53 mg, 0.09 mmol, 1.0 equiv.) in DCM (2 mL) cooled to 0 °C was added TIPS (100 µL, 0.49 mmol, 5.3 equiv.) and trifluoroacetic acid (2 mL). The reaction mixture was stirred at 0 °C for 1.5 h. Then, sat. $NaHCO_3$ was added carefully and the aqueous layer was extracted with EtOAc (3 x 10 mL). The combined organic layers were washed with brine, dried over Na_2SO_4 and evaporated under reduced pressure. The crude TFA salt was dissolved in methanol (1 mL) and 0.1M HCl (1 mL, 0.10 mmol, 1.1 equiv.) was added. The mixture was then lyophilized and the procedure was repeated once. The product (2S,3S)-2-Amino-*N*-[2-[2,2-bis(4-hydroxyphenyl)propyl]-3*H*-benzimidazole-5-yl]-3-methyl-pentanamide hydrochloride (44 mg, 0.09 mmol, 99%) was afforded as a light brown solid: ^{1}H NMR (400 MHz, MeOD-d$_4$): **δ** 0.95 (t, *J* = 7.4 Hz, 3H, H-14), 0.99 (d, *J* = 6.9 Hz, 3H, H-12), 1.14-1.21 (m, 1H, H-13), 1.61-1.69 (m, 1H, H-13), 1.76 (s, 3H, H-4), 2.00-2.04 (m, 1H, H-11), 3.91 (s, 2H, H-5), 4.03-4.08 (m, 1H, H-10), 6.69 (m, 4H, H-3), 7.00 (m, 4H, H-2), 7.66 (d, *J* = 8.8 Hz, 1H, H-8), 7.71 (d, *J* = 8.8 Hz, 1H, H-7), 8.25 (s, 1H, H-6), 9.42 (s, 1H, H-1), 11.54 (s, 1H, H-1), 14.81 (s, 1H, H-1). ^{13}C NMR (100 MHz, MeOD-d$_4$): **δ** 11.0 (C-14), 14.5 (C-12), 24.1 (C-13), 28.5 (C-4), 36.2 (C-11), 45.4 (C-17), 57.0 (C-10), 115.0 (C-3), 127.7 (C-2), 136.0 (C-9), 137.3 (C-9), 137.4 (C-9), 155.6 (C-9), 167.2 (C-15). LC-MS *m/z* (% relative intensity): 473.3 $[M+H]^+$ (100), 945.5 $[M+H]^+$ (7). HR-ESI-MS (*m/z*): calcd for $C_{28}H_{33}N_4O_3$, 473.2547 found, 473.2547. IR (neat) $\tilde{\nu}_{max}$ (cm^{-1}): 2968 (O-H, N-H), 1688 (C=O). r_f 0.76 (DCM:MeOH 9:1).

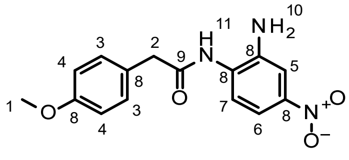

***N*-(2-Amino-4-nitrophenyl)-2-(4-methoxyphenyl)acetamide (AUJ-168, 189):** 4-Methoxyphenylacetic acid (**188**, 1.15 g, 6.89 mmol, 1.0 equiv.), 4-nitrophenylenediamine (**174**, 1.04 g, 6.81 mmol, 1.0 equiv.) and 1-[bis(dimethylamino)methylene]-1*H*-1,2,3-triazolo[4,5-*b*]pyridinium-3-oxide hexafluorophosphate (HATU, 2.91 g, 7.64 mmol, 1.1 equiv.) were dissolved in DCM (20 mL). DIPEA (3.5 mL, 20.58 mmol, 3.0 equiv.) were added and the reaction mixture was stirred for 2.5 h. The resulting precipitate was filtered off, washed with DCM and dried under high vacuum to afford *N*-(2-amino-4-nitrophenyl)-2-(4-methoxyphenyl)acetamide (1.34 g, 4.45 mmol, 65%) as a brown solid: ^{1}H NMR (400 MHz, DMSO-d$_6$): **δ** 3.63 (s, 2H, H-2), 3.74 (s, 3H, H-1), 6.50 (s, 2H, H-10), 6.77 (d, *J* = 9.04 Hz, 1H, H-7), 6.90 (m, 2H, H-4), 7.28 (m, 2H, H-3), 7.84 (dd, *J* = 9.05 Hz, *J* = 2.70 Hz 1H, H-6), 8.23 (d, *J* = 2.52 Hz, 1H, H-5), 9.39 (s, 1H, H-11). ^{13}C NMR (100 MHz, DMSO-d$_6$): **δ** 41.7 (C-2), 55.0 (C-1), 113.7 (C-7, C-4), 121.1 (C-5), 121.6 (C-8), 122.7 (C-6), 127.7 (C-8), 130.2 (C-3), 135.5 (C-8), 148.8 (C-8), 158.0 (C-8), 170.1 (C-9). LC-MS *m/z* (% relative intensity): 302.1 [M+H]$^+$ (100), 603.2 [2M+H]$^+$ (16), 121.1 [CH$_2$PhOMe]$^+$ (63). HR-ESI-MS (*m/z*): calcd for $C_{15}H_{15}N_3NaO_4$, 324.0955 found, 324.0956. IR (neat) $\tilde{v}_{max}$ (cm^{-1}): 3439, 3327 (N-H), 1632 (C=O). r$_f$ 0.33 (CH:EtOAc 1:2).

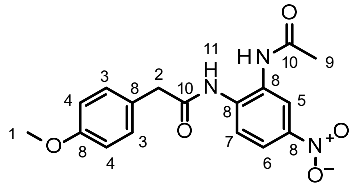

N-(2-Acetamido-4-nitro-phenyl)-2-(4-methoxyphenyl)acetamide (AUJ-172, 190): *N*-(2-Amino-4-nitro-phenyl)-2-(4-methoxyphenyl)acetamide (**AUJ-168**, **189**, 523 mg, 1.74 mmol, 1.0 equiv.) was suspended in acetic anhydride (5.0 mL) and stirred at room temperature for 24 h. The precipitate was then collected, washed with EtOAc and cyclohexane and dried under high vacuum to yield *N*-(2-acetamido-4-nitro-phenyl)-2-(4-methoxyphenyl)acetamide (483 mg, 1.41 mmol, 81%) as an off-white solid: ^{1}H NMR (600 MHz, DMSO-d$_6$): **δ** 2.14 (s, 3H, H-9), 3.70 (s, 2H, H-2), 3.75 (s, 3H, H-1), 6.92 (m, 2H, H-4), 7.29 (m, 2H, H-3), 7.95 (d, *J* = 9.01 Hz, 1H, H-7), 8.02 (dd, *J* = 9.03 Hz, *J* = 2.67 Hz, 1H, H-6), 8.47 (m, 1H, H-5), 9.67 (s, 1H, H-11), 9.72 (s, 1H, H-11). ^{13}C NMR (150 MHz, DMSO-d$_6$): **δ** 23.8 (C-9), 42.0 (C-2), 55.0 (C-1), 113.8 (C-4), 119.5 (C-5), 119.9 (C-6), 123.8 (C-7), 127.2 (C-8), 129.9 (C-8), 130.3 (C-3), 136.6 (C-8), 143.0 (C-8), 158.1 (C-8), 159.1 (C-10), 170.3 (C-10). LC-MS *m/z* (% relative intensity): 344.1 [M+H]$^+$ (100), 366.1 [M+Na]$^+$ (37), 709.2 [2M+Na]$^+$ (33). HR-ESI-MS (*m/z*): calcd for $C_{17}H_{17}N_3NaO_5$, 366.1060 found, 366.1062. IR (neat) $\tilde{v}_{max}$ (cm^{-1}): 3225, 3193 (N-H), 1677 (C=O). r$_f$ 0.22 (CH:EtOAc 1:2).

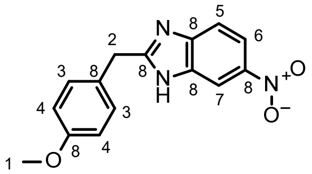

2-[(4-Methoxyphenyl)methyl]-6-nitro-1*H*-benzimidazole (AUJ-169, 191): *N*-(2-Acetamido-4-nitro-phenyl)-2-(4-methoxyphenyl)acetamide (**AUJ-172**, **190**, 329 mg, 0.96 mmol, 1.0 equiv.) and *para*-toluenesulfonic acid monohydrate (350 mg, 1.84 mmol, 1.9 equiv.) were dissolved in toluene (10 mL) and heated to reflux for 17 h. The solvent was then removed under reduced pressure and the residue was partitioned between EtOAc + 1% MeOH and water. The aqueous layer was extracted with EtOAc + 1% MeOH (3 x 20 mL). The combined organic layers were washed with brine, dried over Na_2SO_4 and the solvent was removed *in vacuo*. The crude 2-[(4-methoxyphenyl)methyl]-6-nitro-1*H*-benzimidazole (218 mg, 0.77 mmol, 80%), a light brown solid, was used without further purification: ^{1}H NMR (400 MHz, MeOD-d$_4$): **δ** 3.78 (s, 3H, H-1), 4.26 (s, 2H, H-2), 6.91 (m, 2H, H-4), 7.27 (m, 2H, H-3), 7.63 (d, *J* = 8.84 Hz, 1H, H-5), 8.17 (dd, *J* = 8.87 Hz, *J* = 2.20 Hz, 1H, H-6), 8.44 (d, *J* = 1.96 Hz, 1H, H-7). ^{13}C NMR (100 MHz, MeOD-d$_4$): **δ** 35.3 (C-2), 55.7 (C-1), 112.5 (C-7), 114.8 (C-5), 115.4 (C-4), 119.3 (C-6), 128.9 (C-8), 131.0 (C-3), 131.3 (C-8), 139.3 (C-8), 143.0 (C-8), 144.9 (C-8), 160.4 (C-8). LC-MS *m/z* (% relative intensity): 284.1 $[M+H]^+$ (100). HR-ESI-MS (*m/z*): calcd for $C_{15}H_{14}N_3O_3$, 284.1030 found, 284.1028. IR (neat) $\tilde{\nu}_{max}$ (cm^{-1}): 2929 (N-H). r_f 0.35 (CH:EtOAc 1:1).

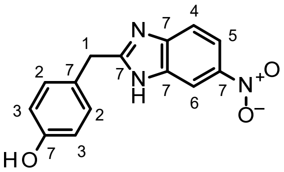

4-[(6-Nitro-1*H*-benzimidazole-2-yl)methyl]phenol (AUJ-183, 192): To a solution of 2-[(4-methoxyphenyl)methyl]-6-nitro-1*H*-benzimidazole (**AUJ-169**, **191**, 21 mg, 66 µmol, 1.0 equiv.) in DCM (2.0 mL) cooled to 0 °C was added dropwise a 1M solution of boron tribromide in DCM (130 µL, 130 µmol, 2.0 equiv.). The resulting mixture was stirred at room temperature for 21 h. Then, ice was added and the aqueous layer was extracted with EtOAc (3 x 20 mL). The combined organic layers were washed with brine, dried over Na_2SO_4 and evaporated to dryness. The crude product (19 mg) was purified by column chromatography (CH:EtOAc 2:1 → 1:1) to afford 4-[(6-nitro-1*H*-benzimidazole-2-yl)methyl]phenol (17 mg, 62 µmol, 93%) as a light brown solid: ^{1}H NMR (400 MHz, Acetone-d$_6$): **δ** 4.25 (s, 2H, H-1), 6.80 (m, 2H, H-3), 7.20 (m, 2H, H-2), 7.64 (d, *J* = 8.84 Hz, 1H, H-4), 8.10 (dd, *J* = 8.84 Hz, *J* = 2.20 Hz, 1H, H-5), 8.43 (m, 1H, H-6). ^{13}C NMR (100 MHz, Acetone-d$_6$): **δ** 36.0 (C-1), 113.2 (C-6), 115.6 (C-4), 116.7 (C-7), 117.1 (C-3), 119.0 (C-5), 127.3 (C-7), 128.6 (C-7), 131.6 (C-2), 131.9 (C-7), 144.7 (C-7), 148.1 (C-7), 160.9 (C-7). LC-MS *m/z* (% relative intensity): 268.1 [M-H]$^-$ (100). HR-ESI-MS (*m/z*): calcd for $C_{14}H_{10}N_3O_3$, 268.0728 found, 268.0726. IR (neat) $\tilde{\nu}_{max}$ (cm^{-1}): 3282 (O-H). r_f 0.44 (CH:EtOAc 1:2).

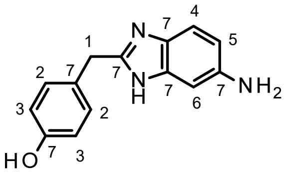

4-[(6-Amino-1*H*-benzimidazole-2-yl)methyl]phenol (AUJ-185, 193): 4-[(6-Nitro-1*H*-benzimidazole-2-yl)methyl]phenol (**AUJ-183**, **192**, 106 mg, 394 µmol, 1.0 equiv.) and 10% palladium on charcoal (48 mg, 45 µmol, 0.1 equiv.) were suspended in methanol (10.0 mL). The mixture was purged with hydrogen (3 x) and then stirred at room temperature for 4.5 h. The suspension was then filtered through a pad of celite. The filtrate was concentrated *in vacuo* to afford 4-[(6-amino-1*H*-benzimidazole-2-yl)methyl]phenol (80 mg, 334 µmol, 85%) as a light brown solid: ^{1}H NMR (400 MHz, MeOD-d$_4$): **δ** 4.07 (s, 2H, H-1), 6.72 (m, 1H, H-5), 6.76 (m, 2H, H-3), 6.86 (d, *J* = 1.92 Hz, 1H, H-6), 7.10 (m, 2H, H-2), 7.28 (d, *J* = 8.52 Hz, 1H, H-4). ^{13}C NMR (100 MHz, MeOD-d$_4$): **δ** 34.8 (C-1), 100.3 (C-6), 114.4 (C-5), 116.2 (C-4), 116.6 (C-3), 128.5 (C-7), 130.8 (C-2), 132.9 (C-7), 138.7 (C-7), 144.6 (C-7), 154.2 (C-7), 157.5 (C-7). LC-MS *m/z* (% relative intensity): 240.1 [M+H]$^+$ (100). HR-ESI-MS (*m/z*): calcd for $C_{14}H_{14}N_3O$, 240.1131 found, 240.1130. IR (neat) $\tilde{\nu}_{max}$ (cm^{-1}): 3323, 2919 (N-H, O-H). r_f 0.08 (Chloroform + 5% MeOH).

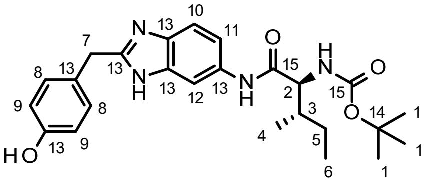

***tert*-Butyl-*N*-[(1S,2S)-1-[[2-[(4-hydroxyphenyl)methyl]-3*H*-benzimidazole-5-yl]carbamoyl]-2-methyl-butyl]carbamate (AUJ-186, 194):** 4-[(6-Amino-1*H*-benzimidazole-2-yl)methyl]phenol (**AUJ-185**, **193**, 80 mg, 0.33 mmol, 1.0 equiv.), Boc-Ile-OH (89 mg, 0.36 mmol, 1.1 equiv.) and 1-[bis(dimethylamino)methylene]-1*H*-1,2,3-triazolo[4,5-*b*]pyridinium-3-oxide hexafluorophosphate (HATU, 188 mg, 0.49 mmol, 1.5 equiv.) were dissolved in DMF (3.0 mL). Then, DIPEA (170 µL, 1.00 mmol, 3.0 equiv.) was added and the mixture was stirred at room temperature for 19.5 h. Sat. $NaHCO_3$ was added and the aqueous layer was extracted with EtOAc (3 x 15 mL). The combined organic layers were washed with brine, dried over Na_2SO_4 and concentrated under reduced pressure. The crude product was purified by column chromatography (Chloroform + 2-5% MeOH) to afford *tert*-butyl-*N*-[(1S,2S)-

1-[[2-[(4-hydroxyphenyl)methyl]-3*H*-benzimidazole-5-yl]carbamoyl]-2-methyl-butyl]carbamate (44 mg, 0.10 mmol, 29%) as an off-white solid: ^{1}H NMR (600 MHz, MeOD-d$_4$): **δ** 0.95 (t, *J* = 7.47 Hz, 3H, H-6), 1.01 (d, *J* = 6.84 Hz, 3H, H-4), 1.26 (m, 1H, H-5), 1.45 (s, 9H, H-1), 1.63 (m, 1H, H-5), 1.87 (m, 1H, H-3), 4.08 (m, 1H, H-2), 4.10 (s, 2H, H-7), 6.76 (m, 2H, H-9), 7.13 (m, 2H, H-8), 7.26 (m, 1H, H-11), 7.43 (m, 1H, H-10), 7.90 (s, 1H, H-12). ^{13}C NMR (150 MHz, MeOD-d$_4$): **δ** 11.4 (C-6), 16.0 (C-4), 26.0 (C-5), 28.7 (C-1), 35.3 (C-7), 38.6 (C-3), 61.2 (C-2), 80.6 (C-14), 107.6 (C-12), 115.8 (C-10), 116.5 (C-9), 117.3 (C-11), 128.8 (C-13), 130.8 (C-8), 130.9 (C-13), 131.1 (C-13), 134.2 (C-13), 156.5 (C-15), 157.5 (C-13), 157.9 (C-13), 173.1 (C-15). LC-MS *m/z* (% relative intensity): 453.2 [M+H]$^+$ (100), 905.5 [2M+H]$^+$ (28). HR-ESI-MS (*m/z*): calcd for $C_{25}H_{33}N_4O_4$, 453.2496 found, 453.2513. IR (neat) $\tilde{\nu}_{max}$ (cm^{-1}): 3205, 2963, 2919 (N-H, O-H). r$_f$ 0.49 (Chloroform +5% MeOH).

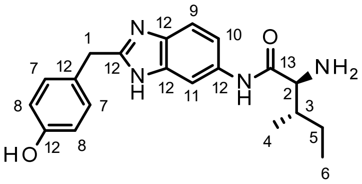

(2S,3S)-2-Amino-*N*-[2-[(4-hydroxyphenyl)methyl]-3*H*-benzimidazole-5-yl]-3-methylpentanamide (AUJ-193, 187): *tert*-Butyl-*N*-[(1S,2S)-1-[[2-[(4-hydroxyphenyl)methyl]-3*H*-benzimidazole-5-yl]carbamoyl]-2-methylbutyl]carbamate (**AUJ-186**, **194**, 37 mg, 82 µmol, 1.0 equiv.) was dissolved in DCM and cooled to 0 °C. Then, tri*iso*propylsilane (80 µL, 0.39 mmol, 4.8 equiv.) and trifluoroacetic acid (500 µL, 6.53 mmol, 79.9 equiv.) were added dropwise. The resulting mixture was stirred at 0 °C for 2 h. Then, the solvent was removed under reduced pressure and the residue was subjected to column chromatography (Chloroform + 5-10% MeOH + 0.1% TEA) to yield (2S,3S)-2-amino-*N*-[2-[(4-hydroxyphenyl)methyl]-3*H*-benzimidazole-5-yl]-3-methyl-pentanamide (18 mg, 51 µmol, 62%) as a colorless solid: ^{1}H NMR (600 MHz, MeOD-d$_4$): **δ** 0.97 (t, *J* = 7.44 Hz, 3H, H-6), 1.04 (d, *J* = 6.84 Hz, 3H, H-4), 1.27 (m, 1H, H-5), 1.65 (m, 1H, H-5), 1.86 (m, 1H, H-3), 3.40 (d, *J* = 5.88 Hz, 1H, H-2), 4.12 (s, 2H, H-1), 6.76 (m, 2H, H-8), 7.14 (m, 2H, H-7), 7.27 (m, 1H, H-10), 7.46 (d, *J* = 8.64 Hz, 1H, H-9), 7.93 (m, 1H, H-11). ^{13}C NMR (150 MHz, MeOD-d$_4$): **δ** 11.9 (C-6), 16.1 (C-4), 25.5 (C-5), 35.3 (C-1), 40.5 (C-3), 61.4 (C-2), 116.6 (C-8), 117.2 (C-10), 128.9 (C-12), 130.8 (C-7), 134.2 (C-12), 156.6 (C-12), 157.5 (C-12), 175.3 (C-13). LC-MS *m/z* (% relative intensity): 353.2 [M+H]$^+$ (100), 705.4 [2M+H]$^+$ (13), 375.2 [M+Na]$^+$ (4). HR-ESI-MS (*m/z*): calcd for $C_{20}H_{25}N_4O_2$, 353.1972 found, 353.1974. IR (neat) $\tilde{\nu}_{max}$ (cm^{-1}): 2926 (N-H, O-H), 1669 (C=O). r$_f$ 0.24 (Chloroform + 10% MeOH + 0.1% TEA).

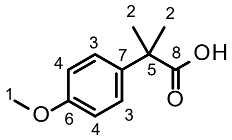

2-(4-Methoxyphenyl)-2-methyl-propanoic acid (AUJ-158, 195): To a solution of diisopropylamine (3.30 mL, 23.48 mmol, 3.8 equiv.) in THF (20 mL) cooled to -10 °C was added a 2.5M solution of *n*-BuLi in hexane (9.5 mL, 23.75 mmol, 3.8 equiv.). After stirring for 15 min, 4-methoxyphenylacetic acid (**188**, 1.03 g, 6.17 mmol, 1.0 equiv.) was added in small portions. The mixture was stirred at -10 °C for further 30 min. Then, iodomethane (2.30 mL, 36.78 mmol, 6.0 equiv.) was added and the reaction mixture was allowed to warm up to room temperature over night. After stirring for 19 h, sat. NH_4Cl was added and the aqueous layer was extracted with DCM (3 x 30 mL). The combined organic layers were washed with brine, dried over Na_2SO_4 and concentrated under reduced pressure. The crude product was purified by column chromatography (DCM:MeOH 50:1) to afford 2-(4-methoxyphenyl)-2-methyl-propanoic acid (275 mg, 1.42 mmol, 23%) as a colorless solid: ^{1}H NMR (600 MHz, $CDCl_3$): **δ** 1.61 (s, 6H, H-2), 3.83 (s, 3H, H-1), 6.90 (m, 2H, H-4), 7.36 (m, 2H, H-3). ^{13}C NMR (150 MHz, $CDCl_3$): **δ** 26.3 (C-2), 45.5 (C-5), 55.2 (C-1), 113.8 (C-4), 127.0 (C-3), 136.0 (C-7), 158.4 (C-6), 183.1 (C-8). LC-MS *m/z* (% relative intensity): 193.1 $[M-H]^-$. HR-ESI-MS (*m/z*): calcd for $C_{11}H_{13}O_3$, 193.0870 found, 193.0869. IR (neat) $\tilde{v}_{max}$ (cm^{-1}): 2976 (O-H), 1692 (C=O). r_f 0.45 (CH:EtOAc 7:3).

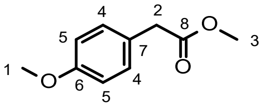

Methyl 2-(4-methoxyphenyl)acetate (AUJ-161, 197): A solution of 4-methoxyphenylacetic acid (**188**, 5.18 g, 31.18 mmol, 1.0 equiv.) in methanol (50 mL) was cooled to 0 °C prior to slowly adding thionyl chloride (5.0 mL, 68.92 mmol, 2.2 equiv.). The mixture was then heated to reflux for 4 h. The solvent was removed under reduced pressure and the residue was partitioned between EtOAc and sat. $NaHCO_3$. The aqueous layer was extracted with EtOAc (3 x 20 mL). The combined organic layers were washed with brine, dried over Na_2SO_4 and evaporated to dryness. The crude methyl 2-(4-methoxyphenyl)acetate (5.55 g, 30.82 mmol, 99%), obtained as a colorless oil, was used without further purification: ^{1}H NMR (400 MHz, $CDCl_3$): **δ** 3.59 (s, 2H, H-2), 3.71 (s, 3H, H-3), 3.81 (s, 3H, H-1), 6.89 (m, 2H, H-5), 7.22 (m, 2H, H-4). ^{13}C NMR (100 MHz, $CDCl_3$): **δ** 40.2 (C-2), 51.9 (C-3), 55.2 (C-1), 114.0 (C-5), 126.0 (C-7), 130.2 (C-4), 158.7 (C-6), 172.3 (C-8). LC-MS *m/z* (% relative intensity): 121.1 $[M-CO_2Me]^+$ (100). HR-APCI-MS (*m/z*): calcd for $C_{10}H_{12}O_3$, 180.0786 found, 180.0819. IR (neat) $\tilde{v}_{max}$ (cm^{-1}): 1733 (C=O). r_f 0.45 (CH:EtOAc 8:2).

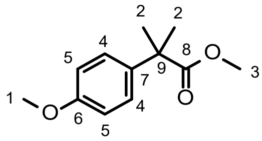

Methyl 2-(4-methoxyphenyl)-2-methyl-propanoate (AUJ-162, 198): To a solution of methyl 2-(4-methoxyphenyl)acetate (**AUJ-161**, **197**, 2.40 g, 13.32 mmol, 1.0 equiv.) in THF (50 mL) cooled to -78 °C was added iodomethane (2.50 mL, 39.98 mmol, 3.0 equiv.). Then, KO^tBu (4.92 g, 43.87 mmol, 3.3 equiv.) was added portionwise and the mixture was stirred at -78 °C for further 30 min before removing the cooling bath. The mixture was stirred for another 3.5 h at room temperature. Then, water was added and the aqueous layer was extracted with EtOAc (3 x 30 mL). The combined organic layers were washed with brine, dried over Na_2SO_4 and concentrated under reduced pressure. The crude product (3.00 g) was purified chromatographically (CH:EtOAc 9:1) to give methyl 2-(4-methoxyphenyl)-2-methylpropanoate (2.44 g, 11.72 mmol, 88%) as a colorless oil: ^{1}H NMR (600 MHz, $CDCl_3$): **δ** 1.59 (s, 6H, H-2), 3.67 (s, 3H, H-3), 3.82 (s, 3H, H-1), 6.89 (m, 2H, H-5), 7.29 (m, 2H, H-4). ^{13}C NMR (150 MHz, $CDCl_3$): **δ** 26.6 (C-2), 45.8 (C-9), 52.1 (C-3), 55.2 (C-1), 113.7 (C-5), 126.7 (C-4), 136.8 (C-7), 158.3 (C-6), 177.4 (C-8). LC-MS *m/z* (% relative intensity): 209.1 $[M+H]^+$ (6), 149.1 $[M-CO_2Me]^+$ (100), 231.1 $[M+Na]^+$ (2). HR-ESI-MS (*m/z*): calcd for $C_{12}H_{16}NaO_3$, 231.0992 found, 231.0990. IR (neat) $\tilde{v}_{max}$ (cm^{-1}): 1728 (C=O). r_f 0.61 (CH:EtOAc 8:2).

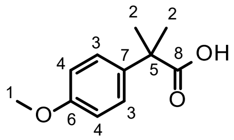

2-(4-Methoxyphenyl)-2-methylpropanoic acid (AUJ-165, 195): To a solution of methyl 2-(4-methoxyphenyl)-2-methyl-propanoate (**AUJ-162**, **198**, 5.38 g, 25.82 mmol, 1.0 equiv.) in a mixture of methanol/THF 3:2 (50 mL) a 8M solution of NaOH in water (26.0 mL, 208.19 mmol, 8.1 equiv.) was added slowly. The mixture was stirred at room temperature for 17.5 h. The solvent was removed under reduced pressure and the residue was diluted with water. The aqueous layer was washed with DCM and then acidified with conc. HCl. The precipitate was extracted with EtOAc (3 x 30 mL). The combined organic layers were washed with brine, dried over Na_2SO_4 and evaporated *in vacuo*. The crude 2-(4-methoxyphenyl)-2-methylpropanoic acid (4.69 g, 24.14 mmol, 94%), obtained as a colorless solid, was used without further purification: ^{1}H NMR (600 MHz, Acetone-d_6): **δ** 1.56 (s, 6H, H-2), 3.79 (s, 3H, H-1), 6.90 (m, 2H, H-4), 7.36 (m, 2H, H-3). ^{13}C NMR (150 MHz, Acetone-d_6): **δ** 27.7 (C-2), 46.7 (C-5), 56.1 (C-1), 115.1 (C-4), 128.3 (C-3), 138.6 (C-7), 160.0 (C-6), 178.9 (C-8). LC-MS *m/z* (% relative intensity): 193.1 $[M-H]^-$ (100). HR-ESI-MS (*m/z*): calcd for $C_{11}H_{13}O_3$, 193.0870 found, 193.0872. IR (neat) $\tilde{v}_{max}$ (cm^{-1}): 2953 (O-H), 1677 (C=O). r_f 0.42 (CH:EtOAc 7:3).

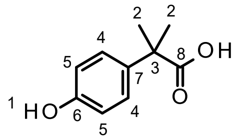

2-(4-Hydroxyphenyl)-2-methylpropanoic acid (AUJ-163, 196): To a solution of 2-(4-methoxyphenyl)-2-methylpropanoic acid (**AUJ-165**, **195**, 619 mg, 3.19 mmol, 1.0 equiv.) in DCM (10 mL) cooled to -78 °C was added a 1M boron tribromide solution in DCM (4.80 mL, 4.80 mmol, 1.5 equiv.) over 30 min. The mixture was then allowed to warm up to 0 °C and stirred for another 1.5 h. Then water was added and the aqueous layer was washed with DCM (3 x 20 mL) and then extracted with EtOAc (3 x 20 mL). The EtOAc layers were combined, dried over Na_2SO_4 and the solvent was removed to afford 2-(4-hydroxyphenyl)-2-methylpropanoic acid (361 mg, 2.00 mmol, 63%) as a colorless solid: ^{1}H NMR (600 MHz, Acetone-d_6): **δ** 1.54 (s, 6H, H-2), 6.81 (m, 2H, H-5), 6.26 (m, 2H, H-4), 8.18 (s, 1H, H-1). ^{13}C NMR (150 MHz, Acetone-d_6): **δ** 27.8 (C-2), 46.7 (C-3), 116.5 (C-5), 128.3 (C-4), 137.5 (C-7), 157.5 (C-6), 178.9 (C-8). LC-MS *m/z* (% relative intensity): 179.1 $[M+H]^+$ (33), 201.1 $[M+Na]^+$ (18). HR-ESI-MS (*m/z*): calcd for $C_{10}H_{11}O_3$, 179.0714 found, 179.0708. IR (neat) $\tilde{\nu}_{max}$ (cm^{-1}): 3195 (O-H), 1669 (C=O). r_f 0.6 (CH:EtOAc 1:1).

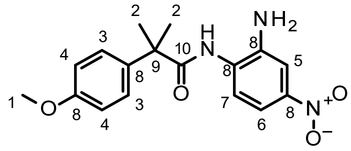

***N*-(2-Amino-4-nitrophenyl)-2-(4-methoxyphenyl)-2-methylpropanamide (AUJ-166, 200):** 2-(4-methoxyphenyl)-2-methylpropanoic acid (**AUJ-165**, **195**, 630 mg, 3.24 mmol, 1.0 equiv.), 4-nitrophenylenediamine (**174**, 511 mg, 3.34 mmol, 1.0 equiv.) and 1-[bis(dimethylamino)methylene]-1*H*-1,2,3-triazolo[4,5-*b*]pyridinium-3-oxide hexafluorophosphate (HATU, 1.31 g, 3.44 mmol, 1.1 equiv.) were dissolved in DMF (10 mL). DIPEA (1.70 mL, 10.00 mmol, 3.1 equiv.) was added and the reaction mixture was stirred at room temperature for 19 h. Then, sat. $NaHCO_3$ was added and the aqueous layer was extracted with EtOAc (3 x 20 mL). The combined organic layers were washed with brine, dried over Na_2SO_4 and evaporated to dryness. The crude product was purified by column chromatography (CH:EtOAc 9:1 → 8:2) to afford *N*-(2-amino-4-nitrophenyl)-2-(4-methoxyphenyl)-2-methylpropanamide (728 mg, 2.21 mmol, 68%) as a yellow solid: ^{1}H NMR (400 MHz, $CDCl_3$): **δ** 1.90 (s, 6H, H-2), 3.86 (s, 3H, H-1), 7.01 m(, 2H, H-4), 7.42 (dd, J = 8.36 Hz, J = 4.54 Hz, 1H, H-6), 7.52 (m, 2H, H-3), 8.41 (dd, J = 8.38 Hz, J = 1.42 Hz, 1H, H-7), 8.73 (dd, J = 4.50 Hz, J = 1.83 Hz, 1H, H-5). ^{13}C NMR (100 MHz, $CDCl_3$): **δ** 26.8 (C-2), 45.9 (C-9), 55.3 (C-1), 114.2 (C-4), 120.7 (C-6), 127.0 (C-3), 129.3 (C-7), 134.0 (C-8), 134.9 (C-8), 140.6 (C-8), 151.7 (C-5), 159.0 (C-8), 172.9 (C-10). LC-MS *m/z* (% relative intensity): 313.1 $[M-NH_2]^+$ (20), 149.1

$[C(CH_3)_2PhOMe]^+$ (100). HR-ESI-MS (*m/z*): calcd for $C_{17}H_{18}N_3O_4$, 328.1303 found, 328.1303. IR (neat) $\tilde{v}_{max}$ (cm^{-1}): 2953 (N-H), 1678 (C=O). r_f 0.14 (CH:EtOAc 8:2).

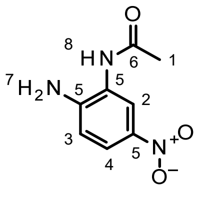

***N*-(2-Amino-5-nitro-phenyl)acetamide (AUJ-184, 203):** To a solution of 4-nitrophenylenediamine (**174**, 507 mg, 3.31 mmol, 1.0 equiv.) in DCM (10 mL) was added acetic anhydride (350 µL, 3.70 mmol, 1.1 equiv.) and TEA (920 µL, 6.64 mmol, 2.0 equiv.) at 0 °C. The reaction mixture was stirred at room temperature for 4 days. The precipitate was filtered off, washed with cyclohexane and dried under high vacuum to give *N*-(2-amino-5-nitro-phenyl)acetamide (277 mg, 1.42 mmol, 43%) as a red-brown solid: ^{1}H NMR (600 MHz, Acetone-d$_6$): **δ** 2.14 (s, 3H, H-1), 5.89 (s, 2H, H-7), 6.36 (m, 1H, H-3), 7.37 (m, 1H, H-4), 7.96 (s, 1H, H-2), 8.73 (s, 1H, H-8). ^{13}C NMR (100 MHz, Acetone-d$_6$): **δ** 24.4 (C-1), 115.0 (C-3), 122.1 (C-2), 123.4 (C-4), 123.5 (C-5), 137.5 (C-5), 149.7 (C-5), 170.1 (C-6). LC-MS *m/z* (% relative intensity): 196.1 $[M+H]^+$ (69), 218.1 $[M+Na]^+$ (36), $[M-Ac]^+$ (100). HR-ESI-MS (*m/z*): calcd for $C_8H_{10}N_3O_3$, 196.0717 found, 196.0716. IR (neat) $\tilde{v}_{max}$ (cm^{-1}): 3306, 3204 (N-H). r_f 0.05 (CH:EtOAc 1:1).

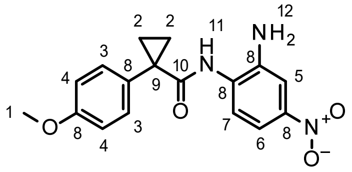

***N*-(2-Amino-4-nitrophenyl)-1-(4-methoxyphenyl)cyclopropanecarboxamide (AUJ-191, 206):** 1-(4-Methoxyphenyl)-1-cyclopropancarboxylic acid (**205**, 1.00 g, 5.20 mmol, 1.0 equiv.), 4-nitrophenylenediamine (**174**, 792 mg, 5.17 mmol, 1.0 equiv.) and 1-[bis(dimethylamino)methylene]-1*H*-1,2,3-triazolo[4,5-*b*]pyridinium-3-oxide hexafluorophosphate (HATU, 2.22 g, 5.83 mmol, 1.1 equiv.) were dissolved in DCM (50 mL) and DIPEA (2.50 mL, 14.44 mmol, 2.8 equiv.) were added. The reaction mixture was then stirred at room temperature for 19.5 h. Then, sat. $NaHCO_3$ was added and the aqueous layer was extracted with EtOAc (3 x 50 mL). The combined organic layers were washed with brine, dried over Na_2SO_4 and evaporated under reduced pressure. The crude product was purified by column chromatography (CH:EtOAc 2:1) to yield *N*-(2-amino-4-nitrophenyl)-1-(4-methoxyphenyl)cyclopropanecarboxamide (1.44 g, 4.41 mmol, 85%) as a light yellow solid: ^{1}H NMR (600 MHz, Acetone-d$_6$): **δ** 1.12 (m, 2H, H-2), 1.59 (m, 2H, H-2), 3.82 (s, 3H, H-1), 5.53 (bs, 2H, H-12), 6.86 (d, *J* = 9.00 Hz, 1H, H-7), 6.97 (m, 2H, H-4), 7.55 (m, 2H, H-3), 7.77 (bs, 1H, H-11), 7.87 (m, 1H, H-6), 8.07 (m, 1H, H-5). ^{13}C NMR (150 MHz, Acetone-d$_6$): **δ** 17.3 (C-2), 31.3 (C-9), 56.3 (C-1), 115.9 (C-4), 116.2 (C-7), 124.3 (C-6), 124.4 (C-8), 124.5 (C-5), 133.7(C-3), 139.1 (C-8), 146.1 (C-8), 151.1 (C-8), 161.0 (C-8), 174.6 (C-10), . LC-MS *m/z* (% relative intensity): 328.1 $[M+H]^+$ (100), 655.2 $[2M+H]^+$ (15). HR-ESI-MS (*m/z*): calcd for $C_{17}H_{18}N_3O_4$, 328.1292 found, 328.1296. IR (neat) $\tilde{\nu}_{max}$ (cm^{-1}): 3440, 3388, 3329, 3216 (N-H), 1679 (C=O). r_f 0.21 (CH:EtOAc 2:1).

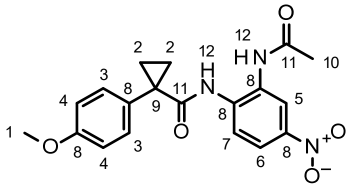

***N*-(2-Acetamido-4-nitrophenyl)-1-(4-methoxyphenyl)cyclopropanecarboxamide (AUJ-192, 207):** *N*-(2-Amino-4-nitrophenyl)-1-(4-methoxyphenyl)cyclopropanecarboxamide (**AUJ-191**, **206**, 1.42 g, 4.32 mmol, 1.0 equiv.) was dissolved in acetic anhydride (15 mL) and the mixture was stirred at room temperature for 23 h. Then, water was added and the aqueous layer was extracted with EtOAc (3 x 50 mL). The combined organic layers were washed with brine, dried over Na_2SO_4 and evaporated to dryness. The crude product was purified chromatographically (CH:EtOAc 1:1) to afford *N*-(2-acetamido-4-nitrophenyl)-1-(4-methoxyphenyl)cyclopropanecarboxamide (1.21 g, 3.27 mmol, 76%) as a colorless solid: ^{1}H NMR (400 MHz, CDCl$_3$): **δ** 1.24 (m, 2H, H-2), 1.71 (m, 2H, H-2), 2.03 (s, 3H, H-10), 3.85 (s, 3H, H-1), 6.97 (m, 2H, H-4), 7.41 (m, 2H, H-3), 7.60 (d, *J* = 8.92 Hz, 1H, H-7), 7.65 (bs, 1H, H-12), 7.93 (dd, *J* = 8.92 Hz, *J* = 2.56 Hz, 1H, H-6), 8.22 (d, *J* = 1.80 Hz, 1H, H-5), 8.44 (bs, 1H, H-12). ^{13}C NMR (100 MHz, CDCl$_3$): **δ** 17.2 (C-2), 23.7 (C-10), 30.3 (C-9), 55.3 (C-1), 114.8 (C-4), 119.8 (C-5), 120.8 (C-6), 124.8 (C-7), 129.9 (C-8), 130.5 (C-8), 132.2 (C-3), 135.9 (C-8), 144.5 (C-8), 159.7 (C-8), 169.0 (C-11), 174.7 (C-11). LC-MS *m/z* (% relative intensity): 370.1 $[M+H]^+$ (100), 392.1 $[M+Na]^+$ (16), 761.3 $[2M+Na]^+$ (22), 147.1 $[C(c\text{-}propyl)\text{-}PhOMe]^+$ (84). HR-ESI-MS (*m/z*): calcd for $C_{19}H_{19}N_3NaO_5$, 392.1217 found, 392.1216. IR (neat) $\tilde{\nu}_{max}$ (cm^{-1}): 3388, 3302 (N-H), 1687, 1669 (C=O). r_f 0.20 (CH:EtOAc 1:1).

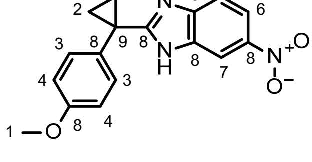

2-[1-(4-Methoxyphenyl)cyclopropyl]-6-nitro-1*H*-benzimidazole (AUJ-194, 208): *N*-(2-Acetamido-4-nitrophenyl)-1-(4-methoxyphenyl)cyclopropanecarboxamide (**AUJ-192**, **207**, 1.07 g, 2.90 mmol, 1.0 equiv.) and *para*-toluenesulfonic acid monohydrate (1.15 g, 6.06 mmol, 2.1 equiv.) were dissolved in toluene (50 mL) and heated to reflux for 18.5 h. The solvent was then removed under reduced pressure and the resulting residue was partitioned between water and EtOAc. The aqueous layer was extracted with EtOAc (3 x 40 mL). The combined organic layers were washed with brine, dried over Na_2SO_4 and evaporated *in vacuo*. The crude product was purified by column chromatography (CH:EtOAc 8:2) to give 2-[1-(4-methoxyphenyl) cyclopropyl]-6-nitro-1*H*-benzimidazole (742 mg, 2.40 mmol, 83%) as a light yellow solid: ^{1}H NMR (400 MHz, Acetone-d$_6$): **δ** 1.43 (m, 2H, H-2), 1.81 (m, 2H, H-2), 3.82 (s, 3H, H-1), 6.95 (m, 2H, H-4), 7.45 (m, 2H, H-3), 7.54 (bs, 1H, H-5), 8.06 (dd, *J* = 8.86 Hz, *J* = 2.18 Hz, 1H, H-6), 8.31 (bs, 1H, H-7). ^{13}C NMR (100 MHz, Acetone-d$_6$): **δ** 19.1 (C-2), 26.3 (C-9), 56.3 (C-1), 115.8 (C-4), 118.8 (C-6), 133.2 (C-3), 133.4 (C-8), 144.5 (C-8), 160.9 (C-8). LC-MS *m/z* (% relative intensity): 310.1 $[M+H]^+$ (100). HR-ESI-MS (*m/z*): calcd for $C_{17}H_{16}N_3O_3$, 310.1186 found, 310.1185. IR (neat) $\tilde{v}_{max}$ (cm^{-1}): 3245 (N-H). r_f 0.26 (CH:EtOAc 2:1).

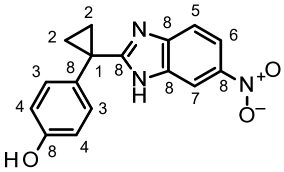

4-[1-(6-Nitro-1*H*-benzimidazole-2-yl)cyclopropyl]phenol (AUJ-195, 209): To a solution of 2-[1-(4-methoxyphenyl)cyclopropyl]-6-nitro-1*H*-benzimidazole (**AUJ-194**, **208**, 60 mg, 194 µmol, 1.0 equiv.) in DCM (5.0 mL) cooled to 0 °C was slowly added a 1M solution of boron tribromide in DCM (400 µL, 400 µmol, 2.1 equiv.) and the resulting mixture was stirred at 0 °C for 3 h. Then, the mixture was added to an ice-cold sat. solution of $NaHCO_3$. The aqueous layer was extracted with EtOAc (3 x 15 mL). The combined organic layers were washed with brine, dried over Na_2SO_4 and concentrated under reduced pressure. The crude product was purified by column chromatography (CH:EtOAc 2:1) to afford 4-[1-(6-nitro-1*H*-benzimidazole-2-yl)cyclopropyl]phenol (47 mg, 159 µmol, 82%) as a light brown solid: ^{1}H NMR (600 MHz, Acetone-d$_6$): **δ** 1.43 (m, 2H, H-2), 1.80 (m, 2H, H-2), 6.88 (m, 2H, H-4), 7.36 (m, 2H, H-3), 7.55 (d, *J* = 8.88 Hz, 1H, H-5), 8.06 (dd, *J* = 8.80 Hz, *J* = 2.18 Hz, 1H, H-6), 8.32 (d, *J* = 2.10 Hz, 1H, H-7). ^{13}C NMR (150 MHz, Acetone-d$_6$): **δ** 19.1 (C-2), 26.3 (C-1), 112.5 (C-7), 115.6 (C-5), 117.3 (C-4), 118.8 (C-6), 132.1 (C-8), 133.2 (C-3), 144.4 (C-8), 158.7 (C-8), 165.8 (C-8). LC-MS *m/z* (% relative intensity): 294.1 $[M-H]^-$ (100). HR-ESI-MS (*m/z*): calcd for $C_{16}H_{12}N_3O_3$, 294.0884 found, 294.0885. IR (neat) $\tilde{v}_{max}$ (cm^{-1}): 3238 (N-H, O-H). r_f 0.49 (CH:EtOAc 1:1).

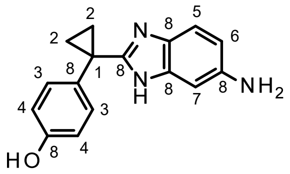

4-[1-(6-Amino-1*H*-benzimidazole-2-yl)cyclopropyl]phenol (AUJ-197, 210a): 4-[1-(6-Nitro-1*H*-benzimidazole-2-yl)cyclopropyl]phenol (**AUJ-195**, **209**, 47 mg, 159 µmol, 1.0 equiv.) and 10% palladium on charcoal (18 mg, 17 µmol, 0.1 equiv.) were suspended in methanol. The resulting mixture was purged with hydrogen (3 x) and then stirred at room temperature for 1.5 h. The suspension was filtered through a pad of celite which was thoroughly rinsed with methanol. The filtrate was concentrated *in vacuo* to give 4-[1-(6-amino-1*H*-benzimidazole-2-yl)cyclopropyl]phenol (42 mg, 158 µmol, 99%) as a colorless solid: ^{1}H NMR (600 MHz, MeOD-d$_4$): **δ** 1.33 (m, 2H, H-2), 1.59 (m, 2H, H-2), 6.69 (dd, *J* = 8.55 Hz, *J* = 2.07 Hz, 1H, H-6), 6.82 (m, 3H, H-4, H-7), 7.24 (m, 3H, H-3, H-5). ^{13}C NMR (150 MHz, MeOD-d$_4$): **δ** 16.9 (C-2), 25.3 (C-1), 100.4 (C-7), 114.1 (C-6), 116.0 (C-5), 116.6 (C-4), 131.7 (C-3), 144.2 (C-8), 157.9 (C-8). LC-MS *m/z* (% relative intensity): 264.2 [M-H]$^-$ (100). HR-ESI-MS (*m/z*): calcd for $C_{16}H_{14}N_3O$, 264.1142 found, 264.1141. IR (neat) $\tilde{v}_{max}$ (cm^{-1}): 3328-2920 (N-H, O-H). r_f 0.09 (chloroform + 5% MeOH).

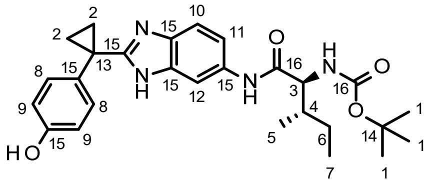

***tert*-Butyl-*N*-[(1S,2S)-1-[[2-[1-(4-hydroxyphenyl)cyclopropyl]-3*H*-benzimidazole-5-yl]carbamoyl]-2-methyl-butyl]carbamate (AUJ-198, 211a):** 4-[1-(6-Amino-1*H*-benzimidazole-2-yl)cyclopropyl]phenol (**AUJ-197**, **210a**, 40 mg, 0.15 mmol, 1.0 equiv.), Boc-Ile-OH (42 mg, 0.17 mmol, 1.1 equiv.) and 1-[bis(dimethylamino)methylene]-1*H*-1,2,3-triazolo[4,5-*b*]pyridinium-3-oxide hexafluorophosphate (HATU, 79 mg, 0.21 mmol, 1.4 equiv.) were dissolved in DMF (2.0 mL). To this, DIPEA (80 µL, 0.47 mmol, 3.1 equiv.) was added and the resulting mixture was stirred for 15 h at room temperature. The crude product was purified by column chromatography (chloroform + 2-5% MeOH) to yield *tert*-butyl-*N*-[(1S,2S)-1-[[2-[1-(4-hydroxyphenyl)cyclopropyl]-3*H*-benzimidazole-5-yl]carbamoyl]-2-methylbutyl]carbamate (30 mg, 63 µmol, 42%) as a colorless solid: ^{1}H NMR (400 MHz, MeOD-d$_4$): **δ** 0.95 (m, 3H, H-7), 1.01 (m, 3H, H-5), 1.25 (m, 1H, H-6), 1.35 (m, 2H, H-2), 1.46 (s, 9H, H-1), 1.63 (m, 3H, H-2, H-6), 1.86 (m, 1H, H-4), 4.06 (m, 1H, H-3), 6.81 (m, 2H, H-9), 7.24 (m, 1H, H-11), 7.27 (m, 2H, H-8), 7.38 (d, *J* = 8.60 Hz, 1H, H-10), 7.83 (m, 1H, H-12),. ^{13}C NMR (100 MHz, MeOD-d$_4$): **δ** 11.4 (C-7), 16.0 (C-5), 17.1 (C-2), 26.0 (C-6), 28.7 (C-1), 38.6 (C-4), 61.3 (C-3), 80.6 (C-14), 107.6 (C-10/C-12), 115.6 (C-10/C-12), 116.6 (C-), 117.2 (C-11), 123.0 (C-15), 129.8 (C-15), 131.9 (C-8), 133.0 (C-15), 134.0 (C-15), 157.9 (C-16), 161.0 (C-15), 173.0 (C-16), . LC-MS *m/z* (% relative intensity): 479.2 $[M+H]^+$ (100), 957.5 $[2M+H]^+$ (16). HR-ESI-MS (*m/z*): calcd for $C_{27}H_{35}N_4O_4$, 479.2653 found, 479.2664. IR (neat) $\tilde{v}_{max}$ (cm^{-1}): 3395 (N-H), 2920 (O-H), 1633 (C=O). r_f 0.17 (Chloroform + 5% MeOH).

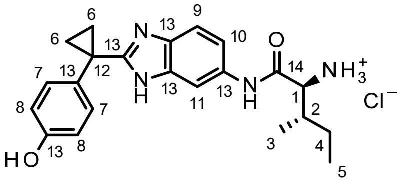

(2S,3S)-2-Amino-*N*-[2-[1-(4-hydroxyphenyl)cyclopropyl]-3*H*-benzimidazole-5-yl]-3-methyl-pentanamide hydrochloride (AUJ-199, 204a): *tert*-Butyl-*N*-[(1S,2S)-1-[[2-[1-(4-hydroxyphenyl)cyclopropyl]-3*H*-benzimidazole-5-yl]carbamoyl]-2-methylbutyl]carbamate (**AUJ-198**, **211a**, 25 mg, 52 µmol, 1.0 equiv.) was dissolved in DCM (2.0 mL) and cooled to 0 °C. Then, triisopropylamine (50 µL, 244 µmol, 4.7 equiv.) and trifluoroacetic acid (500 µL, 653 µmol, 125.0 equiv.) were added dropwise and the resulting mixture was stirred at 0 °C for 2.5 h. The solvent was evaporated to afford the crude TFA-salt which was dissolved in methanol (500 µL) and 0.1M HCl (1000 µL, 100 µmol, 1.9 equiv.) and the mixture was lyophilized to afford the corresponding hydrochloride. The procedure was repeated once to yield (2S,3S)-2-amino-*N*-[2-[1-(4-hydroxyphenyl)cyclopropyl]-3*H*-benzimidazole-5-yl]-3-methyl-pentanamide hydrochloride (24 mg, 52 µmol, 100%) as a colorless solid: ^1H NMR (600 MHz, MeOD-d_4): **δ** 1.02 (m, 3H, H-5), 1.13 (m, 3H, H-3), 1.31 (m, 1H, H-4), 1.68 (m, 1H, H-4), 1.77 (m, 2H, H-6), 1.88 (m, 2H, H-6), 2.08 (m, 1H, H-2), 3.93 (m, 1H, H-1), 6.91 (m, 2H, H-8), 7.39 (m, 2H, H-7), 7.59 (m, 1H, H-9/C-10), 7.63 (m, 1H, H-9/H-10), 8.26 (m, 1H, H-11). ^{13}C NMR (150 MHz, MeOD-d_4): **δ** 11.5 (C-5), 15.2 (C-3), 19.5 (C-6), 25.4 (C-4), 38.2 (C-2), 59.7 (C-1), 105.6 (C-11), 114.9 (C-9/C-10), 117.3 (C-8), 120.0 (C-9/C-10), 128.8 (C-13), 129.3 (C-13), 132.6 (C-7), 137.4 (C-13), 159.4 (C-13), 160.0 (C-13), 168.4 (C-14). LC-MS *m/z* (% relative intensity): 379.2 $[M+H]^+$ (100), 757.4 $[2M+H]^+$ (30). HR-ESI-MS (*m/z*): calcd for $C_{22}H_{27}N_4O_2$, 379.2129 found, 379.2128. IR (neat) $\tilde{v}_{max}$ (cm^{-1}): 3384 (N-H), 2916 (O-H), 1624 (C=O).

6.3. Synthesis of ligands to bind to the MIA protein

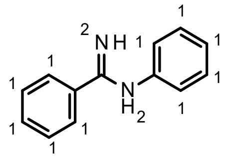

***N*-Phenylbenzamidine (AUJ-110, 230):** In a bulb suitable for Kugelrohr distillation, aniline (**228**, 180 µL, 1.97 mmol, 1.0 equiv.) and benzonitrile (**229**, 200 µL, 1.96 mmol, 1.0 equiv.) were mixed and aluminium trichloride (264.7 mg, 1.99 mmol, 1.0 equiv.) was added portionswise. The mixture was then heated to 200 °C for 30 min. After cooling down to room temperature, the residue was dissolved in ethyl acetate, filtered and the solvent was removed under reduced pressure. The crude product (137.7 mg) was purified by column chromatography (CH:EtOAc 7:3 + 0.1% triethylamine) yielding *N*-phenylbenzamidine (137.2 mg, 0.7 mmol, 36%) as a colorless solid: ^{1}H NMR (400 MHz, DMSO-d$_6$): **δ** 6.21 (bs, 2H, H-2), 6.87 (bs, 2H, H-1), 6.99 (t, *J* = 7.28 Hz, 1H, H-1), 7.32 (t, *J* = 7.62 Hz, 2H, H-1), 7.45 (m, 3H, H-1), 7.97 (m, 2H, H-1). ^{13}C NMR (100 MHz, DMSO-d$_6$): **δ** 121.5 (C-1), 121.8 (C-1), 127.0 (C-1), 128.0 (C-1), 129.2 (C-1), 130.0 (C-1). LC-MS *m/z* (% relative intensity): 197.1 [M+H]$^+$ (100). HR-ESI-MS (*m/z*): calcd for $C_{13}H_{13}N_2$, 197.1073 found, 197.1072. IR (neat) $\tilde{\nu}_{max}$ (cm^{-1}): 3345 (N-H), 1614 (-CN$_2$). r$_f$ 0.20 (CH:EtOAc 7:3 + 0.1% triethylamine).

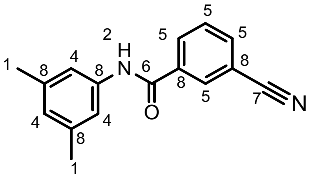

3-Cyano-*N*-(3,5-dimethylphenyl)benzamide (AUJ-113, 232): To a solution of 3-cyanobenzoic acid (**234**, 93.1 mg, 0.63 mmol, 1.1 equiv.), 3,5-dimethylaniline (**233**, 70 µL, 0.56 mmol, 1.0 equiv.), DIPEA (120 µL, 0.71 mmol, 1.3 equiv.) and hydroxybenzotriazole hydrate (94.4 mg, 0.62 mmol, 1.1 equiv.) in DMF (1 mL) was added 1-ethyl-3-(3-dimethylaminopropyl)carbodiimide hydrochloride (EDC, 122.2 mg, 0.64 mmol, 1.1 equiv.). The reaction mixture was stirred at room temperature for 18 h. The organic phase was washed with 1M hydrochloric acid and the aqueous layer was extracted with DCM (3 x 20 mL). The combined organic layers were dried over sodium sulfate, filtered and concentrated under reduced pressure. The crude product was purified by column chromatography (CH:EtOAc 8:2 to 1:1) to yield 3-cyano-*N*-(3,5-dimethylphenyl)benzamide (132.8 mg, 0.53 mmol, 95%) as a colorless solid: ^{1}H NMR (600 MHz, CDCl$_3$): **δ** 2.34 (s, 6H, H-1), 3.86 (s, 1H, H-2), 6.88 (m, 1H, H-4), 7.34 (m, 2H, H-4), 7.68 (m, 1H, H-5), 7.87 (m, 1H, H-5), 8.26 (m, 2H, H-5). ^{13}C NMR (150 MHz, CDCl$_3$): **δ** 21.1 (C-1), 112.4 (C-8), 118.0 (C-8), 118.7 (C-4), 126.6 (C-4), 129.5 (C-5), 131.1 (C-5), 131.9 (C-5), 134.6 (C-5), 136.3 (C-8), 137.5 (C-8), 138.5 (C-8), 164.4 (C-6). LC-MS *m/z* (% relative intensity): 251.1 [M+H]$^+$ (100), 273.1 [M+Na]$^+$ (3), 523.2 [2M+Na]$^+$ (2). HR-ESI-MS (*m/z*): calcd for $C_{16}H_{15}N_2O$, 251.1179 found, 251.1157. IR (neat) $\tilde{\nu}_{max}$ (cm^{-1}): 3248 (N-H), 2229 (-CN), 1643 (C=O). r_f 0.23 (CH:EtOAc 7:3).

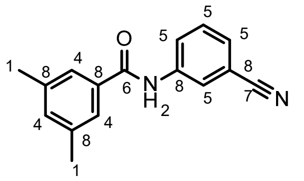

***N*-(3-Cyanophenyl)-3,5-dimethyl-benzamide (AUJ-111, 231):** To a solution of 1-ethyl-3-(3-dimethylaminopropyl)carbodiimide hydrochloride (EDC, 95.8 mg, 0.50 mmol, 1.5 equiv.) and 4-dimethylaminopyridine (61.1 mg, 0.50 mmol, 1.5 equiv.) in DCM (5 mL) was added 3-aminobenzonitrile (**236**, 59.7 mg, 0.51 mmol, 1.5 equiv.) and the resulting solution was stirred for 5 min. Then, 3,5-dimethylbenzoic acid (**235**, 50.4 mg, 0.34 mmol, 1.0 equiv.) was added and the reaction mixture was stirred at room temperature for 22 h. The organic phase was washed with 1M hydrochloric acid and the aqueous layer was extracted with DCM (3 x 15 mL). The combined organic layers were dried over sodium sulfate, filtered and concentrated under reduced pressure. The crude product was purified by column chromatography (CH:EtOAc 7:3) to yield *N*-(3-cyanophenyl)-3,5-dimethyl-benzamide (42.9 mg, 0.17 mmol, 51%) as a colorless solid: ^{1}H NMR (400 MHz, $CDCl_3$): **δ** 2.40 (s, 6H, H-1), 7.22 (m, 1H, H-4), 7.43 (m, 1H, H-5), 7.45 (m, 3H, H-4, H-5), 7.89 (m, 1H, H-5), 8.03 (bs, 1H, H-2), 8.06 (m, 1H, H-5). ^{13}C NMR (100 MHz, $CDCl_3$): **δ** 21.2 (C-1), 113.1 (C-7), 118.5 (C-8), 123.2 (C-5), 124.2 (C-5), 124.8 (C-4/C-5), 127.8 (C-5), 129.9 (C-4/C-5), 134.0 (C-4), 134.1 (C-8), 138.7 (C-8), 138.9 (C-8), 166.3 (C-6). LC-MS *m/z* (% relative intensity): 251.1 [M+H]$^+$ (100), 273.1 [M+Na]$^+$ (2), 523.2 [2M+Na]$^+$ (6). HR-ESI-MS (*m/z*): calcd for $C_{16}H_{14}N_2NaO$, 273.0998 found, 273.0991. IR (neat) $\tilde{\nu}_{max}$ (cm^{-1}): 3245 (N-H), 1654 (C=O). r_f 0.11 (CH:EtOAc 7:3).

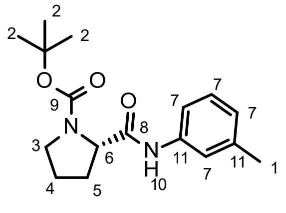

***tert*-Butyl (2S)-2-(*m*-tolylcarbamoyl)pyrrolidine-1-carboxylate (AUJ-071, 246):** A solution of *N*-Boc-L-Proline (**244**, 506.8 mg, 2.35 mmol, 1.0 equiv.), *m*-toluidine (**245**, 260.0 µL, 2.41 mmol, 1.0 equiv.) and 1-hydroxybenzotriazole hydrate (440.0 mg, 2.87 mmol, 1.2 equiv.) in DCM (5 mL) was cooled to 0 °C. 1-[3-(dimethylamino)propyl]-3-ethylcarbodiimide hydrochloride (545.9 mg, 2.85 mmol, 1.2 equiv) was added and the resulting mixture was stirred for 30 h at room temperature. The reaction mixture was then washed with 1M HCl and the aqueous layer was extracted with DCM (3 x 25 mL). The combined organic layers were washed with brine, dried over Na_2SO_4 and concentrated under reduced pressure. The crude product (788.9 mg) was purified by column chromatography (CH:EtOAc 7:3) to yield *tert*-butyl (2S)-2-(*m*-tolylcarbamoyl)pyrrolidine-1-carboxylate (628.1 mg, 2.06 mmol, 88%) as a colorless solid: ^{1}H NMR (400 MHz, $CDCl_3$): **δ** 1.51 (s, 9H, H-2), 1.93 (m, 2H, H-4), 2.00 (m, 1H, H-5), 2.32 (s, 3H, H-1), 2.48 (m, 1H, H-5), 3.47 (m, 2H, H-3), 4.48 (m, 1H, H-6), 6.89 (m, 1H, H-7), 7.17 (m, 1H, H-7), 7.28 (m, 1H, H-7), 7.40 (m, 1H, H-7), 9.41 (s, 1H, H-13). ^{13}C NMR (100 MHz, $CDCl_3$): **δ** 21.4 (C-1), 24.5 (C-4), 27.3 (C-5), 28.3 (C-2), 47.1 (C-3), 60.5 (C-6), 80.7 (C-9), 116.7 (C-7), 120.2 (C-7), 128.6 (C-7), 138.7 (C-11), 170.0 (C-8). LC-MS *m/z* (% relative intensity): 205.1356 $[M\text{-}Boc+H]^+$ (100). HR-ESI-MS (*m/z*): calcd for $C_{17}H_{24}N_2NaO_3$, 327.1679 found, 327.1678. IR (neat) $\tilde{\nu}_{max}$ (cm^{-1}): 1666 (C=O). r_f 0.16 (CH:EtOAc 7:3).

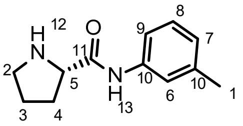

(2S)-*N*-(*m*-tolyl)pyrrolidine-2-carboxamide (AUJ-073, 247): At 0 °C, to a solution of *tert*-butyl (2S)-2-(*m*-tolylcarbamoyl)pyrrolidine-1-carboxylate (**AUJ-071**, **246**, 574.6 mg, 1.89 mmol, 1.0 equiv.) in DCM (5 mL) was added trifluoroacetic acid (1.5 mL, 19.59 mmol, 10.38 equiv.). The reaction mixture was stirred at room temperature for 3h. Then, sat. aq. $NaHCO_3$ was added and the aqueous layer was extracted with EtOAc (3 x 10 mL). The organic layer was washed with brine, dried with Na_2SO_4 and concentrated *in vacuo*. The crude (2S)-*N*-(*m*-tolyl)pyrrolidine-2-carboxamide (269.4 mg, 1.81 mmol, 96%) was used in the next reaction without further purification: ^{1}H NMR (400 MHz, $CDCl_3$): **δ** 1.96 (qui, *J* = 6.99 Hz, 2H, H-3), 2.11 (m, 1H, H-4), 2.30 (s, 3H, H-1), 2.44 (m, 1H, H-4), 3.32 (m, 2H, H-2), 4.65 (m, 1H, H-5), 6.93 (d, *J* = 7.36 Hz, 1H, H-9), 7.17 (t, *J* = 7.80 Hz, 1H, H-8), 7.32 (d, *J* = 8.26 Hz, 1H, H-7), 7.37 (s, 1H, H-6), 10.18 (s, 1H, H-13). ^{13}C NMR (100 MHz, $CDCl_3$): **δ** 21.4 (C-1), 24.9 (C-3), 30.2 (C-4), 46.7 (C-2), 60.3 (C-5), 117.1 (C-7), 120.6 (C-6), 125.6 (C-9), 128.7 (C-8), 137.3 (C-10), 138.9 (C-10), 168.0 (C-11). LC-MS *m/z* (% relative intensity): 205.1392 $[M+H]^+$ (100). HR-ESI-MS (*m/z*): calcd for $C_{12}H_{17}N_2O$, 205.1335 found, 205.1333. IR (neat) $\tilde{\nu}_{max}$ (cm^{-1}): 3271 (N-H), 1668 (C=O). r_f 0.08 (CH:EtOAc 1:1).

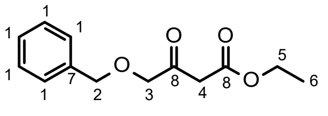

Ethyl 4-benzyloxy-3-oxobutanoate (AUJ-082, 249): To a suspension of sodium hydride (787.0 mg, 32.79 mmol, 2.2 equiv.) in THF (10 mL) cooled to 0 °C was added benzyl alcohol (1.6 mL, 15.46 mmol, 1.04 equiv.) and the mixture was stirred at room temperature for 2h. Ethyl

4-chloroacetoacetate (**248**, 2.0 mL, 14.80 mmol, 1.0 equiv.) was then added drop wise and the reaction mixture was stirred at room temperature for further 22h. The mixture was then poured into 1M HCl at 0 °C and the aqueous layer was extracted with EtOAc (3 x 20 mL). The combined organic layers were washed with sat. $NaHCO_3$ (2 x 10 mL) and brine and were dried over Na_2SO_4. The solvent was evaporated under reduced pressure. The crude product (3.39 g) was purified by column chromatography (CH:EtOAc 19:1) yielding ethyl 4-benzyloxy-3-oxobutanoate (3.22 g, 13.62 mmol, 92%) as a light yellow oil: ^{1}H NMR (400 MHz, $CDCl_3$): **δ** 1.27 (t, *J* = 7.14 Hz, 3H, H-6), 3.55 (s, 2H, H-4), 4.16 (s, 2H, H-3), 4.19 (q, *J* = 7.12 Hz, 2H, H-5), 4.61 (s, 2H, H-2), 7.37 (m, 5H, H-1). ^{13}C NMR (100 MHz, $CDCl_3$): **δ** 14.0 (C-6), 46.0 (C-4), 61.3 (C-5), 73.4 (C-2), 74.8 (C-3), 127.8 (C-1), 128.0 (C-1), 128.5 (C-1), 136.9 (C-7), 166.9 (C-8), 201.6 (C-8). LC-MS *m/z* (% relative intensity): 259.0972 $[M+Na]^+$ (100). HR-ESI-MS (*m/z*): calcd for $C_{13}H_{16}NaO_4$, 259.0941 found, 259.0941. IR (neat) $\tilde{v}_{max}$ (cm^{-1}): 1720 (C=O). r_f 0.34 (CH:EtOAc 8:2).

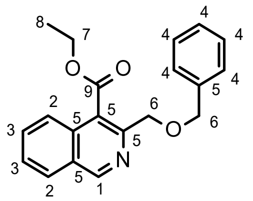

Ethyl 3-(benzyloxymethyl)isoquinoline-4-carboxylate (AUJ-084, 250): To a suspension of potassium carbonate (280.0 mg, 2.03 mmol, 3.0 equiv.) in isopropanol (3 mL) were added copper iodide (18.0 mg, 0.09 mmol, 0.14 equiv.), 2-bromobenzylamine (122.0 mg, 0.66 mmol, 1.0 equiv.) and ethyl 4-benzyloxy-3-oxobutanoate (**AUJ-082**, **249**, 313.0 mg, 1.32 mmol, 2.0 equiv.) subsequently. The resulting mixture was heated at reflux for 24h under argon. After cooling to room temperature, the mixture was stirred for further 22h under air. The mixture was then diluted with water and extracted with DCM (3 x 10 mL). The combined organic layers were washed with brine, dried over Na_2SO_4 and concentrated *in vacuo*. The crude product (478.5 mg) was purified by column chromatography (CH:EtOAc 3:1) to give ethyl 3-(benzyloxymethyl)isoquinoline-4-carboxylate (102.3 mg, 0.32 mmol, 59%) as a yellowish oil: ^{1}H NMR (600 MHz, $CDCl_3$): **δ** 1.37 (t, *J* = 7.17 Hz, 3H, H-8), 4.42 (q, *J* = 7.16 Hz, 2H, H-7), 4.62 (s, 2H, H-6), 5.00 (s, 2H, H-6), 7.35 (m, 5H, H-4), 7.67 (m, 1H, H-2), 7,79 (m, 1H, H-2), 7.99 (m, 1H, H-3), 8.03 (m, 1H, H-3), 9.28 (s, 1H, H-1). ^{13}C NMR (150 MHz, $CDCl_3$): **δ** 14.1 (C-8). 61.7 (C-7), 72.6 (C-6), 73.0 (C-6), 124.0 (C-3), 127.0 (C-4), 127.6 (C-2), 127.9 (C-3), 128.3 (C-4), 128.5 (C-4), 131.5 (C-2), 133.3 (C-5), 137.9 (C-5), 140.9 (C-5), 149.2 (C-5), 153.2 (C-5), 167.9 (C-9). LC-MS *m/z* (% relative intensity): 322.1468 $[M+H]^+$ (100). HR-ESI-MS (*m/z*): calcd for $C_{20}H_{20}NO_3$, 322.1438 found, 322.1437. IR (neat) $\tilde{v}_{max}$ (cm^{-1}): 1720 (C=O). r_f 0.46 (CH:EtOAc 2:1).

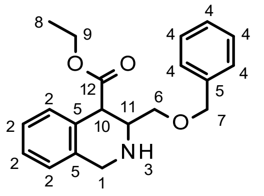

Ethyl 3-(benzyloxymethyl)-1,2,3,4-tetrahydroisoquinoline-4-carboxylate (AUJ-088, 248): A suspension of ethyl 3-(benzyloxymethyl)isoquinoline-4-carboxylate (**AUJ-084**, **250**, 106.6 mg, 0.33 mmol, 1.0 equiv.) and PtO_2 (9.4 mg, 0.04 mmol, 0.12 equiv.) were hydrogenated at room temperature for 19h. The reaction mixture was then filtered through celite and concentrated under reduced pressure. The residue was dissolved in DCM and extracted with aq. sat. $NaHCO_3$. The aqueous layer was extracted with DCM (3 x 10 mL) and the combined organic layers were dried and concentrated *in vacuo*. The crude product (75 mg) was purified by column chromatography (CH:EtOAc 2:1) to give ethyl 3-(benzyloxymethyl)-1,2,3,4-tetrahydroisoquinoline-4-carboxylate (34.8 mg, 0.11 mmol, 32%) as a yellow oil: ^{1}H NMR (400 MHz, $CDCl_3$): **δ** 1.23 (t, *J* = 7.10 Hz, 3H, H-8), 3.33 (m, 1H, H-11), 3.60 (m, 1H, H-6), 3.77 (m, 1H, H-6), 3.84 (m, 1H, H-10), 4.10 (m, 2H, H-9), 4.14 (m, 2H, H-7), 4.54 (d, *J* = 11.89 Hz, 1H, H-1), 4.61 (d, *J* = 11.89 Hz, 1H, H-1), 7.11 (m, 1H, H-2), 7.19 (m, 1H, H-2), 7.22 (m, 1H, H-2), 7.27 (m, 1H, H-2), 7.37 (m, 5H, H-4). ^{13}C NMR (100 MHz, $CDCl_3$): **δ** 14.1 (C-8), 44.0 (C-10), 47.9 (C-7), 55.2 (C-11), 60.6 (C-9), 71.5 (C-6), 73.4 (C-1), 126.2 (C-2), 126.3 (C-2), 127.4 (C-2), 127.6 (C-4), 127.7 (C-4), 128.3 (C-4), 129.3 (C-2), 132.2 (C-5), 136.0 (C-5), 138.0 (C-5), 172.9 (C-12). LC-MS *m/z* (% relative intensity): 326.1795 $[M+H]^+$ (100). HR-ESI-MS (*m/z*): calcd for $C_{20}H_{24}NO_3$, 326.1751 found, 326.1749. IR (neat) $\tilde{v}_{max}$ (cm^{-1}): 1724 (C=O). r_f 0.12 (CH:EtOAc 1:1).

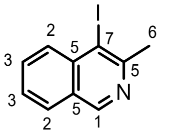

4-Iodo-3-methyl-isoquinoline (AUJ-095, 260): A mixture of 3-methylisoquinoline (**259**, 310.5 mg, 2.17 mmol, 1.0 equiv.) and *N*-iodosuccinimide (802.2 mg, 3.57 mmol, 1.6 equiv.) in glacial acetic acid (10 mL) was stirred at 80 °C for 7h. The reaction mixture was then cooled to room temperature and then concentrated under reduced pressure. The residue was dissolved in EtOAc and washed with aq. $NaHCO_3$ and brine. The aqueous layer was extracted with EtOAc and the combined organic layers were dried over Na_2SO_4. The solvent was then evaporated and the crude product (727.1 mg) was purified by column chromatography (CH:EtOAc 9:1) to give 4-iodo-3-methyl-isoquinoline (420.9 mg, 1.56 mmol, 72%) as a brownish crystalline solid: ^{1}H NMR (600 MHz, $CDCl_3$): **δ** 3.02 (s, 3H, H-6), 7.60 (m, 1H, H-3), 7.76 (m, 1H, H-3), 7.89 (m, 1H, H-2), 8.10 (m, 1H, H-2), 9.05 (s, H-1). ^{13}C NMR (150 MHz, $CDCl_3$): **δ** 30.2 (C-6), 99.1 (C-7), 127.1 (C-3), 127.5 (C-5), 127.8 (C-2), 131.0 (C-2), 131.8 (C-3), 138.3 (C-5), 151.7 (C-1), 154.9

(C-5). LC-MS m/z (% relative intensity): 270.0 $[M+H]^+$ (100). HR-ESI-MS (m/z): calcd for $C_{10}H_9IN$, 269.9774 found, 269.9769. IR (neat) $\tilde{v}_{max}$ (cm^{-1}): 1614 (C=N). r_f 0.47 (CH:EtOAc 1:1).

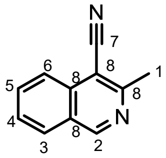

3-Methylisoquinoline-4-carbonitrile (AUJ-099, 261): To a mixture of 4-iodo-3-methylisoquinoline (**AUJ-095**, **260**, 292 mg, 1.09 mmol, 1.0 equiv.) and zinc cyanide (114 mg, 0.97 mmol, 0.9 equiv.) in degassed dry DMF was added tetrakis(triphenylphosphine)palladium(0) (78 mg, 0.07 mmol, 0.06 equiv.). The reaction mixture was then stirred at 120 °C for 21 h. After cooling to room temperature, the mixture was filtered and diluted with EtOAc. The organic layer was washed with $NaHCO_3$ and brine. After drying over Na_2SO_4 and evaporation of the solvent, the crude product was purified by column chromatography (CH:EtOAc 8:2) to afford 3-methylisoquinoline-4-carbonitrile (171 mg, 1.01 mmol, 94%) as reddish-brown crystals: ^1H NMR (400 MHz, $CDCl_3$): **δ** 2.95 (s, 3H, H-1), 7.69 (m, 1H, H-5), 7.87 (m, 1H, H-4), 8.03 (m, 1H, H-6), 8.12 (m, 1H, H-3), 9.30 (s, 1H, H-2). ^{13}C NMR (100 MHz, $CDCl_3$): **δ** 23.8 (C-1), 103.7 (C-8), 116.1 (C-7), 123.7 (C-3), 125.8 (C-8), 128.0 (C-5), 128.3 (C-6), 132.9 (C-4), 135.3 (C-8), 155.2 (C-2), 158.0 (C-8). LC-MS m/z (% relative intensity): 169.1 $[M+H]^+$ (100). HR-ESI-MS (m/z): calcd for $C_{11}H_9N_2$, 169.0760 found, 169.0761. IR (neat) $\tilde{v}_{max}$ (cm^{-1}): 2217 (C≡N). r_f 0.31 (CH:EtOAc 1:1).

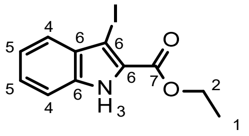

Ethyl 3-iodo-1*H*-indole-2-carboxylate (AUJ-072, 264): Ethyl indole-2-carboxylate (**262**, 1.01 g, 5.35 mmol, 1.0 equiv.) and *N*-iodosuccinimide (1.23 g, 5.47 mmol, 1.0 equiv.) were dissolved in DCM (20 mL) and stirred at room temperature for 2.5 h. The reaction mixture was then quenched with aqueous $Na_2S_2O_3$. The aqueous layer was extracted with DCM (2 x 50 mL). The combined organic layers were washed with brine, dried over Na_2SO_4 and concentrated *in vacuo*. The crude product (1.80 g) were purified by column chromatography (CH:EtOAc 19:1). Ethyl 3-iodo-1*H*-indole-2-carboxylate (1.63 g, 5.16 mmol, 96%) was obtained as a light yellow solid: ^1H NMR (600 MHz, $CDCl_3$): **δ** 1.51 (t, *J* = 7.17 Hz, 3H, H-1), 4.51 (q, *J* = 7.14 Hz, 2H, H-2), 7.26 (m, 1H, H-4), 7.41 (m, 2H, H-5), 7.60 (m, 1H, H-4), 9.52 (s, 1H, H-3). ^{13}C NMR (150 MHz, $CDCl_3$): **δ** 14.3 (C-1), 61.5 (C-2), 66.0 (C-6), 112.0 (C-5), 121.6 (C-4), 123.5 (C-4), 126.5 (C-5), 128.2 (C-6), 131.5 (C-6), 136.2 (C-6), 161.0 (C-7). LC-MS m/z (% relative intensity):

316.0 $[M+H]^+$ (100). HR-ESI-MS (*m/z*): calcd for $C_{11}H_{10}INNaO_2$, 337.9648 found, 337.9645. IR (neat) $\tilde{\nu}_{max}$ (cm^{-1}): 3293 (N-H), 1683 (C=O). r_f 0.21 (CH:EtOAc 9:1).

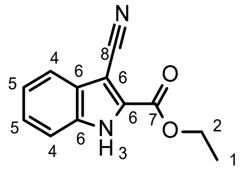

Ethyl 3-cyano-1H-indole-2-carboxylate (AUJ-074, 263): To a solution of ethyl 3-iodo-1H-indole-2-carboxylate (**AUJ-072**, **264**, 252.8 mg, 0.80 mmol, 1.0 equiv.), in degassed DMF/THF 1:1 (8 mL) were added copper cyanide (168.1 mg, 1.88 mmol, 2.3 equiv.), tetraethylammonium cyanide (62.7 mg, 0.40 mmol, 0.5 equiv.) and the mixture was purged with argon for 15 min. Then, tris(dibenzylideneacetone)dipalladium(0) (41.2 mg, 0.04 mmol, 0.06 equiv.) and 1,1′-bis(diphenylphosphino)ferrocene (68.0 mg, 0.12 mmol, 0.15 equiv.) were added and the reaction mixture was heated to 120 °C for 12h. Sat. aq. $NaHCO_3$ was then added and the mixture was filtered. The aqueous layer was extracted with EtOAc (3 x 30 mL). The combined organic layers were washed with brine, dried over Na_2SO_4 and concentrated under reduced pressure. The crude product (255.6 mg) was purified chromatographically (CH:EtOAc 7:3) to give ethyl 3-cyano-1H-indole-2-carboxylate (142.5 mg, 0.67 mmol, 83%) as a colorless solid: ^{1}H NMR (400 MHz, $CDCl_3$): **δ** 1.40 (t, *J* = 7.12 Hz, 3H, H-1), 4.43 (q, *J* = 7.11 Hz, 2H, H-2), 7.26 (m, 1H, H-5), 7.37 (m, 1H, H-5), 7.57 (m, 1H, H-4), 7.67 (m, 1H, H-4), 12.91 (s, 1H, H-3). ^{13}C NMR (100 MHz, $CDCl_3$): **δ** 13.9 (C-1), 61.5 (C-2), 88.9 (C-6), 113.6 (C-5), 114.3 (C-8), 119.5 (C-4), 122.6 (C-4), 125.9 (C-5), 127.4 (C-6), 131.9 (C-6), 135.7 (C-6), 158.9 (C-7). LC-MS *m/z* (% relative intensity): 215.0678 $[M+H]^+$ (100), 237.0484 $[M+Na]^+$ (39). HR-ESI-MS (*m/z*): calcd for $C_{12}H_{10}N_2NaO_2$, 237.0634 found, 237.0637. IR (neat) $\tilde{\nu}_{max}$ (cm^{-1}): .3276 (N-H), 2219 (C≡N), 1689 (C=O) r_f 0.21 (CH:EtOAc 9:1).

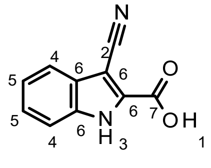

3-Cyano-1H-indole-2-carboxylic acid (AUJ-077, 265): Ethyl 3-cyano-1H-indole-2-carboxylate (**AUJ-074**, **263**, 545.0 mg, 2.54 mmol, 1.0 equiv.) and potassium hydroxide (312.0 mg, 5.56 mmol, 2.2 equiv.) were dissolved in water/ethanol 1:2.5 and heated to 60 °C for 1.5h. The solvent was then evaporated and the residue was suspended in water (20 mL) and acidified with concentrated HCl. The precipitate was collected and dried to yield 3-cyano-1H-indole-2-carboxylic acid (473.5 mg, 2.54 mmol, 100%) as an off-white solid: ^{1}H NMR (600 MHz, ACN-D_3): **δ** 6.78 (m, 1H, H-5), 6.89 (m, 1H, H-5), 7.08 (m, 1H, H-4), 7.21 (m, 1H, H-4), 11.91 (s, 1H, H-1). ^{13}C NMR (150 MHz, ACN-D$_3$): **δ** 114.6 (C-4), 115.7 (C-2), 120.7 (C-4), 123.6 (C-5), 126.9 (C-5), 128.8 (C-6), 135.1 (C-6), 136.8 (C-6). LC-MS *m/z* (% relative intensity): 141.0637 [M-CO$_2$H]$^-$ (100), 185.0582 [M-H]$^-$ (14). HR-ESI-MS (*m/z*): calcd for $C_{10}H_6N_2NaO_2$, 209.0321 found, 209.0325. IR (neat) $\tilde{v}_{max}$ (cm^{-1}): 2218 (C≡N), 1696 (C=O). r$_f$ 0.18 (CH:EtOAc 1:1 + 0.1% AcOH).

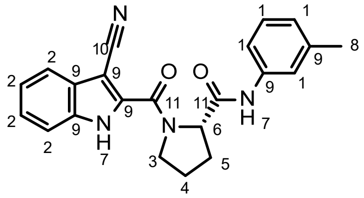

(2S)-1-(3-Cyano-1*H*-indole-2-carbonyl)-*N*-(*m*-tolyl)pyrrolidine-2-carboxamide (AUJ-083, 266): A suspension of 3-cyano-1H-indole-2-carboxylic acid (**AUJ-077**, **265**, 58.9 mg, 0.32 mmol, 1.0 equiv.) in DCM (10 mL) was cooled to 0 °C. Then, (2S)-*N*-(*m*-tolyl)pyrrolidine-2-carboxamide (**AUJ-073**, **247**, 260.0 mg, 1.27 mmol, 4.0 equiv.), 4-dimethylaminopyridine (11.7 mg, 0.10 mmol, 0.3 equiv.) and 1-ethyl-3-(3-dimethylaminopropyl)carbodiimide hydrochloride (EDC, 127.2 mg, 0.66 mmol, 2.1 equiv.) were added and the reaction mixture was stirred at 0 °C for 30 min and at room temperature for 3h. The mixture was then washed with water (1 x 10 mL) and the organic layer was dried over Na$_2$SO$_4$. After evaporation of the solvent, the crude product (199 mg) was purified chromatographically (CH:EtOAc 3:1) to give (2S)-1-(3-cyano-1*H*-indole-2-carbonyl)-*N*-(*m*-tolyl)pyrrolidine-2-carboxamide (77.0 mg, 0.21 mmol, 65%) as a light yellow solid: ^1H NMR (600 MHz, CDCl$_3$): **δ** 1.90 (m, 1H, H-4), 2.10 (m, 1H, H-4), 2.13 (s, 3H, H-8), 2.22 (m, 1H, H-5), 2.28 (m, 1H, H-5), 3.84 (m, 1H, H-3), 3.96 (m, 1H, H-3), 4.92 (m, 1H, H-6), 6.82 (m, 1H, H-1), 7.02 (m, 1H, H-1), 7.22 (m, 2H, H-1), 7.28 (m, 2H, H-2), 7.46 (m, 1H, H-2), 7.74 (m, 1H, H-2), 8.90 (s, 1H, H-7), 11.45 (s, 1H, H-7). ^{13}C NMR (150 MHz, CDCl$_3$): **δ** 21.3 (C-8), 25.4 (C-4), 29.6 (C-5), 50.1 (C-3), 62.3 (C-6), 87.6 (C-9), 113.3 (C-2), 115.6 (C-10), 117.5 (C-1), 119.8 (C-2), 121.0 (C-1), 123.0 (C-2), 125.4 (C-1), 125.8 (C-2), 127.1 (C-9), 128.6 (C-1), 135.3 (C-9), 137.0 (C-9), 137.3 (C-9), 138.7 (C-9), 161.6 (C-11), 169.9 (C-11). LC-MS *m/z* (% relative intensity): 373.2 [M+H]$^+$ (100). HR-ESI-MS (*m/z*): calcd for $C_{22}H_{20}N_4NaO_2$, 395.1478 found, 395.1478. IR (neat) $\tilde{v}_{max}$ (cm^{-1}): 3283 (N-H), 2223 (C≡N), 1668 (C=O). r$_f$ 0.27 (CH:EtOAc 1:1).

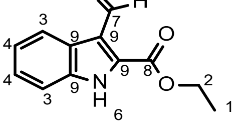

Ethyl 3-formyl-1*H*-indole-2-carboxylate (AUJ-109, 270): Phosphorous oxychloride (220 µL, 2.41 mmol, 1.1 equiv.) was added dropwise to DMF cooled to 0 °C. A solution of ethyl indole-2-

carboxylate (**262**, 398 mg, 2.10 mmol, 1.0 equiv.) in DMF was then added and the mixture was stirred at room temperature for 1h and then at 70 °C for 21 h. After cooling to room temperature, the mixture was poured into ice cold water and neutralized by addition of 2M NaOH. The yellow precipitate was collected and purified chromatographically (CH:EtOAc 7:3 → 1:1) to yield ethyl 3-formyl-1*H*-indole-2-carboxylate (456 mg, 2.10 mmol, quant.) as a yellow powder: ^{1}H NMR (600 MHz, CDCl$_3$): **δ** 1.42 (t, *J* = 7.10 Hz, 3H, H-1), 4.46 (q, *J* = 7.11 Hz, 2H, H-2), 7.27 (m, 1H, H-4), 7.34 (m, 1H, H-4), 7.56 (d, *J* = 8.24 Hz, 1H, H-3), 8.26 (d, *J* = 8.00 Hz, 1H, H-3), 10.62 (s, 1H, H-5), 12.69 (s, 1H, H-6). ^{13}C NMR (150 MHz, CDCl$_3$): **δ** 14.0 (C-1), 61.5 (C-2), 112.9 (C-3), 118.4 (C-9), 122.4 (C-3), 123.2 (C-4), 124.7 (C-9), 125.6 (C-4), 132.4 (C-9), 135.7 (C-9), 160.1 (C-8), 187.3 (C-7). LC-MS *m/z* (% relative intensity): 218.1 [M+H]$^+$ (43), 172.0 [M-CO$_2$]$^+$ (100). HR-ESI-MS (*m/z*): calcd for $C_{12}H_{11}NaO_3$, 240.0631 found, 240.0628. IR (neat) $\tilde{\nu}_{max}$ (cm^{-1}): 1720 (C=O), 1630 (C=O). r_f 0.14 (CH:EtOAc 7:3).

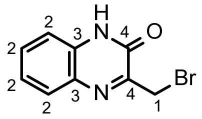

3-(Bromomethyl)-1H-quinoxalin-2-one (AUJ-120, 289): Freshly recrystallized 1,2-Phenylenediamine (**288**, 302.7 mg, 2.52 mmol, 1.0 equiv.) was dissolved in THF (10 mL). After addition of 3-bromopyruvic acid (455.4 mg, 2.65 mmol, 1.05 equiv.), the mixture was stirred at room temperature for 1 h. The precipitate was collected (330.0 mg) and recrystallized from DCM to yield 3-(bromomethyl)-1H-quinoxalin-2-one (252.0 mg, 1.05 mmol, 42%) as a brown solid: ^{1}H NMR (400 MHz, DMSO-d$_6$): **δ** 4.61 (s, 2H, H-1), 7.34 (m, 2H, H-2), 7.56 (m, 1H, H-2), 7.77 (m, 1H, H-2). ^{13}C NMR (150 MHz, DMSO-d$_6$): **δ** 29.6 (C-1), 116.1 (C-2), 124.4 (C-2), 129.4 (C-2), 131.6 (C-2), 132.5 (C-3), 133.2 (C-3), 154.4 (C-4), 157.0 (C-4). LC-MS *m/z* (% relative intensity): 239.0 [M(^{79}Br)+H]$^+$ (81), 241 [M(^{81}Br)+H]$^+$ (84), 160.1 [M-Br$^-$]$^+$ (100). HR-ESI-MS (*m/z*): calcd for $C_9H_8BrN_2O$, 238.9815 and 240.9795 found, 238.9814 and 240.9778. IR (neat) $\tilde{\nu}_{max}$ (cm^{-1}): 1657 (C=O). r_f 0.30 (CH:EtOAc 9:1).

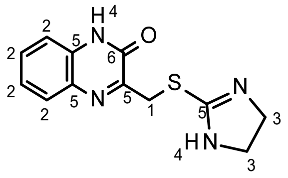

3-(4,5-Dihydro-1*H*-imidazole-2-ylsulfanylmethyl)-1*H*-quinoxalin-2-one (AUJ-125, 278): To a solution of 3-(bromomethyl)-1H-quinoxalin-2-one (**AUJ-120**, **289**, 237.0 mg, 0.99 mmol, 1.0 equiv.) in dry ethanol imidazolidinethione (104.0 mg, 1.02 mmol, 1.0 equiv.) was added and the mixture was stirred at 85 °C for 22 h. After cooling to room temperature, the solvent was removed under reduced pressure and the crude product (338.5 mg) was prepurified by column chromatography (EtOAc) followed by preparative HPLC (water:ACN 80:20) to give 3-(4,5-dihydro-1*H*-imidazole-2-ylsulfanylmethyl)-1*H*-quinoxalin-2-one (85.5 mg, 0.33 mmol, 33%) as a brown solid: ^{1}H NMR (400 MHz, DMSO-d_6): **δ** 3.88 (m, 4H, H-3), 4.71 (s, 2H, H-1), 7.33 (m, 1H, H-2), 7.49 (m, 1H, H-2), 7.57 (m, 1H, H-2), 7.75 (m, 1H, H-2), 10.23 (bs, 1H, H-4), 12.66 (bs, 1H, H-4). ^{13}C NMR (100 MHz, DMSO-d_6): **δ** 33.78 (C-1), 44.1 (C-5), 45.2 (C-3), 115.6 (C-2), 123.6 (C-2), 128.3 (C-2), 130.6 (C-2), 131.1 (C-5), 132.2 (C-5), 154.5 (C-5), 169.0 (C-6). LC-MS *m/z* (% relative intensity): 261.1 $[M+H]^+$ (100). HR-ESI-MS (*m/z*): calcd for $C_{12}H_{13}N_4OS$, 261.0805 found, 261.0806. IR (neat) $\tilde{\nu}_{max}$ (cm^{-1}): 3377, 3044 (N-H), 1666, 1620 (C=O). r_f 0.33 (CH:EtOAc 1:1).

7. Appendix

In the following paragraph, the NMR overlays of excess titrations of the non- or weak binding compound are shown. In some cases, a shift of the so-called Histidine-tag (His-tag) can be observed. The His-tag is added to the recombinant protein during expression in *E. coli* as it simplifies purification of the protein. The peak for the amine proteins is labeled in the spectra. The shift results from DMSO addition and is usually reflected in most of the other peaks shifting in the spectrum. Therefore, shifts in spectra showing a His-tag shift need to excess the range of the His-tag shift to be considered relevant a criteria that does not apply to the NMR data shown in the following.

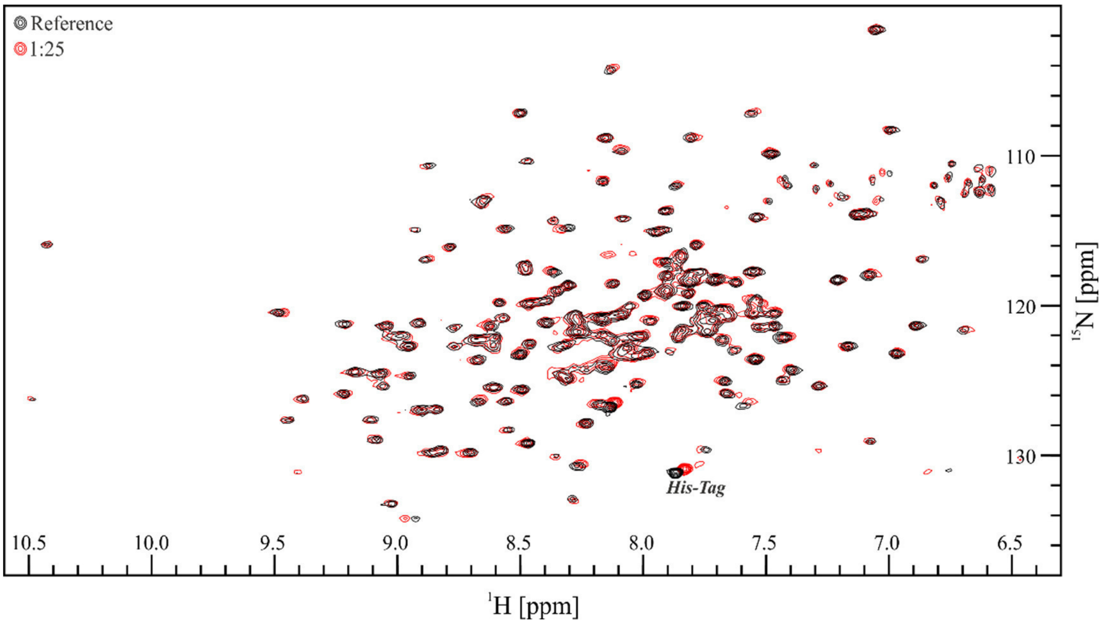

Figure 103: NMR titration of di-methoxy BPA ***136a*** *in excess to the protein K-Ras showing no shifts for the relevant peaks.*

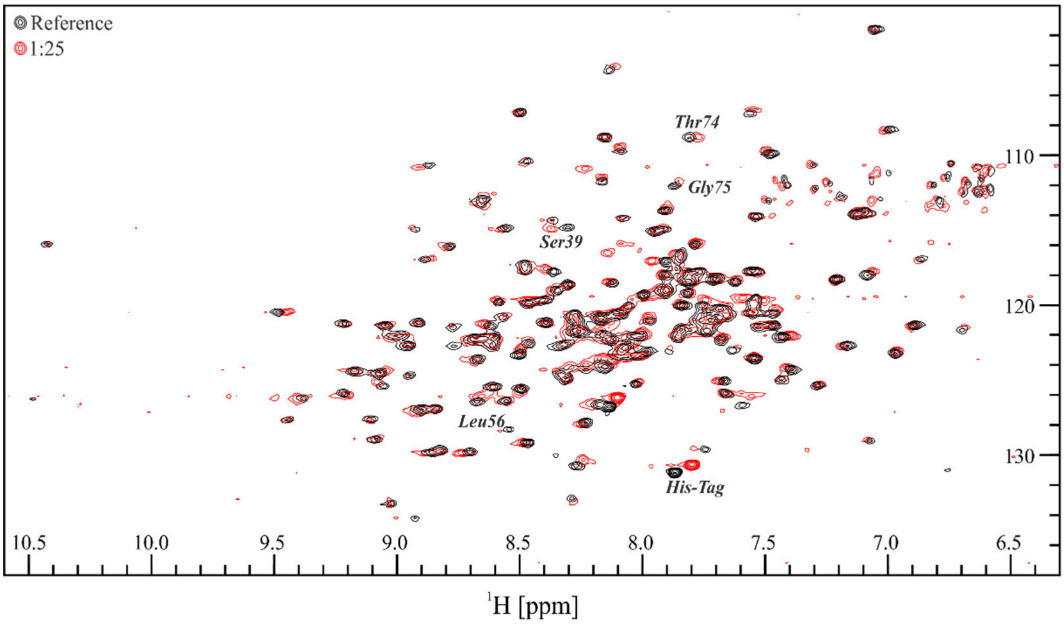

*Figure 104: NMR titration of mono-methoxy BPA **136b** in excess to the protein K-Ras showing minor shifts for only a few of the relevant peaks.*

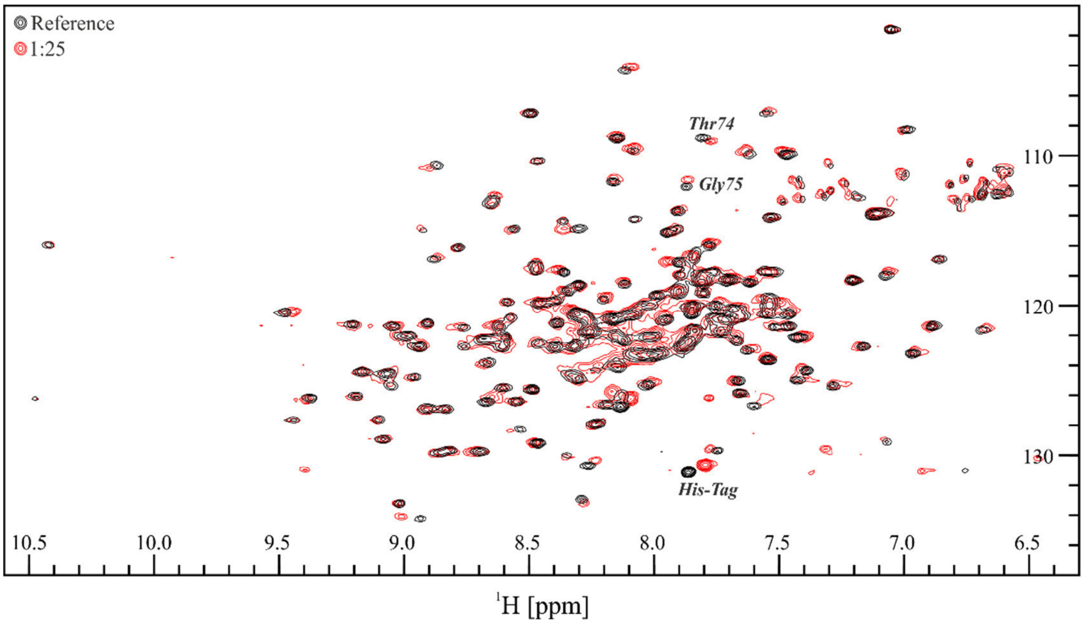

*Figure 105: NMR titration of bis-3-indole A **151** in excess to the protein K-Ras showing minor shifts for only a few of the relevant peaks.*

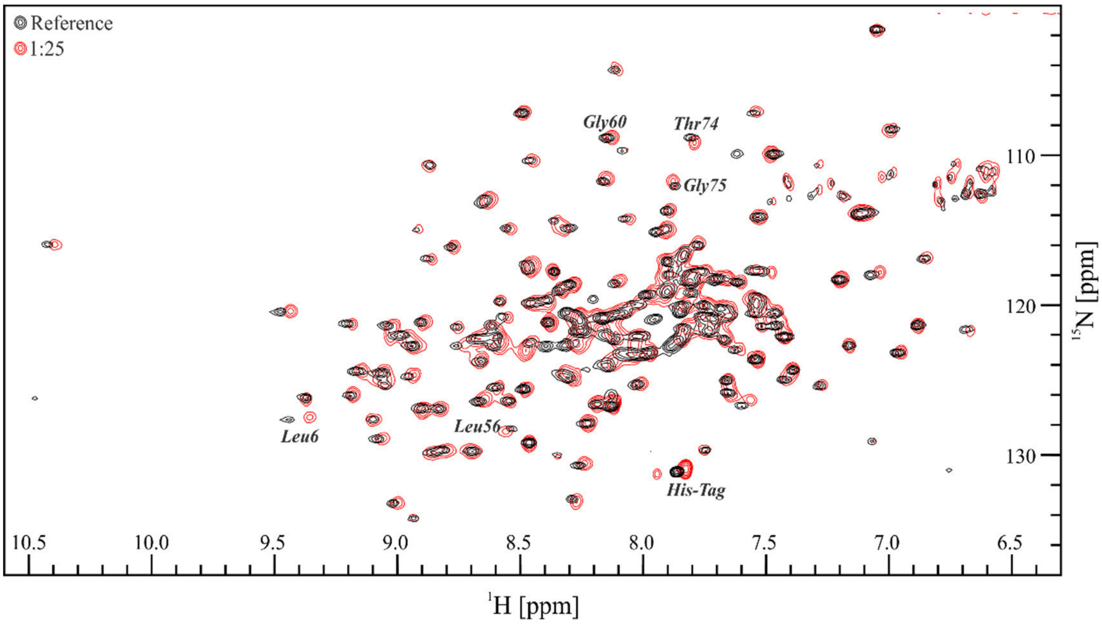

*Figure 106: NMR titration of BPA acetic-acid (**160**) in excess to the protein K-Ras showing minor shifts for only a few of the relevant peaks.*[102]

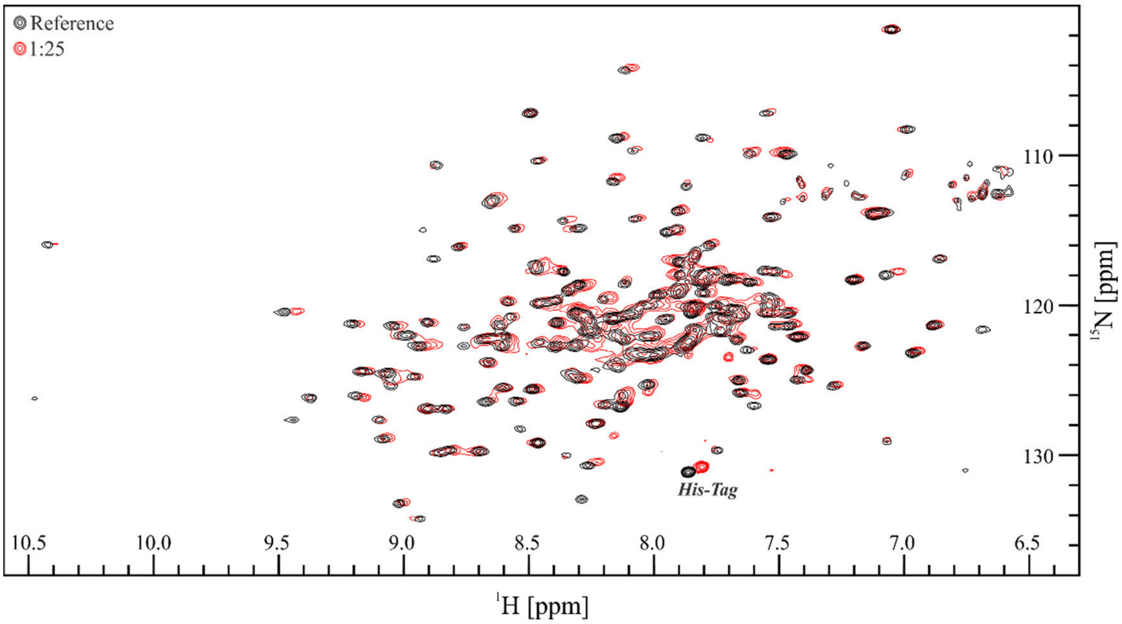

*Figure 107: NMR titration of amide **170** in excess to the protein K-Ras showing no shifts for the relevant peaks.*

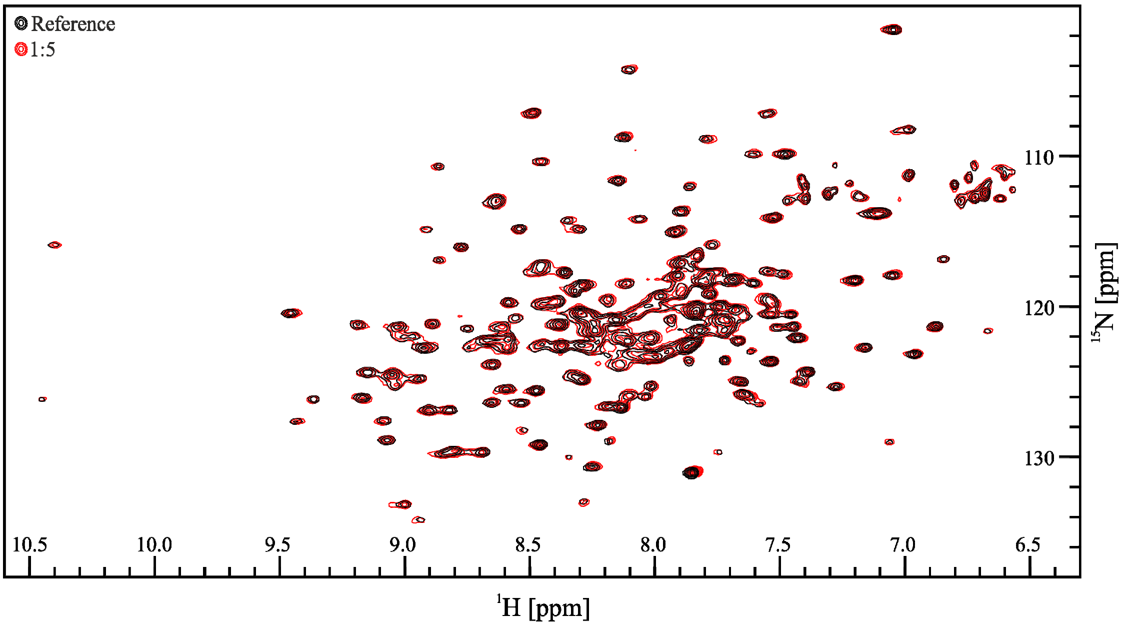

Figure 108: NMR titration of amide ***172*** *in excess to the protein K-Ras showing no shifts for the relevant peaks.*

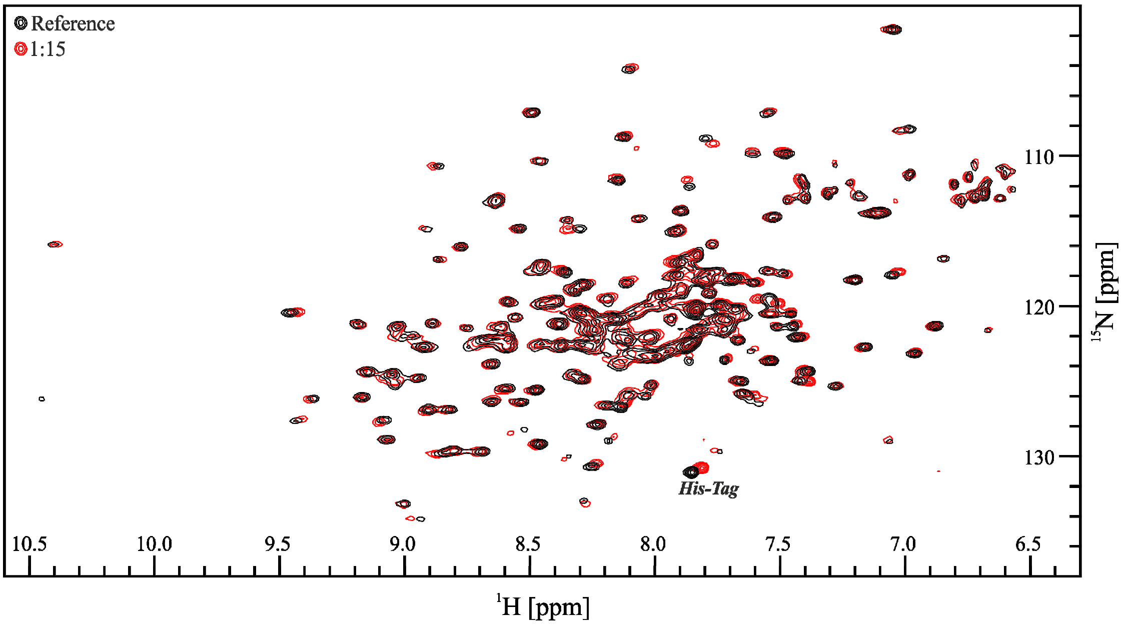

Figure 109: NMR titration of amide ***173*** *in excess to the protein K-Ras showing no shifts for the relevant peaks.*

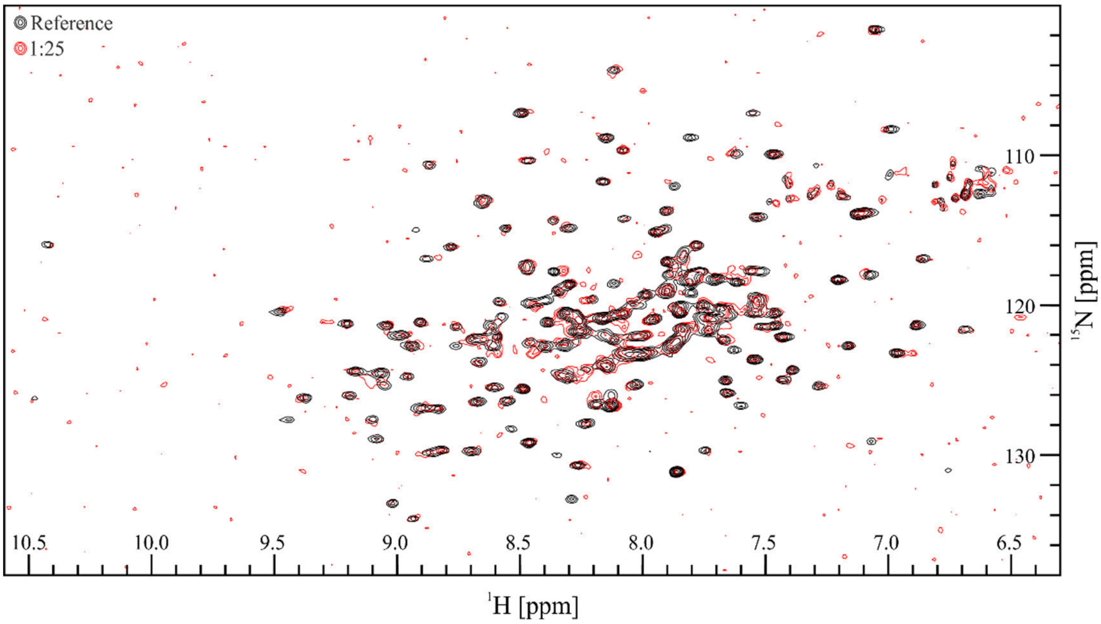

Figure 110: NMR titration of hybrid molecule ***179*** *in excess to K-Ras showing no shifts for the relevant peaks.*

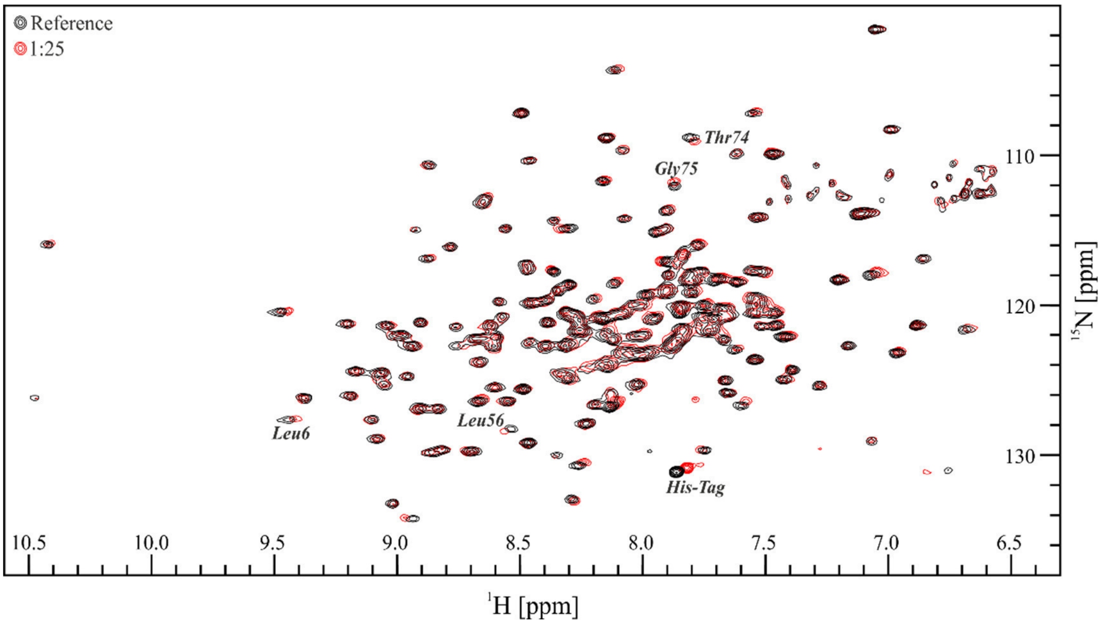

Figure 111: NMR titration of amine ***182*** *in excess to the protein K-Ras showing no shifts for the relevant peaks.*

8. Literature

(1) Stewart, B. W.; Wild, C. P. *World Cancer Report 2014*; 2014.

(2) World Health Organization (WHO) http://www.who.int/en/ (accessed Jan 20, 2018).

(3) Bos, J. L.; Rehmann, H.; Wittinghofer, A. *Cell* **2007**, *129* (5), 865–877.

(4) Rajalingam, K.; Schreck, R.; Rapp, U. R.; Albert, Š. *Biochim. Biophys. Acta - Mol. Cell Res.* **2007**, *1773* (8), 1177–1195.

(5) Lu, S.; Jang, H.; Muratcioglu, S.; Gursoy, A.; Keskin, O.; Nussinov, R.; Zhang, J. *Chem. Rev.* **2016**, *116* (11), 6607–6665.

(6) Prior, I. A.; Lewis, P. D.; Mattos, C. *Cancer Res.* **2012**, *72* (10), 2457–2467.

(7) Wittinghofer, A.; Waldmann, H. *Angew. Chemie* **2000**, *39* (23), 4192–4214.

(8) Takashima, A.; Faller, D. V. *Expert Opin. Ther. Targets* **2013**, *17* (5), 507–531.

(9) Heard, J. J.; Fong, V.; Bathaie, S. Z.; Tamanoi, F. *Cell. Signal.* **2014**, *26* (9), 1950–1957.

(10) Ehrkamp, A.; Herrmann, C.; Stoll, R.; Heumann, R. *Cancers (Basel).* **2013**, *5* (2), 639–661.

(11) Karassek, S.; Berghaus, C.; Schwarten, M.; Goemans, C. G.; Ohse, N.; Kock, G.; Jockers, K.; Neumann, S.; Gottfried, S.; Herrmann, C.; Heumann, R.; Stoll, R. *J. Biol. Chem.* **2010**, *285* (44), 33979–33991.

(12) John, J.; Schlichting, I.; Schiltz, E.; Rösch, P.; Wittinghofer, A. *J. Biol. Chem.* **1989**, *264* (22), 13086–13092.

(13) Gideon, P.; John, J.; Frech, M.; Lautwein, A.; Clark, R.; Scheffler, J. E.; Wittinghofer, A. *Mol. Cell. Biol.* **1992**, *12* (5), 2050–2056.

(14) Goody, R. S.; Frech, M.; Wittinghofer, A. *Trends Biochem. Sci.* **1991**, *16*, 327–328.

(15) Cherfils, J.; Zeghouf, M. *Physiol. Rev.* **2013**, *93* (1), 269–309.

(16) Spoerner, M.; Herrmann, C.; Vetter, I. R.; Kalbitzer, H. R.; Wittinghofer, A. *Proc. Natl. Acad. Sci.* **2001**, *98* (9), 4944–4949.

(17) Rudack, T.; Xia, F.; Schlitter, J.; Kötting, C.; Gerwert, K. *Biophys. J.* **2012**, *103* (2), 293–302.

(18) RCSB - PDB Protein Data Bank http://www.rcsb.org/pdb/home/home.do (accessed Jan 31, 2018).

(19) Yu, Y.; Li, S.; Xu, X.; Li, Y.; Guan, K.; Arnold, E.; Ding, J. *J. Biol. Chem.* **2005**, *280* (17), 17093–17100.

(20) Schöpel, M.; Jockers, K. F. G.; Düppe, P. M.; Autzen, J.; Potheraveedu, V. N.; Ince, S.; Yip, K. T.; Heumann, R.; Herrmann, C.; Scherkenbeck, J.; Stoll, R. *J. Med. Chem.* **2013**, *56* (23), 9664–9672.

(21) Downward, J. *Nat. Rev. Cancer* **2003**, *3* (1), 11–22.

(22) Wang, Y.; Kaiser, C. E.; Frett, B.; Li, H. Y. *J. Med. Chem.* **2013**, *56* (13), 5219–5230.

(23) Clark, G. J.; Kinch, M. S.; Rogers-Graham, K.; Sebti, S. M.; Hamilton, A. D.; Der, C. J. *J. Biol. Chem.* **1997**, *272* (16), 10608–10615.

(24) Im, E.; von Lintig, F. C.; Chen, J.; Zhuang, S.; Qui, W.; Chowdhury, S.; Worley, P. F.; Boss, G. R.; Pilz, R. B. *Oncogene* **2002**, *21* (41), 6356–6365.

(25) Armijo, M. E.; Campos, T.; Fuentes-Villalobos, F.; Palma, M. E.; Pincheira, R.; Castro, A. F. *Int. J. Cancer* **2016**, *138* (8), 1815–1823.

(26) Aspuria, P.-J.; Tamanoi, F. *Cell. Signal.* **2004**, *16* (10), 1105–1112.

(27) Ma, D.; Bai, X.; Zou, H.; Lai, Y.; Jiang, Y. *J. Biol. Chem.* **2010**, *285* (12), 8621–8627.

(28) Sun, Y.; Fang, Y.; Yoon, M.-S.; Zhang, C.; Roccio, M.; Zwartkruis, F. J.; Armstrong, M.; Brown, H. A.; Chen, J. *Proc. Natl. Acad. Sci.* **2008**, *105* (24), 8286–8291.

(29) Cox, A. D.; Fesik, S. W.; Kimmelman, A. C.; Luo, J.; Der, C. J. *Nat. Rev. Drug Discov.* **2014**, *13* (11), 828–851.

(30) Catalogue Of Somatic Mutation In Cancer (COSMIC) v79 http://cancer.sanger.ac.uk/cosmic (accessed Jan 26, 2018).

(31) Gremer, L.; Gilsbach, B.; Reza Ahmadian, M.; Wittinghofer, A. *Biol. Chem.* **2008**, *389* (9), 1163–1171.

(32) Lim, S. M.; Westover, K. D.; Ficarro, S. B.; Harrison, R. A.; Choi, H. G.; Pacold, M. E.; Carrasco, M.; Hunter, J.; Kim, N. D.; Xie, T.; Sim, T.; Jänne, P. A.; Meyerson, M.; Marto, J. A.; Engen, J. R.; Gray, N. S. *Angew. Chem. Int. Ed.* **2014**, *53* (1), 199–204.

(33) Mazhab-Jafari, M. T.; Marshall, C. B.; Ho, J.; Ishiyama, N.; Stambolic, V.; Ikura, M. *J. Biol. Chem.* **2014**, *289* (18), 12195–12201.

(34) Blesch, A.; Bosserhoff, A.-K.; Apfel, R.; Behl, C.; Hessdoerfer, B.; Schmitt, A.; Jachimczak, P.; Lottspeich, F.; Buettner, R.; Bogdahn, U. *Cancer Res.* **1994**, *54* (21), 5695–5701.

(35) Bosserhoff, A.-K.; Kaufmann, M.; Kaluza, B.; Bartke, I.; Zirngibl, H.; Hein, R.; Stolz, W.; Buettner, R. *Cancer Res.* **1997**, *57*, 3149–3153.

(36) Stoll, R.; Bosserhoff, A.-K. *Curr. Protein Pept. Sci.* **2008**, *9* (3), 221–226.

(37) Cancer Facts and Figures 2017 https://www.cancer.org/research/cancer-facts-statistics/all-cancer-facts-figures/cancer-facts-figures-2017.html.

(38) Stoll, R.; Renner, C.; Zweckstetter, M.; Brüggert, M.; Ambrosius, D.; Palme, S.; Engh, R. A.; Golob, M.; Breibach, I.; Buettner, R.; Voelter, W.; Holak, T. A.; Bosserhoff, A.-K. *EMBO J.* **2001**, *20* (3), 340–349.

(39) Lougheed, J. C.; Holton, J. M.; Alber, T.; Bazan, J. F.; Handel, T. M. *Proc. Natl. Acad. Sci.* **2001**, *98* (10), 5515–5520.

(40) Bosserhoff, A.-K. *Pigment Cell Res.* **2005**, *18* (6), 51012082332003.

(41) Schmidt, J.; Riechers, A.; Stoll, R.; Amann, T.; Fink, F.; Spruss, T.; Gronwald, W.; König, B.; Hellerbrand, C.; Bosserhoff, A.-K. *PLoS One* **2012**, *7* (5), e37941.

(42) Schmidt, J.; Friebel, K.; Schönherr, R.; Coppolino, M. G.; Bosserhoff, A.-K. *Cell Res.* **2010**, *20* (11), 1224–1238.

(43) Schmidt, J.; Riechers, A.; Bosserhoff, A.-K. *Histol. Histopathol.* **2013**, *28* (4), 421–426.

(44) van Zundert, G. C. P.; Rodrigues, J. P. G. L. M.; Trellet, M.; Schmitz, C.; Kastritis, P. L.; Karaca, E.; Melquiond, A. S. J.; van Dijk, M.; de Vries, S. J.; Bonvin, A. M. J. J. *J. Mol. Biol.* **2016**, *428* (4), 720–725.

(45) Bauer, R.; Humphries, M.; Fässler, R.; Winklmeier, A.; Craig, S. E.; Bosserhoff, A.-K. *J. Biol. Chem.* **2006**, *281* (17), 11669–11677.

(46) Schmidt, J.; Bosserhoff, A.-K. *Int. J. Cancer* **2009**, *125* (7), 1587–1594.

(47) Ledford, H. *Nature* **2015**, *520* (7547), 278–280.

(48) Keeton, A. B.; Salter, E. A.; Piazza, G. A. *Cancer Res.* **2017**, *77* (2), 221–226.

(49) Wang, W.; Fang, G.; Rudolph, J. *Bioorg. Med. Chem. Lett.* **2012**, *22* (18), 5766–5776.

(50) Dong, D. L.; Liu, R.; Sherlock, R.; Wigler, M. H.; Nestler, H. P. *Chem. Biol.* **1999**, *6* (3), 133–141.

(51) Sebti, S. M.; Hamilton, A. D. *Expert Opin. Investig. Drugs* **2000**, *9* (12), 2767–2782.

(52) Cox, A. D.; Der, C. J. *Curr. Opin. Pharmacol.* **2002**, *2* (4), 388–393.

(53) Singh, S. B.; Lingham, R. B. *Curr. Opin. Drug Discov. Devel.* **2002**, *5* (2), 225–244.

(54) Gysin, S.; Salt, M.; Young, A.; McCormick, F. *Genes Cancer* **2011**, *2* (3), 359–372.

(55) Taveras, A. G.; Remiszewski, S. W.; Doll, R. J.; Cesarz, D.; Huang, E. C.; Kirschmeier, P.; Pramanik, B. N.; Snow, M. E.; Wang, Y. S.; del Rosario, J. D.; Vibulbhan, B.; Bauer, B. B.; Brown, J. E.; Carr, D.; Catino, J.; Evans, C. A.; Girijavallabhan, V.; Heimark, L.; James, L.; Liberles, S.; Nash, C.; Perkins, L.; Senior, M. M.; Tsarbopoulos, A.; Ganguly, A. K.; Aust, R.; Brown, E.; Delisle, D.; Fuhrman, S.; Hendrickson, T.; Kissinger, C.; Love, R.; Sisson, W.; Villafranca, E.; Webber, S. E. *Bioorg. Med. Chem.* **1997**, *5* (1), 125–133.

(56) Colombo, S.; Peri, F.; Tisi, R.; Nicotra, F.; Martegani, E. *Ann. N. Y. Acad. Sci.* **2004**, *1030* (1), 52–61.

(57) Palmioli, A.; Sacco, E.; Airoldi, C.; Di Nicolantonio, F.; D'Urzo, A.; Shirasawa, S.; Sasazuki, T.; Di Domizio, A.; De Gioia, L.; Martegani, E.; Bardelli, A.; Peri, F.; Vanoni, M. *Biochem. Biophys. Res. Commun.* **2009**, *386* (4), 593–597.

(58) Xiong, Y.; Lu, J.; Hunter, J.; Li, L.; Scott, D.; Choi, H. G.; Lim, S. M.; Manandhar, A.; Gondi, S.; Sim, T.; Westover, K. D.; Gray, N. S. *ACS Med. Chem. Lett.* **2017**, *8* (1), 61–66.

(59) Palmioli, A.; Sacco, E.; Abraham, S.; Thomas, C. J.; Domizio, A. Di; Gioia, L. De; Gaponenko, V.; Vanoni, M.; Peri, F. *Bioorg. Med. Chem. Lett.* **2009**, *19* (15), 4217–4222.

(60) Rudolph, J.; Stokoe, D. *Angew. Chem. Int. Ed.* **2014**, *53* (15), 3777–3779.

(61) Müller, M. P.; Jeganathan, S.; Heidrich, A.; Campos, J.; Goody, R. S. *Sci. Rep.* **2017**, *7* (1), 3687.

(62) Ostrem, J. M.; Peters, U.; Sos, M. L.; Wells, J. A.; Shokat, K. M. *Nature* **2013**, *503* (7477), 548–551.

(63) Erlanson, D. A.; Braisted, A. C.; Raphael, D. R.; Randal, M.; Stroud, R. M.; Gordon, E. M.; Wells, J. A. *Proc. Natl. Acad. Sci.* **2000**, *97* (17), 9367–9372.

(64) Ma, R.; Wang, P.; Wu, J.; Ruan, K. *Molecules* **2016**, *21* (7), 854.

(65) Sakamoto, K.; Kamada, Y.; Sameshima, T.; Yaguchi, M.; Niida, A.; Sasaki, S.; Miwa, M.; Ohkubo, S.; Sakamoto, J.; Kamaura, M.; Cho, N.; Tani, A. *Biochem. Biophys. Res. Commun.* **2017**, *484* (3), 605–611.

(66) Marín-Ramos, N. I.; Piñar, C.; Vázquez-Villa, H.; Martín-Fontecha, M.; González, Á.; Canales, Á.; Algar, S.; Mayo, P. P.; Jiménez-Barbero, J.; Gajate, C.; Mollinedo, F.; Pardo, L.; Ortega-Gutiérrez, S.; Viso, A.; López-Rodríguez, M. L. *Chem. - A Eur. J.* **2017**, *23* (7), 1676–1685.

(67) Sogabe, S.; Kamada, Y.; Miwa, M.; Niida, A.; Sameshima, T.; Kamaura, M.; Yonemori, K.; Sasaki, S.; Sakamoto, J.; Sakamoto, K. *ACS Med. Chem. Lett.* **2017**, *8* (7), 732–736.

(68) Spoerner, M.; Graf, T.; König, B.; Kalbitzer, H. R. *Biochem. Biophys. Res. Commun.* **2005**, *334* (2), 709–713.

(69) Rosnizeck, I. C.; Graf, T.; Spoerner, M.; Tränkle, J.; Filchtinski, D.; Herrmann, C.; Gremer, L.; Vetter, I. R.; Wittinghofer, A.; König, B.; Kalbitzer, H. R. *Angew. Chem. Int. Ed.* **2010**, *49* (22), 3830–3833.

(70) Shima, F.; Yoshikawa, Y.; Ye, M.; Araki, M.; Matsumoto, S.; Liao, J.; Hu, L.; Sugimoto, T.; Ijiri, Y.; Takeda, A.; Nishiyama, Y.; Sato, C.; Muraoka, S.; Tamura, A.; Osoda, T.; Tsuda, K.; Miyakawa, T.; Fukunishi, H.; Shimada, J.; Kumasaka, T.; Yamamoto, M.; Kataoka, T. *Proc. Natl. Acad. Sci.* **2013**, *110* (20), 8182–8187.

(71) Welsch, M. E.; Kaplan, A.; Chambers, J. M.; Stokes, M. E.; Bos, P. H.; Zask, A.; Zhang, Y.; Sanchez-Martin, M.; Badgley, M. A.; Huang, C. S.; Tran, T. H.; Akkiraju, H.; Brown, L. M.; Nandakumar, R.; Cremers, S.; Yang, W. S.; Tong, L.; Olive, K. P.; Ferrando, A.; Stockwell, B. R. *Cell* **2017**, *168* (5), 878–889.e29.

(72) Maurer, T.; Garrenton, L. S.; Oh, A.; Pitts, K.; Anderson, D. J.; Skelton, N. J.; Fauber, B. P.; Pan, B.; Malek, S.; Stokoe, D.; Ludlam, M. J. C.; Bowman, K. K.; Wu, J.; Giannetti, A. M.; Starovasnik, M. A.; Mellman, I.; Jackson, P. K.; Rudolph, J.; Wang, W.; Fang, G. *Proc. Natl. Acad. Sci.* **2012**, *109* (14), 5299–5304.

(73) Sun, Q.; Burke, J. P.; Phan, J.; Burns, M. C.; Olejniczak, E. T.; Waterson, A. G.; Lee, T.; Rossanese, O. W.; Fesik, S. W. *Angew. Chem. Int. Ed.* **2012**, *51* (25), 6140–6143.

(74) Scott, D. E.; Coyne, A. G.; Hudson, S. A.; Abell, C. *Biochemistry* **2012**, *51*, 4990–5003.

(75) Spies, M. A. *ACS Med. Chem. Lett.* **2013**, *4* (10), 895–897.

(76) Harner, M. J.; Frank, A. O.; Fesik, S. W. *J. Biomol. NMR* **2013**, *56* (2), 65–75.

(77) Shuker, S. B.; Hajduk, P. J.; Meadows, R. P.; Fesik, S. W. *Science (80-.).* **1996**, *274* (5292), 1531–1534.

(78) Hajduk, P. J.; Greer, J. *Nat. Rev. Drug Discov.* **2007**, *6* (3), 211–219.

(79) Sun, Q.; Phan, J.; Friberg, A. R.; Camper, D. V.; Olejniczak, E. T.; Fesik, S. W. *J. Biomol. NMR* **2014**, *60* (1), 11–14.

(80) Morris, G. M.; Huey, R.; Lindstrom, W.; Sanner, M. F.; Belew, R. K.; Goodsell, D. S.; Olson, A. J. **2009**, *30* (16), 2785–2791.

(81) Trott, O.; Olson, A. J. *J. Comput. Chem.* **2009**, NA-NA.

(82) Cosconati, S.; Forli, S.; Perryman, A. L.; Harris, R.; Goodsell, D. S.; Olson, A. J. *Expert Opin. Drug Discov.* **2010**, *5* (6), 597–607.

(83) Schrödinger Suite 2012 Protein Preparation Wizard; Epik version 2.3, Schrödinger, LLC, New York, NY, 2012; Impact version 5.8, Schrödinger, LLC, New York, NY, 2012; Prime version 3.1, Schrödinger, LLC, New York, NY, 2012.Schrödinger Suite 2012 Protein Pre, 2012. .

(84) Olsson, M. H. M.; Søndergaard, C. R.; Rostkowski, M.; Jensen, J. H. *J. Chem. Theory Comput.* **2011**, *7* (2), 525–537.

(85) LigPrep, version 2.5, Schrödinger, LLC, New York, NY, **2012**.

(86) Glide, version 5.8, Schrödinger, LLC, New York, NY, **2012**.

(87) Friesner, R. A.; Banks, J. L.; Murphy, R. B.; Halgren, T. A.; Klicic, J. J.; Mainz, D. T.; Repasky, M. P.; Knoll, E. H.; Shelley, M.; Perry, J. K.; Shaw, D. E.; Francis, P.; Shenkin, P. S. *J. Med. Chem.* **2004**, *47* (7), 1739–1749.

(88) Halgren, T. A.; Murphy, R. B.; Friesner, R. A.; Beard, H. S.; Frye, L. L.; Pollard, W. T.; Banks, J. L. *J. Med. Chem.* **2004**, *47* (7), 1750–1759.

(89) Friesner, R. A.; Murphy, R. B.; Repasky, M. P.; Frye, L. L.; Greenwood, J. R.; Halgren, T. A.; Sanschagrin, P. C.; Mainz, D. T. *J. Med. Chem.* **2006**, *49* (21), 6177–6196.

(90) MacroModel, version 9.9, Schrödinger, LLC, New York, NY, 2012. .

(91) Dominguez, C.; Boelens, R.; Bonvin, A. M. J. J. *J. Am. Chem. Soc.* **2003**, *125* (7), 1731–1737.

(92) de Vries, S. J.; van Dijk, A. D. J.; Krzeminski, M.; van Dijk, M.; Thureau, A.; Hsu, V.; Wassenaar, T.; Bonvin, A. M. J. J. *Proteins Struct. Funct. Bioinforma.* **2007**, *69* (4), 726–733.

(93) Irwin, J. J.; Shoichet, B. K. *J. Chem. Inf. Model.* **2005**, *45* (1), 177–182.

(94) Irwin, J. J.; Sterling, T.; Mysinger, M. M.; Bolstad, E. S.; Coleman, R. G. *J. Chem. Inf. Model.* **2012**, *52* (7), 1757–1768.

(95) Yip, K. T.; Zhong, X. Y.; Seibel, N.; Pütz, S.; Autzen, J.; Gasper, R.; Hofmann, E.; Scherkenbeck, J.; Stoll, R. *Sci. Rep.* **2016**, *6* (1), 25119.

(96) The NMR measurement was conducted by Dr. Katharina Jockers at the Ruhr Universität Bochum.

(97) Lionetti, D.; Medvecz, A. J.; Ugrinova, V.; Quiroz-Guzman, M.; Noll, B. C.; Brown, S. N. *Inorg. Chem.* **2010**, *49* (10), 4687–4697.

(98) Mamane, V.; Hannen, P.; Fürstner, A. *Chem. - A Eur. J.* **2004**, *10* (18), 4556–4575.

(99) Brun, K. A.; Linden, A.; Heimgartner, H. **2002**, *85*, 3422–3443.

(100) McNulty, J.; Das, P. *European J. Org. Chem.* **2009**, *2009* (24), 4031–4035.

(101) Mori, K.; Kawasaki, T.; Akiyama, T. **2012**, No. 3, 14–17.

(102) The NMR measurement was conducted by Miriam Schöpel at the Ruhr Universität Bochum.

(103) Ziarek, J. J.; Peterson, F. C.; Lytle, B. L.; Volkman, B. F. 2011; pp 241–275.

(104) Chu, W.; Li, X.; Hou, Y.; Wang, H.; Li, H.; Yuan, X.; Sun, Z. *Appl. Organomet. Chem.* **2012**, *26* (9), 478–482.

(105) Roelens, F.; Heldring, N.; Dhooge, W.; Bengtsson, M.; Comhaire, F.; Gustafsson, J.-Å.; Treuter, E.; De Keukeleire, D. *J. Med. Chem.* **2006**, *49* (25), 7357–7365.

(106) The NMR measurement was conducted by Oleksandr Shkura at the Ruhr Universität Bochum.

(107) Aoyama, A.; Endo-Umeda, K.; Kishida, K.; Ohgane, K.; Noguchi-Yachide, T.; Aoyama, H.; Ishikawa, M.; Miyachi, H.; Makishima, M.; Hashimoto, Y. *J. Med. Chem.* **2012**, *55* (17), 7360–7377.

(108) Diemer, V.; Chaumeil, H.; Defoin, A.; Carré, C. *Tetrahedron* **2010**, *66* (4), 918–929.

(109) Starčević, Š.; Brožič, P.; Turk, S.; Cesar, J.; Lanišnik Rižner, T.; Gobec, S. *J. Med. Chem.* **2011**, *54* (1), 248–261.

(110) Kolasa, T.; Gunn, D. E.; Bhatia, P.; Basha, A.; Craig, R. A.; Stewart, A. O.; Bouska, J. B.; Harris, R. R.; Hulkower, K. I.; Malo, P. E.; Bell, R. L.; Carter, G. W.; Brooks, C. D. W. *J. Med. Chem.* **2000**, *43* (17), 3322–3334.

(111) Woo, L. W. L.; Wood, P. M.; Bubert, C.; Thomas, M. P.; Purohit, A.; Potter, B. V. L. *ChemMedChem* **2013**, *8* (5), 779–799.

(112) Lin, D. W.; Masuda, T.; Biskup, M. B.; Nelson, J. D.; Baran, P. S. *J. Org. Chem.* **2011**, *76* (4), 1013–1030.

(113) Kaller, M.; Tussetschläger, S.; Fischer, P.; Deck, C.; Baro, A.; Giesselmann, F.; Laschat, S. *Chem. - A Eur. J.* **2009**, *15* (37), 9530–9542.

(114) Pouységu, L.; Chassaing, S.; Dejugnac, D.; Lamidey, A.-M.; Miqueu, K.; Sotiropoulos, J.-M.; Quideau, S. *Angew. Chem. Int. Ed.* **2008**, *47* (19), 3552–3555.

(115) Moreman, J.; Lee, O.; Trznadel, M.; David, A.; Kudoh, T.; Tyler, C. R. *Environ. Sci. Technol.* **2017**, *51* (21), 12796–12805.

(116) Corrales, J.; Kristofco, L. A.; Steele, W. B.; Yates, B. S.; Breed, C. S.; Williams, E. S.; Brooks, B. W. *Dose-Response*

2015, *13* (3), 155932581559830.

(117) Wang, A.; Padula, A.; Sirota, M.; Woodruff, T. J. *Fertil. Steril.* **2016**, *106* (4), 905–929.

(118) Suvorov, A.; Waxman, D. J. *Reprod. Toxicol.* **2015**, *57*, 59–72.

(119) Umweltbundesamt. Bisphenol A: Massenchemikalie mit unerwünschten Nebenwirkungen https://www.umweltbundesamt.de/sites/default/files/medien/publikation/long/3782.pdf (accessed Dec 12, 2017).

(120) Bund - Friends of the Earth Germany https://www.bund.net/chemie/hormonelle-schadstoffe/bisphenol-a/ (accessed Dec 12, **2017**).

(121) Schöpel, M.; Herrmann, C.; Scherkenbeck, J.; Stoll, R. *FEBS Lett.* **2016**, *590* (3), 369–375.

(122) Unbuplished results by Dr. Miriam Schöpel.

(123) Chen, D.; Kannan, K.; Tan, H.; Zheng, Z.; Feng, Y.-L.; Wu, Y.; Widelka, M. *Environ. Sci. Technol.* **2016**, *50* (11), 5438–5453.

(124) Gul, W.; Hammond, N. L.; Yousaf, M.; Peng, J.; Holley, A.; Hamann, M. T. *Biochim. Biophys. Acta - Gen. Subj.* **2007**, *1770* (11), 1513–1519.

(125) Bao, Y.-S.; Baiyin, M.; Agula, B.; Jia, M.; Zhaorigetu, B. *J. Org. Chem.* **2014**, *79* (14), 6715–6719.

(126) Ren, Y.; Matthew, S.; Lantvit, D. D.; Ninh, T. N.; Chai, H.; Fuchs, J. R.; Soejarto, D. D.; de Blanco, E. J. C.; Swanson, S. M.; Kinghorn, A. D. *J. Nat. Prod.* **2011**, *74* (5), 1117–1125.

(127) Shiri, M.; Zolfigol, M. A.; Ayazi-Nasrabadi, R. *Tetrahedron Lett.* **2010**, *51* (2), 264–268.

(128) Azizian, J.; Teimouri, F.; Mohammadizadeh, M. R. *Catal. Commun.* **2007**, *8* (7), 1117–1121.

(129) Zhang, Z.-H.; Yin, L.; Wang, Y.-M. *Synthesis (Stuttg).* **2005**, *2005* (12), 1949–1954.

(130) Smithen, D. A.; Cameron, T. S.; Thompson, A. *Org. Lett.* **2011**, *13* (21), 5846–5849.

(131) Das, P. J.; Das, J. *Tetrahedron Lett.* **2012**, *53* (35), 4718–4720.

(132) Seward, E. M.; Hopkins, R. B.; Sauerer, W.; Tam, S. W.; Diederich, F. *J. Am. Chem. Soc.* **1990**, *112* (5), 1783–1790.

(133) Carta, M.; Msayib, K. J.; Budd, P. M.; McKeown, N. B. *Org. Lett.* **2008**, *10* (13), 2641–2643.

(134) Nemmara, V. V.; Adediran, S. A.; Dave, K.; Duez, C.; Pratt, R. F. *Biochemistry* **2013**, *52* (15), 2627–2637.

(135) Thirumalai Rajan, S.; Eswraiah, S.; Venkat Reddy, G. Process for the Preparation of DPP-IV Inhibitor. WO 2013/111158 A2, **2013**.

(136) Banoglu, E.; Çalışkan, B.; Luderer, S.; Eren, G.; Özkan, Y.; Altenhofen, W.; Weinigel, C.; Barz, D.; Gerstmeier, J.; Pergola, C.; Werz, O. *Bioorg. Med. Chem.* **2012**, *20* (12), 3728–3741.

(137) Salikov, R. F.; Platonov, D. N.; Frumkin, A. E.; Lipilin, D. L.; Tomilov, Y. V. *Tetrahedron* **2013**, *69* (16), 3495–3505.

(138) Charton, J.; Girault-Mizzi, S.; Sergheraert, C. *Chem. Pharm. Bull. (Tokyo).* **2005**, *53* (5), 492–497.

(139) Palkowitz, A. D.; Steinberg, M. I.; Thrasher, K. J.; Reel, J. K.; Hauser, K. L.; Zimmerman, K. M.; Wiest, S. A.; Whitesitt, C. A.; Simon, R. L. *J. Med. Chem.* **1994**, *37* (26), 4508–4521.

(140) Coterón, J. M.; Catterick, D.; Castro, J.; Chaparro, M. J.; Díaz, B.; Fernández, E.; Ferrer, S.; Gamo, F. J.; Gordo, M.; Gut, J.; de las Heras, L.; Legac, J.; Marco, M.; Miguel, J.; Muñoz, V.; Porras, E.; de la Rosa, J. C.; Ruiz, J. R.; Sandoval, E.; Ventosa, P.; Rosenthal, P. J.; Fiandor, J. M. *J. Med. Chem.* **2010**, *53* (16), 6129–6152.

(141) Rousseaux, S.; Davi, M.; Sofack-Kreutzer, J.; Pierre, C.; Kefalidis, C. E.; Clot, E.; Fagnou, K.; Baudoin, O. *J. Am. Chem. Soc.* **2010**, *132* (31), 10706–10716.

(142) Chaumontet, M.; Piccardi, R.; Audic, N.; Hitce, J.; Peglion, J.; Clot, E.; Baudoin, O. *J. Am. Chem. Soc.* **2008**, *130* (45), 15157–15166.

(143) Baloglu, E.; Ghosh, S.; Lobera, M.; Schmidt, D. R. Compounds and Methods. WO 2013/019635 A1, **2013**.

(144) Baloglu, E.; Bohnert, Gary, J.; Gosh, S.; Lobera, M.; Schmidt, D. R.; Sung, L. Compounds and Methods. WO 2013/019682 A1, 2013.

(145) Trieu, T. H.; Dong, J.; Zhang, Q.; Zheng, B.; Meng, T.-Z.; Lu, X.; Shi, X.-X. *European J. Org. Chem.* **2013**, *2013* (16), 3271–3277.

(146) Lee, H. K.; Lee, Y. S.; Roh, E. J.; Rhim, H.; Lee, J. Y.; Shin, K. J. *Bioorg. Med. Chem. Lett.* **2008**, *18* (15), 4424–4427.

(147) Sherman, D.; Kawakami, J.; He, H.-Y.; Dhun, F.; Rios, R.; Liu, H.; Pan, W.; Xu, Y.-J.; Hong, S.; Arbour, M.; Labelle, M.; Duncton, M. A. J. *Tetrahedron Lett.* **2007**, *48* (51), 8943–8946.

(148) Brückner, C.; Reißig, H.-U. *Chem. Ber.* **1987**, *120* (4), 617–626.

(149) Brückner, C.; Reißig, H.-U. *Chem. Ber.* **1987**, *120* (4), 627–629.

(150) Li, F.-N.; Kim, N.-J.; Paek, S.-M.; Kwon, D.-Y.; Min, K. H.; Jeong, Y.-S.; Kim, S.-Y.; Park, Y.-H.; Kim, H.-D.; Park, H.-G.; Suh, Y.-G. *Bioorg. Med. Chem.* **2009**, *17* (10), 3557–3567.

(151) Ferreira, L. M.; Marques, M. M. B.; Glória, P. M. C.; Chaves, H. T.; Franco, J.-P. P.; Mourato, I.; Antunes, J.-R. T.; Rzepa, H. S.; Lobo, A. M.; Prabhakar, S. *Tetrahedron* **2008**, *64* (33), 7759–7770.

(152) Tuhina, K.; Bhowmik, D. R.; Venkateswaran, R. V. *Chem. Commun.* **2002**, No. 6, 634–635.

(153) Ghosh, S.; Tuhina, K.; Bhowmik, D. R.; Venkateswaran, R. V. *Tetrahedron* **2007**, *63* (3), 644–651.

(154) Roy, A.; Tuhina, K.; Biswas, B.; Venkateswaran, R. V. *Tetrahedron* **2012**, *68* (32), 6575–6580.

(155) Gilbert, A. M.; Katz, T. J.; Geiger, W. E.; Robben, M. P.; Rheingold, A. L. *J. Am. Chem. Soc.* **1993**, *115* (8), 3199–3211.

(156) Ke, Y.; Zhi, X.; Yu, X.; Ding, G.; Yang, C.; Xu, H. *Comb. Chem. High Throughput Screen.* **2014**, *17* (1), 89–95.

(157) Chancellor, D. R.; Davies, K. E.; De Moor, O.; Dorgan, C. R.; Johnson, P. D.; Lambert, A. G.; Lawrence, D.; Lecci, C.; Maillol, C.; Middleton, P. J.; Nugent, G.; Poignant, S. D.; Potter, A. C.; Price, P. D.; Pye, R. J.; Storer, R.; Tinsley, J. M.; van Well, R.; Vickers, R.; Vile, J.; Wilkes, F. J.; Wilson, F. X.; Wren, S. P.; Wynne, G. M. *J. Med. Chem.* **2011**, *54* (9), 3241–3250.

(158) The NMR measurement was conducted by King Yip Tuo at the Ruhr Universität Bochum.

(159) Wang, Y.; Wang, H.; Peng, J.; Zhu, Q. *Org. Lett.* **2011**, *13* (17), 4604–4607.

(160) The NMR measurement was conducted by Xueyin Zhong at the Ruhr Universität Bochum.

(161) Hausler, N. E.; Devine, S. M.; McRobb, F. M.; Warfe, L.; Pouton, C. W.; Haynes, J. M.; Bottle, S. E.; White, P. J.; Scammells, P. J. *J. Med. Chem.* **2012**, *55* (7), 3521–3534.

(162) Galley, G.; Groebke Zbinden, K.; Norcross, R.; Stalder, H. The Use of Benzamide Derivatives for the Treatment of CNS Disorders. WO 2009016088 A1, **2009**.

(163) Moorthy, J. N.; Saha, S. *European J. Org. Chem.* **2008**, No. 5, NA-NA.

(164) Lee, D.; Long, S. A.; Murray, J. H.; Adams, J. L.; Nuttall, M. E.; Nadeau, D. P.; Kikly, K.; Winkler, J. D.; Sung, C.; Ryan, M. D.; Levy, M. A.; Keller, P. M. **2015**, 2015–2026.

(165) Fan, W.; Li, W.; Ma, X.; Tao, X.; Li, X.; Yao, Y.; Xie, X.; Zhang, Z. *J. Org. Chem.* **2011**, *76* (22), 9444–9451.

(166) Shi, L.; Ye, Z.-S.; Cao, L.-L.; Guo, R.-N.; Hu, Y.; Zhou, Y.-G. *Angew. Chem. Int. Ed.* **2012**, *51* (33), 8286–8289.

(167) Carmen Bernabeu, M.; Luis Díaz, J.; Jiménez, O.; Lavilla, R. *Synth. Commun.* **2004**, *34* (1), 137–149.

(168) Liguori, A.; Sindona, G.; Romeo, G.; Uccella, N. *Synthesis (Stuttg).* **1987**, *1987* (2), 168–168.

(169) Rakshit, S.; Grohmann, C.; Besset, T.; Glorius, F. *J. Am. Chem. Soc.* **2011**, *133* (8), 2350–2353.

(170) Suzuki, Y.; Moriyama, K.; Togo, H. *Tetrahedron* **2011**, *67* (41), 7956–7962.

(171) Miller, J. F.; Gudmundsson, K. S.; Richardson, L. D.; Jenkinson, S.; Spaltenstein, A.; Thomson, M.; Wheelan, P. *Bioorg. Med. Chem. Lett.* **2010**, *20* (10), 3026–3030.

(172) Tsuzuki, Y.; Sawamoto, D.; Sakamoto, T.; Kato, T.; Niwa, Y. Sulfonamide Compounds having TRPM8 Antagonistic Activity. WO2012124825 A1, **2012**.

(173) Elliott, R.; Gancia, E.; Heald, R.; Heffron, T.; Safina, B.; Seward, E. M.; Staben, S.; Sutherlin, D. P.; Waszkowycz, B.; Wei, B. Benzoxazepin Compounds Selective for PI3K P110 Delta and Methods of Use. WO2012126901 A1, 2012.

(174) Kagabu, S. *Synth. Commun.* **2006**, *36* (9), 1235–1245.

(175) Liu, G.; Sham, H. L.; Szczepankiewicz, B. G.; Xin, Z.; Zhao, H.; Serby, M. D.; Liu, B.; Liu, M. Inhibitors of c-Jun N-Terminal Kinases. US2006173050 A1, **2006**.

(176) Singer, A. W.; McElvain, S. M. *Org. Synth.* **1940**, *20*, 79.

(177) Reddy, B. V. S.; Begum, Z.; Reddy, Y. J.; Yadav, J. S. *Tetrahedron Lett.* **2010**, *51* (25), 3334–3336.

(178) Nazaré, M.; Will, D. W.; Matter, H.; Schreuder, H.; Ritter, K.; Urmann, M.; Essrich, M.; Bauer, A.; Wagner, M.;

Czech, J.; Lorenz, M.; Laux, V.; Wehner, V. *J. Med. Chem.* **2005**, *48* (14), 4511–4525.

(179) Nazaré, M.; Essrich, M.; Will, D. W.; Matter, H.; Ritter, K.; Wehner, V. Indole-2-carboxamides as Factor Xa Inhibitors, **2001**.

(180) Font, M.; Monge, A.; Cuartero, A.; Elorriaga, A.; Martínez-Irujo, J. J.; Alberdi, E.; Santiago, E.; Prieto, I.; Lasarte, J. J.; Sarobe, P.; Borrás, F. *Eur. J. Med. Chem.* **1995**, *30* (12), 963–971.

(181) Hewlett, N. M.; Tepe, J. J. *Org. Lett.* **2011**, *13* (17), 4550–4553.

(182) Caron, S.; Wei, L.; Douville, J.; Ghosh, A. *J. Org. Chem.* **2010**, *75* (3), 945–947.

(183) Güven, A.; Jones, R. A. *Tetrahedron* **1993**, *49* (48), 11145–11154.

(184) Kuuloja, N.; Tois, J.; Franzén, R. *Tetrahedron: Asymmetry* **2011**, *22* (4), 468–475.

(185) Yoshikawa, K.; Yokomizo, A.; Naito, H.; Haginoya, N.; Kobayashi, S.; Yoshino, T.; Nagata, T.; Mochizuki, A.; Osanai, K.; Watanabe, K. *Bioorg. Med. Chem.* **2009**, *17* (24), 8206–8220.

(186) Andreani, A.; Rambaldi, M.; Bonazzi, D.; Andreani, F.; Bossa, R.; Galatulas, I. *Arch. Pharm. (Weinheim).* **1984**, *317* (10), 847–851.

(187) Kutschy, P.; Suchý, M.; Andreani, A.; Dzurilla, M.; Kováčik, V.; Alföldi, J.; Rossi, M.; Gramatová, M. *Tetrahedron* **2002**, *58* (44), 9029–9039.

(188) Blunt, R.; Eatherton, A. J.; Garzya, V.; Healy, M. P.; Myatt, J.; Porter, R. Benzoxazinone Derivatives for the Treatment of Glytl Mediated Disorders. WO 2011012622 A1, **2011**.

(189) Hall, C. M.; Johnson, H. G. Quinoxalinone Compounds Useful for Expanding the Lumina or Air Passages in Mammals. US 4181724 A, **1980**.

(190) Foti, R. S.; Rock, D. A.; Han, X.; Flowers, R. A.; Wienkers, L. C.; Wahlstrom, J. L. *J. Med. Chem.* **2012**, *55* (3), 1205–1214.

(191) Světlik, J.; Tureček, F.; Goljer, I. *J. Org. Chem.* **1990**, *55* (15), 4740–4744.

(192) Kawaguchi, M.; Okabe, T.; Okudaira, S.; Hanaoka, K.; Fujikawa, Y.; Terai, T.; Komatsu, T.; Kojima, H.; Aoki, J.; Nagano, T. *J. Am. Chem. Soc.* **2011**, *133* (31), 12021–12030.

(193) Berghaus, C.; Schwarten, M.; Heumann, R.; Stoll, R. *Biomol. NMR Assign.* **2007**, *1* (1), 45–47.

(194) Vo, U.; Embrey, K. J.; Breeze, A. L.; Golovanov, A. P. *Biomol. NMR Assign.* **2013**, *7* (2), 215–219.

(195) Stoll, R.; Renner, C.; Ambrosius, D.; Golob, M.; Voelter, W.; Buettner, R.; Bosserhoff, A. K.; Holak, T. A. *J. Biomol. NMR* **2000**, *17* (1), 87–88.